Noise, Sensitivity, and Distortion Analysis of Switched Analog Circuits

by

Fei Yuan

A thesis
presented to the University of Waterloo
in fulfilment of the
thesis requirement for the degree of
Doctor of Philosophy
in
Electrical Engineering

Waterloo, Ontario, Canada, 1999

©Fei Yuan 1999

National Library of Canada
Acquisitions and Bibliographic Services
395 Wellington Street
Ottawa ON K1A 0N4
Canada

Bibliothèque nationale du Canada
Acquisitions et services bibliographiques
395, rue Wellington
Ottawa ON K1A 0N4
Canada

Your file Votre référence

Our file Notre référence

The author has granted a non-exclusive licence allowing the National Library of Canada to reproduce, loan, distribute or sell copies of this thesis in microform, paper or electronic formats.

L'auteur a accordé une licence non exclusive permettant à la Bibliothèque nationale du Canada de reproduire, prêter, distribuer ou vendre des copies de cette thèse sous la forme de microfiche/film, de reproduction sur papier ou sur format électronique.

The author retains ownership of the copyright in this thesis. Neither the thesis nor substantial extracts from it may be printed or otherwise reproduced without the author's permission.

L'auteur conserve la propriété du droit d'auteur qui protège cette thèse. Ni la thèse ni des extraits substantiels de celle-ci ne doivent être imprimés ou autrement reproduits sans son autorisation.

0-612-44783-9

Canada

The University of Waterloo requires the signatures of all persons using or photocopying this thesis. Please sign below, and give address and date.

Abstract

This thesis deals with the analysis of noise, sensitivity, and distortion of analog circuits containing externally clocked switches in the frequency domain.

The phasor representation of the network variables of multi-phase periodically switched linear (PSL) circuits is introduced. Tellegen's theorem for PSL circuits in phase domain is derived and the theory of the adjoint network of PSL circuits is developed. Two novel theorems, namely, frequency reversal theorem and transfer function theorem are introduced and their usefulness in computing the aliasing transfer functions of PSL circuits is investigated. The theory of the adjoint network is applied to noise analysis of PSL circuits and an algorithm that is orders of magnitude faster than the conventional brute-force method is obtained.

The developed Tellegen's theorem is further applied to sensitivity analysis of PSL circuits. The frequency-domain sensitivity of PSL circuits is obtained. The sensitivity network of PSL circuits is also introduced and its usefulness in sensitivity analysis is compared with that of the adjoint network approach. To analyze switched nonlinear circuits in frequency domain, time-varying Volterra functional series is further developed by introducing time-varying network functions and multi-frequency transforms. The complete spectrum of nonlinear time-varying systems is obtained. The theory is applied to distortion analysis of multi-phase periodically switched nonlinear circuits. Both the harmonic and intermodulation distortion are analyzed.

The theories presented in this thesis have been implemented in three computer programs that compute the noise and sensitivity of periodically switched linear circuits, and the distortion of periodically switched nonlinear circuits.

Acknowledgements

I am deeply indebted to Professor Ajoy Opal for his enthusiastic support, constant guidance and inspiration throughout the course of this research. His intuition, rigorism and patience have made the journey of my doctoral work full of enjoyment.

My heartfelt gratitude goes to Professors James Barby and George Kesidis from the Department of E&CE, Professor John Vanderkooy from the Department of Physics, University of Waterloo, and Professor Timothy N. Trick from the Department of E&CE, University of Illinois at Urbana-Champaign for their participation in my comprehensive examination and defense. My special thanks also go to Professor Anthony Vannelli for many invaluable advises, and Mr. Phil Regier for his prompt response in trouble-shooting system malfunctions over the years.

I am grateful to the Natural Sciences and Engineering Research Council (NSERC) of Canada for providing me with the post-graduate scholarships (PGS-B) during 1997-1998.

Finally, It is my sincere wish to dedicate this thesis to my abiding wife, Jing, for her love, patience, and understanding. This work could not have been completed without her unending support and the joyfulness that our little boy and girl, Jonathan and Michelle, have brought to us.

Fei Yuan

May 3rd, 1999

GLOSSARY

1. Abbreviations

BJT	Bipolar junction transistor
CAD	Computer-aided design
CMOS	Complementary metal-oxide-semiconductor
CCVS	Current-controlled voltage source
CCCS	Current-controlled current source
DFT	Discrete Fourier transform
IF	Immediate frequency
LO	Local oscillator
LNA	Low-noise amplifier
LTI	Linear time-invariant
LTV	Linear time-varying
LPTV	Linear periodically time-varying
MISO	Multiple-input single-output
MNA	Modified nodal analysis
MOS	Metal-oxide-semiconductor
MOSFET	Metal-oxide-semiconductor field-effect transistor
MS	Mean-square
NTI	Nonlinear time-invariant
NTV	Nonlinear time-varying
NPTV	Nonlinear periodically time-varying
Op amp	Operational amplifier
PSL	Periodically switched linear
PSN	Periodically switched nonlinear

PSD	Power spectral density
RF	Radio frequency
S/H	Sampled-and-held
SC	Switched capacitor
SCN	Switched capacitor network
SI	Switched current
SISO	Single-input single-output
SIMO	Single-input multiple-output
SLCNAP	Switched linear circuit noise analysis program
SLCSAP	Switched linear circuit sensitivity analysis program
SNCDAP	Switched nonlinear circuit distortion analysis program
VCVS	Voltage-controlled voltage source
VCCS	Voltage-controlled current source

2. Symbols

$\mathbf{A}_2$	Constant matrix depicting the 2nd-order nonlinearities
$\mathbf{A}_3$	Constant matrix depicting the 3rd-order nonlinearities
C_g	Gate-channel capacitance
C_{ol}	Gate-channel overlapping capacitance
C_{gb}	Gate-substrate capacitance
C_{sb}	Source-substrate diffusion capacitance
C_{db}	Drain-substrate diffusion capacitance
C_o	Depletion layer capacitance at zero-biasing
C_{ox}	Gate-channel capacitance per unit area

$\mathbf{C}_k$	Capacitance matrix in phase k
$\mathbf{d}$	Constant vector specifying the output nodes.
$E[.]$	Mathematical expectation operator
f	frequency (Hz)
$\mathcal{F}[.]$	Fourier transform operator
$\mathcal{F}^{-1}[.]$	Inverse Fourier transform operator
g_m	Gate transconductance
g_{mb}	Substrate transconductance
g_{DS}	Channel conductance
g_{DS_o}	Channel conductance at $v_{DS} = 0$
$\mathbf{G}_k$	Conductance matrix in phase k
$\mathbf{g}_k$	Constant vector specifying the input nodes
$h(t,\tau)$	First-order impulse response
$h_1(t,\tau)$	First-order Volterra kernel
$h_2(t,\tau_1,\tau_2)$	Second-order Volterra kernel
$h_3(t,\tau_1,\tau_2,\tau_3)$	Third-order Volterra kernel
$h_n(t,\tau_1,...,\tau_n)$	nth-order Volterra kernel
$H(t,\omega)$	First-order time-varying transfer function
$H_1(t,\omega)$	First-order time-varying transfer function
$H_2(t,\omega_1,\omega_2)$	Second-order time-varying transfer function
$H_3(t,\omega_1,\omega_2,\omega_3)$	Third-order time-varying transfer function
$H_n(t,\omega_1,...,\omega_n)$	nth-order time-varying transfer function
$\mathcal{H}(\omega_1,\omega_2)$	Bi-frequency transfer function
$\mathcal{H}_1(\omega_1,\omega_2)$	Bi-frequency transfer function
$\mathcal{H}_2(\omega_1,\omega_2,\omega_3)$	Tri-frequency transfer function
$\mathcal{H}_3(\omega_1,...\omega_n)$	multi-frequency transfer function

$\mathcal{H}(\omega, \omega + n\omega_s)$	Aliasing transfer function, $\omega + n\omega_s$ = input freq., ω = output freq.
$i_b(t)$	Branch current
$\Delta i_b(t)$	Increment in $i_b(t)$
$I_b(\omega_o + n\omega_s)$	Phasor of $i_b(t)$ at $\omega_o + n\omega_s$
$\Delta I_b(\omega_o + n\omega_s)$	Increment in $I_b(\omega_o + n\omega_s)$
I_{DS}	Drain-source DC current
$\overline{i^2(t)}$	Mean-square value of $i(t)$
k	Boltzmann constant ($1.3806226 \times 10^{-23}$ J/K)
K_f	Flicker noise coefficient
$\mathcal{L}[.]$	Laplace transform operator
$\mathcal{L}^{-1}[.]$	Inverse Laplace transform operator
L	Channel length of MOS transistor
L_{eff}	Effective channel length of MOS transistor
$\mathbf{M}_k$	State-transition matrix in phase k
$\mathbf{N}_k$	Quasi-state-transition matrix in phase k
$\mathcal{N}$	Original circuit
$\hat{\mathcal{N}}$	Adjoint network of $\mathcal{N}$
$\mathcal{N}_\lambda$	Sensitivity network of λ
$\hat{\mathcal{N}}_\lambda$	Adjoint network of $\mathcal{N}_\lambda$
$\mathbf{P}_k$	Zero-state response vector in phase k
q	Charge on an electron ($-1.6021918 \times 10^{-19}$ C)

r_b	Base resistance
r_e	Emitter resistance
r_c	Collector resistance
r_g	Gate resistance
r_s	Source resistance
r_d	Drain resistance
$\mathcal{R}_{xx}(t_1, t_2)$	Autocorrelation function of $x(t)$
$\mathcal{R}_{xx}(t)$	Average power of $x(t)$
s	Laplace variable
$\mathcal{S}_{xx}(\omega)$	PSD of $x(t)$ at ω
$\mathcal{S}_{xx}(t, \omega)$	Time-varying PSD of $x(t)$
$\mathcal{S}_{xx}(\omega_1, \omega_2)$	2-dimensional PSD of $x(t)$
$\mathcal{S}_i(\omega)$	PSD of the input at ω
$\mathcal{S}_o(\omega)$	PSD of the output at ω
t	Time variable of the original circuit
T	Absolute temperature in degrees Kelvin
T_s	Clock period
$v_b(t)$	Branch voltage
$V_b(\omega_o + n\omega_s)$	Phasor of $v_b(t)$ at $\omega_o + n\omega_s$
$v_n(t)$	Nodal voltage
V_T	Threshold voltage of MOS transistor
v_{GS}	Gate-source voltage
v_{DS}	Drain-source voltage
$\mathbf{v}_k(t)$	Network variable in phase k
$\mathbf{v}_k(nT + \sigma_k^-)$	$\mathbf{v}_k(t)$ at $t = nT + \sigma_k^-$

$\mathbf{V}_k(j\omega)$	Fourier transform of $\mathbf{v}_k(t)$
$\mathbf{V}(j\omega)$	Fourier transform of $\mathbf{v}(j\omega)$
$\mathbf{V}^{(1)}(j\omega)$	Fourier transform of the response of the 1st-order Volterra circuit
$\mathbf{V}^{(2)}(j\omega)$	Fourier transform of the response of the 2nd-order Volterra circuit
$\mathbf{V}^{(3)}(j\omega)$	Fourier transform of the response of the 3rd-order Volterra circuit
W	Channel width
W_{eff}	Effective channel width
$\mathbf{w}^{(1)}(t)$	Input vector of the 1st-order Volterra circuit
$\mathbf{w}^{(2)}(t)$	Input vector of the 2nd-order Volterra circuit
$\mathbf{w}^{(3)}(t)$	Input vector of the 3rd-order Volterra circuit
$\otimes$	Convolution operator

3. Greek Letters

μ	Surface mobility of carriers in channel
μ_{eff}	Effective surface mobility of carriers in channel
τ	Time variable of the adjoint network
τ_k	Width of phase k
ω_s	Clock frequency
ω_o	Input frequency
$\xi_k(t)$	Window function in phase k
ϵ	Relative difference

Contents

1 Introduction 1

1.1 Noise Analysis of PSL Circuits 2

1.2 Sensitivity Analysis of PSL Circuits 9

1.3 Distortion Analysis of PSN Circuits 11

1.4 Original Contributions 15

1.5 Scope of The Thesis 17

2 Noise of LPTV Systems 19

2.1 Basic Concepts 19

2.2 Time-Varying Transfer Functions 21

2.3 PSD of LPTV Systems 25

2.4 Summary 32

3 Adjoint Network of PSL Circuits 33

3.1 Network Variable Theorem 33

3.2 Tellegen's Theorem for PSL Circuits in Phasor Domain 35

3.3 Adjoint Network of PSL Circuits 39
3.3.1 Interreciprocity and Adjoint Network 39
3.3.2 Ideal Switches 41
3.3.3 LTI Resistors 41
3.3.4 LTI Capacitors and Inductors 42
3.3.5 Controlled Sources 43
3.3.6 Operational Amplifiers 44
3.3.7 Complex Devices 44
3.4 Frequency Reversal Theorem 45
3.5 Transfer Function Theorem 51
3.6 Solution of The Adjoint Network 53
3.7 Numerical Examples 59
3.7.1 Parasitic-insensitive Switched-capacitor Integrator 60
3.7.2 Switched-capacitor Band pass Filter 62
3.8 Summary 63

4 Noise Analysis of PSL Circuits **67**

4.1 Noise Sources 67
4.1.1 Thermal noise 68
4.1.2 Shot noise 68
4.1.3 Flicker noise ($1/f$ noise) 70
4.1.4 Clock Jitter 71

4.2 Equivalent Circuits 72
4.2.1 Resistors 72
4.2.2 Bipolar Junction Transistors 73
4.2.3 MOS Transistors 74
4.2.4 Operational Amplifiers (Op amp) 78
4.3 Noise Analysis of PSL Circuits 79
4.4 Numerical Examples 82
4.4.1 Noise of SC Low-pass 82
4.4.2 Noise of SC Integrator 83
4.4.3 Noise of SC Band-pass Filter 88
4.5 Summary 89

5 Sensitivity Analysis of PSL Circuits **92**

5.1 Introduction 92
5.2 Incremental Form of Tellegen's Theorem in Phasor Domain 94
5.3 Frequency-Domain Sensitivity of PSL Circuits 95
5.3.1 Resistors 96
5.3.2 Capacitors and Inductors 97
5.3.3 Controlled Sources 98
5.3.4 Ideal Switches 98
5.3.5 Input and Output 99

5.4 Sensitivity Analysis of PSL Circuits Using The Sensitivity Network Approach 103

5.4.1 Sensitivity Networks of PSL Circuits 103

5.4.2 Sensitivity Analysis of PSL Circuits Using The Sensitivity Network Approach 104

5.5 Numerical Examples 108

5.5.1 Sensitivity of Stray-insensitive Switched-capacitor Integrator 108

5.5.2 Sensitivity of Switched-capacitor Band pass Filter 111

5.6 Summary 112

6 Distortion Analysis of PSN Circuits 118

6.1 Volterra Series of Nonlinear Time-Invariant Systems 119

6.2 Volterra Series of Nonlinear Time-Varying Systems 120

6.3 Frequency Response of Nonlinear Time-Varying Systems 122

6.3.1 Time-Varying Transfer Functions 122

6.3.2 Multi-Frequency Transform 124

6.3.3 Frequency Response of Nonlinear Time-Varying Systems 125

6.4 Nonlinear Periodically Time-Varying Systems 127

6.5 Distortion Analysis of PSN Circuits 132

6.5.1 Nonlinear Elements 132
6.5.2 Volterra Series Representation of Network Variables 138
6.5.3 Distortion Analysis of PSN Circuits 141
6.6 Harmonic Distortion of PSN Circuits 146
6.6.1 The First-order Volterra Circuit $\mathcal{N}^{(1)}$ 146
6.6.2 The Second-order Volterra Circuit $\mathcal{N}^{(2)}$ 147
6.6.3 The Third-order Volterra Circuit $\mathcal{N}^{(3)}$ 148
6.6.4 The Fold-over Effect 150
6.7 Intermodulation Distortion of PSN Circuits 151
6.7.1 The Solution of $\mathcal{N}^{(1)}$ 151
6.7.2 The Solution of $\mathcal{N}^{(2)}$ 152
6.7.3 The Solution of $\mathcal{N}^{(3)}$ 152
6.8 Numerical Examples 153
6.8.1 Harmonic Distortion of Modulator 153
6.8.2 Harmonic Distortion of Stray-insensitive SC Integrator 154
6.9 Summary 162

7 Conclusions **168**

A Numerical Inversion of Laplace Transform **171**

Bibliography **174**

List of Tables

3.1 Frequency reversal theorem 50

3.2 Transfer function theorem 52

3.3 Relation between original and adjoint networks 59

3.4 Parameter values of SC integrator 60

3.5 Responses of switched-capacitor integrator and its adjoint network . 63

3.6 Parameter value of Switched-capacitor band pass filter 64

3.7 Responses of Switched-capacitor band pass filter and its adjoint network 66

4.1 Parameter values of SC low-pass 82

4.2 Parameter values of SC integrator 85

5.1 Sensitivity of PSL circuits 101

5.2 Parameter values of stray-insensitive Switched-capacitor integrator 109

6.1 Parameter values of modulator 154

6.2 Harmonic distortion of modulator 155

6.3 Parameter values of stray-insensitive SC integrator 155

6.4 Harmonic distortion of stray-insensitive integrator 157

6.5 Parameter values of stray-insensitive SC integrator 158

6.6 Harmonic distortion of stray-insensitive integrator ($a_1 = 100, a_2 = 0, a_3 = 10$) 161

6.7 Harmonic distortion of stray-insensitive integrator ($a_1 = 100, a_2 = 10, a_3 = 10$) 162

6.8 Harmonic distortion using adjoint network and brute-force methods 164

6.9 Intermodulation distortion 165

6.10 Harmonic distortion of stray-insensitive integrators with nonlinear capacitors 165

List of Figures

1.1 Ideal sampler 4

1.2 Effect of coupling. (L) Direct noise, (R) S/H noise 4

1.3 Effect of aliasing. (L) Direct noise, (R) S/H noise 5

1.4 Input referred noise 6

1.5 Block diagram of the front end of receiver 11

2.1 Input-output mappings of LTI and LPTV systems 24

2.2 Sampling of stationary random signal 28

2.3 Aliasing effect of band-limited noise signals 30

3.1 Time reversal of adjoint network 39

3.2 Configuration of LTI circuit and its adjoint network 39

3.3 Elements and their counterparts in the adjoint network 45

3.4 Frequency reversal theorem 46

3.5 Impulse response and transfer function of linear time-varying system 48

3.6 Frequency reversal theorem 51

3.7 Inputs and outputs of original and adjoint networks 53

3.8 Clock phase 54

3.9 Parasitic-insensitive switched-capacitor integrator and its adjoint network 61

3.10 Models of op amp and its adjoint network 62

3.11 Switched-capacitor band pass filter 65

3.12 adjoint network of Switched-capacitor band pass 65

4.1 Equivalent circuits of resistors. (a) Norton equivalent, (b) Thevenin equivalent 72

4.2 A high-frequency small-signal equivalent circuit of BJTs biased in forward active region 74

4.3 A low-frequency equivalent circuit of MOSFET switch 77

4.4 A high-frequency small-signal Equivalent circuit of MOS transistor . 78

4.5 Equivalent circuits of operational amplifier. (a) Complete equivalent circuit, (b) Simplified equivalent circuit. 79

4.6 SC low-pass 83

4.7 PSD of SC low-pass 84

4.8 SC integrator 86

4.9 PSD of SC integrator 87

4.10 CPU time 88

4.11 Speedup 89

4.12 Equivalent circuit of band-pass filter 90

4.13 PSD of band-pass filter 91

5.1 Sensitivity analysis of PSL circuits 96

5.2 Fold-over effect in sensitivity analysis of PSL circuits 102

5.3 Sensitivity networks of basic elements 105

5.4 Sensitivity network of PSL circuits (a) PSL circuit $\mathcal{N}$, (b) Sensitivity networks $\mathcal{N}_{C,k}, k = 0, \pm 1, ...,$ (c) Adjoint network of $\mathcal{N}$ 106

5.5 Stray-insensitive Switched-capacitor integrator 109

5.6 Sensitivity of the response of integrator to C1 (Real part) 110

5.7 Sensitivity of the response of integrator to C1 (Imaginary part) . . 111

5.8 Normalized sensitivity of the response of integrator to C1 112

5.9 Voltage of C1 of Switched-capacitor integrator 113

5.10 Voltage of C1 of the adjoint network of Switched-capacitor integrator 114

5.11 Sensitivity of the response of band pass to C2 (Real part) 114

5.12 Sensitivity the response of band pass to C2 (Imaginary part) 115

5.13 Normalized sensitivity of response of band pass 115

5.14 Relative difference 116

5.15 Voltage of C2 of band pass filter 116

5.16 Voltage of C2 of the adjoint network of band pass filter 117

6.1 Gilbert-cell RF mixer 121

6.2 Spectrum of PSN circuits with input $x(t) = A\cos\omega_o t$ 131

6.3 Spectrum of PSN circuits with input $x(t) = A(\cos\omega_1 t + \cos\omega_2 t)$ . . . 133

6.4 Equivalent circuits of nonlinear VCVS 135

6.5 Equivalent circuits of linear and nonlinear capacitors in phase k. (a) Linear capacitor, (b) Nonlinear capacitor 139

6.6 Stamps for nonlinear capacitors 140

6.7 Block diagram of PSN circuits. IC - initial condition, FC - final condition 142

6.8 Fold-over effect in distortion analysis 150

6.9 Modulator 153

6.10 Convergence of 2nd-order harmonic of modulator 156

6.11 Stray-insensitive SC integrator 157

6.12 Convergence of 2nd-order harmonic of stray-insensitive SC integrator 158

6.13 SC integrator 160

6.14 Harmonic distortion of SC integrator 163

6.15 Harmonic distortion of SC integrator 164

6.16 Intermodulation distortion of SC integrator 166

6.17 Intermodulation distortion of SC integrator 166

6.18 Harmonic distortion of SC integrator with nonlinear capacitors . . . 167

Chapter 1

Introduction

The objective of this research is to develop efficient methods for noise and sensitivity analysis of periodically switched linear circuits, and distortion analysis of periodically switched mildly nonlinear circuits. In this chapter, a brief review of the theories and algorithms available for noise, sensitivity, and distortion analysis of these circuits is presented.

Periodically switched networks are analog circuits containing externally clocked switches. Switched capacitor networks (SCNs), switched current (SI) networks, modulators, frequency mixers, etc. are typical examples. These mixed analog-digital circuits are widely encountered in telecommunication systems [1]. The trend towards portable and wireless electronic systems, such as personal communication systems, note-book computers, wireless networks, etc. has pushed the design of these circuits towards ultra low power consumption and high degree of integration. Noise has become a critical issue in the design of these circuits [2–4]. For instance, the resolution of switched capacitor sigma-delta modulators is limited by the thermal noise generated by the operational amplifiers and MOSFET switches of the

modulators [5,6]. The minimization of the silicon chip area of switched-capacitor networks tends to reduce the signal-to-noise ratio (SNR) of the circuits [7]. The physical dimension and layout of semiconductor devices directly affect the noise of the devices [8]. An accurate analysis of noise is vital to the design of these circuits.

The performance of electronic circuits is not only affected by the quality of the circuits at the design stage, it is also affected by the fabrication process in which the circuits are fabricated and the environment in which the circuits are operated. Circuits tolerating a large variation in element values are highly desirable. Sensitivity plays a key role in measuring the robustness of circuit design. This thesis explores novel theories and efficient algorithms for sensitivity analysis of PSL circuits in frequency domain.

In addition to noise and sensitivity, distortion is another key factor affecting the performance of switched analog circuits. The design of most analog circuits is based on the local linearization of the non-ideal characteristics of electronic devices. This thesis makes no attempt to address the analysis of general nonlinear switched circuits. Rather, our attention is focused upon periodically switched analog circuits containing weak nonlinearities only. This is because a large number of analog circuits encountered in telecommunication systems are designed to operate at specific operating points such that the nonlinearities encountered are weak.

1.1 Noise Analysis of PSL Circuits

The noise of linear time-invariant circuits is usually investigated in frequency domain and is well understood [9]. A universal way to compute the output noise power of a given linear time-invariant circuit is to approximate the input noise

signal within a small frequency range $\Delta\omega$ by a sinusoidal excitation whose mean-square (MS) value is determined by the PSD of the input noise source. The circuit is analyzed in frequency domain and the MS value of the response gives the output noise power of the circuit in $\Delta\omega$. This approach is valid for linear time-invariant circuits only.

Noise analysis of switched-capacitor networks, a special subset of general PSL circuits, has received considerable attention since the launch of switched-capacitor technique in the early 1970s [10]. The early investigations of noise behavior of switched-capacitor networks were primarily focused upon the techniques that decompose the output noise into the so-called direct noise caused by the feed-through of the noise sources and the sampled-and-held (S/H) noise caused by the noise sampled by the shunt capacitors in the circuits [11–14]. The behavior of these two types of noise is best illustrated using an ideal sampler shown in Fig.1.1. The input noise source is assumed to be white of unity power and the switching frequency f_s is 10 r/s. The PSD of the direct noise, denoted by $S_o^d(\omega)$ and that of the S/H noise, denoted by $S_o^{S/H}(\omega)$, of the output are given by

$$\begin{aligned} S_o^d(\omega) &= \left(\frac{a}{T_s}\right)^2 \sum_{n=-\infty}^{\infty} \mathrm{sinc}^2\left(\frac{n\omega_s a}{2}\right) S_i(\omega - n\omega_s) \\ S_o^{S/H}(\omega) &= \left[\frac{T_s - a}{T_s}\right]^2 \mathrm{sinc}^2\left[\frac{(T_s - a)\omega}{2}\right] \sum_{n=-\infty}^{\infty} S_i(\omega - n\omega_s) \end{aligned} \tag{1.1}$$

where $\omega_s = 2\pi f_s$, $T_s = 1/f_s$, $S_i(\omega)$ is the PSD of the input noise source. Fig.1.2 shows the effect of the direct coupling between the input noise source and the response with the input noise band width $10\omega_s$. It is seen that the power of the direct noise is independent of frequency and is negligibly small as compared with that of the S/H noise. The power of the S/H noise is frequency-dependent. It rises

with the decrease in the direct coupling. Fig.1.3 shows the effect of aliasing with $a = 0.3T_s$. It is seen that the power of the S/H noise increases with the increase in the number of side bands folded over.

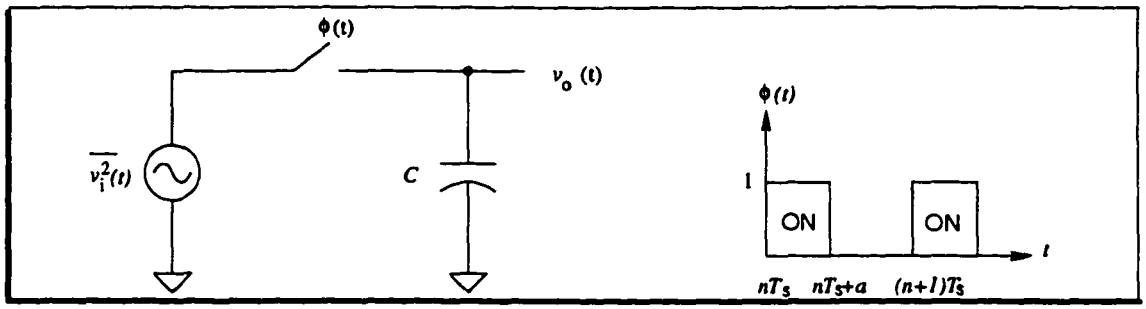


Figure 1.1: Ideal sampler

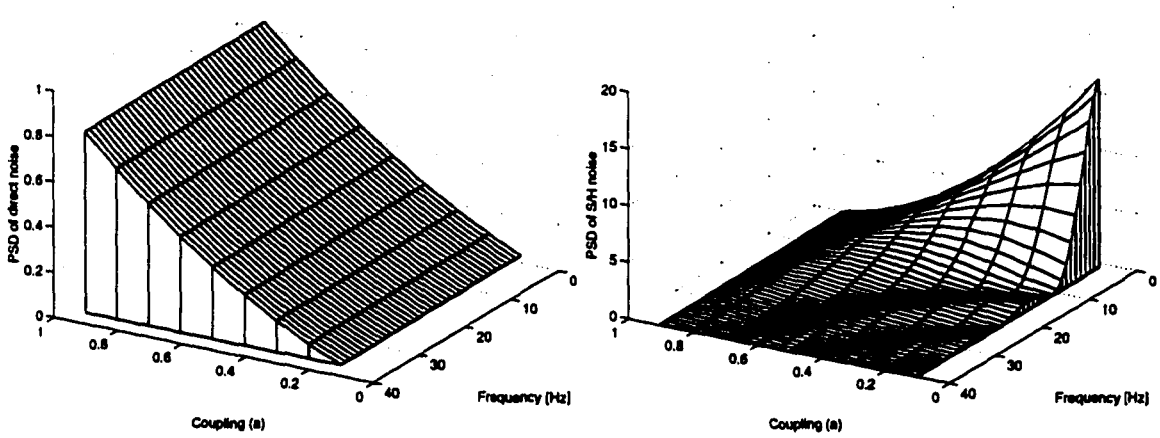


Figure 1.2: Effect of coupling. (L) Direct noise, (R) S/H noise

Eqs.(1.1) were deduced directly from the autocorrelation function of $v_o(t)$. This approach is often referred to as the *analytical approach*. The analytical approach provides a clear insight into the noise behavior of switched-capacitor networks. Its application, however, is limited to simple circuit configurations for which the analytical expressions of the response and its autocorrelation function are obtainable using the pen and paper approach.

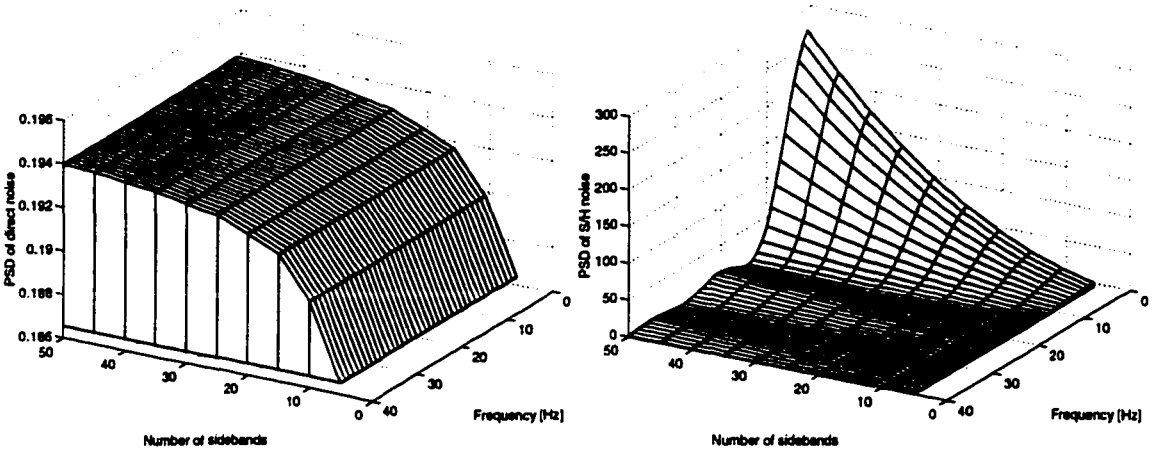


Figure 1.3: Effect of aliasing. (L) Direct noise, (R) S/H noise

Techniques that utilize conventional circuit simulators, such as SPICE, to analyze the noise of switched-capacitor networks, were also investigated [15]. These techniques are categorized as the *equivalent-circuit* approach. The essence of this method is to transform a switched-capacitor network into an equivalent continuous RC circuit. The output noise power of the switched-capacitor network is obtained by multiplying that of the RC circuit by the number of side bands that fall in the noise band width of the network. The method is in favor of many circuit designers owing to its simplicity. However, due to the difficulty in determining the noise band width of switched-capacitor networks prior to simulation, an estimated noise band width is used. Consequently, the obtained output noise power is only an approximation of the actual value.

With the increase in the complexity of switched-capacitor network configuration, computationally efficient methods are critically needed. The *input-referred noise generator* technique is an elegant approach that is widely adopted in noise analysis of complex electronic circuits. In this method, a pair of fictitious input-referred

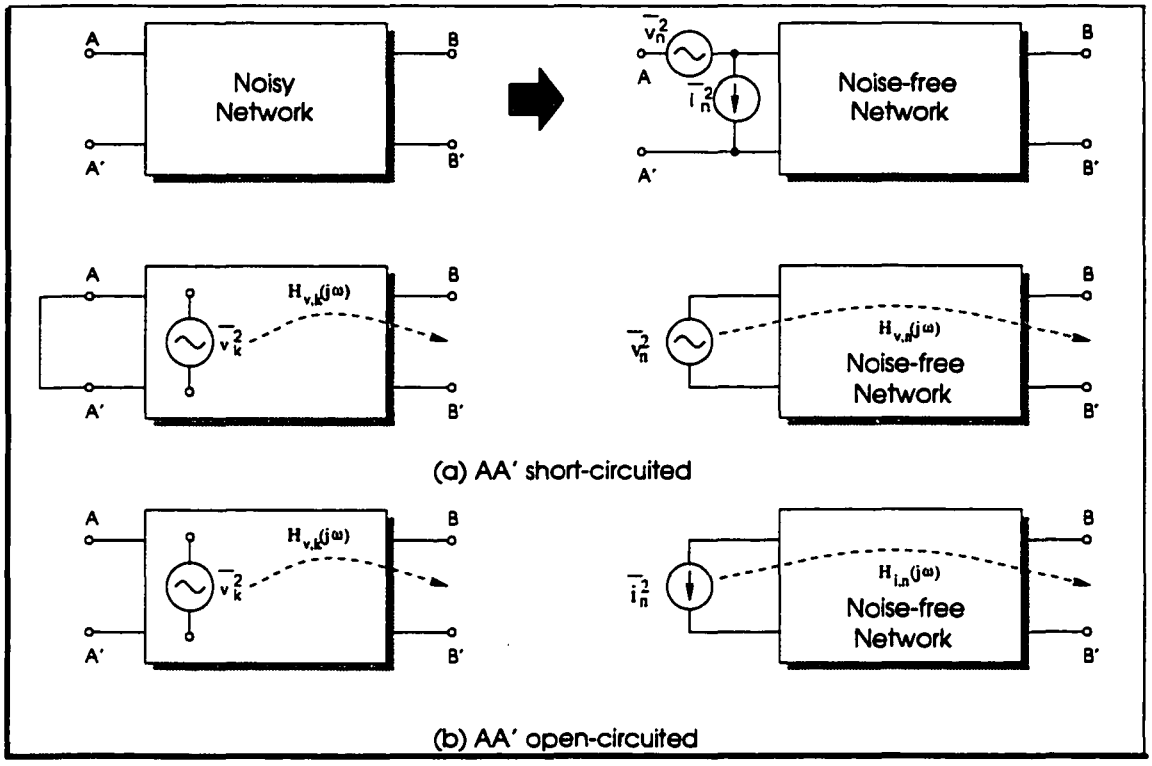


Figure 1.4: Input referred noise

noise-voltage and noise-current generators are employed at the input of a noisy circuit (usually two-port) to represent the effect of all the noise sources in the circuit. The entire circuit is thereby treated as noise-free [16], as shown in Fig. 1.4. To obtain the noise-voltage source, the input is shorted. To compute the noise-current source, the input is open-circuited. Specifically, to obtain the input-referred voltage representative of the kth noise source whose MS value is $\overline{v_k^2}$, the transfer function from the noise source to the output of the noisy network $H_{v,k}(j\omega)$ and that from the input-referred noise-voltage source to the output of the noise-free network $H_{v,n}(j\omega)$ are required. The MS values of the input-referred noise sources

are obtained from

$$\begin{cases} \overline{v_n^2}(j\omega) = \dfrac{1}{|H_{v,n}(j\omega)|^2} \displaystyle\sum_{k=1}^{M} |H_{v,k}(j\omega)|^2 \overline{v_k^2} \\ \overline{i_n^2}(j\omega) = \dfrac{1}{|H_{i,n}(j\omega)|^2} \displaystyle\sum_{k=1}^{M} |H_{v,k}(j\omega)|^2 \overline{v_k^2} \end{cases} \tag{1.2}$$

where M is the number of noise sources in the circuit. Eqs.(1.2) are valid only if all the physical noise sources in the circuit are uncorrelated. The input-referred noise source approach is very effective in simplifying the noise analysis of complex circuits, calculating the signal-to-noise ratio and determining the minimum input signal level. The application of this approach, however, is affected by the following factors : (a) The input-referred noise sources are, in general, correlated because they are originated from the same physical noise sources. (b) The power of the input-referred noise sources is frequency-dependent. This is because the transfer functions required to derive these noise sources are functions of frequency. They must be re-calculated every time frequency changes. (c) The power of the input-referred noise sources is affected by the biasing condition. This is because many small-signal parameters of integrated devices, such as the transconductances of MOSFETs and BJTs, are functions of DC biasing currents/voltages. For switched capacitor networks, it is generally difficult to obtain the input-referred noise sources due to the folding effect. However, this method can be applied to linear time-invariant subcircuits in switched-capacitor networks, such as op amps, to greatly simplify noise analysis.

State-space approach is an effective method widely used in the theoretical study of electronic circuits. A pioneer work on the noise analysis of switched-capacitor networks using the state-space approach was carried out by Liou and Kuo [17], and was also studied by other authors [18–20]. The state-space approach is not par-

ticularly convenient for equation formulation of electronic circuits on digital computers [21, 22], particularly if the circuits are complex and contain ideal switches. Modern CAD tools almost exclusively use the modified nodal analysis to formulate circuit equations [22]

Adjoint network is well known as one of the most efficient methods in computing the transfer functions from multiple inputs to the single output of linear time-invariant circuits [23–25]. Its advantages in noise analysis of linear time-invariant circuits were demonstrated in [26]. The adjoint network theory for linear time-invariant circuits was also extended to switched-capacitor networks with S/H inputs [27–29], and its usefulness in noise analysis of switched-capacitor networks was explored as well [30–32].

The application of SCN-based CAD tools is limited by the following factors : (i) No current-related elements, such as resistors, current-related controlled sources, etc. are permitted in the configuration of switched-capacitor networks. This makes it impossible to analyze the effect of some nonidealities, such as the channel resistance of MOSFET switches, the finite input and output resistances of op amps of practical switched-capacitor networks. (ii) The analysis of switched-capacitor networks is based on the assumption that the charge transfer occurs instantaneously at switching instants. This assumption is often violated when switched-capacitor networks are used for high-frequency applications. In this case, the effect of incomplete charge transfer must be taken into account. (iii) The accurate modeling of integrated devices, such as MOSFETs and BJTs, requires taking into account the characteristics of the devices, such as the intrinsic and extrinsic resistances, contact resistances, the body effect of MOS transistors, the clock feed-through of MOSFET switches, etc. Modeling of these effects requires the presence of resistors and current-related controlled sources. Contrary to switched-capacitor networks,

resistors, inductors, and all types of controlled sources are basic elements of PSL circuits. Many nonidealities of practical switched-capacitor networks can be handled conveniently using PSL circuits.

As compared with switched-capacitor networks, noise analysis of general PSL circuits, however, has received little attention in the past. In [33,34], the output noise power of PSL circuits was analyzed by discretizing the circuit equation using the Backward Euler approximation. The accuracy of this method is affected by the errors introduced in discretization and the assumption that the time-varying transfer function of PSL circuits is piece-wise constant in each phase. In [35,36], a noise analysis method for nonideal switched-capacitor networks was proposed. The method approximates the continuous response of PSL circuits with the sampled-data response. It yields good approximation only if the clock frequency is much higher than the signal frequency and may give erroneous results when the two frequencies become comparable. In [37], a method using the time-varying transfer functions to compute the noise of RF mixers was proposed. However, the efficiency of the method is undermined by the DFT operation used to compute the aliasing transfer functions. Also, no attempt was made in implementing the algorithm on digital computers. The above review demonstrates that despite the practical importance, accurate and efficient noise analysis methods for PSL circuits are not available.

1.2 Sensitivity Analysis of PSL Circuits

In addition to noise analysis, efficient and accurate computational methods for sensitivity analysis of PSL circuits are needed. Sensitivity plays an essential role in optimization and tolerance design of electronic circuits [38,39]. It provides a

mathematical measure in determining the quality of designed circuits. The exact sensitivity of a given circuit can be obtained if the analytical response of the circuit is available. This approach is only feasible for simple circuit configurations and becomes irrelevant once circuits are complex. Early investigations on computer methods for sensitivity analysis of linear time-invariant circuits were primarily focused on perturbation and incremental network techniques [25, 40, 41]. These methods, however, suffer from the poor numerical accuracy and the lack of efficiency. The adjoint network method was introduced as an efficient means for sensitivity analysis of linear time-invariant circuits [23–25, 42] more than a decade after the publication of the original theorem by B. Tellegen [43], now known as Tellegen's theorem. The application of Tellegen's theorem was later extended to switched-capacitor networks with S/H inputs [27, 28, 31, 44, 45] and piece-wise linear circuits [46]. A careful examination shows the difficulties in extending this approach directly to sensitivity analysis of PSL circuits. This is because there is no closed-form solution available for general PSL circuits. Opal and Vlach [47] proposed an accurate frequency-domain method to compute the sensitivity of general PSL circuits. The method is capable of handling arbitrary types of input (continuous or S/H) and the number of the phases in each clock period. However, it is only capable of computing sensitivities of all network variables with respect to one element at a time. Computation becomes prohibitively expensive if sensitivities of one variable with respect to a large number of elements are required. Shang and Sewell [36, 48, 49] improved the computational efficiency of Opal-Vlach method by considering the discrete response of PSL circuits only. The method yields a good approximation of the sensitivity only if the clock frequency is much higher than the signal frequency. It gives erroneous results if the frequencies of the clock and signal are close. Circuits of this characteristic can be found in many areas of telecommunications, such as

mixers in which the frequencies of the carriers and the local oscillator are nearly the same. Efficient and accurate computer methods for sensitivity analysis of general PSL circuits are critically needed.

1.3 Distortion Analysis of PSN Circuits

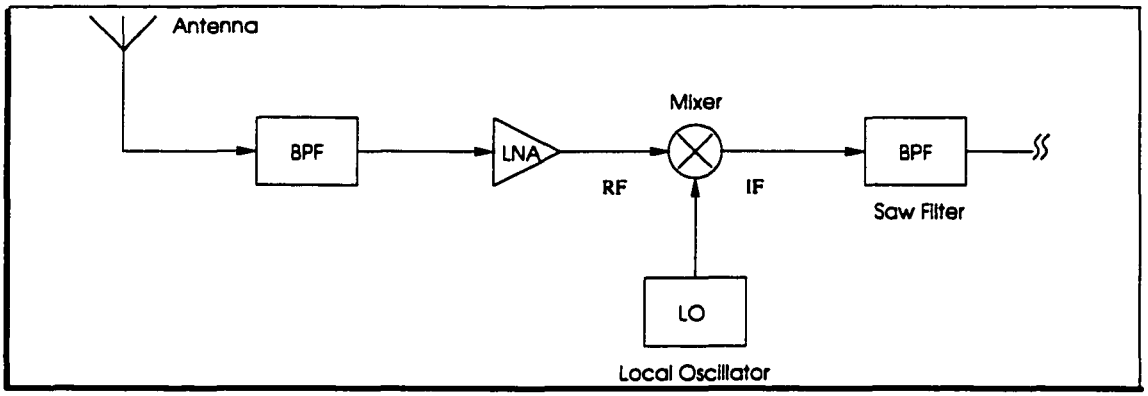


Figure 1.5: Block diagram of the front end of receiver

Distortion is a key factor affecting the design of switched circuits [50]. Circuits of superior linearity are highly desirable. Nonlinearities inherent to analog circuits integrated on silicon chips, such as depletion layer capacitances, the transconductance of MOS transistors, the slew-rate and saturation of operational amplifiers, etc. deteriorate the performance of the circuits. An illustrative example is the front-end of a RF receiver shown in Fig.1.5. The dynamic range of the receiver is directly affected by the distortion generated by the low-noise amplifier (LNA) and the mixer.

Distortion of nonlinear circuits is usually analyzed by carrying out direct numerical integration of the circuit equations in time-domain and post discrete Fourier transform (DFT) analysis of the steady-state response data of the circuits. These

methods are referred to as the *DFT-based approach.* The DFT-based method is effective and universal in determining both the harmonic and intermodulation distortion of nonlinear circuits in steady state. It is also capable of handling both harsh and weak nonlinearities. The application of this approach, however, is often limited by the excessive cost of computation, particularly, if the circuits contain periodically operated ideal switches. Many efficient methods, such as shooting methods [51–53], were developed to accelerate integration process. To speed up integration, variable step size is always preferred. Since FFT analysis requires equidistant time points, interpolation is needed [22]. Recently, an elegant method was proposed by Bedrosian and Vlach [54–56] to speed up the transient analysis of switched nonlinear circuits. This method makes use of the 2-step algorithm initially developed by Opal and Vlach [57–59] to compute the initial conditions of the states. The overhead caused by small step size is eliminated.

Harmonic balance [60–63] is a well-known method for distortion analysis of nonlinear circuits with periodic excitations in steady state. It is based on the assumption that the steady-state response of nonlinear circuits with periodic excitations is a linear combination of a set of sinusoidals that are harmonically related. The amplitude and phase of the response are obtained by solving the so-called determining equations using numerical techniques. In principle, the harmonic balance method is capable of handling arbitrary nonlinearities that in general can not be described adequately by 3rd-order polynomials. However, in order to depict strong nonlinearities accurately, many sine and cosine functions will be needed. This drastically increases the cost of computation and memory resource requirement. The situation becomes formidable once the excitations are multiple tones. A piece-wise harmonic balance method was proposed by Nakhla and Vlach [62, 64] to eliminate this drawback by decomposing a given nonlinear circuit into linear and nonlinear subcircuits. The

linear subcircuits are solved using conventional frequency response methods while the nonlinear subcircuits are solved using the harmonic balance technique. The results are matched at the junctions of the subcircuits. Because the resulting nonlinear subcircuits are much smaller in scale the burden of excessive computation is hence reduced. This method is also known as the *substitution* method [65,66]. The application of this method is in general limited to circuits containing a few nonlinearities. PSN circuits encountered in telecommunication systems, such as mixers, modulators, etc. are usually driven by inputs of multiple tones. The steady-state waveforms of these circuits contain many frequency components due to the combination of the fundamental frequencies of the forced inputs and those generated by the nonlinearities in the circuits. In this case, the harmonic balance method becomes inefficient as a large set of determining equations must be solved.

Recently, the conventional *describing function* approach was extended to distortion analysis of nonlinear time-invariant electronic circuits [67]. Describing function is an extended version of the popular frequency response method used in linear network analysis. It has been used extensively in control system design to predict the existence of limit cycles [68] and normally only the fundamental frequency component is used. The author extended this approach by also including harmonic components. This method can be used for distortion analysis of circuits containing soft nonlinearities. Hard nonlinearities with a rapidly decaying harmonic spectrum can also be analyzed.

In the past decade, much attention was focused upon analytical means to analyze the harmonic distortion of nonlinear switched capacitor filters [45, 69, 70]. In these approaches, The harmonic components of the output are obtained directly from the Taylor series expansion of the response of the circuits. This method is much in favor of IC designers as it provides an insight into the sources of dis-

tortion. The application of this method, however, is limited to circuits of simple configurations for which analytical solutions are obtainable using the pen and paper approach.

Investigations on systematic approaches and computer methods for distortion analysis of nonlinear switched-capacitor networks were also carried out. The usefulness of Volterra functional series in distortion analysis of nonlinear time-invariant circuits has been investigated extensively. Volterra series-based approach is a generalization of the well-known power series method [71]. As compared with those reviewed earlier, this method is a direct frequency-domain approach. Because there is no numerical integration involved this method is computationally efficient. An extensive coverage of the theory and applications of time-invariant Volterra functional series can be found in [72–75]. Alper [76, 77] and Bush [78] modified the time-invariant Volterra series by incorporating the characteristics of sampled-data systems and discrete Volterra series emerged. Discrete Volterra series has been used in distortion analysis of nonlinear switched-capacitor networks [27, 28, 79, 80]. Because of the constraints of sampled-data systems, only nonlinear switched-capacitor networks with S/H inputs can be analyzed.

Distortion analysis of general switched nonlinear circuits has received little attention in the past despite its practical importance. An analytical approach [81, 82] was proposed to compute the harmonic distortion of CMOS Gilbert cell RF mixers [83–85]. The nonlinear characteristic of the transconductances of the amplifying MOS transistors is identified as the dominant source of distortion. The signal from the local oscillator (LO) which drives the mixing MOS transistors is represented by Fourier time series. The output of the mixer is a time-domain product of the carrier (RF) and LO signals. This approach neglects the effect of the transfer of the charges stored in the parasitic capacitances between LO states. The effect of

charge transfer is vital to the analysis of switched circuits, as demonstrated in [47]. As a result, only low-frequency distortion can be predicted.

1.4 Original Contributions

This thesis contains original contributions in noise and sensitivity analysis of periodically switched linear circuits, and distortion analysis of periodically switched nonlinear circuits. The major contributions of this thesis are summarized as follows:

(1) Tellegen's theorem for PSL circuits in phasor domain is developed. It is shown that Tellegen's theorem for linear time-invariant circuits is a special case of that for PSL circuits.

(2) Two novel theorems, namely, the transfer function theorem and frequency reversal theorem of PSL circuits are introduced. Both rigorous proofs and numerical verification are given.

(3) The interreciprocity concept of linear time-invariant circuits is extended to PSL circuits. The theory of adjoint network of PSL circuits is developed. The theory handles periodically operated multiphase switches and all types of linear elements.

(4) The intrinsic relationship between the original PSL circuits and the corresponding adjoint networks is explored. It is shown that both the state transition matrix and zero-state response vector of the adjoint network can be obtained directly from those of the original circuit. It is also shown that the adjoint network of a given PSL circuit can be solved efficiently provided that the solution of the original PSL circuit is available.

(5) An adjoint network-based frequency-domain noise analysis algorithm for general PSL circuits is developed. The method is exact and is orders of magnitude

faster than the brute-force method. The algorithm has been implemented in a computed program. The PSDs of several PSL circuits are analyzed and the results are in very good agreement with measurements.

(6) The incremental form of Tellegen's theorem for PSL circuits in phasor domain is developed. The frequency-domain sensitivity of periodically switched linear circuits is obtained. The method yields sensitivities of the response of PSL circuits with respect to all circuit elements in one frequency analysis. It is shown that frequency-domain sensitivity of PSL circuit is a series summation of the network variables. Both the base band and side band components contribute to the sensitivity computed in the base band. It is also shown that the sensitivity of linear time-invariant circuits is a special case of that of PSL circuits.

(7) The sensitivity networks of PSL circuits are introduced. It is demonstrated that the sensitivities obtained from adjoint network approach are identical to those from sensitivity network technique.

(8) A general theory of time-varying Volterra functional series for nonlinear time-varying system is developed. High-order time-varying transfer functions and multi-frequency transforms are introduced to characterize the behavior of nonlinear time-varying systems. The network variable theorem of periodically switched nonlinear circuits is introduced and the complete spectra of the systems to both single-tone and double-done inputs are obtained.

(9) A Volterra series-based frequency-domain method for distortion analysis of periodically switched nonlinear circuits is developed. It is shown that the behavior of a periodically switched nonlinear circuit can be characterized by a set of intrinsically related PSL circuits. It is also shown that the fold-over effect, a phenomenon encountered in noise analysis of PSL circuits, also exists in distortion analysis of

periodically switched nonlinear circuits. The cost of computation for distortion analysis can be minimized by using the adjoint network theory of PSL circuits. The distortion of several practical circuits are analyzed and the results are in an excellent agreement with SPICE simulation.

1.5 Scope of The Thesis

This thesis deals with the analysis of noise, sensitivity, and distortion of switched analog circuits in frequency domain.

Chapter 2 investigates the stochastic behavior of linear periodically time-varying systems. The PSD of these systems with uncorrelated stationary inputs is derived. This chapter lays a theoretical foundation for noise analysis of general PSL circuits.

Chapter 3 is devoted to the development of the adjoint network of PSL circuits. The network variable theorem of PSL circuits is developed. Tellegen's theorem for PSL circuits in phasor domain, transfer function theorem, and frequency reversal theorem are introduced. The relationship between the original PSL circuits and the adjoint networks is investigated. The effectiveness of these theorems is assessed using numerical examples.

In chapter 4, noise sources inherent to switched analog integrated circuits are investigated. The equivalent circuits of integrated devices are presented. An adjoint network-based noise analysis algorithm for general PSL circuit is developed. The output noise power of a number of practical switched-capacitor networks is analyzed and the results are compared with measurements.

In chapter 5, the incremental form of Tellegen's theorem for PSL circuits in phasor domain is introduced and the frequency-domain sensitivity of PSL circuits

is obtained. The sensitivity networks of PSL circuits are also introduced and a comparison with the adjoint network approach is made. The sensitivities of a number of PSL circuits are computed and the results are compared with those from other CAD tools.

In chapter 6, a theory of time-varying Volterra series is introduced. The time-varying network function and bi-frequency transform initially introduced by Zadeh for linear time-varying (LTV) systems are extended to nonlinear time-varying (NTV) systems. The network variable theorem of periodically switched nonlinear circuits is derived and the complete spectra of these circuits to both single-tone and double-tone inputs are obtained. Also developed in this chapter is a Volterra series-based frequency-domain method for distortion analysis of periodically switched nonlinear circuits. Both harmonic and inter-modulation distortion of are analyzed. The distortion of several practical circuits is analyzed and the results are compared with SPICE simulation.

Chapter 7 summarizes the important results obtained from this research. It also outlines the areas that the results of this thesis can be directly extended to. Finally, a brief review of numerical Laplace inversion is suffixed to make the thesis self-contained.

Chapter 2

Noise of LPTV Systems

Periodically switched linear circuits are linear periodically time-varying (LPTV) systems. This chapter investigates the noise behavior of LPTV systems. Some useful concepts of stochastic processes and linear time-varying systems, which are to be used throughout the thesis, are reviewed in Sections 2.1 and 2.2. The average PSD of LPTV systems with stationary noise input is obtained in Section 2.3.

2.1 Basic Concepts

Noise is a random signal with zero mean. The behavior of a noise signal is characterized by its *autocorrelation function* in time domain and *power spectral density* in frequency domain. The autocorrelation function of a noise signal $x(t)$, denoted by $\mathcal{R}_{xx}(t_1, t_2)$, is the joint moment of $x(t_1)$ and $x^*(t_2)$ [86]

$$\mathcal{R}_{xx}(t_1, t_2) = E[x(t_1)x^*(t_2)] \tag{2.1}$$

where $E[.]$ is the expectation operator, the asterisk denotes complex conjugation, t_1 and t_2 are two time instants. $\mathcal{R}_{xx}(t_1, t_2)$ quantifies the connection between $x(t_1)$ and $x(t_2)$ statistically. If $t_1 = t_2 = t$, then $\mathcal{R}_{xx}(t, t) = E[|x(t)|^2]$, which is the mean-square (MS) value, or average power of $x(t)$. The *autocovariance* of $x(t)$, denoted by $\mathcal{C}_{xx}(t_1, t_2)$, is defined as the joint moment of $x(t_1) - E[x(t_1)]$ and $x^*(t_2) - E[x^*(t_2)]$ and it relates to the autocorrelation function by

$$\mathcal{C}_{xx}(t_1, t_2) = \mathcal{R}_{xx}(t_1, t_2) - E[x(t_1)]E[x^*(t_2)]. \tag{2.2}$$

$x(t_1)$ and $x(t_2)$ are said to be uncorrelated if $\mathcal{C}_{xx}(t_1, t_2) = 0$. A stochastic process is said to be *stationary* in the strict sense if all of its statistical properties are time-invariant. It is stationary in the wide sense if its mean is constant and its autocorrelation function satisfies

$$\mathcal{R}_{xx}(t_1, t_2) = \mathcal{R}_{xx}(\tau) \tag{2.3}$$

where $\tau = t_2 - t_1$. Note that the wide-sense stationarity involves only the 1st and 2nd-order moments. Because it is generally difficult to evaluate the high-order moments of a given stochastic process, the wide-sense stationarity is of practical usefulness. If both the mean and autocorrelation function of a wide-sense stationary noise signal are periodic in time, the noise signal is said to be wide-sense *cyclo-stationary.*

In frequency domain, the PSD of a noise signal $x(t)$, denoted by $\mathcal{S}_{xx}(\omega)$, depicts the spectrum of the noise power. It is defined as the Fourier transform of the autocorrelation function of $x(t)$. $\mathcal{S}_{xx}(\omega)$ and $\mathcal{R}_{xx}(\tau)$ relate to each other via the

pair of transforms

$$\begin{cases} \mathcal{S}_{xx}(\omega) = \int_{-\infty}^{\infty} \mathcal{R}_{xx}(\tau) e^{-j\omega\tau} d\tau \\ \mathcal{R}_{xx}(\tau) = \dfrac{1}{2\pi} \int_{-\infty}^{\infty} \mathcal{S}_{xx}(\omega) e^{j\omega\tau} d\omega \end{cases} . \tag{2.4}$$

Eq.(2.4) is also known as Wiener-Khintchine theorem [88]. If $\mathcal{S}_{xx}(\omega) = A$, where A is a constant, then $\mathcal{R}_{xx}(\tau) = A\delta(\tau)$. Processes of such are said to be *white*. For a wide-sense process $x(t)$, if $\tau = 0$, i.e. $t_1 = t_2 = t$, then

$$\mathcal{R}_{xx}(0) = E[|x(t)|^2] = \frac{1}{2\pi} \int_{-\infty}^{\infty} \mathcal{S}_{xx}(\omega) d\omega. \tag{2.5}$$

Eq.(2.5) reveals that the area under $\mathcal{S}_{xx}(\omega)/2\pi$ specifies the MS value of $x(t)$. If $\mathcal{S}_{xx}(\omega)$ is band-limited and has a constant value A within $[\omega_1, \omega_2]$ and zero outside the interval, then

$$E[|x(t)|^2] = \frac{A}{2\pi} \Delta\omega \tag{2.6}$$

where $\Delta\omega = \omega_2 - \omega_1$, Eq.(2.6) reveals that once $\mathcal{S}_{xx}(\omega)$ is known, the power of $x(t)$ in $[\omega_1, \omega_2]$ is determined. The PSDs of noise sources encountered in integrated devices have been investigated extensively and are readily computable. Noise analysis is often a task of how to compute the output noise power of a given circuit containing a large number of noise sources.

2.2 Time-Varying Transfer Functions

In steady state, the characteristics of a linear time-varying system in time domain are described by the impulse response of the system $h(t, \tau)$, which is a function of

both the *excitation time* τ at which the impulse is launched and the *observation time* t at which the response is measured. The input $x(t)$ and output $y(t)$ of the system are related to each other in time domain by

$$y(t) = \int_{-\infty}^{\infty} h(t,\tau)x(\tau)d\tau. \tag{2.7}$$

The time-varying transfer function $H(t,\omega)$ is defined as [89]

$$H(t,\omega) = \int_{-\infty}^{\infty} h(t,\tau)e^{-j\omega(t-\tau)}d\tau. \tag{2.8}$$

The impulse response can be derived from $H(t,\omega)$ using

$$h(t,\tau) = \frac{1}{2\pi}\int_{-\infty}^{\infty} H(t,\omega)e^{j\omega(t-\tau)}d\omega. \tag{2.9}$$

Substituting (2.9) into (2.7) gives

$$y(t) = \frac{1}{2\pi}\int_{-\infty}^{\infty} H(t,\omega)X(\omega)e^{j\omega t}d\omega \tag{2.10}$$

where $X(\omega)$ is the Fourier transform of $x(t)$. Eq.(2.10) indicates that once $H(t,\omega)$ is known, the time domain response of the system is defined completely.

If a system is linear periodically time-varying (LPTV), then it can be shown that $H(t,\omega)$ is also periodic in t [87]. Assume that $H(t,\omega)$ satisfies Dirichlet-Jordan criterion [1]. Due to its periodicity, $H(t,\omega)$ can be represented by the Fourier series

$$H(t,\omega) = \sum_{n=-\infty}^{\infty} H_n(\omega)e^{jn\omega_s t} \tag{2.11}$$

[1] i.e. $H(t,\omega)$ is bounded, piecewise continuous, and has at most a finite number of minima, maxima, and discontinuities per period.

where $\omega_s = 2\pi/T_s$. The coefficients of the Fourier series are determined from

$$H_n(\omega) = \frac{1}{T_s}\int_0^{T_s} H(t,\omega)e^{-jn\omega_s t}dt. \tag{2.12}$$

The Frequency response of the output, denoted by $Y(\omega)$, is obtained by taking Fourier transform of (2.10)

$$Y(\omega) = \frac{1}{2\pi}\int_{-\infty}^{\infty}\int_{-\infty}^{\infty} H(t,\Omega)X(\Omega)e^{j\Omega t}e^{-j\omega t}d\Omega dt. \tag{2.13}$$

Further making use of (2.11), (2.13) becomes

$$Y(\omega) = \frac{1}{2\pi}\sum_{n=-\infty}^{\infty}\int_{-\infty}^{\infty} H_n(\Omega)X(\Omega)\left[\int_{-\infty}^{\infty} e^{-j(\omega-\Omega-n\omega_s)t}dt\right]d\Omega. \tag{2.14}$$

Because

$$\int_{-\infty}^{\infty} e^{-j(\omega-\Omega-n\omega_s)t}dt = 2\pi\delta(\omega-\Omega-n\omega_s) \tag{2.15}$$

therefore

$$Y(\omega) = \sum_{n=-\infty}^{\infty} H_n(\omega-n\omega_s)X(\omega-n\omega_s). \tag{2.16}$$

Eq.(2.16) reveals that $H_n(\omega-n\omega_s)$ represents the *aliasing transfer function* of the LPTV system with the input at frequency $\omega - n\omega_s$ and the response at frequency ω. Aliasing transfer function is a generalization of the traditional transfer function. If the input signal has a broad-band spectrum, then the response at ω consists of the contributions of both the base band ($n = 0$) and side bands ($n\neq 0$) components of the input. It is worth noting that if the system is LTI, then (2.16) is simplified

to

$$Y(\omega) = H_o(\omega)X(\omega). \tag{2.17}$$

a well-known relation of linear time-invariant systems. Clearly, for linear time-invariant systems, there is a one-to-one mapping between the input and output frequency components whereas for LPTV systems, the mapping is multiple-to-one, as illustrated in Fig.2.1.

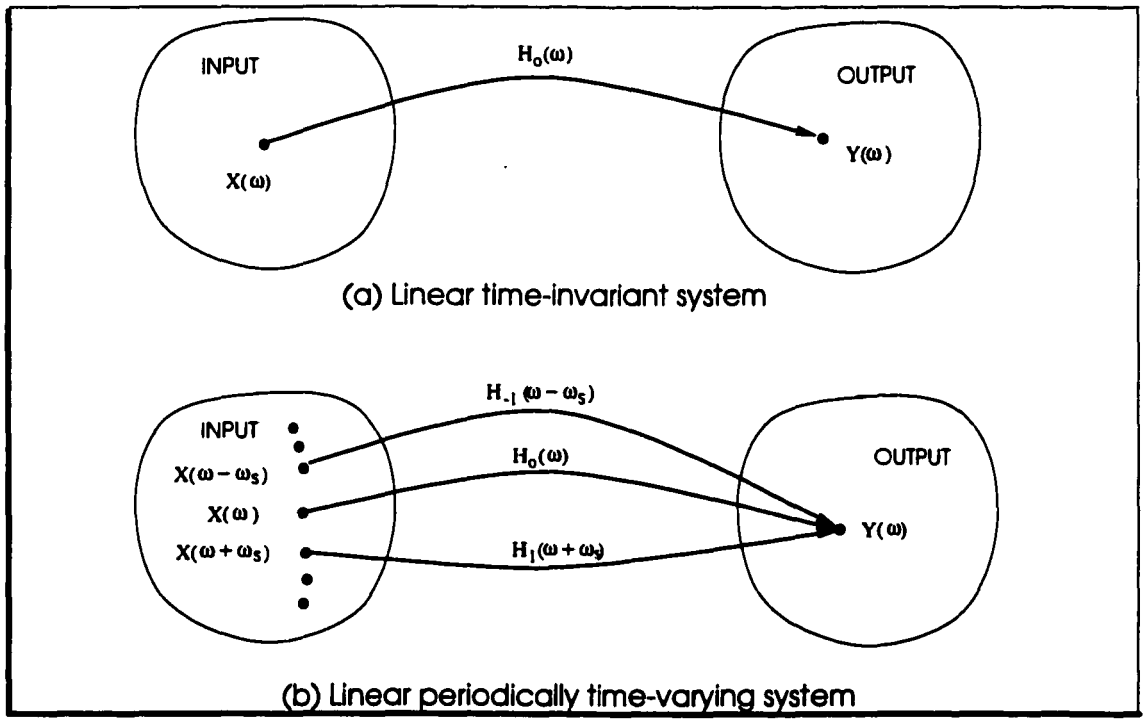


Figure 2.1: Input-output mappings of LTI and LPTV systems

2.3 PSD of LPTV Systems

If the input of a LPTV system $x(t)$ is a stochastic process, then the response of the system $y(t)$ is also a stochastic process. From (2.10), the autocorrelation function of the response is given by [86]

$$\begin{aligned}\mathcal{R}_{yy}(t_1,t_2) &= E[y(t_1)y^*(t_2)] \\ &= \frac{1}{4\pi^2}\int_{-\infty}^{\infty}\int_{-\infty}^{\infty} H(t_1,\omega_1)E[X(\omega_1)X^*(\omega_2)]H^*(t_2,\omega_2)e^{j\omega_1 t_1}e^{-j\omega_2 t_2}d\omega_1 d\omega_2.\end{aligned} \tag{2.18}$$

The 2-dimensional PSD of $x(t)$, denoted by $S_{xx}(\omega_1,\omega_2)$, is defined as the 2-dimensional Fourier transform of the autocorrelation function of $x(t)$ [86]

$$\begin{aligned}S_{xx}(\omega_1,\omega_2) &= \int_{-\infty}^{\infty}\int_{-\infty}^{\infty}\mathcal{R}_{xx}(t_1,t_2)e^{-j\omega_1 t_1}e^{j\omega_2 t_2}dt_1 dt_2 \\ &= \int_{-\infty}^{\infty}\int_{-\infty}^{\infty}E[x(t_1)x^*(t_2)]e^{-j\omega_1 t_1}e^{j\omega_2 t_2}dt_1 dt_2 \\ &= E[X(\omega_1)X^*(\omega_2)]\end{aligned} \tag{2.19}$$

where $X(\omega_1)$ and $X(\omega_2)$ are the Fourier transform of $x(t_1)$ and $x(t_2)$, respectively. Substituting (2.19) into (2.18) gives

$$\mathcal{R}_{yy}(t_1,t_2) = \frac{1}{4\pi^2}\int_{-\infty}^{\infty}\int_{-\infty}^{\infty} H(t_1,\omega_1)S_{xx}(\omega_1,\omega_2)H^*(t_2,\omega_2)e^{j\omega_1 t}e^{-j\omega_2 t_2}d\omega_1 d\omega_2. \tag{2.20}$$

Using (2.11), (2.20) is further simplified to

$$\mathcal{R}_{yy}(t_1,t_2) = \frac{1}{4\pi^2}\sum_{n=-\infty}^{\infty}\sum_{m=-\infty}^{\infty}\int_{-\infty}^{\infty}\int_{-\infty}^{\infty} H_n(\omega_1)S_{xx}(\omega_1,\omega_2)H_m^*(\omega_2)$$

$$e^{j(\omega_1+n\omega_s)t_1}e^{-j(\omega_2+m\omega_s)t_2}d\omega_1 d\omega_2. \tag{2.21}$$

Thus

$$\begin{aligned} S_{yy}(\omega_1,\omega_2) &= \int_{-\infty}^{\infty}\int_{-\infty}^{\infty}\mathcal{R}_{yy}(t_1,t_2)e^{-j\omega_1 t_1}e^{j\omega_2 t_2}dt_1dt_2 \\ &= \frac{1}{4\pi^2}\sum_{n=-\infty}^{\infty}\sum_{m=-\infty}^{\infty}\int_{-\infty}^{\infty}\int_{-\infty}^{\infty}\Bigg[H_n(\Omega_1)S_{xx}(\Omega_1,\Omega_2)H_m^*(\Omega_2) \\ &\quad \int_{-\infty}^{\infty}e^{-j(\omega_1-\Omega_1-n\omega_s)t_1}dt_1\int_{-\infty}^{\infty}e^{j(\omega_2-\Omega_2-m\omega_s)t_2}dt_2\Bigg]d\Omega_1 d\Omega_2. \end{aligned} \tag{2.22}$$

Because

$$\int_{-\infty}^{\infty}f(t)\delta(t-t_o)dt = f(t_o) \tag{2.23}$$

therefore

$$S_{yy}(\omega_1,\omega_2) = \sum_{n=-\infty}^{\infty}\sum_{m=-\infty}^{\infty}H_n(\omega_1-n\omega_s)S_{xx}(\omega_1-n\omega_s,\omega_2-m\omega_s)H_m^*(\omega_2-m\omega_s). \tag{2.24}$$

Eq.(2.24) is valid for general LPTV systems regardless of whether the input is wide-sense stationary or not. If $x(t)$ is wide-sense stationary, then $\mathcal{R}_{xx}(t_1,t_2) = \mathcal{R}_{xx}(t_1-t_2)$. Consequently

$$S_{xx}(\omega_1,\omega_2) = \int_{-\infty}^{\infty}\int_{-\infty}^{\infty}\mathcal{R}_{xx}(t_1-t_2)e^{-j\omega_1 t_1}e^{j\omega_2 t_2}dt_1dt_2. \tag{2.25}$$

Let $t_1 - t_2 = \tau$, then

$$\begin{aligned} \mathcal{S}_{xx}(\omega_1, \omega_2) &= \left[\int_{-\infty}^{\infty} \mathcal{R}_{xx}(\tau) e^{-j\omega_1 \tau} d\tau\right]\left[\int_{-\infty}^{\infty} e^{j(\omega_2 - \omega_1)t_2} dt_2\right] \\ &= 2\pi \mathcal{S}_{xx}(\omega_1)\delta(\omega_2 - \omega_1). \end{aligned} \tag{2.26}$$

Consequently

$$\mathcal{S}_{xx}(\omega_1 - n\omega_s, \omega_2 - m\omega_s) = 2\pi \mathcal{S}_{xx}(\omega_1 - n\omega_s)\delta[\omega_1 - \omega_2 - (n-m)\omega_s]. \tag{2.27}$$

Substituting (2.27) into (2.24) yields

$$\begin{aligned} \mathcal{S}_{yy}(\omega_1, \omega_2) &= 2\pi \sum_{n=-\infty}^{\infty} \sum_{m=-\infty}^{\infty} H_n(\omega_1 - n\omega_s)\mathcal{S}_{xx}(\omega_1 - n\omega_s)H_m^*(\omega_2 - m\omega_s) \\ &\quad \delta[\omega_1 - \omega_2 - (n-m)\omega_s]. \end{aligned} \tag{2.28}$$

The time-varying PSD of the response $\mathcal{S}(t, \omega)$ is obtained by taking the inverse transform of the 2-dimensional PSD $\mathcal{S}_{yy}(\omega_1, \omega_2)$ with respect to the frequency variable corresponding to the excitation time

$$\mathcal{S}_{yy}(t, \omega) = \frac{1}{2\pi} \int_{-\infty}^{\infty} S_{yy}(\Omega, \omega) e^{-j(\Omega - \omega)t} d\Omega. \tag{2.29}$$

Therefore

$$\begin{aligned} \mathcal{S}_{yy}(t, \omega) &= \sum_{n=-\infty}^{\infty} \sum_{m=-\infty}^{\infty} \int_{-\infty}^{\infty} H_n(\Omega - n\omega)\mathcal{S}_{xx}(\Omega - n\omega)H_m^*(\omega - m\omega_s) \\ &\quad \delta[\Omega - \omega - (n-m)\omega_s] e^{-j(\Omega - \omega)t} d\Omega \\ &= \sum_{n=-\infty}^{\infty} \sum_{m=-\infty}^{\infty} H_n(\omega - m\omega_s)\mathcal{S}_{xx}(\omega - m\omega_s)H_m^*(\omega - m\omega_s) e^{j(m-n)\omega_s t}. \end{aligned} \tag{2.30}$$

Define

$$S_{m,n}(\omega) = H_n(\omega - n\omega_s)S_{xx}(\omega - n\omega_s)H_m^*(\omega - m\omega_s) \tag{2.31}$$

then

$$S_{yy}(t,\omega) = \sum_{n=-\infty}^{\infty}\sum_{m=-\infty}^{\infty} S_{m,n}(\omega)e^{j(m-n)\omega_s t}. \tag{2.32}$$

As can be seen that $S_{yy}(\omega,t)$ is periodic in t with period $2\pi/\omega_s$. Fig.2.2 illustrates the sampling of a stationary random input using a sample-and-hold mechanism.

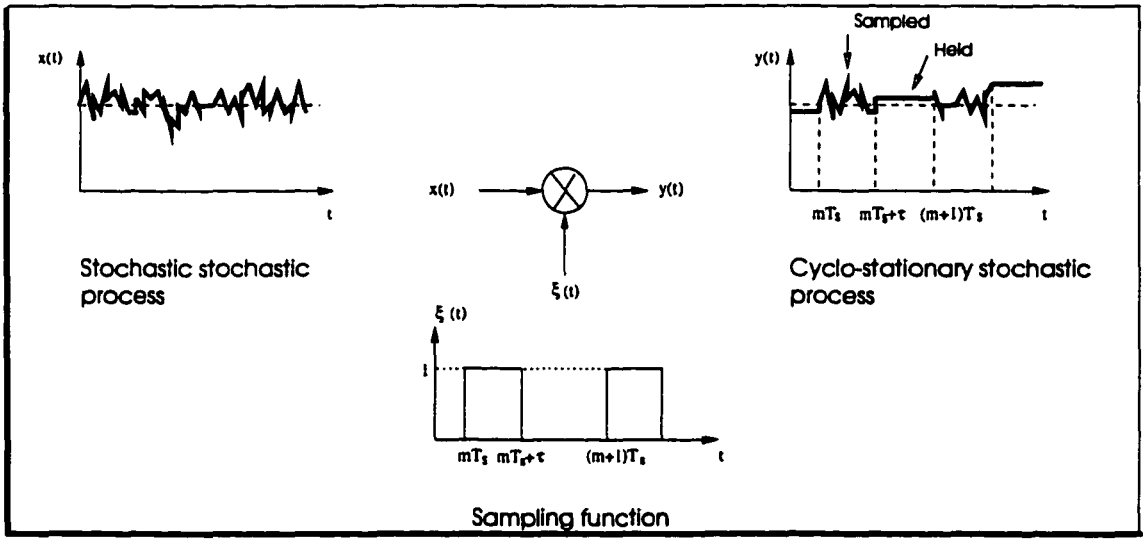


Figure 2.2: Sampling of stationary random signal

The average PSD of the response over a period, denoted by $S_{yy}(\omega)$, is computed from

$$S_{yy}(\omega) = \frac{1}{T_s}\int_0^{T_s} S_{yy}(t,\omega)dt$$

$$= \frac{1}{T_s} \sum_{n=-\infty}^{\infty} \sum_{m=-\infty}^{\infty} \mathcal{S}_{m,n}(\omega) \int_0^{T_s} e^{j(n-m)\omega_s t} dt. \tag{2.33}$$

Because

$$\int_0^{T_s} e^{j(n-m)\omega_s t} dt = \begin{cases} T_s & \text{if } n = m \\ 0 & \text{otherwise} \end{cases} \tag{2.34}$$

we obtain

$$\mathcal{S}_{yy}(\omega) = \sum_{n=-\infty}^{\infty} |H_n(\omega - n\omega_s)|^2 \mathcal{S}_{xx}(\omega - n\omega_s). \tag{2.35}$$

Eq.(2.35) characterizes the PSD of the response of LPTV systems with stationary inputs. Because periodically switched linear circuits are LPTV systems and noise sources encountered in these circuits are stationary, Eq. (2.35) can be used to compute the output noise power of general periodically switched linear circuits. A few comments in regard to (2.35) are made.

(1) If the power spectrum of the input noise is broad-band, Nyquist sampling theorem is violated. As a result, the side band components of the input noise are folded back to the base band. A pictorial illustration is given in Fig.2.3. In this example, the band width of the input noise is $10\omega_s$, the band width of the circuit is assumed to be infinite and the gain is unity. Due to the aliasing effect, the output noise power is 11 times that of the input noise. The power folded over from the side band components of the input noise sources clearly dominates the total output noise power.

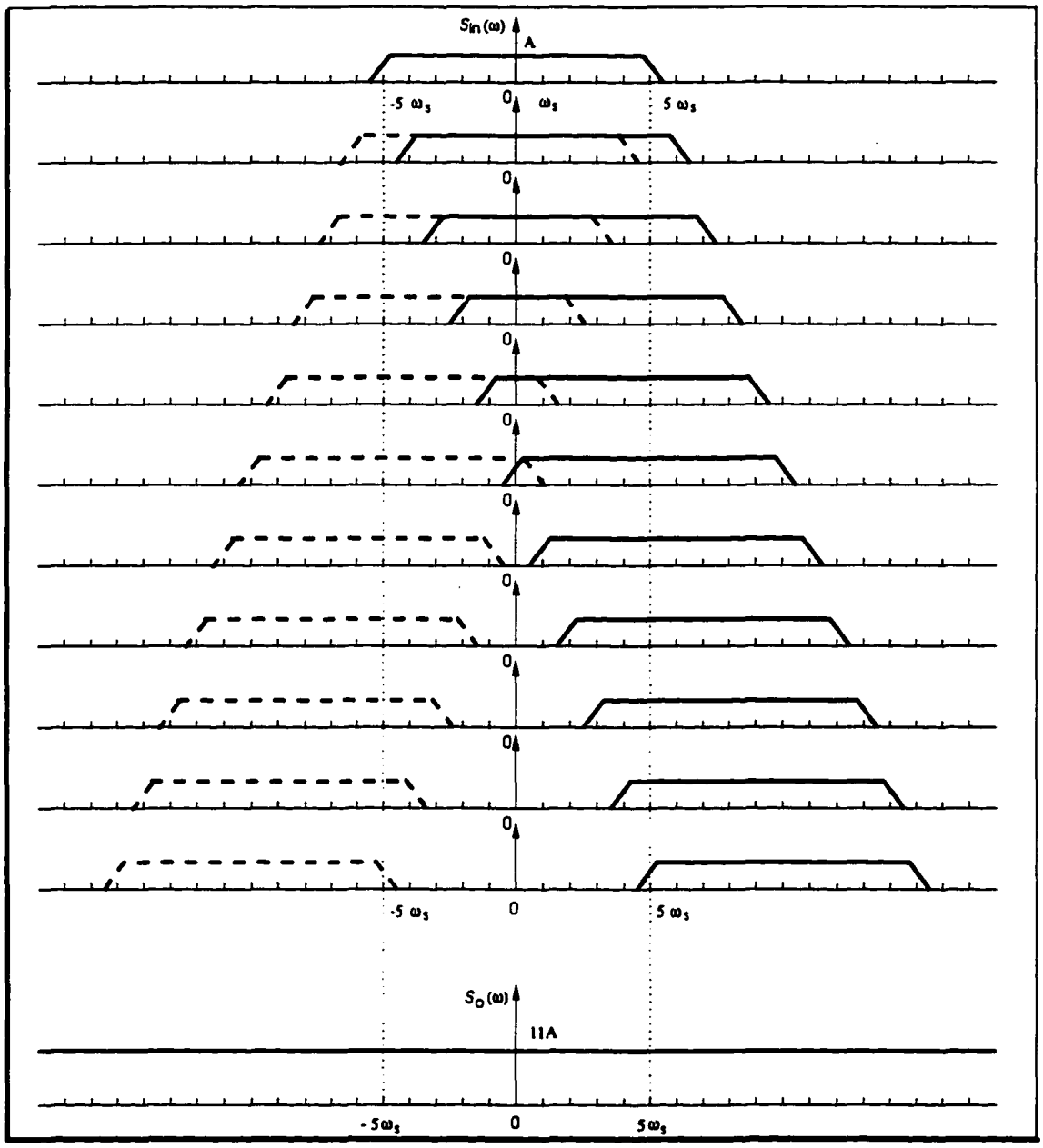


Figure 2.3: Aliasing effect of band-limited noise signals

(2) If there is no switching in the circuits, i.e. $n\equiv 0$, Eq.(2.35) simplifies to the familiar expression for linear time-invariant circuits.

$$S_{ww}(\omega) = |H_o(\omega)|^2 S_{xx}(\omega). \tag{2.36}$$

It is evident that even though the input noise is broad-band, the side band components of the noise signal, however, do not affect the output noise power in the base band.

(3) If there are a total of M uncorrelated noise sources in a linear time-invariant circuit, the output noise power is obtained from

$$S_{yy}(\omega) = \sum_{i=1}^{M} |H_n^{(i)}(\omega)|^2 S_{xx}^{(i)}(\omega) \tag{2.37}$$

where $H_n^{(i)}(\omega)$ is the transfer function from the ith noise source to the output at ω, $S_{xx}^{(i)}(\omega)$ is the PSD of the ith noise source at ω. Eq.(2.37) can also be written as

$$S_{yy}(\omega) = \mathbf{H}^T[S]\mathbf{H}^* \tag{2.38}$$

where $\mathbf{H} = [H_1\ H_2\ ...\ H_M]^T$, $\mathbf{H}^* = [H_1^*\ H_2^*\ ...\ H_M^*]^T$ and $[S] = diag[S_{xx}^{(1)}\ S_{xx}^{(2)}\ ...\ S_{xx}^{(M)}]$. $[S]$ is called the noise matrix [88]. If correlation among the noise sources exists, $[S]$ will contain cross-PSD terms.

If it is a periodically switched linear circuit, then the output noise power is computed from

$$\begin{aligned} S_{yy}(\omega) &= \sum_{i=1}^{M} \sum_{n=-\infty}^{\infty} |H_n^{(i)}(\omega - n\omega_s)|^2 S_{xx}^{(i)}(\omega - n\omega_s) \\ &\approx \sum_{i=1}^{M} \sum_{n=-N}^{N} |H_n^{(i)}(\omega - n\omega_s)|^2 S_{xx}^{(i)}(\omega - n\omega_s) \end{aligned} \tag{2.39}$$

where $|H_{\pm N}^{(i)}(\omega \pm N\omega_s)|^2 S_{xx}^{(i)}(\omega \pm N\omega_s) \ll max\{|H_n^{(i)}(\omega - n\omega_s)|^2 S_{xx}^{(i)}(\omega - n\omega_s), n = 0, \pm 1, ...\}$. It is seen that the computational cost in noise analysis of periodically switched lin-

ear circuits arises from (a) a large number of noise sources and (b) the aliasing effect. Methods that compute the output noise power directly from (2.39) is often referred to as the *Brute-force* method. This is because not only the contribution of each noise source needs to be computed separately, the contribution of every sideband component of the same noise source must also be calculated separately.

2.4 Summary

The PSD of LPTV with stationary input noise sources was derived using the time-varying transfer function and 2-dimensional Fourier transform. It is seen that both the base band and side band components of the input noise sources contribute to the output noise power in the base band. The cost of computation in noise analysis arises due to a large number of noise sources and the aliasing effect. In the next chapter, novel theorems and efficient computational methods will be developed to speed up noise analysis.

Chapter 3

Adjoint Network of PSL Circuits

This chapter presents the theory of the adjoint network of periodically switched linear circuits [91]. The application of the theory to noise, sensitivity, and distortion analyses of switched circuits will be given in chapters that follow. In Section 3.1, we introduce the network variable theorem of PSL circuits. Tellegen's theorem for PSL circuits in phasor domain is developed in Section 3.2. In Sections 3.4 and 3.5, frequency reversal theorem and transfer function theorem are derived. The relationship between the original PSL circuit and its adjoint network is investigated in Section 3.6. The theory is assessed in Section 3.7 with the help of numerical examples. Finally, the chapter is summarized in Section 3.8.

3.1 Network Variable Theorem

It was shown in Chapter 2, the characteristics of a linear time-varying system are described by the impulse response $h(t,\tau)$ and the time-varying transfer function $H(t,\omega)$ of the system. If the input of the system is an exponential function of time,

then

$$x(t) = e^{j\omega_o t} \tag{3.1}$$

where ω_o is the frequency of the input, because $X(\omega) = 2\pi\delta(\omega - w_o)$, using (2.10), we obtain the response of the system

$$y(t) = H(t, \omega_o)e^{j\omega_o t}. \tag{3.2}$$

If the system is further LPTV then $H(t, \omega_o)$ can be represented in the Fourier series given in (2.11) with ω replaced by ω_o. Substituting the corresponding results into (3.2) gives

$$y(t) = \sum_{n=-\infty}^{\infty} H_n e^{j(\omega_o + n\omega_s)t} \tag{3.3}$$

where H_n is the coefficient of the Fourier series given by (2.12). The above result reveals that the response of the LPTV system contains an infinite number of frequency components even though its input is a single tone. Also, H_n specifies the magnitude of $y(t)$ at frequency $\omega_o + n\omega_s$ in the complex plane. It is the phasor representation of $y(t)$ at $\omega_o + n\omega_s$. Eq. (3.3) establishes the relationship between the time and frequency domain quantities of the network variable. The application of the above result to PSL circuits leads to the following theorem

Theorem 3.1 (Network Variable Theorem of PSL Circuits) *In steady-state, the network variables of a PSL circuit with clock frequency ω_s and input $e^{j\omega_o t}$ contain an infinite number of frequency components. They can be represented by the Fourier series*

$$v_b(t) = \sum_{n=-\infty}^{\infty} V_b(\omega_o + n\omega_s)e^{j(\omega_o + n\omega_s)t} \tag{3.4}$$

where $V_b(\omega_o + n\omega_s)$ is the phasor of $v_b(t)$ at $\omega_o + n\omega_s$.

Corollary 3.1.1 *The network variable of a PSL circuit, $v_b(t)$, satisfies $v_b(t) = 0\ \forall t$ if and only if $V_b(\omega_o + n\omega_s) = 0\ \forall n$.*

3.2 Tellegen's Theorem for PSL Circuits in Phasor Domain

Tellegen's theorem, introduced by B. Tellegen almost half a century ago is a fundamental law for lumped electrical networks [43]. It has found applications in many areas of electrical engineering [92,93]. Tellegen's theorem is based on Kirchoff's current law (KCL) and voltage law (KVL) for lumped LTI circuits. In time-domain, it is given by

$$\sum_{b=1}^{B} v_b(t) i_b(t) = 0 \tag{3.5}$$

where $v_b(t)$ and $i_b(t)$ denote the branch voltages and currents of the LTI circuit, respectively. B is the number of branches in the circuit. Eq.(3.5) also holds for any two LTI circuits $\mathcal{N}$ and $\hat{\mathcal{N}}$ having the same topology

$$\sum_{b=1}^{B} v_b(t) \hat{i}_b(\tau) = 0, \qquad \sum_{b=1}^{B} i_b(t) \hat{v}_b(\tau) = 0 \tag{3.6}$$

where $\hat{i}_b(\tau)$ and $\hat{v}_b(\tau)$ denote respectively the branch currents and voltages of $\hat{\mathcal{N}}$, t and τ are the time variables of $\mathcal{N}$ and $\hat{\mathcal{N}}$, respectively.

PSL circuits differ from LTI networks by including externally clocked switches. A switch is modeled as either a short or open circuits, depending upon the state of the switch. The topology of the circuits remains unchanged during switching. For

a given PSL circuit $\mathcal{N}$, we can construct another network $\hat{\mathcal{N}}$ of the same topology as that of $\mathcal{N}$ irrespective of switching. As a result, Eqs.(3.6) also hold for PSL circuits. Subtracting the equations in (3.6) yields

$$\sum_{b=1}^{B}\Big[v_b(t)\hat{i}_b(\tau) - i_b(t)\hat{v}_b(\tau)\Big] = 0. \tag{3.7}$$

Eqs.(3.6) and (3.7) are respectively the *strong* and *weak* forms of Tellegen's theorem for PSL circuits in time domain. The weak form of Tellegen's theorem incorporates the branch voltages and currents of $\mathcal{N}$ and $\hat{\mathcal{N}}$. It is of particular usefulness in characterizing the relationship between $\mathcal{N}$ and $\hat{\mathcal{N}}$.

As is well known, in AC steady state, LTI circuits can be analyzed conveniently in phasor domain. Consequently, Tellegen's theorem for LTI circuits also holds in phasor domain and is given by [25]

$$\sum_{b=1}^{B}\Big[V_b(j\omega)\hat{I}_b(j\omega) - I_b(j\omega)\hat{V}_b(j\omega)\Big] = 0 \tag{3.8}$$

where $V_b(j\omega)$ and $I_b(j\omega)$, $\hat{V}_b(j\omega)$ and $\hat{I}_b(j\omega)$ are the voltages and currents of the $v_b(t)$ and $i_b(t)$, $\hat{v}_b(\tau)$ and $\hat{i}_b(\tau)$, respectively. Recall that Theorem 3.1 establishes a bridge between the time and phasor domain quantities of PSL circuits. To find out the relationship between the phasors of the network variables of two distinct PSL circuits $\mathcal{N}$ and $\hat{\mathcal{N}}$ having the same topology, let the clock frequency of $\hat{\mathcal{N}}$ be identical to that of $\mathcal{N}$. Representing each variable in (3.7) using (3.4)

$$\sum_{b=1}^{B}\sum_{n=-\infty}^{\infty}\sum_{m=-\infty}^{\infty}\Big[V_b(\omega_o+n\omega_s)\hat{I}_b(\omega_o+m\omega_s) - I_b(\omega_o+n\omega_s)\hat{V}_b(\omega_o+m\omega_s)\Big]$$
$$e^{j\omega_o(t+\tau)}e^{j\omega_s(nt+m\tau)} = 0 \tag{3.9}$$

where $V_b(\omega_o + n\omega_s)$ and $I_b(\omega_o + n\omega_s)$ are respectively the phasors of $v_b(t)$ and $i_b(t)$ at $\omega_o + n\omega_s$, $\hat{V}_b(\omega_o + m\omega_s)$ and $\hat{I}_b(\omega_o + m\omega_s)$ are the phasors of $\hat{v}_b(\tau)$ and $\hat{i}_b(\tau)$ at $\omega_o + m\omega_s$, respectively. Note in (3.9), there are two time variables, namely, t and τ. To extract the relationship between the phasors of the network variables of $\mathcal{N}$ and $\hat{\mathcal{N}}$ from (3.9), we first eliminate τ by imposing the constraint

$$t + \tau = 0 \tag{3.10}$$

on $\hat{\mathcal{N}}$ and then integrate (3.9) with respect to t from 0 to T_s

$$\sum_{b=1}^{B} \sum_{n=-\infty}^{\infty} \sum_{m=-\infty}^{\infty} \left[V_b(\omega_o + n\omega_s)\hat{I}_b(\omega_o + m\omega_s) - I_b(\omega_o + n\omega_s)\hat{V}_b(\omega_o + m\omega_s) \right] \int_0^{T_s} e^{j\omega_s(n-m)t} dt = 0. \tag{3.11}$$

Using the results of (2.34), we obtain

$$\sum_{b=1}^{B} \sum_{n=-\infty}^{\infty} \left[V_b(\omega_o + n\omega_s)\hat{I}_b(\omega_o + n\omega_s) - I_b(\omega_o + n\omega_s)\hat{V}_b(\omega_o + n\omega_s) \right] = 0. \tag{3.12}$$

Following the similar procedures, it can also be shown that

$$\begin{aligned} \sum_{b=1}^{B} \sum_{n=-\infty}^{\infty} V_b(\omega_o + n\omega_s)\hat{I}_b(\omega_o + n\omega_s) &= 0 \\ \sum_{b=1}^{B} \sum_{n=-\infty}^{\infty} I_b(\omega_o + n\omega_s)\hat{V}_b(\omega_o + n\omega_s) &= 0 \end{aligned} \tag{3.13}$$

Eq.(3.12) bears a resemblance to (3.8). It incorporates the phasors of $\mathcal{N}$ and $\hat{\mathcal{N}}$ in a single notation.

Theorem 3.2 (Tellegen's Theorem for PSL Circuits in Phasor Domain) *In steady state, for a given lumped PSL circuit, there exists another lumped PSL circuit having the same topology, switching frequency, and reversed time. The weak and strong forms of Tellegen's theorem in phasor domain are given by (3.12) and (3.13), respectively.*

A few comments are made prior to further development. (a) The phasors of the branch voltages and currents of both $\mathcal{N}$ and $\hat{\mathcal{N}}$ in (3.12) and (3.13) are evaluated at the same frequency. Its necessity will become evident when we derive the adjoint network of PSL circuits in the next section. (b) The constraint imposed on the time variable τ of $\hat{\mathcal{N}}$ in (3.10) reveals that the time of $\hat{\mathcal{N}}$ proceeds in the reverse direction, as compared with that of $\mathcal{N}$. Consequently, the switching clock sequence of $\hat{\mathcal{N}}$ is also reversed. To be specific, consider a PSL circuit with five non-overlapping clock phases shown in Fig.3.1. The width of the kth phase is denoted by τ_k. In addition, σ_k is defined as

$$\sigma_k = \sum_{j=1}^{k} \tau_j \qquad\qquad k = 1, 2, ..., 5. \tag{3.14}$$

By definition, $\sigma_o = 0$ and $\sigma_5 = T_s$. The width of each clock phase of $\hat{\mathcal{N}}$ equals to that of the corresponding phase of $\mathcal{N}$.

(c) The difference between Tellegen's theorems for PSL and LTI circuits is the extra summation over n for PSL circuits. This summation represents a fundamental characteristic of PSL circuits. Also note if $n \equiv 0$, Eq.(3.12) simplies to Tellegen's theorem for LTI circuits in phasor domain.

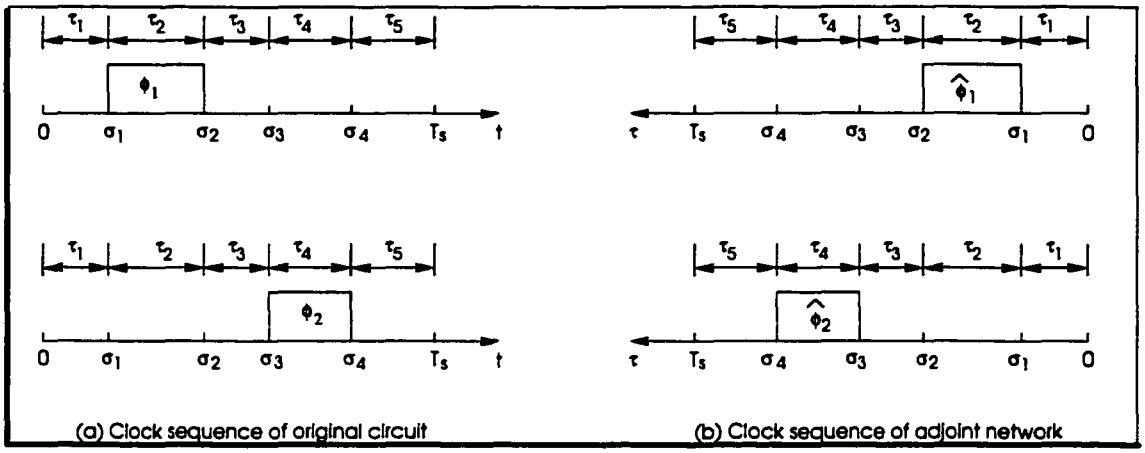


Figure 3.1: Time reversal of adjoint network

3.3 Adjoint Network of PSL Circuits

3.3.1 Interreciprocity and Adjoint Network

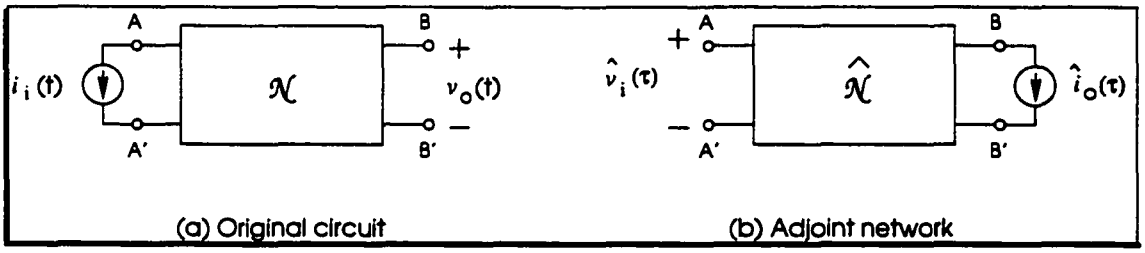


Figure 3.2: Configuration of LTI circuit and its adjoint network

The adjoint network of LTI circuits is based on the concept of interreciprocity [25, 94, 95]. In AC steady state, the interreciprocity of LTI circuits can also be defined in phasor domain. Consider two LTI network $\mathcal{N}$ and $\hat{\mathcal{N}}$ shown in Fig. 3.2. $\hat{\mathcal{N}}$ is said to be interreciprocal to $\mathcal{N}$ if for $I_i(j\omega) = \hat{I}_o(j\omega)$, we have $V_o(j\omega) = \hat{V}_i(j\omega)$. It was shown in [25] that if each element in $\mathcal{N}$ and its counterpart in $\hat{\mathcal{N}}$ satisfy

$$V_b(j\omega)\hat{I}_b(j\omega) - I_b(j\omega)\hat{V}_b(j\omega) = 0 \tag{3.15}$$

then $\mathcal{N}$ and $\hat{\mathcal{N}}$ are interreciprocal to each other. It can be shown that two interreciprocal LTI circuits satisfy Tellegen's theorem [25]. However, two LTI circuits satisfying Tellegen's theorem might not be interreciprocal. Tellegen's theorem is not a sufficient but rather a necessary condition of interreciprocity.

In the preceding section, it was shown that if two PSL circuits $\hat{\mathcal{N}}$ and $\mathcal{N}$ have the same topology, clock frequency, and their time variables are related via (3.10), then they satisfy (3.12). We now determine both the type and value of the elements of $\hat{\mathcal{N}}$ by further imposing the constraint of interreciprocity. Analogous to LTI circuits, for each element in $\hat{\mathcal{N}}$ and its counterpart in $\mathcal{N}$, we impose

$$\sum_{n=-\infty}^{\infty} \left[V_b(\omega_o + n\omega_s)\hat{I}_b(\omega_o + n\omega_s) - I_b(\omega_o + n\omega_s)\hat{V}_b(\omega_o + n\omega_s) \right] = 0 \qquad (3.16)$$

or equivalently

$$v_b(t)\hat{i}_b(\tau) - i_b(t)\hat{v}_b(\tau) = 0. \qquad (3.17)$$

Note (3.17) must be satisfied for $t, \tau \in (-\infty, \infty)$. This is because (3.16) was derived using Fourier transform. For multi-branch elements, such as controlled sources, the network variables of all the branches of the elements must be included in evaluating (3.16) or (3.17). Elements that satisfy (3.16) or (3.17) are said to be *interreciprocal.* The network $\hat{\mathcal{N}}$ constructed in this way is called the *adjoint network* of $\mathcal{N}$. Clearly, $\mathcal{N}$ and $\hat{\mathcal{N}}$ satisfy the Tellegen's theorem. The adjoint network constructed in this way manifests its advantages in deriving the aliasing transfer function of $\mathcal{N}$, as will be seen shortly.

Since the aliasing transfer functions of a PSL circuit is only concerned with the inputs and outputs of the circuit, it is advantageous to partition the branches of the circuit into (a) the internal branches associated with all interreciprocal elements and (b) the input/output branches. Substituting (3.16) into (3.12) for all internal

branches results in

$$\sum_{b=1}^{B_1} \left[v_b(t)\hat{i}_b(\tau) - i_b(t)\hat{v}_b(\tau) \right] = 0 \tag{3.18}$$

where B_1 is the number of input/output branches in the circuit. In the following subsections, we derive the adjoint networks of PSL circuits.

3.3.2 Ideal Switches

Ideal switches are essential components of PSL circuits. An ideal switch has, at most, two distinct states : OPEN and CLOSED, depending upon the clock signal. In the OPEN state, the current through the switch is zero and the voltage across the switch is determined by the rest of the circuit. An OPEN switch is characterized by $i_b(t) = 0$ and $v_b(t) = \textit{arbitrary}$. Substituting these conditions into (3.17), we obtain $\hat{i}_b(\tau) = 0$. So the counterpart of an OPEN switch in $\mathcal{N}$ is also an OPEN switch in $\hat{\mathcal{N}}$. In the CLOSED state, the switch is characterized by $v_b(t) = 0$ and $i_b(t) = \textit{arbitrary}$. Substituting these conditions into (3.17) yields $\hat{v}_b(\tau) = 0$. The counterpart of a CLOSED switch in $\mathcal{N}$ is a also CLOSED switch in $\hat{\mathcal{N}}$. We conclude that an OPEN/CLOSED ideal switch in $\mathcal{N}$ maps to an OPEN/CLOSED ideal switch in $\hat{\mathcal{N}}$.

3.3.3 LTI Resistors

The phasors of the voltage and current of a LTI resistor in a PSL circuit are related to each other by $V_R(\omega_o + n\omega_s) = RI_R(\omega_o + n\omega_s), \forall n$, where R is the resistance of

the resistor. Substituting this relationship into (3.16) for a specific n, we obtain

$$I_R(\omega_o + n\omega_s)\left[\hat{V}_R(\omega_o + n\omega_s) - R\hat{I}_R(\omega_o + n\omega_s)\right] = 0 \tag{3.19}$$

where $\hat{V}_R(\omega_o + n\omega_s)$ and $\hat{I}_R(\omega_o + n\omega_s)$ are the phasors of the voltage and current of the counterpart of the resistor in $\hat{\mathcal{N}}$, respectively. To have (3.19) hold for arbitrary $I_R(\omega_o + n\omega_s)$, clearly

$$\hat{V}_R(\omega_o + n\omega_s) = R\hat{I}_R(\omega_o + n\omega_s) \tag{3.20}$$

The element characterized by (3.20) is a LTI resistor. We conclude that the counterpart of a LTI resistor in $\mathcal{N}$ is also a LTI resistor in $\hat{\mathcal{N}}$ of the same resistance.

3.3.4 LTI Capacitors and Inductors

Consider a LTI capacitor in a PSL circuit. Representing the voltage and current of the capacitor using (3.4) and substituting them into the constitutive equation of the capacitor give

$$\sum_{n=-\infty}^{\infty} I_C(\omega_o + n\omega_s)e^{j(\omega_o+n\omega_s)t} = \sum_{n=-\infty}^{\infty} j(\omega_o + n\omega_s)CV_C(\omega_o + n\omega_s)e^{j(\omega_o+n\omega_s)t} \tag{3.21}$$

Using the identity of orthogonality of exponential series, we obtain

$$I_C(\omega_o + n\omega_s) = j(\omega_o + n\omega_s)CV_C(\omega_o + n\omega_s) \qquad \forall n. \tag{3.22}$$

Eq.(3.22) is the phasor-domain representation of the constitutive equation of LTI capacitor in PSL circuits. Clearly, if $n\equiv 0$, it becomes the phasor domain relation of

capacitors in LTI circuits. Substituting the voltages and currents of the capacitor into (3.16) for a specific n, we obtain

$$V_C(\omega_o + n\omega_s)\Big[\hat{I}_C(\omega_o + n\omega_s) - j(\omega_o + n\omega_s)C\hat{V}_C(\omega_o + n\omega_s)\Big] = 0. \tag{3.23}$$

To validate (3.23) for arbitrary $V_C(\omega_o + n\omega_s)$, the following must be true

$$\hat{I}_C(\omega_o + n\omega_s) - j(\omega_o + n\omega_s)C\hat{V}_C(\omega_o + n\omega_s) = 0 \tag{3.24}$$

Elements characterized by (3.24) are LTI capacitors. We conclude that the counterpart of a LTI capacitor in $\mathcal{N}$ is a LTI capacitor of the same capacitance in $\hat{\mathcal{N}}$. In a very like manner, one can also show that a LTI inductor in $\mathcal{N}$ maps to a LTI inductor of the same inductance in $\hat{\mathcal{N}}$.

3.3.5 Controlled Sources

Consider a voltage-controlled voltage source (VCVS) with voltage gain a. Let the network variables of the controlling branch of the VCVS be identified with the subscript "1" and those of the controlled branch with "2". Because $i_1(t) = 0, v_2(t) = gv_1(t)\forall t$, using Corollary 3.1.1, we have, $I_1(\omega_o + n\omega_s) = 0$, $V_2(\omega_o + n\omega_s) = aV_1(\omega_o + n\omega_s)\ \forall n$. Substituting these variables into (3.16) for a specific n gives

$$V_1(\omega_o + n\omega_s)\Big[\hat{I}_1(\omega_o + n\omega_s) + a\hat{I}_2(\omega_o + n\omega_s)\Big] - I_2(\omega_o + n\omega_s)\hat{V}_2(\omega_o + n\omega_s) = 0. \tag{3.25}$$

To have (3.25) hold for arbitrary $V_1(\omega_o + n\omega_s)$ and $I_2(\omega_o + n\omega_s)$, we set

$$\begin{cases} \hat{V}_2(\omega_o + n\omega_s) = 0 \\ \hat{I}_1(\omega_o + n\omega_s) = -a\hat{I}_2(\omega_o + n\omega_s) \end{cases}. \tag{3.26}$$

The element characterized by (3.26) is a current-controlled current source (CCCS). The controlling and controlled branches of the CCCS are interchanged as compared with those of the VCVS. The current gain of the CCCS has the same magnitude as that of the voltage gain of the VCVS but the opposite sign. The counterparts of other controlled sources in the adjoint network were also derived in a similar manner and the results are given in Fig 3.3.

3.3.6 Operational Amplifiers

Operational amplifiers are building blocks of PSL circuits. They are usually modeled using either single-pole or multi-pole macro models, depending upon the speed and accuracy of simulation [39,96]. These macro models are essentially LTI circuits consisting of resistors, capacitors and controlled sources. Their adjoint networks are constructed element by element. Fig.3.3 summarizes the elements that are often encountered in PSL circuits and their counterparts in the adjoint network.

3.3.7 Complex Devices

The adjoint networks of complex devices, such as BJTs and MOSFETs, are obtained by first replacing these devices with appropriate equivalent circuits and then finding out the adjoint networks of these equivalent circuits.

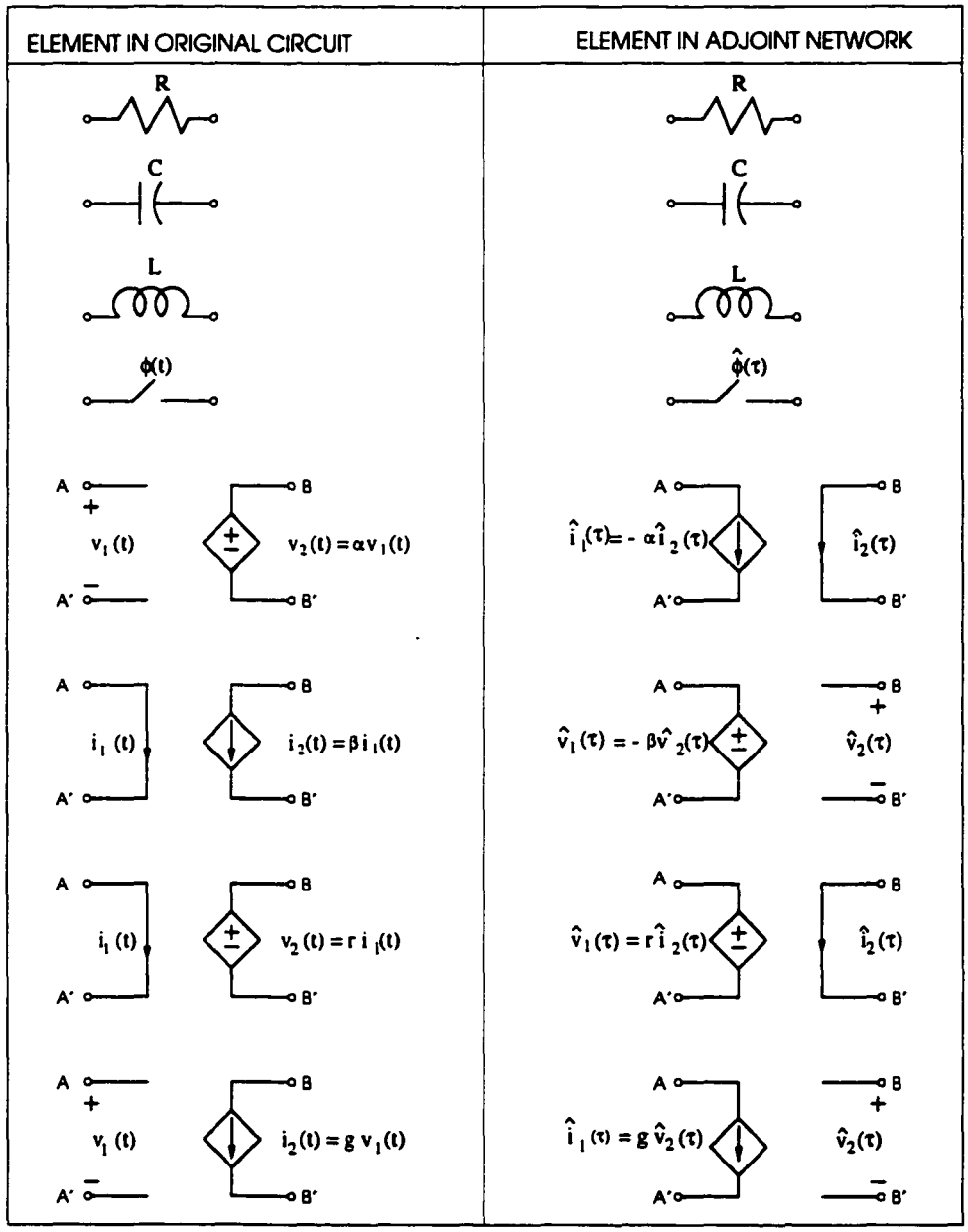


Figure 3.3: Elements and their counterparts in the adjoint network

3.4 Frequency Reversal Theorem

In this section, we make use of the characteristics of PSL circuits and the corresponding adjoint networks to develop a novel theorem. Further, we will show

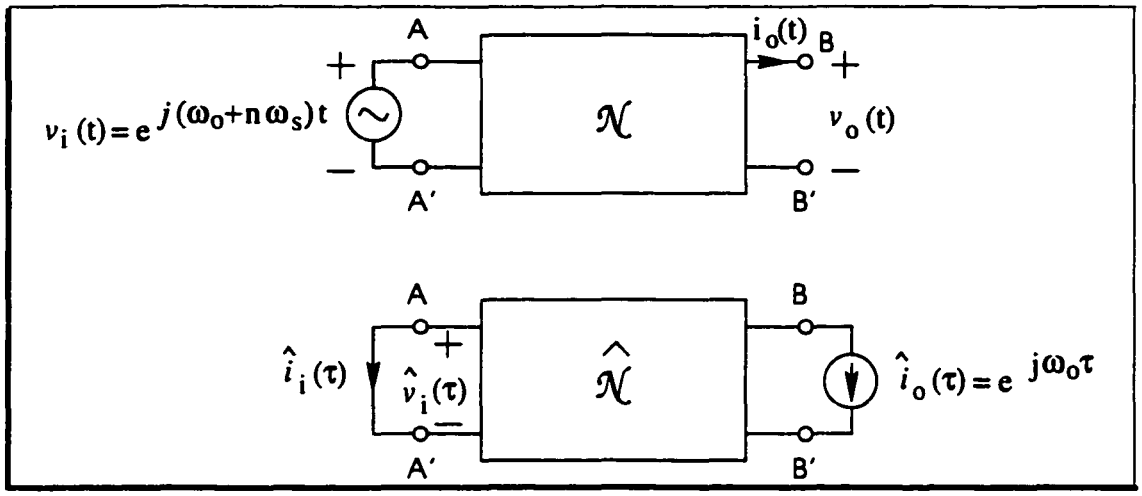


Figure 3.4: Frequency reversal theorem

that the computational cost of the noise analysis of PSL circuits can be reduced dramatically by making use of the theorem.

Consider a single-input single-output (SISO) PSL circuit $\mathcal{N}$ shown in Fig. 3.4. Its adjoint network is also shown in the figure. Eq. (3.18) can be written as

$$\left[v_o(t)\hat{i}_o(\tau) - i_o(t)\hat{v}_o(\tau)\right] + \left[v_i(t)\hat{i}_i(\tau) - i_i(t)\hat{v}_i(\tau)\right] = 0 \tag{3.27}$$

where the subscripts o and i identify the network variables of the output and input branches, respectively. Because $i_o(t) = 0, \forall t$ and $\hat{v}_i(\tau) = 0, \forall \tau$

$$v_o(t)\hat{i}_o(\tau) + v_i(t)\hat{i}_i(\tau) = 0 \tag{3.28}$$

Representing the responses of $\mathcal{N}$ and $\hat{\mathcal{N}}$ using (3.2), substituting the inputs of $\mathcal{N}$ and $\hat{\mathcal{N}}$ into (3.28), and making use of the time reversal characteristic of $\hat{\mathcal{N}}$, we

obtain

$$H(t, \omega_o + n\omega_s) + \hat{H}(-t, \omega_o) = 0. \tag{3.29}$$

Note $H(t, \omega_o + n\omega_s)$ and $\hat{H}(-t, \omega_o)$ contain an infinite number of frequency components due to their periodicity in t. To find out the relationship between the response of $\mathcal{N}$ at ω_o and that of $\hat{\mathcal{N}}$ at $\omega_o + n\omega_s$, we have noticed that the bi-frequency transfer function of linear time-varying systems introduced by Zadeh [89] incorporates the input and output of the systems at different frequencies in a single notation. The bi-frequency transfer function is defined as

$$\mathcal{H}(\Omega, \omega) = \int_{-\infty}^{\infty} H(t, \omega) e^{-j(\Omega - \omega)t} dt \tag{3.30}$$

where Ω and ω are the output and input frequencies of the system, respectively. It is easy to verify that $\mathcal{H}(\Omega, \omega)$ is the 2-dimensional Fourier transform of $h(t, \tau)$. The time-varying transfer function is obtained from the bi-frequency transfer function through the inverse transform

$$H(t, \omega) = \frac{1}{2\pi} \int_{-\infty}^{\infty} \mathcal{H}(\Omega, \omega) e^{j(\Omega - \omega)t} d\Omega \tag{3.31}$$

It can be shown that the Fourier transform of the output of the system is computed from

$$Y(\Omega) = \frac{1}{2\pi} \int_{-\infty}^{\infty} \mathcal{H}(\Omega, \omega) X(\omega) d\omega. \tag{3.32}$$

Eq.(3.32) establishes the frequency-domain relationship between the output $y(t)$ at frequency Ω and the input $x(t)$ at frequency ω of linear time-varying systems.

Its counterpart in the time-domain is given by (2.7). A graphical representation is given in Fig.3.5. Because

$$V_i(\omega) = \mathcal{F}[v_i(t)] = 2\pi\delta(\omega - \omega_o - n\omega_s) \tag{3.33}$$

where $\mathcal{F}[.]$ denotes taking Fourier transform. Making use of (3.32), we obtain the output of $\mathcal{N}$ at ω_o

$$V_o(\omega_o) = \frac{1}{2\pi}\int_{-\infty}^{\infty} \mathcal{H}_{VV}(\omega_o, \omega)V_i(\omega)d\omega = \mathcal{H}_{VV}(\omega_o, \omega_o + n\omega_s). \tag{3.34}$$

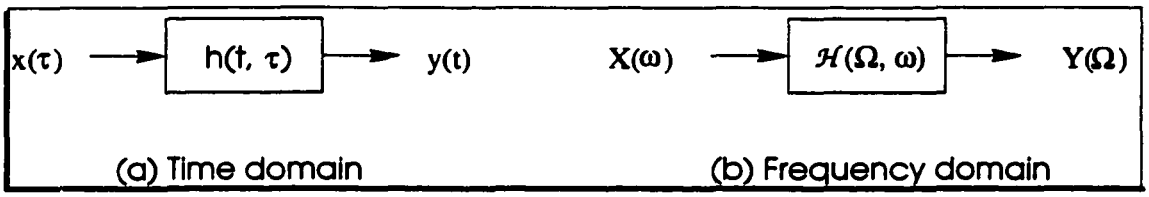


Figure 3.5: Impulse response and transfer function of linear time-varying system

where $\mathcal{H}_{VV}(\omega_o, \omega_o + n\omega_s)$ is the aliasing transfer function from the voltage input at $\omega_o + n\omega_s$ to the voltage output at ω_o. Further representing $\mathcal{H}(\omega_o, \omega_o + n\omega_s)$ in (3.34) using (3.30) gives

$$V_o(\omega_o) = \int_{-\infty}^{\infty} H(t, \omega_o + n\omega_s)e^{jn\omega_s t}dt. \tag{3.35}$$

Similarly, since

$$\hat{I}_o(\omega) = \mathcal{F}[\hat{i}_o(\tau)] = 2\pi\delta(\omega - \omega_o). \tag{3.36}$$

therefore

$$\hat{I}_i(\omega_o + n\omega_s) = \frac{1}{2\pi}\int_{-\infty}^{\infty} \hat{\mathcal{H}}_{II}(\omega_o + n\omega_s, \omega)\hat{I}_o(\omega)d\omega = \hat{\mathcal{H}}_{II}(\omega_o + n\omega_s, \omega_o). \quad (3.37)$$

where $\mathcal{H}_{II}(\omega_o + n\omega_s, \omega_o)$ denotes the aliasing transfer function from the current input at ω_o to the current output at $\omega_o + n\omega_s$. Using (3.30) and the time reversal characteristic of $\hat{\mathcal{N}}$, we can further simplify (3.37) as

$$\hat{I}_i(\omega_o + n\omega_s) = \int_{-\infty}^{\infty} \hat{H}(-t, \omega_o)e^{jn\omega_s t}dt. \quad (3.38)$$

Summing up (3.38) and (3.35) and making use of (3.29) yield

$$V_o(\omega_o) = -\hat{I}_i(\omega_o + n\omega_s). \quad (3.39)$$

Consequently

$$\mathcal{H}_{VV}(\omega_o, \omega_o + n\omega_s) = -\hat{\mathcal{H}}_{II}(\omega_o + n\omega_s, \omega_o). \quad (3.40)$$

Eq.(3.40) reveals that the magnitude of the aliasing transfer function of $\mathcal{N}$ from the input at $\omega_o + n\omega_s$ to the output at ω_o is equal to that of $\hat{\mathcal{N}}$ from the input at ω_o to the output at $\omega_o + n\omega_s$. Similar results were also obtained for circuits with other input/output configurations and are tabulated in Table 3.1. The variables in the table are defined graphically in Fig. 3.2. These relationships are fundamental characteristics of PSL circuits. Although the above derivation was done for SISO circuits, it can readily be extended to multiple-input single-output (MISO) circuits.

Theorem 3.3 (Frequency Reversal Theorem of PSL Circuits) *The magnitude of the aliasing transfer functions from multiple inputs at frequency* $\omega_o + n\omega_s$

Table 3.1: Frequency reversal theorem

Original		Adjoint		Aliasing
Input	Output	Input	Output	transfer function
$i_i(t) = e^{j(\omega_o+n\omega_s)t}$	$v_o(t)$	$\hat{i}_o(\tau) = e^{j\omega_o\tau}$	$\hat{v}_i(\tau)$	$V_o(\omega_o) = \hat{V}_i(\omega_o + n\omega_s)$
$v_i(t) = e^{j(\omega_o+n\omega_s)t}$	$v_o(t)$	$\hat{i}_o(\tau) = e^{j\omega_o\tau}$	$\hat{i}_i(\tau)$	$V_o(\omega_o) = -\hat{I}_i(\omega_o + n\omega_s)$
$i_i(t) = e^{j(\omega_o+n\omega_s)t}$	$i_o(t)$	$\hat{v}_o(\tau) = e^{j\omega_o\tau}$	$\hat{v}_i(\tau)$	$I_o(\omega_o) = -\hat{V}_i(\omega_o + n\omega_s)$
$v_i(t) = e^{j(\omega_o+n\omega_s)t}$	$i_o(t)$	$\hat{v}_o(\tau) = e^{j\omega_o\tau}$	$\hat{i}_i(\tau)$	$I_o(\omega_o) = \hat{I}_i(\omega_o + n\omega_s)$

to the single output at frequency ω_o of a PSL circuit is equal to that of the aliasing transfer functions of the adjoint network from the single input at ω_o to the multiple output at $\omega_o + n\omega_s$.

The significance of the frequency reversal theorem consists in the fact that the computation of the aliasing transfer functions from inputs at $\omega_o + n\omega_s$ to the output at ω_o of $\mathcal{N}$ requires solving the circuit at multiple frequencies $\omega_o + n\omega_s, n = 0, \pm1, \pm2, ...$, which requires repetitive numerical integration of the circuit equations. This amounts to an excessive amount of computation. With the frequency reversal theorem, these aliasing transfer functions can be obtained by solving the adjoint network $\hat{\mathcal{N}}$ at ω_o only. A significant reduction in CPU time is achieved. The frequency reversal theorem was not known before. It is one of the contributions of this research.

The frequency reversal theorem is visualized in Fig.3.6. The upper portion of the diagram illustrates the aliasing transfer functions from the input at multiple input frequencies $\omega_o + n\omega_s$, $n = 0, \pm1, \ldots$, to the output at a single frequency ω_o of $\mathcal{N}$ whereas the lower portion depicts those of $\hat{\mathcal{N}}$ from the input at the single frequency ω_o to the output at multiple frequencies $\omega_o + n\omega_s$.

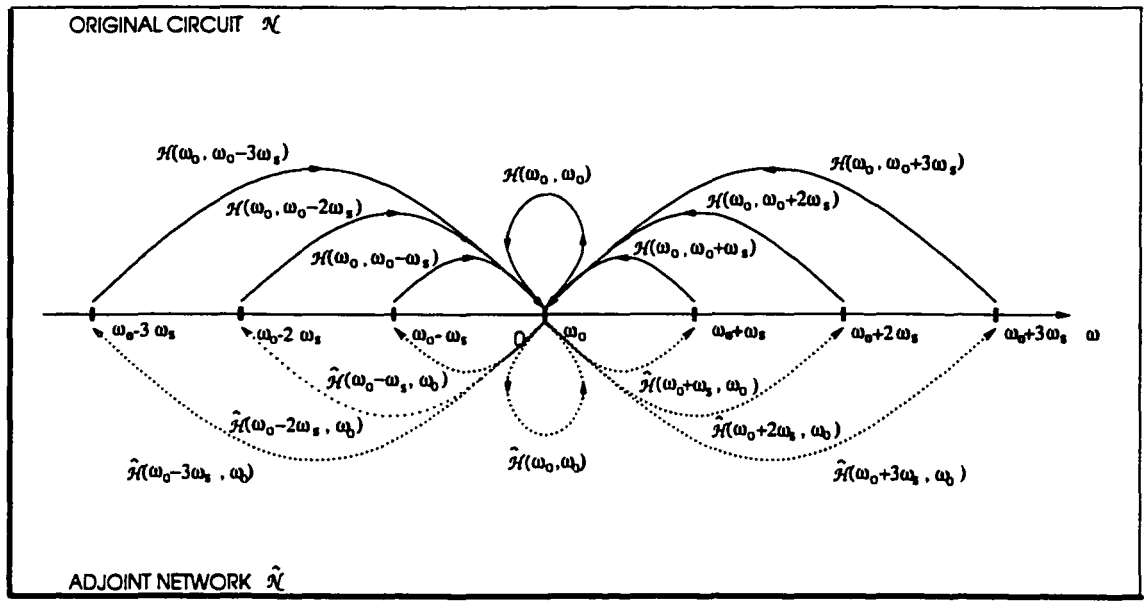


Figure 3.6: Frequency reversal theorem

3.5 Transfer Function Theorem

A special case of the frequency reversal theorem is when the frequencies of the inputs and output are the same, i.e. n is zero. In this case, (3.39) simplifies to

$$V_o(\omega_o) = -\hat{I}_i(\omega_o) \tag{3.41}$$

Consequently

$$\mathcal{H}_{VV}(\omega_o, \omega_o) = -\hat{\mathcal{H}}_{II}(\omega_o, \omega_o) \tag{3.42}$$

where $\mathcal{H}_{VV}(\omega_o, \omega_o)$ and $\hat{\mathcal{H}}_{II}(\omega_o, \omega_o)$ are the transfer functions of $\mathcal{N}$ and $\hat{\mathcal{N}}$ at frequency ω_o, respectively. Similar results were also obtained for circuits with other input/output configurations and are given in Table 3.2.

Table 3.2: Transfer function theorem

Original		Adjoint		Transfer function
Input	Output	Input	Output	
$i_i(t) = e^{j\omega_o t}$	$v_o(t)$	$\hat{i}_o(\tau) = e^{j\omega_o \tau}$	$\hat{v}_i(\tau)$	$V_o(\omega_o) = \hat{V}_i(\omega_o)$
$v_i(t) = e^{j\omega_o t}$	$v_o(t)$	$\hat{i}_o(\tau) = e^{j\omega_o \tau}$	$\hat{i}_i(\tau)$	$V_o(\omega_o) = -\hat{I}_i(\omega_o)$
$i_i(t) = e^{j\omega_o t}$	$i_o(t)$	$\hat{v}_o(\tau) = e^{j\omega_o \tau}$	$\hat{v}_i(\tau)$	$I_o(\omega_o) = -\hat{V}_i(\omega_o)$
$v_i(t) = e^{j\omega_o t}$	$i_o(t)$	$\hat{v}_o(\tau) = e^{j\omega_o \tau}$	$\hat{i}_i(\tau)$	$I_o(\omega_o) = \hat{I}_i(\omega_o)$

Theorem 3.4 (Transfer Function Theorem of PSL Circuits) *The magnitude of the transfer functions from multiple input sources to the single output of a PSL circuit at frequency ω_o is equal to that of the transfer functions of the adjoint network from the single input to multiple outputs at ω_o.*

The efficiency gained from employing the transfer function theorem is evident. With the transfer function theorem, we need to solve the adjoint network at the frequency at which the transfer functions from multiple inputs to the single output of the original circuit are to be evaluated *only once* to yield all the transfer functions of the original circuit. For circuits in which a large number of input sources exist, a tremendous amount of computation can be saved. It is worth noting that a similar result exists for LTI circuits [25].

It is also interesting to note that the transfer function theorem bears a resemblance to the characteristics of controlled sources. For instance, the relationship between $i_i(t)$ to $v_o(t)$ in Fig.3.7 can be considered as a CCVS with the transimpedance to be the transfer function. Using the fact that the adjoint network of a

CCVS is also a CCVS with the same trans-impedance, we obtain the desired adjoint network. Similar comparison can be made for other input/output configurations.

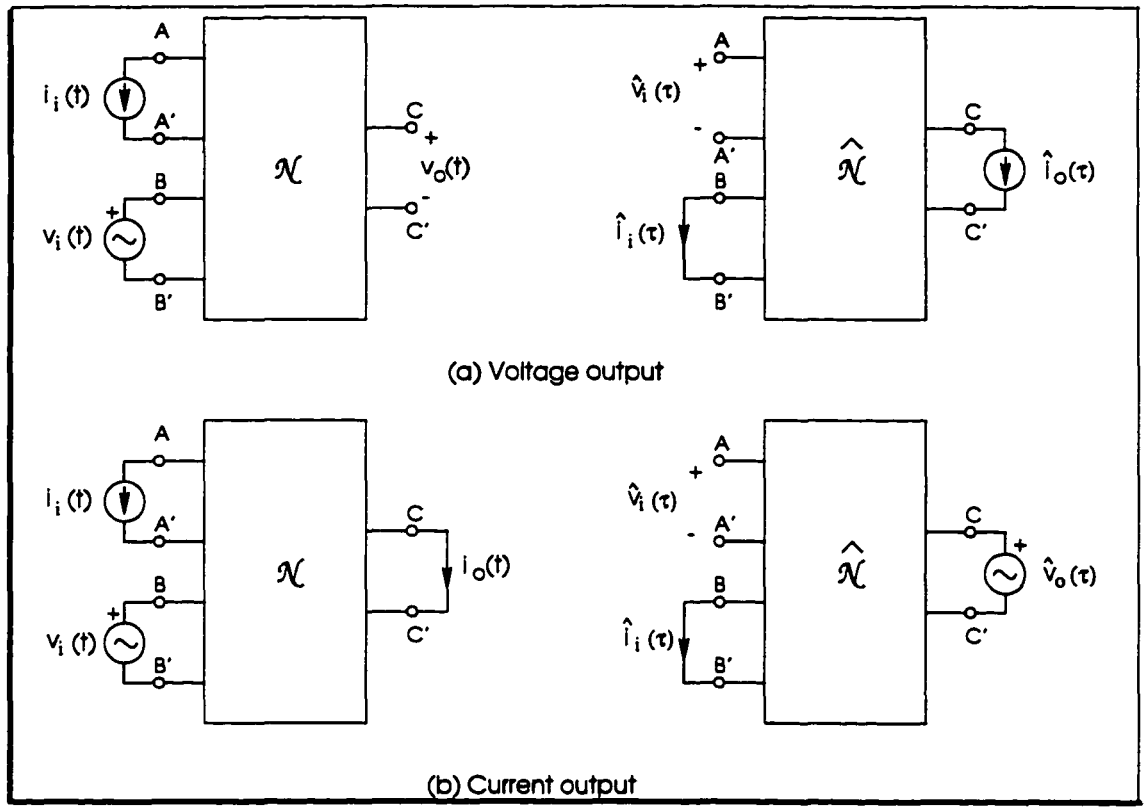


Figure 3.7: Inputs and outputs of original and adjoint networks

3.6 Solution of The Adjoint Network

The implementation of both the frequency reversal theorem and transfer function theorem requires the solution of the adjoint network. In this section, we show that the adjoint network of a given PSL circuit can be solved efficiently by utilizing the intrinsic relationship of these two circuits.

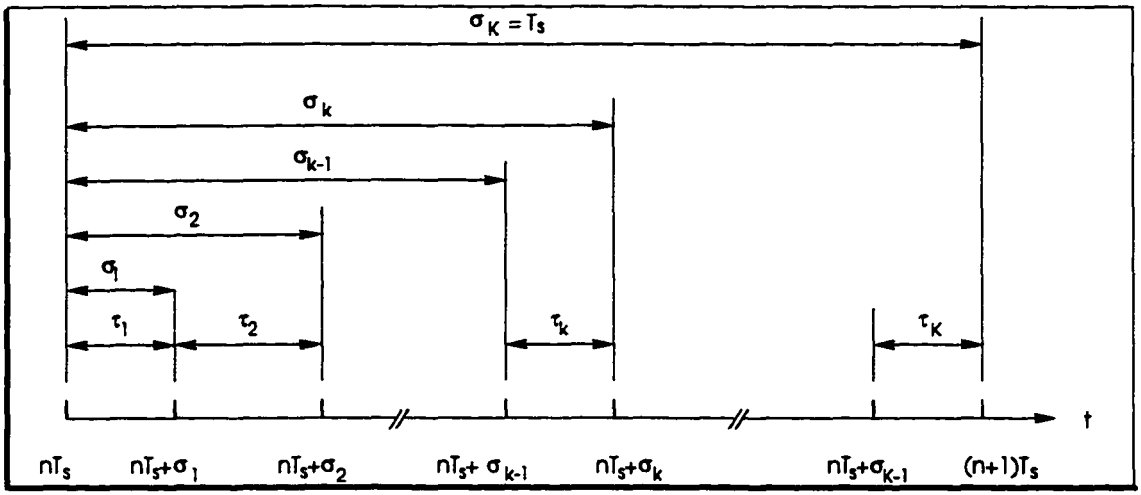


Figure 3.8: Clock phase

Without losing generality, let the input of a multi-phase PSL circuit $\mathcal{N}$ be an exponential signal $w(t) = e^{j\omega_o t}$. Let there be a total of K non-overlapping clock phases in a clock period, as shown in Fig.3.8. The widths of the phases are arbitrary. The adjoint network $\hat{\mathcal{N}}$ of $\mathcal{N}$ is constructed accordingly. The frequency domain analysis of PSL circuits was developed by Opal and Vlach in [47]. We make use of some of the essential results here without further explanation. In steady state, the constitutive equation of $\mathcal{N}$ in time domain is given by

$$\begin{aligned} \mathbf{G}_k\mathbf{v}_k(t) + \mathbf{C}_k\frac{d\mathbf{v}_k(t)}{dt} &= \mathbf{g}_k w(t)\xi_k(t) \\ &+ \mathbf{C}_k\mathbf{v}_{k-1}(nT+\sigma_{k-1}^+)\delta(t-nT-\sigma_{k-1}^+) \\ &- \mathbf{C}_k\mathbf{v}_k(nT+\sigma_k^-)\delta(t-nT-\sigma_k^-) \\ &\quad -\infty < t < \infty,\ n = 0, \pm 1, \pm 2, \ldots \end{aligned} \tag{3.43}$$

where $\mathbf{v}_k(t)$ is the network variable vector. $\mathbf{G}_k$ and $\mathbf{C}_k$ are conductance and capacitance matrices, respectively. $w(t)$ is the input and $\mathbf{g}_k$ is a constant vector specifying

the location of the input. $\xi_k(t)$ is the kth window function defined as

$$\xi_k(t) = \begin{cases} 1 & nT + \sigma_{k-1} < t \leq nT + \sigma_k \\ 0 & \text{elsewhere} \end{cases}. \tag{3.44}$$

The Dirac delta terms at $t = nT + \sigma_{k-1}^+$ and $t = nT + \sigma_k^-$ represent the injection of the initial conditions and the extraction of final conditions. The frequency response of the circuit is obtained by taking Fourier transform of (3.43)

$$\begin{aligned} \mathbf{T}_k(j\omega)\mathbf{V}_k(j\omega) &= \mathcal{F}[\mathbf{g}_k w(t)\xi_k(t)] \\ &+ \mathbf{C}_k\mathcal{F}[\mathbf{v}_{k-1}(nT + \sigma_{k-1}^+)\delta(t - nT - \sigma_{k-1}^+)] \\ &- \mathbf{C}_k\mathcal{F}[\mathbf{v}_k(nT + \sigma_k^-)\delta(t - nT - \sigma_k^-)] \\ &\quad n = 0, \pm 1, \pm 2, \ldots \end{aligned} \tag{3.45}$$

where $\mathbf{T}_k(j\omega) = \mathbf{G}_k + j\omega\mathbf{C}_k$. The Fourier transform of the first term on the right hand side of (3.45) can be computed analytically for both continuous and S/H input and is readily available [47]. The other two terms are obtained using numerical integration as follows :

During each clock phase, the circuit is essentially linear time-invariant. The LTI circuit in phase k is characterized by

$$\mathbf{G}_k\mathbf{v}_k(t) + \mathbf{C}_k\frac{d\mathbf{v}_k(t)}{dt} = \mathbf{g}_k e^{j\omega_o t}, \quad \mathbf{v}_k(t)|_{t=nT+\sigma_{k-1}} = \mathbf{v}_{k-1}. \tag{3.46}$$

Taking Laplace transform

$$\mathbf{V}_k(s) = \mathbf{T}_k^{-1}(s)\mathbf{C}_k\mathbf{v}_{k-1} + \mathbf{T}_k^{-1}(s)\frac{\mathbf{g}_k}{s - j\omega_o} \tag{3.47}$$

where $\mathbf{T}_k(s) = \mathbf{G}_k + s\mathbf{C}_k$. The superscript "-1" denotes matrix inversion. Because

$$\mathbf{T}_k^{-1}(s)\frac{\mathbf{g}_k}{s - j\omega_o} \Longleftrightarrow \mathcal{L}^{-1}\left[\mathbf{T}_k^{-1}(s)\right] \otimes \mathbf{g}_k e^{j\omega_o t} \tag{3.48}$$

where $\otimes$ denotes convolution, $\mathcal{L}^{-1}[.]$ is inverse Laplace transform operator and $\Longleftrightarrow$ denotes convolution theorem. The response of the circuit at $t = nT + \sigma_k^-$, denoted by $\mathbf{v}_k$, is obtained from (3.47) by taking inverse Laplace transform

$$\mathbf{v}_k = \mathbf{N}_k\mathbf{C}_k\mathbf{v}_{k-1} + \mathbf{P}_k e^{j\omega_o(nT+\sigma_{k-1}^+)} \tag{3.49}$$

where

$$\begin{aligned} \mathbf{N}_k &= \mathcal{L}^{-1}\left[\mathbf{T}_k^{-1}(s)\right]_{t=nT+\sigma_k^-} \\ \mathbf{P}_k &= e^{j\omega_o\tau_k}\left[\int_0^\infty \mathbf{N}_k(\tau)e^{-j\omega_o\tau}d\tau\right]\mathbf{g}_k. \end{aligned} \tag{3.50}$$

It becomes clear that $\mathbf{N}_k\mathbf{C}_k$ is the state transition matrix and $\mathbf{P}_k$ is the zero-state response of the circuit at $t = nT + \sigma_k^-$ with the input at $t = nT + \sigma_{k-1}^+$. The state transition matrix is solely determined by the topology of the circuit. It is independent of the input and frequency. $\mathbf{P}_k$, however, is input and frequency dependent. Fourier transform of (3.49) gives the last two terms on the right hand side of (3.43).

The computational cost of frequency analysis of PSL circuits mainly consists of the cost for computing (a) $\mathbf{N}_k$ matrix, (b) $\mathbf{P}_k$ vector and (c) LU-factorization of $\mathbf{T}_k(j\omega)$. $\mathbf{G}_k$ and $\mathbf{C}_k$ matrices are formulated using the modified nodal analysis. When taking into account the time reversal characteristic of the adjoint network,

it can be shown that $\mathbf{G}_k$ and $\mathbf{C}_k$ of $\mathcal{N}$ relate to those of $\hat{\mathcal{N}}$ by

$$\begin{aligned}\hat{\mathbf{G}}_k &= \mathbf{G}^T_{K-k+1} \\ \hat{\mathbf{C}}_k &= \mathbf{C}^T_{K-k+1} \\ \hat{\mathbf{T}}_k(s) &= \mathbf{T}^T_{K-k+1}(s) \\ \hat{\tau}_k &= \tau_{K-k+1}\end{aligned} \tag{3.51}$$

where $\hat{\mathbf{G}}_k$ and $\hat{\mathbf{C}}_k$ are the conductance and capacitance matrices of $\hat{\mathcal{N}}$, $\hat{\mathbf{T}}_k(s) = \hat{\mathbf{G}}_k + s\hat{\mathbf{C}}_k$. The superscript T denotes matrix transpose. Since $(\mathbf{A}^{-1})^T = (\mathbf{A}^T)^{-1}$, where $\mathbf{A}$ is a non-singular square matrix, also because $\mathcal{L}^{-1}\left([.]^T\right) = \left(\mathcal{L}^{-1}[.]\right)^T$, we have

$$\hat{\mathbf{T}}_k^{-1}(j\omega) = \left[\mathbf{T}^{-1}_{K-k+1}(j\omega)\right]^T. \tag{3.52}$$

Therefore, the LU-factorization of $\hat{\mathbf{T}}_k(j\omega)$ can be obtained directly from that of $\mathbf{T}_k(j\omega)$ without additional computation. Also, because

$$\begin{aligned}\hat{\mathbf{N}}_k(\tau) &= \mathcal{L}^{-1}\left[\hat{\mathbf{T}}_k^{-1}(s)\right] \\ &= \mathcal{L}^{-1}\left(\left[\mathbf{T}^{-1}_{K-k+1}(s)\right]^T\right) \\ &= \left(\mathcal{L}^{-1}\left[\mathbf{T}^{-1}_{K-k+1}(s)\right]\right)^T \\ &= \mathbf{N}^T_{K-k+1}(t).\end{aligned} \tag{3.53}$$

The state transition matrix of $\hat{\mathcal{N}}$ can also be obtained from that of $\mathcal{N}$ without numerical integration.

The zero-state response $\mathbf{P}_k$ is input-dependent. It is the solution of (3.46) at $t = nT + \sigma_k^-$ when the input is applied at $t = nT + \sigma_{k-1}^+$ and the initial condition is zero. Using numerical Laplace inversion of order 19 [97-99] [1], it can be shown that $\mathbf{P}_k$ is computed from

$$\mathbf{P}_k = \mathbf{Q}_k(\tau_k)\mathbf{g}_k \tag{3.54}$$

where

$$\mathbf{Q}_k(\tau_k) = -\frac{1}{\tau_k}\sum_{i=1}^{10} K_i \mathbf{T}_{k,i}^{-1}\left(\frac{z_i}{\tau_k}\right)\frac{1}{\frac{z_i}{\tau_k} - j\omega_o} \tag{3.55}$$

K_i and z_i are two sets of precomputed complex numbers readily available [39]. Because

$$\hat{\mathbf{T}}_{k,i}\left(\frac{z_i}{\hat{\tau}_k}\right) = \mathbf{T}_{K-k+1,i}^T\left(\frac{z_i}{\tau_{K-k+1}}\right) \tag{3.56}$$

we obtain

$$\hat{\mathbf{Q}}_k = \mathbf{Q}_{K-k+1}^T \tag{3.57}$$

Consequently

$$\hat{\mathbf{P}}_k = \mathbf{Q}_{K-k+1}^T \hat{\mathbf{g}}_k \tag{3.58}$$

where $\hat{\mathbf{g}}_k$ is a constant vector specifying the input location of $\hat{\mathcal{N}}$. It is obtained from $\hat{\mathbf{g}}_k = \mathbf{d}_k$, where $\mathbf{d}_k$ is a constant vector specifying the output location of $\mathcal{N}$. The

[1] A brief review of numerical Laplace inversion is presented in Appendix A.

Table 3.3: Relation between original and adjoint networks

Original circuit	Adjoint network
$\mathbf{G}_k$	$\hat{\mathbf{G}}_k = \mathbf{G}_{K-k+1}^T$
$\mathbf{C}_k$	$\hat{\mathbf{C}}_k = \mathbf{C}_{K-k+1}^T$
$\mathbf{T}_k(j\omega)$	$\hat{\mathbf{T}}_k(j\omega) = \mathbf{T}_{K-k+1}^T(j\omega)$
$\mathbf{T}_k^{-1}(j\omega)$	$\hat{\mathbf{T}}_k^{-1}(j\omega) = \left(\mathbf{T}_{K-k+1}^{-1}(j\omega)\right)^T$
$\mathbf{N}_k$	$\hat{\mathbf{N}}_k = \mathbf{N}_{K-k+1}^T$
$\mathbf{Q}_k$	$\hat{\mathbf{Q}}_k = \mathbf{Q}_{K-k+1}^T$
$\mathbf{P}_k$	$\hat{\mathbf{P}}_k = \mathbf{Q}_{K-k+1}^T \mathbf{d}_k$
$\mathbf{d}_k$	$\hat{\mathbf{d}}_k = \mathbf{g}_k$
$\mathbf{g}_k$	$\hat{\mathbf{g}}_k = \mathbf{d}_k$

above analysis shows that the zero-state response of $\hat{\mathcal{N}}$ can be obtained efficiently from that of $\mathcal{N}$ without numerical integration.

In summary, the adjoint network $\hat{\mathcal{N}}$ of $\mathcal{N}$ can be solved with little extra computation given that the solution of $\mathcal{N}$ is available. The intrinsic relationship between $\mathcal{N}$ and $\hat{\mathcal{N}}$ is summarized in Table 3.3

3.7 Numerical Examples

In this section, the theory developed in this chapter is assessed with the help of numerical examples.

Table 3.4: Parameter values of SC integrator

Parameter	Numerical value	Unit	Remark
C_1	0.01592	μF	
C_2	10	μF	
C_3	1	μF	
R_S	100	Ω	
R_3	22.74	kΩ	
R_O	100	Ω	
R_{ON}	3.5	kΩ	Channel resistance
f_o	889	Hz	Input frequency
f_s	100	kHz	Clock frequency
f_T	700	kHz	Unit-gain frequency of op amp
τ_1	$0.488T_s$	Second	Width of phase 1
τ_2	$0.512T_s$	Second	Width of phase 2
g_1	1	Simen	Transconductance
g_2	4.398×10^4	Simen	Transconductance

3.7.1 Parasitic-insensitive Switched-capacitor Integrator

Consider a parasitic-insensitive switched-capacitor integrator in Fig. 3.9. The schematic of its adjoint network is also shown in the figure. The circuit is not sensitive to the parasitic capacitances between the top/bottom plates of the capacitor and the substrate, as shown in the figure [100, 101]. The op amp is modeled as a single-pole device with unity-gain band width 700 kHz and output resistance 100 Ω. The schematics of the equivalent circuits of op amp and its adjoint network are shown in Fig. 3.10 [39]. The dominant pole is determined by R_3C_3 whereas the

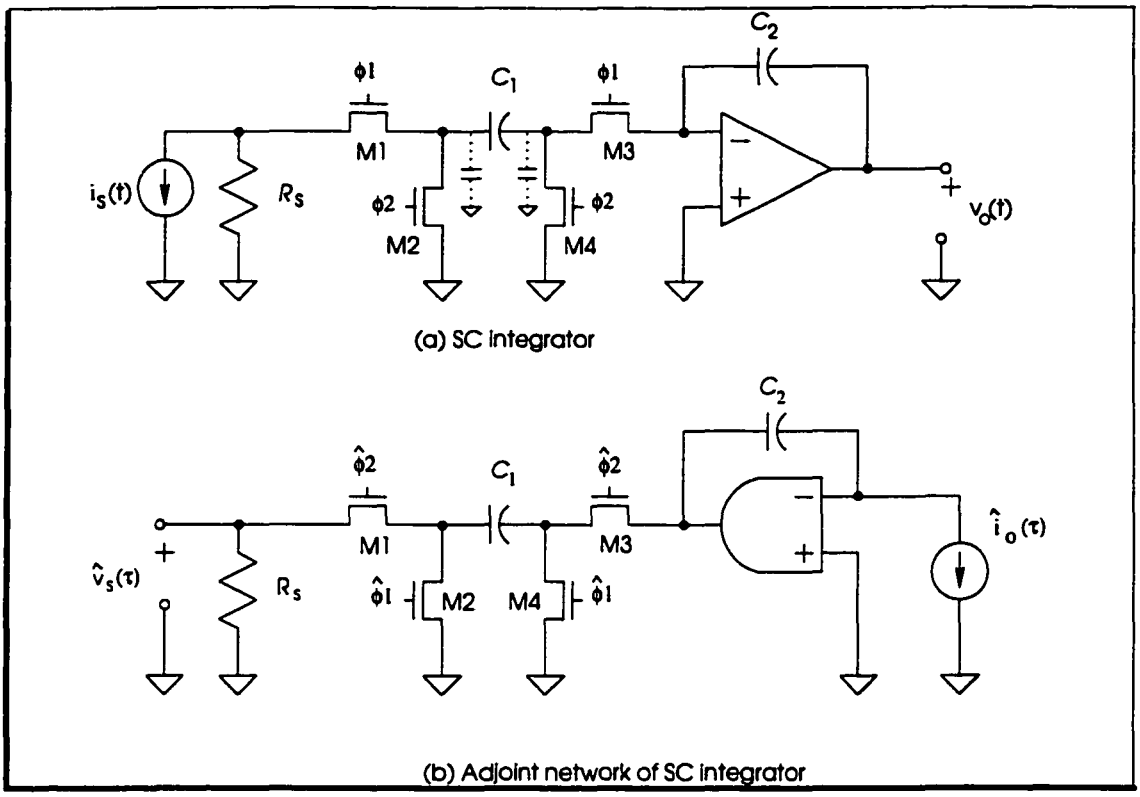


Figure 3.9: Parasitic-insensitive switched-capacitor integrator and its adjoint network

open-loop gain is determined by the second VCCS. Note we have assumed infinite differential input impedance and common-mode input resistances. Other nonidealities, such as finite slew rate, finite CMRR, etc. are also neglected for simplicity. More advanced models [96, 101] can also be employed, however, with a cost of increasing circuit complexity and simulation time. The MOSFETs are modeled as an ideal switch in series with a LTI resistor with resistance 3.5 kΩ. All intrinsic and parasitic capacitances associated with MOSFETs are neglected. The parameters of the circuit are given in Table 3.4. The magnitude of the inputs of both circuits is unity. The circuits were solved using Watsnap [47] and the results are presented

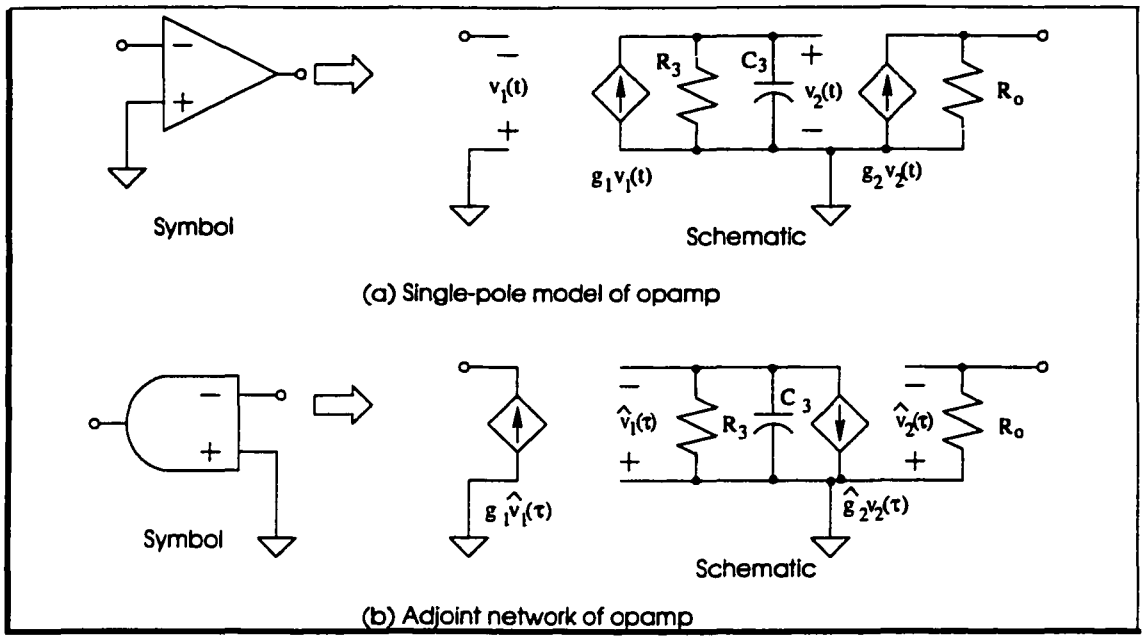


Figure 3.10: Models of op amp and its adjoint network

in Table 3.5. It is seen that the transfer function and aliasing transfer functions of the integrator match those of its adjoint network exactly.

3.7.2 Switched-capacitor Band pass Filter

Consider a second-order switched-capacitor band pass filter with two non-overlapping clock phases. The schematics of the filter and its adjoint network are shown Figs.3.11 and 3.12, respectively. It is a stray-insensitive switched-capacitor realization of the classic Tow-Thomas band pass filter [102]. The value of the parameters of the circuit is given in Table 3.6. The pass-band center frequency is 1 kHz. The models of MOSFETs and op amp are the same as those in the previous example. The magnitude of the inputs of both circuits is unity. The circuits were solved using Watsnap and the results are presented in Table 3.7. It is seen that both the

Table 3.5: Responses of switched-capacitor integrator and its adjoint network

Original Circuit (output at f_o)		Adjoint Network (input at f_o)	
Input freq.	Output	Output freq.	Output
f_o	$2.68218\times10^{-2} - 8.02467\times10^{-2}i$	f_o	$2.68218\times10^{-2} - 8.02467\times10^{-2}i$
$f_o + f_s$	$5.29485\times10^{-2} + 1.6045\times10^{-2}i$	$f_o + f_s$	$5.29485\times10^{-2} + 1.6045\times10^{-2}i$
$f_o + 2f_s$	$-9.60776\times10^{-4} + 2.04816\times10^{-3}i$	$f_o + 2f_s$	$-9.60776\times10^{-4} + 2.04816\times10^{-3}i$
$f_o + 3f_s$	$1.7885\times10^{-2} + 3.83242\times10^{-3}i$	$f_o + 3f_s$	$1.7885\times10^{-2} + 3.83242\times10^{-3}i$
$f_o + 4f_s$	$-5.77075\times10^{-4} + 2.07626\times10^{-3}i$	$f_o + 4f_s$	$-5.77075\times10^{-4} + 2.07626\times10^{-3}i$
$f_o + 5f_s$	$1.07444\times10^{-2} + 1.43950\times10^{-3}i$	$f_o + 5f_s$	$1.07444\times10^{-2} + 1.43950\times10^{-3}i$
$f_o + 6f_s$	$-3.42938\times10^{-4} + 2.08695\times10^{-3}i$	$f_o + 6f_s$	$-3.42938\times10^{-4} + 2.08695\times10^{-3}i$
$f_o + 7f_s$	$7.59345\times10^{-3} + 4.25669\times10^{-4}i$	$f_o + 7f_s$	$7.59345\times10^{-3} + 4.25669\times10^{-4}i$
$f_o + 8f_s$	$-1.47032\times10^{-4} + 2.08153\times10^{-3}i$	$f_o + 8f_s$	$-1.47032\times10^{-4} + 2.08153\times10^{-3}i$
$f_o + 9f_s$	$5.77376\times10^{-3} - 1.21182\times10^{-4}i$	$f_o + 9f_s$	$5.77376\times10^{-3} - 1.21182\times10^{-4}i$

transfer function and aliasing transfer functions of the original circuit match those of the adjoint network exactly.

3.8 Summary

In this chapter, Tellegen's theorem for PSL circuits in phasor domain was introduced and a general theory of the adjoint network of multiphase PSL circuits was developed. Two novel theorems, namely, frequency reversal theorem and transfer function theorem, were also introduced and rigorous proofs were given. The theory derives the transfer functions and aliasing transfer functions from the multiple input

Table 3.6: Parameter value of Switched-capacitor band pass filter

Parameter	Numerical value	Unit	Remark
C_1	0.434567	pF	
C_2	20	pF	
C_3	0.434567	pF	
C_4	20	pF	
C_5	20	pF	
C_6	0.108642	pF	
C_7	0.295097	pF	
R_{ON}	3.5	kΩ	Channel resistance
f_o	889	Hz	Input frequency
f_s	20	kHz	Clock frequency
f_T	700	kHz	Unit-gain frequency of op amp
τ_1	$0.488T_s$	Second	Width of phase 1
τ_2	$0.512T_s$	Second	Width of phase 2

sources to the single output at the base band frequency of a given PSL circuit by solving its adjoint network at the base band only once. The relationship between PSL circuits and the corresponding adjoint networks was investigated. It is shown that the adjoint network can be solved efficiently.

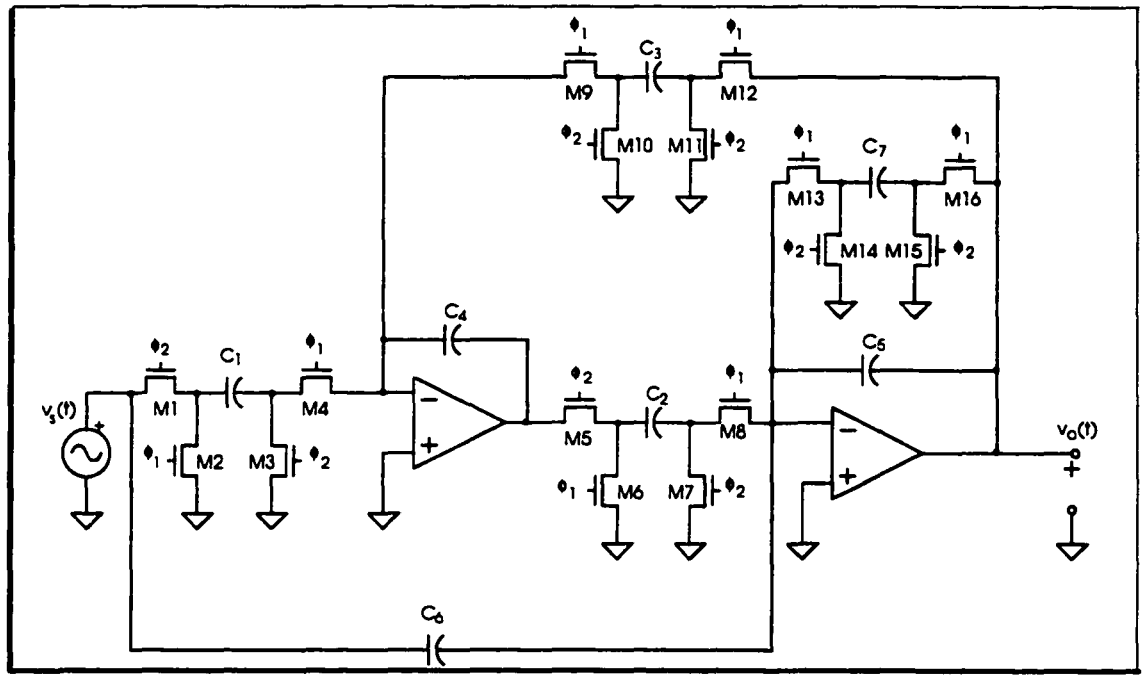


Figure 3.11: Switched-capacitor band pass filter

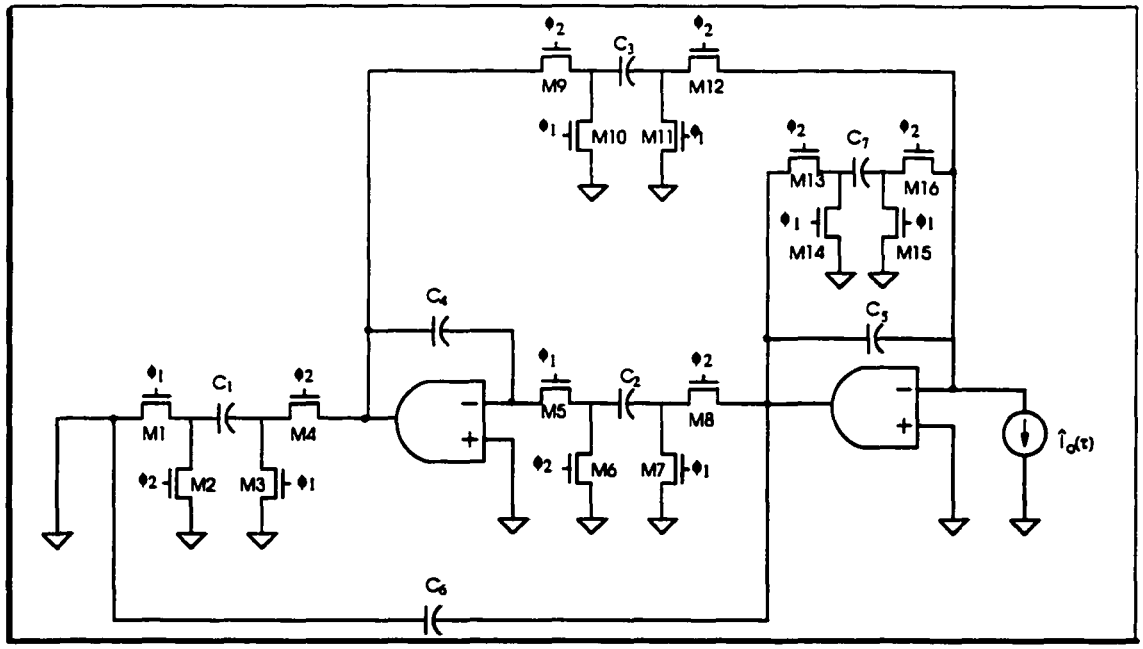


Figure 3.12: adjoint network of Switched-capacitor band pass

Table 3.7: Responses of Switched-capacitor band pass filter and its adjoint network

Original Circuit (output at f_o)		Adjoint Network (input at f_o)	
Input freq.	Output	Output freq.	Output
f_o	$5.08187\times10^{-2} + 4.46942\times10^{-2}i$	f_o	$5.08187\times10^{-2} + 4.46942\times10^{-2}i$
$f_o + f_s$	$-2.94092\times10^{-2} + 3.57741\times10^{-2}i$	$f_o + f_s$	$-2.94092\times10^{-2} + 3.57741\times10^{-2}i$
$f_o + 2f_s$	$-2.60379\times10^{-3} - 2.61331\times10^{-3}i$	$f_o + 2f_s$	$-2.60379\times10^{-3} - 2.61331\times10^{-3}i$
$f_o + 3f_s$	$-8.02836\times10^{-3} + 1.21848\times10^{-3}i$	$f_o + 3f_s$	$-8.02836\times10^{-3} + 1.21848\times10^{-3}i$
$f_o + 4f_s$	$-2.13732\times10^{-3} - 1.46881\times10^{-3}i$	$f_o + 4f_s$	$-2.13732\times10^{-3} - 1.46881\times10^{-3}i$
$f_o + 5f_s$	$-4.12177\times10^{-3} + 7.45969\times10^{-3}i$	$f_o + 5f_s$	$-4.12177\times10^{-3} + 7.45969\times10^{-3}i$
$f_o + 6f_s$	$-1.97140\times10^{-3} - 1.07077\times10^{-3}i$	$f_o + 6f_s$	$-1.97140\times10^{-3} - 1.07077\times10^{-3}i$
$f_o + 7f_s$	$-2.46157\times10^{-3} + 5.38513\times10^{-3}i$	$f_o + 7f_s$	$-2.46157\times10^{-3} + 5.38513\times10^{-3}i$
$f_o + 8f_s$	$-1.89279\times10^{-3} - 8.23294\times10^{-4}i$	$f_o + 8f_s$	$-1.89279\times10^{-3} - 8.23294\times10^{-4}i$
$f_o + 9f_s$	$-5.77376\times10^{-3} + 1.21182\times10^{-4}i$	$f_o + 9f_s$	$-5.77376\times10^{-3} + 1.21182\times10^{-4}i$

Chapter 4

Noise Analysis of PSL Circuits

This chapter deals with noise analysis of periodically switched linear circuits [103]. Noise sources and the equivalent circuits of integrated devices are investigated. An adjoint network-based noise analysis algorithm is developed. The output noise power of a number of PSL circuits is analyzed and the results are compared with measurements.

4.1 Noise Sources

The most commonly encountered types of noise in silicon integrated circuits are thermal noise, shot noise, and flicker noise. These noise sources are inherent to silicon devices. Clock jitter is another source of fluctuation that generates random errors in network variables. It is unique to clocked circuits.

4.1.1 Thermal noise

Thermal noise, often referred to as Johnson noise in recognition of the first observation of the phenomenon by J. B. Johnson [104], is generated by the random thermal agitation of mobile carriers. It is due to the random departure and return of mobile charges in thermal equilibrium. The power of thermal noise is directly proportional to temperature. The band width of thermal noise at room temperature is around 6000 GHz. Time samples separated by 0.17 ps are uncorrelated [105]. In almost all cases, thermal noise is treated as a stationary process. The distribution of thermal noise is Gaussian. The PSD of the thermal noise generated by a resistor is given by Nyquist law

$$S(\omega) = 2kTR \qquad -\infty < \omega < \infty \tag{4.1}$$

where R is the resistance, k is Boltzmann constant, T is the absolute temperature in degrees Kelvin. Eq.(4.1) was first derived by Nyquist [106] from an argument based on thermodynamics and the exchange of energy between resistive elements in thermal equilibrium.

4.1.2 Shot noise

Shot noise is caused by the random combination of electron-hole pairs and the random diffusion of minority carriers across depletion regions in semiconductor devices [107]. This phenomenon is depicted by a stochastic process $Y(t)$, which represents the sum of a large number of independent events occurring at random

time instants at an average rate λ

$$Y(t) = \sum_i \gamma(t - t_i) \tag{4.2}$$

where $\gamma(t)$ is a pulse shape function and t_i is the time at which the pulse occurs. Note $\gamma(t)$ is causal. The distribution of $Y(t)$ is Poisson. The PSD of $Y(t)$ is given by Curson's theorem [108, 109]

$$S_Y(\omega) = 2\lambda|\Gamma(\omega)|^2 \tag{4.3}$$

where $\Gamma(\omega)$ is the Fourier transform of $\gamma(t)$. The band width of shot noise is inversely proportional to the transit time required by the carriers to cross the depletion regions. It is in the high gigahertz range [105]. Shot noise is therefore treated as a stationary white process. In the extreme case where $\gamma(t)$ is approximated by Dirac impulse function $\delta(t)$, because $|\Gamma(\omega)| = 1$, we have the following Schottky's theorem for PN-junction [88]

$$S(\omega) = 2qI_D \tag{4.4}$$

where I_D is the average forward bias current of the pn-junction and q is the charge on an electron. It should be noted that the above result is only valid for $f < f_T = 1/(2\pi\tau)$, where τ is the transit time for mobile carriers to cross the potential barriers.

4.1.3 Flicker noise ($1/f$ noise)

Flicker noise, also known as $1/f$ noise, exists in both active devices and passive resistors. The mechanism of $1/f$ noise has been studied extensively. Numerous papers tend to converge to two basic $1/f$ noise theories : (1) the mobility fluctuation model [110], which is based on the scattering of mobile carriers due to the collision with the crystal lattice of silicon and impurities, and (2) the carrier density fluctuation due to the trapping and de-trapping of the mobile carriers in the traps located in the surface of silicon-oxide interface and within the gate oxide [111]. For MOS transistors, it was found that the mobility fluctuation model only holds when the devices are operated in the triode region where the inverse layer can be approximated by a homogeneous resistor. The density fluctuation theory, on the other hand, predicts $1/f$ noise accurately in all regions of MOS transistors. Flicker noise is always associated with a direct current and is often modeled as a stationary process with PSD given by [16]

$$S(\omega) = \frac{K_f I^a}{f^b} \tag{4.5}$$

where I is the average current, K_f is a process and temperature dependent constant, a and b are constants in the ranges of $0.5 < a < 2$ and $0 < b < 2$, and f is frequency. For most electronic devices, flicker noise surpasses thermal and shot noise at low frequencies. Extensive experiments show that there is no change in the shape of the PSD of flicker noise even at extremely low frequencies [112]. The upper limit of flicker noise is difficult to detect as it is usually masked by the floor of thermal noise. The corner frequency, defined as the frequency at which the PSDs of thermal/shot and flicker noise intercept, is often used as the upper bound of flicker noise.

4.1.4 Clock Jitter

Clock jitter, also known as timing jitter, is caused by the random error in the time of the occurrence of the sampling clock. The cause of clock jitter is mainly due to the phase noise generated in the reference oscillator and the associated circuits in the clock generator [113]. The fluctuation of the oscillator output causes the comparator to detect zero-crossing instants with a random time jitter [114]. Experimental results show that the distribution of clock jitter tends to be Gaussian [115] although uniform distribution is also often used in analyzing jitter effect [6]. The effect of clock jitter on the operation of MOSFET switches are two-fold. Both the amplitude and phase fluctuations of the clock signal affect the ON/OFF instants of MOSFET switches. Among them, the phase fluctuation is dominant as the amplitude fluctuation is usually small. In [116], the effect of timing jitter in sampling systems was investigated. It was shown that for a given signal sampled with a jittered clock, the Fourier transform of the expectation of samples is obtained from mean, variance and high-order moments of the jitter. In [117], an investigation on the effect of clock jitter on the performance of switched-capacitor networks was carried out using a deterministic approach. Time-domain simulation of clock jitter of PSL circuits and sigma-delta converters was also carried out [118]. It was shown that the fluctuation caused by the clock jitter is buried by the floor of the thermal noise of the circuit if the clock frequency is much higher than the signal frequency. However, it becomes the dominant fluctuation source if the frequencies of the clock and signal are comparable. For most switched-capacitor and switched-current networks, the clock period is usually much larger than the charging/discharging RC constants, the effect of the clock jitter is therefore insignificant. Investigation on frequency-domain methods for the analysis of clock jitter effect of general PSL circuit is left as a future research project.

4.2 Equivalent Circuits

The equivalent circuits of integrated devices with noise sources included are presented in this section. These equivalent circuits are used in noise analysis of electronic circuits, including PSL circuits.

4.2.1 Resistors

Physical resistors such as diffusion resistors, polysilicon resistors, etc., generate thermal noise. At low frequencies, a resistor can be modeled as a hypothetical noise-free resistor in series with a random voltage generator or a noise-free conductor in parallel with a random current generator, as shown in Fig. 4.1. At high frequencies, the parasitic capacitances associated with the resistors must also be taken into account in accurate modeling of the resistors.

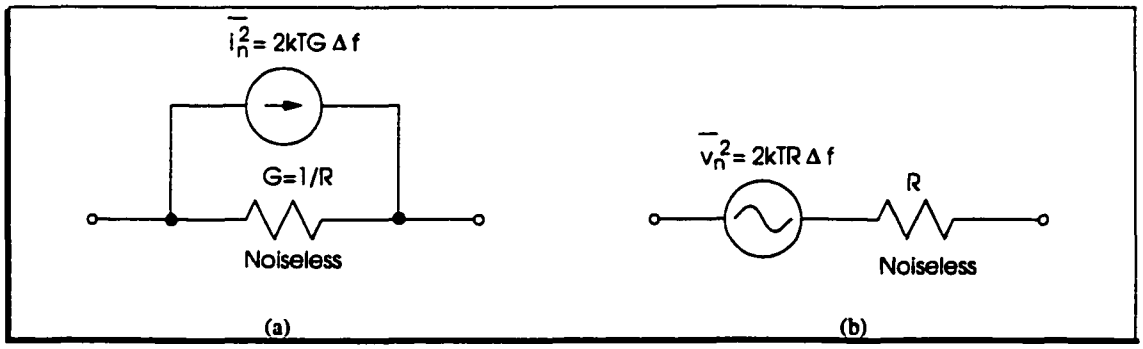


Figure 4.1: Equivalent circuits of resistors. (a) Norton equivalent, (b) Thevenin equivalent

4.2.2 Bipolar Junction Transistors

Bipolar junction transistors (BJTs) are widely used for high-frequency and high-speed applications due to their large f_T. There are four main noise sources associated with a BJT : (1) thermal noise generated by the base resistance, (2) shot noise in the base current, (3) flicker noise in the base current, and (4) shot noise in the collector current.

Flicker noise of BJTs arises mainly due to the generation/recombination processes in the emitter-base depletion region and the trap/de-trap of carriers by the oxide located above the emitter-base junction. The former usually predominates over the later [120]. As compared with MOS transistors, $1/f$ noise of BJTs is much smaller and manifests itself in frequency regions several decades lower [119]. The base resistance consists of the intrinsic and extrinsic base resistances. The intrinsic base resistance is usually larger than the extrinsic [120]. However, due to the effect of current crowding [16], the intrinsic resistance and the associated thermal noise can be reduced by a large collector current. The extrinsic base resistance is made up of the bulk and contact resistances. It can be reduced by increasing the number of contacts in the base and reducing the lateral distance between the emitter and base contacts. The thermal noise generated by other parasitic resistances, such as emitter and collector bulk resistances, also constitute the overall noise of the device. However, because the emitter is heavily doped, the associated thermal noise is small [121]. The thermal noise originating from the collector resistance is often surpassed by the noise of high collector loads. A small-signal equivalent circuit of BJTs biased in the forward active region is given in Fig. 4.2. When a BJT is operated in ON/OFF modes, its equivalent circuit can also be obtained by including the above identified noise sources in the large-signal equivalent circuit of BJTs.

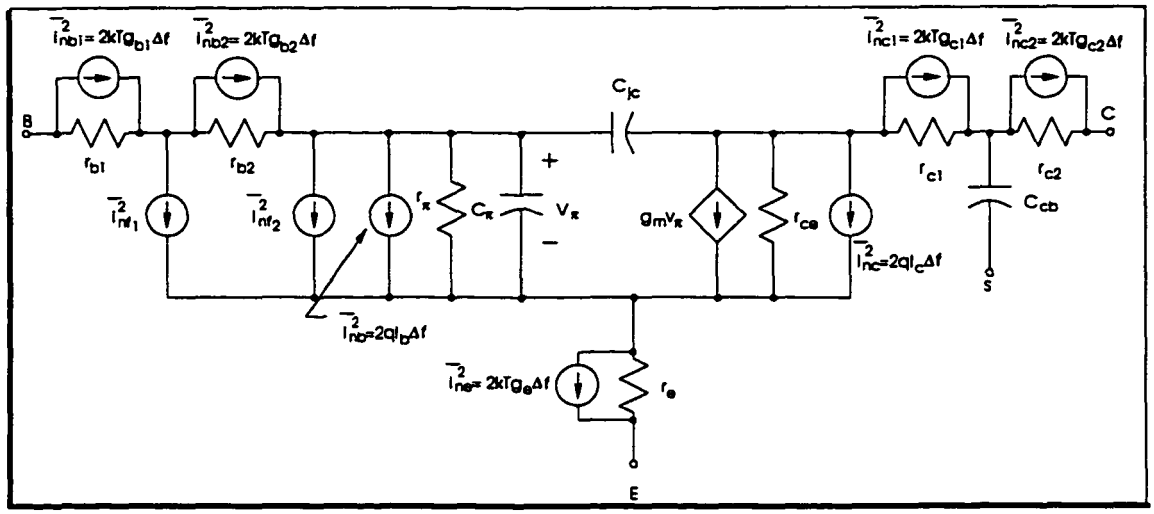


Figure 4.2: A high-frequency small-signal equivalent circuit of BJTs biased in forward active region

4.2.3 MOS Transistors

MOS transistors are building elements of SC and SI circuits. Recent advances in CMOS technology have also made CMOS a viable technology choice for high-speed and RF applications. Noise generated by the intrinsic part of a MOS transistor consists of (1) shot noise in the gate leakage current, (2) thermal noise due to the random thermal motion of mobile carriers in the inversion layer and (3) flicker noise due to channel charge density fluctuation caused by the traps at the oxide-silicon interface [122]. The shot noise of gate leakage current is usually neglected. To ensure stable operation, MOS transistors are usually biased in strong inversion. The power of the flicker noise originating in the channel is given by [119]

$$\overline{i^2}_{nf} = \frac{K_f I_{DS}}{C_{ox} L^2 f} = \frac{K_f g_m^2}{2\mu C_{ox}^2 W L f} \tag{4.6}$$

where I_{DS} is the drain-source quiescent current. W and L are the width and length of the channel, respectively, g_m is the gate transconductance. MOS transistors exhibit the highest $1/f$ noise among all active integrated devices [119]. As compared with BJTs, the corner frequency of the flicker noise of MOS transistors could extend to mega Hertz ranges [16]. The thermal noise generated by a strongly inverted MOS transistor in saturation is mainly due to the fluctuation in the drift current in the channel [123]. The fluctuation in the diffusion current is negligible as the drift current predominates over the diffusion current in strong inversion. The thermal noise of the drift current is given by [124]

$$\overline{i^2}_{nDS} = 2kT\frac{2}{3}(g_m + g_{mb})\Delta f \tag{4.7}$$

where g_m and g_{mb} are the gate and substrate transconductances, respectively. Eq.(4.7) is valid only in the saturation region. It gives erroneous results in the triode region because as $v_{DS}\rightarrow 0$, zero thermal noise is predicted [1]. In [125, 126], g_{DS}, the channel conductance, was added to (4.7) to represent the thermal noise generated by the device in ohmic region.

$$\overline{i^2}_{nDS} = 2kT\alpha(g_m + g_{mb} + g_{DS})\Delta f \tag{4.8}$$

where $\alpha = 1 - v_{DS}/(3V_{DS,SAT})$ if $v_{DS} < V_{DS,SAT}$ and 2/3 if $v_{DS} > V_{DS,SAT}$. $V_{DS,SAT} = v_{GS} - V_T$. Note α varies with v_{DS} linearly from 1 at $v_{DS} = 0$ (where $g_m \approx 0$) to $\frac{2}{3}$ at $v_{DS} = V_{DS,SAT}$ (where g_{DS} is small). The validity of (4.8) was questioned in [127] because it differs from the theoretical results given in [123,128].

[1] In the triode region, since $i_{DS} = \mu C_{ox}\frac{W}{L}[(v_{GS} - V_T)v_{DS} - \frac{1}{2}V_{DS}^2]$, $g_m = \frac{\partial i_{DS}}{\partial v_{GS}} = \mu C_{ox}\frac{W}{L}v_{DS}$. As $v_{DS}\rightarrow 0, g_m \rightarrow 0$.

Moreover, the noise power predicated by (4.8) deviates notably from SPICE simulation when different levels of MOSFET models are used. It was shown in [123] that under quasi-static condition, the power of the thermal noise originating from the drift current in the channel of a strongly inverted MOS transistor is given by [123]

$$\overline{i_{nDS}^2} = 2kT\gamma g_{DS_o}\Delta f \tag{4.9}$$

where $\gamma = \frac{2}{3}$ if $v_{DS} > V_{DS,SAT}$ and $(1 - \lambda + \lambda^2/3)/(1 - \lambda/2)$ if $v_{DS} \leq V_{DS,SAT}$. Here $\lambda = v_{DS}/v_{DS,SAT}$ and g_{DS_o} is the channel conductance when $v_{DS} = 0$. When the first-order approximation [129] is used, it is obtained from

$$g_{DS_o} = \left.\frac{i_{DS}}{v_{DS}}\right|_{v_{DS}=0} = \mu C_{ox}\frac{W}{L}(v_{GS} - V_T) \tag{4.10}$$

It should be noted that (4.9) is only valid for long channel devices. In [130], the modulation of channel length and the degradation of surface mobility due to the high lateral field were also included in modeling the noise of MOS transistors and more complex results were obtained.

Switches in PSL circuits are realized using NMOS transistors operated in the triode region to minimize v_{DS} and the subthreshold regions. CMOS pass-transistor gates with complementary clock are also used extensively to maximize signal dynamic range, minimize ON-resistance and reduce clock feed-through [101, 131]. In the triode region, because v_{DS} is small, the channel can be approximated by a homogeneous conductor with conductance given by

$$g_{DS} = \mu C_{ox}\frac{W}{L}\Big[(v_{GS} - V_T) - v_{DS}\Big] \tag{4.11}$$

The thermal noise generated by the channel is computed in the same way as that of LTI resistors. When the transistor is in subthreshold region, we follow the same treatment as that in CSIM [129], BSIM [132], and set $i_{DS} = 0$. Consequently, the associated noise is zero. A low-frequency equivalent circuit of MOSFET switches is given in Fig. 4.3. This model has been used widely due to its simplicity [11, 12, 14, 15].

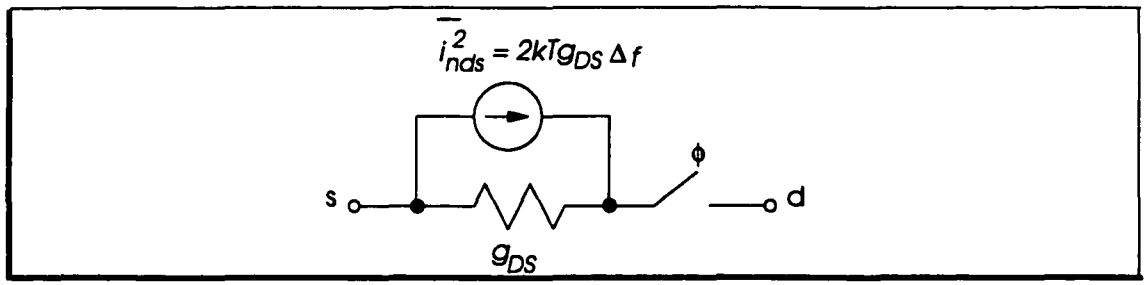


Figure 4.3: A low-frequency equivalent circuit of MOSFET switch

Noise generated by the extrinsic part of the device includes the thermal noise originating from the source and drain bulk resistances, and polysilicon gate resistance. Among them, the thermal noise of the polysilicon gate predominates. To analyze the noise behavior of MOS transistors at high frequencies, both the intrinsic and parasitic capacitances must be included. A high frequency small-signal equivalent circuit of MOS transistors with noise sources included is given in Fig. 4.4. At very high frequencies, the thermal noise generated by substrate resistance should also be taken into consideration as it contributes nearly 20% of the total noise of MOS transistors [133].

It is also worth noting that the so-called gate-current fluctuation [88, 122, 134] is due to the thermal noise originating in the channel and coupled via the gate-channel capacitance at high frequencies. It should not be considered as an independent nor a correlated noise source.

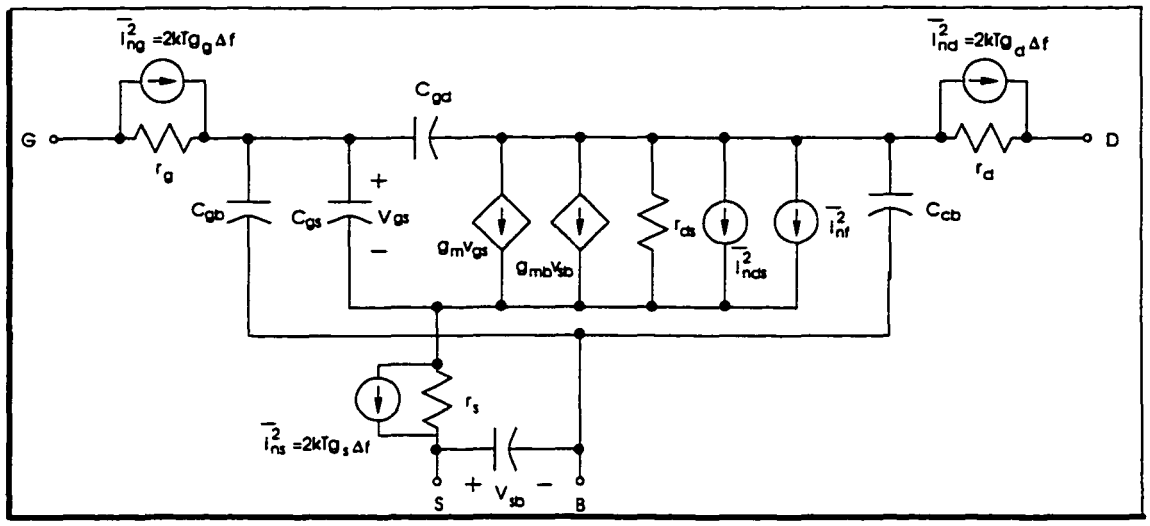


Figure 4.4: A high-frequency small-signal Equivalent circuit of MOS transistor

4.2.4 Operational Amplifiers (Op amp)

Noise generated by an operational amplifier is mainly due to the noise generated in the differential input stage. Noise generated in the following stages is usually negligible. To model the noise of the differential input stage in either open- or short-circuited cases, two pairs of noise-current and noise-voltage generators are needed at the inputs of the op amp and the op amp is thereby treated as a hypothetical noise-free device, as shown in Fig. 4.5(a) in which $\overline{i_{n1}^2}$ and $\overline{i_{n2}^2}$ are current-noise generators, $\overline{v_{n1}^2}$ and $\overline{v_{n2}^2}$ are voltage-noise generators [90]. Because $\overline{i_{n1}^2}$ and $\overline{i_{n2}^2}$ represent common-mode signals, they produce virtually no differential output if CMRR of the op amp is high. Consequently, they can be removed from the equivalent circuit without introducing large errors [16]. Also, because the two voltage-noise generators are in series with the input, they can be combined into a single voltage-noise generator, i.e. $\overline{v_n^2} = \overline{v_{n1}^2} + \overline{v_{n2}^2}$, given the correlation is small. This leads to a simplified equivalent circuit of the op amp shown in Fig. 4.5(b) [135–137]. If the op amp is realized

using BJTs, then $\overline{v_n^2}$ consists of the thermal noise of the base resistances, shot noise in base current and the input-referred noise originating in the collector currents of appropriate transistors in the differential stage. If the input stage is realized using MOS transistors, then $\overline{v_n^2}$ is made of the input-referred thermal and flicker noise originating in the inversion layer of the appropriate MOS transistors in the stage. It should be noted that when the op amp is operated at low frequencies, $\overline{v_n^2}$ is independent of frequency. However, at high frequencies, since the gain of the differential input stage varies with frequency, the input-referred noise source also changes with frequency. Consequently, $\overline{v_n^2}$ is frequency-dependent.

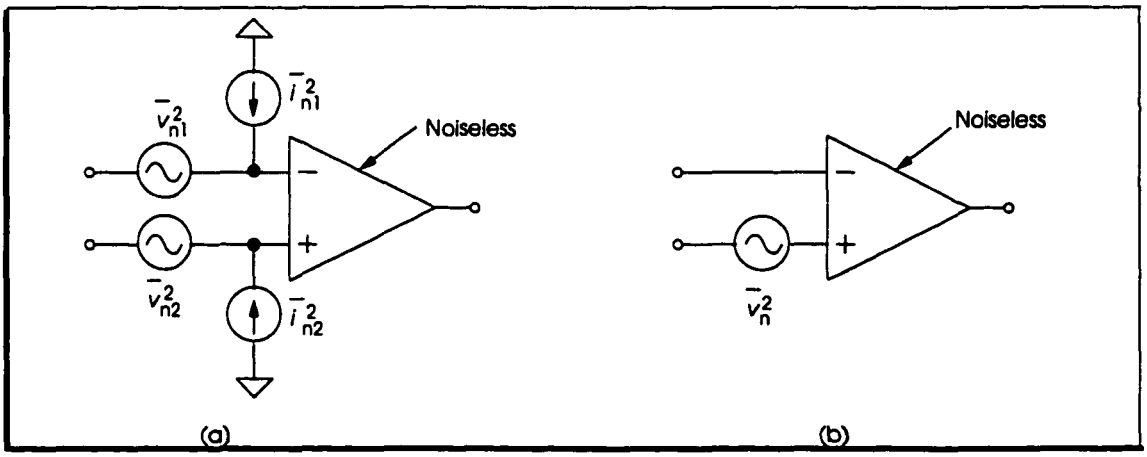


Figure 4.5: Equivalent circuits of operational amplifier. (a) Complete equivalent circuit, (b) Simplified equivalent circuit.

4.3 Noise Analysis of PSL Circuits

The noise behavior of PSL circuits differs from that of LTI circuits due to periodic switching. The band width of noise signals encountered in PSL circuits usually exceeds the clock frequency by orders of magnitude. The under-sampling of the

wide band noise results in strong aliasing effect. The noise power folded over from the side band components of the noise sources dominates the output noise power. In Chapter 2, it was shown that the response of PSL circuits with stationary inputs is cyclo-stationary. Its average PSD is time-independent and is computed from

$$\mathcal{S}_o(\omega) = \sum_{i=1}^{M} \sum_{n=-\infty}^{\infty} |\mathcal{H}_i(\omega, \omega + n\omega_s)|^2 \mathcal{S}_i(\omega + n\omega_s) \tag{4.12}$$

where $\mathcal{S}_i(\omega + n\omega_s)$ is the PSD of the ith noise at $\omega + n\omega_s$, $\mathcal{H}_i(\omega, \omega + n\omega_s)$ is the aliasing transfer function from the ith noise source at $\omega + n\omega_s$ to the output at ω, M is the number of noise sources. Revealed by (4.12) is that the computational cost of noise analysis of PSL circuits arises from a large number of noise sources and the aliasing effect. Both the transfer and aliasing transfer functions from the noise sources to the output are needed in computing the output noise power.

It was shown in Chapter 3 that these transfer and aliasing transfer functions can be computed efficiently by using the adjoint network technique. For a given PSL circuit $\mathcal{N}$ having K non-overlapping clock phases in each clock period, we first replace all noisy elements in the circuit with their corresponding equivalent circuits given earlier and then define a set of constant vectors $\mathbf{g}_i$, $i = 1, 2, .., M$, to specify the nodes to which these noise sources are connected. Further, the output of $\mathcal{N}$ is specified by a constant vector $\mathbf{d}$, i.e. $V_o(j\omega) = \mathbf{d}^T\mathbf{V}(j\omega)$, where $\mathbf{V}(j\omega)$ is the response of $\mathcal{N}$. The adjoint network $\hat{\mathcal{N}}$ of $\mathcal{N}$ is constructed in accordance with the guidelines given in Chapter 3. The circuit equations of $\mathcal{N}$, in particular, the conductance matrices $\mathbf{G}_k$ and capacitance matrices $\mathbf{C}_k$, $k = 1, 2, ..., K$, are formulated using the modified nodal analysis. The system matrices of $\hat{\mathcal{N}}$ are obtained as detailed in Chapter 3. Using Theorem 3.4, the transfer function from the ith noise

source to the output of $\mathcal{N}$ at ω, denoted by $H_i(\omega,\omega)$, is obtained from

$$\mathcal{H}_i(\omega,\omega) = \mathbf{g}_i^T\hat{\mathbf{V}}(\omega) \tag{4.13}$$

where $\hat{\mathbf{V}}(\omega)$ is the response of $\hat{\mathcal{N}}$ at ω with an input of unity amplitude at ω. The location of the input of $\hat{\mathcal{N}}$ is specified by $\mathbf{d}$. Further from Theorem 3.3, the aliasing transfer function from the ith noise source at $\omega + n\omega_s$ to the output at ω, denoted by $\mathcal{H}_i(\omega,\omega+n\omega_s)$, is obtained from

$$\mathcal{H}_i(\omega,\omega+n\omega_s) = \mathbf{g}_i^T\hat{\mathbf{V}}(\omega+n\omega_s) \qquad \forall n \tag{4.14}$$

where $\hat{\mathbf{V}}(\omega+n\omega_s)$ is the nth order frequency component of the response of $\hat{\mathcal{N}}$. The transfer and aliasing transfer functions from other noise sources to the same output of $\mathcal{N}$ can be obtained by substituting appropriate $\mathbf{g}_i$ vectors into (4.13) and (4.14), respectively. Since all noise sources are uncorrelated, the total output noise power of $\mathcal{N}$ is obtained by summing up the contributions of all noise sources.

$$\mathcal{S}_o(\omega) = \sum_{i=1}^{M}\sum_{n=-\infty}^{\infty} |\mathbf{g}_i^T\hat{\mathbf{V}}(\omega+n\omega_s)|^2\mathcal{S}_i(\omega+n\omega_s) \tag{4.15}$$

Eq.(4.15) reveals that for a given PSL circuit, once the location and type of the noise sources are known, the PSD of the output of the circuit at a given base band frequency can be computed efficiently by solving the adjoint network. The above algorithm has been implemented in a computer program SLCNAP (Switched Linear Circuit Noise Analysis Program). An algorithm using the brute-force method has also been implemented for the purpose of comparison.

Table 4.1: Parameter values of SC low-pass

Parameter	Numerical value	Unit	Remark
C_1	51	pF	
C_2	45	pF	
R_{ON_1}	14.2	kΩ	Channel resistance of M1
R_{ON_2}	18.4	kΩ	Channel resistance of M2
f_s	5	kHz	Clock frequency
T_s	$1/f_s$	Second	Clock period
τ_1	$0.25T_s$	Second	Width of phase 1
τ_2	$0.25T_s$	Second	Width of phase 2
τ_3	$0.25T_s$	Second	Width of phase 3
τ_4	$0.25T_s$	Second	Width of phase 4

4.4 Numerical Examples

In this section, the average output noise power of several PSL circuits is analyzed using SLCNAP and the results are compared with measurements.

4.4.1 Noise of SC Low-pass

The schematic of a SC low-pass is shown in Fig. 4.6, and the parameters are given in Table 4.1. Only the thermal noise of MOSFET switches is considered. Five different input noise band widths, 250 kHz, 500 kHz, 1 MHz, 5 MHz ,and 10 MHz were considered. This corresponds to 50, 100, 200, 1000, and 2000 side bands to be folded over. The output noise power was calculated and the results are plotted in Fig. 4.7, together with the measurement data extracted from [12]. It is seen

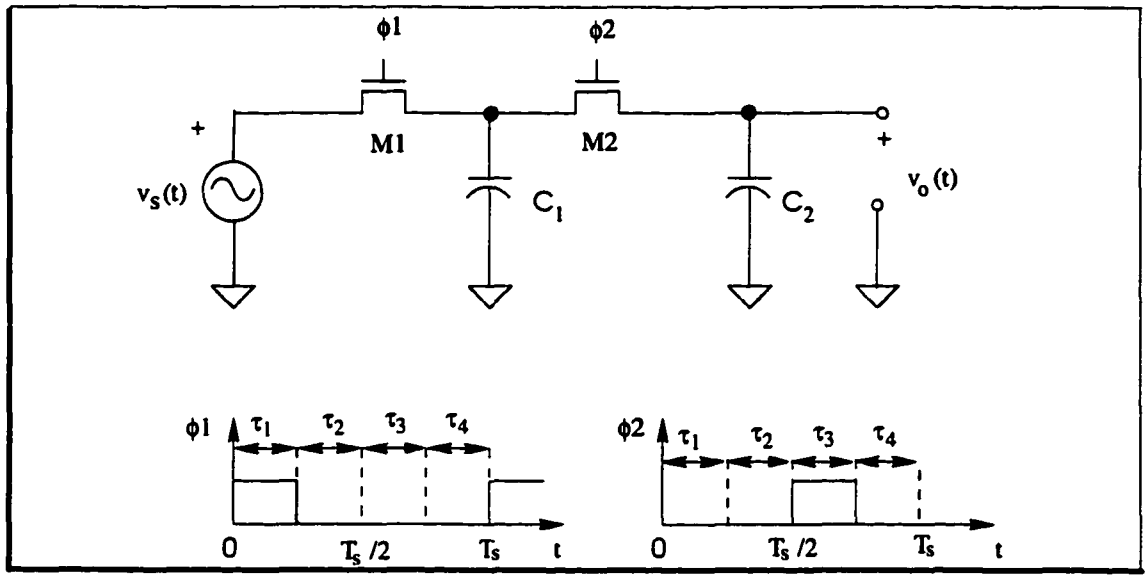


Figure 4.6: SC low-pass

that the output noise power increases initially with the increase in the number of side bands folded over. It eventually converges to a finite power irrespective of any further increase in the number of side bands. This observation reveals the existence of a finite band width of this circuit. The band width of the circuit is due to the low-pass mechanism formed by the channel resistance of the MOSFET switches and the shunting capacitances. It is the finite band width that results in a finite output noise power. It is also seen that simulation results agree very well with the measurements.

4.4.2 Noise of SC Integrator

The second example investigated is a SC integrator with four non-overlapping phases of equal width [13]. The schematic of the integrator is shown in Fig. 4.8, with the parameter values given in Table 4.2. The thermal and shot noise of the

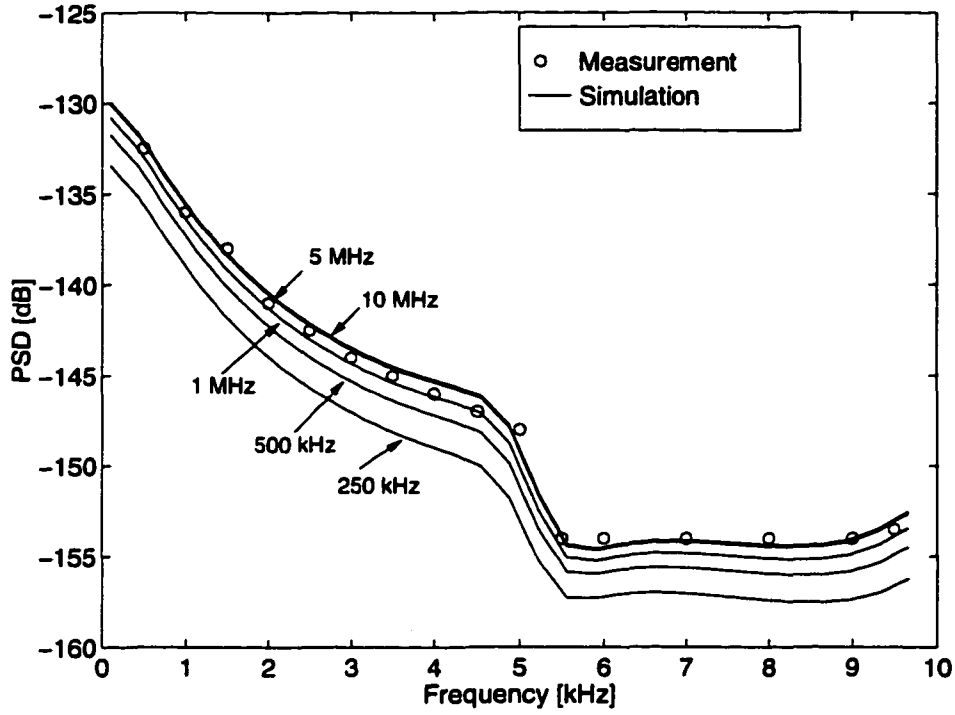


Figure 4.7: PSD of SC low-pass

op amp are represented by an equivalent noise-voltage generator $\overline{v^2}_n = 2kTR_{eq}\Delta f$. The flicker noise of the op amp and MOSFET switches is neglected. The model of the noise-free op amp is the same as that given in Chapter 3. The output noise power was calculated with input noise band width of 250 kHz, 500 kHz, 1 MHz, 5 MHz, and 10 MHz. This translates to 25, 50, 100, 500, and 1000 side bands that need to be folded over. The results are plotted in Fig. 4.9, together with the measurement data extracted from [13]. It is seen that the converged output noise power matches the measurements very well.

The efficiency of the proposed algorithm is demonstrated by comparing the CPU time of our algorithm with that of the brute-force method. Fig. 4.10 shows the CPU time of the proposed algorithm on computing the output noise power of the

Table 4.2: Parameter values of SC integrator

Parameter	Numerical value	Unit	Remark
C_1	10	pF	
C_2	10	pF	
R_{ON}	3.5	kΩ	Channel resistance
R_{eq}	1.55	MΩ	Equivalent resistor of op amp
R_o	100	Ω	Output resistance of op amp
f_s	10	kHz	Clock frequency
f_T	700	kHz	Unit-gain frequency of op amp
T_s	$1/f_s$	Second	Clock period
τ_1	$0.25T_s$	Second	Width of phase 1
τ_2	$0.25T_s$	Second	Width of phase 2
τ_3	$0.25T_s$	Second	Width of phase 3
τ_4	$0.25T_s$	Second	Width of phase 4

SC integrator with (a) only the noise of M1 considered and (b) all noise sources (noise of M_1, M_2, and op amp) considered. As can be seen that the amount of time spent in both cases is nearly the same. This observation validates our earlier statements on the advantages of using the transfer function theorem. Also observed that the cost of computation is linearly proportional to the number of side bands folded over.

The efficiency gained from the frequency reversal theorem over the brute-force method is not as intuitive as that from the transfer function theorem. To investigate the efficiency, the noise sources of M_2 and the op amp are turned off, and only the noise source of M_1 is activated. The output noise power of the integrator was

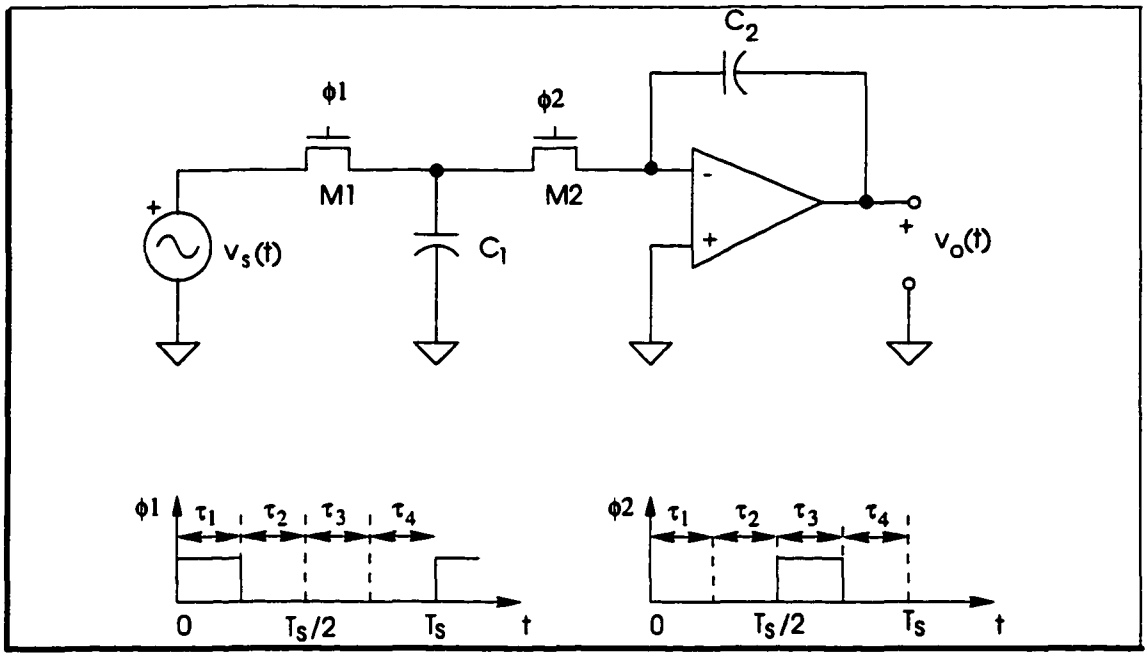


Figure 4.8: SC integrator

computed using both methods. Fig. 4.11 gives the quotient of the CPU time of our method to that of the brute-force with various step sizes used in computing $\mathbf{P}_k$ and $\mathbf{N}_k$. It is seen that the speedup obtained using the frequency reversal theorem is significant. Also, the speedup is step size dependent. It increases dramatically with the decrease in the step size. These results are expected since the lack of efficiency of the brute-force method is due to the repetitive calculation of $\mathbf{P}_k$ at both the base band and side band frequencies [2]. Also, the accuracy of the computation of $\mathbf{P}_k$ is inversely proportional to the step size whereas the computational cost is directly proportional to the step size. The deficiencies of the brute-force method are eliminated completely once the frequency reversal theorem is employed. For every base band frequency, the adjoint network is solved *only once* at the frequency. In

[2] $\mathbf{N}_k$ is input-independent and is computed only once.

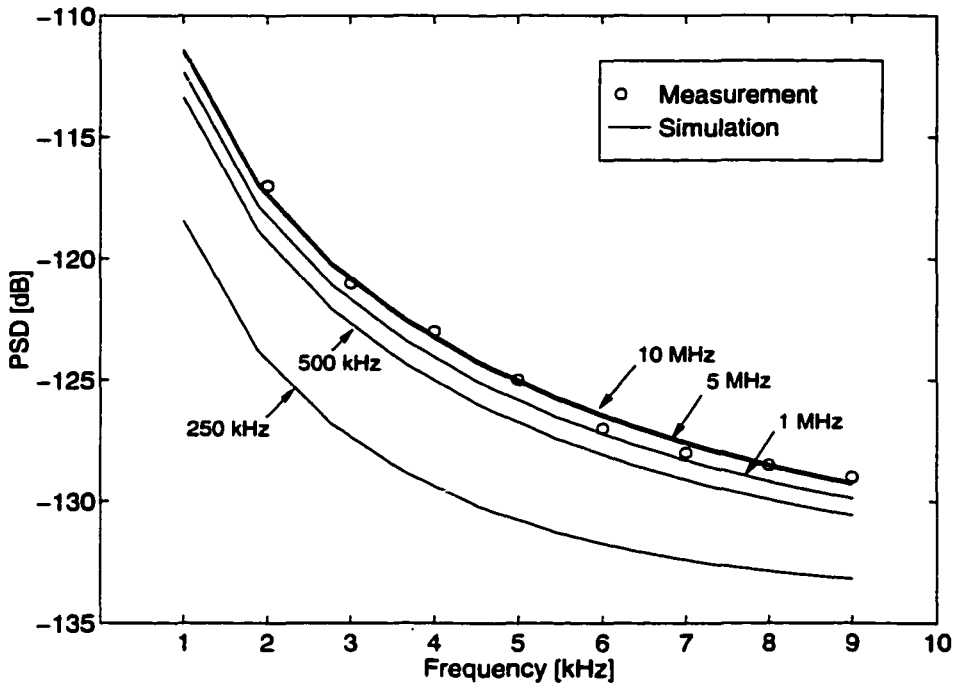


Figure 4.9: PSD of SC integrator

other words, one calculation of $\hat{\mathbf{P}}_k$ of the adjoint network per base band frequency is required. The corresponding high-order frequency components are obtained using LU-factorization and forward/backward substitutions. The computation required for LU-factorization is much less than that of $\mathbf{P}_k$, significant speedup is therefore achieved. For instance, at step size $T_s/200$ and with 100 sidebands considered, the adjoint network-based method is 15 times faster than the brute-force method when only *one* noise source is considered. For circuit containing 100 noise sources (which is quite a small circuit), the adjoint network-based method will be $15 \times 100 = 1500$ times faster !

Also observed is that with the in the number of sidebands to be folded over, the speed up plot in Fig. 4.11 flats. This is because the cost of LU-decomposition of $\mathbf{G}_k + j\omega\mathbf{C}_k$ start to dominate the total cost of computation.

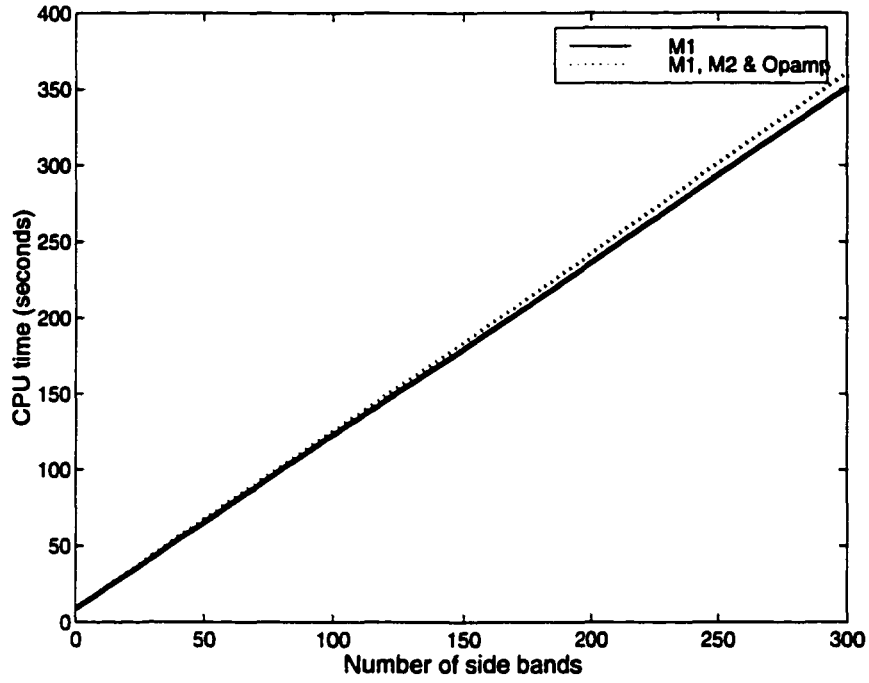


Figure 4.10: CPU time

4.4.3 Noise of SC Band-pass Filter

To further assess the effectiveness of the proposed algorithm, the noise of a SC band-pass filter was investigated. The schematic of the filter is shown in Fig.3.11. The MOSFET switches are modeled as a noisy linear resistor ($R_{on} = 80\Omega$) in series with an ideal switch. The input-referred thermal noise generated by the op amp is assumed to be 20 $nV/\sqrt{Hz}$ [3]. The flicker noise of the op amp is neglected for simplicity. The equivalent circuit of the filter with the noise sources included is shown in Fig.4.12. The MS value of noise sources is given by $\overline{i_{nk}^2} = 2kT/R_{on}\Delta f$, $k = 1, 2, ..., 16$. The output noise power of the band-pass filter is computed using the proposed algorithm and the results are plotted in Fig. 4.13, together with the simu-

[3]We have used the same data as those in [19] in order to compare with their results.

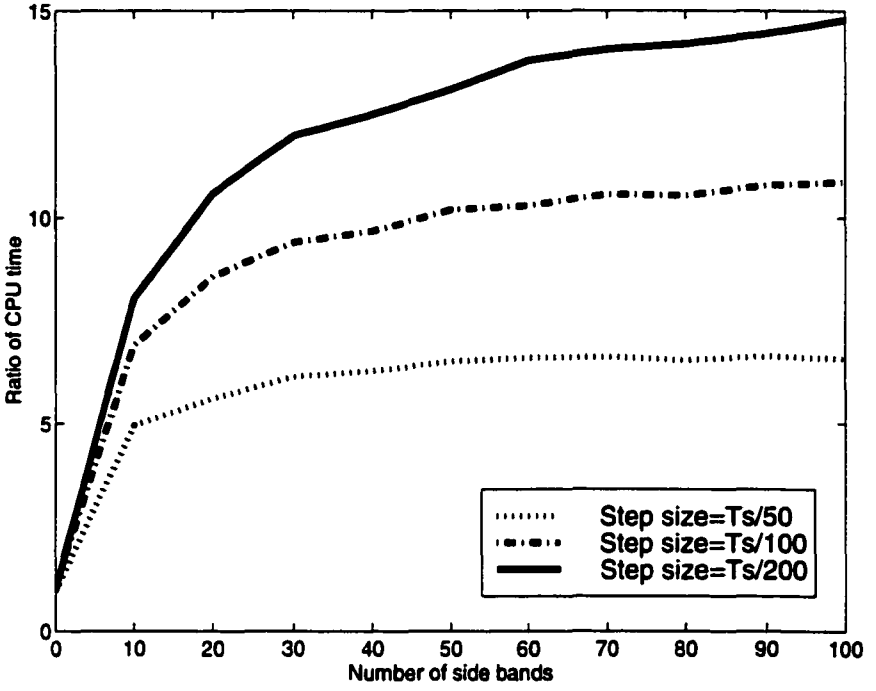


Figure 4.11: Speedup

lation results extracted from [19]. As can be seen that both results are comparable. It should be noted that in [19], a state-space approach was employed to compute the PSD of the band-pass. The excellent agreement once again demonstrates the effectiveness of the algorithm.

4.5 Summary

An efficient algorithm for noise analysis of multiphase periodically switched linear circuits was developed. The algorithm is exact and is orders of magnitude faster than the conventional brute-force method. The numerical results obtained using the proposed algorithm are compared with measurements and published results. An excellent agreement is observed.

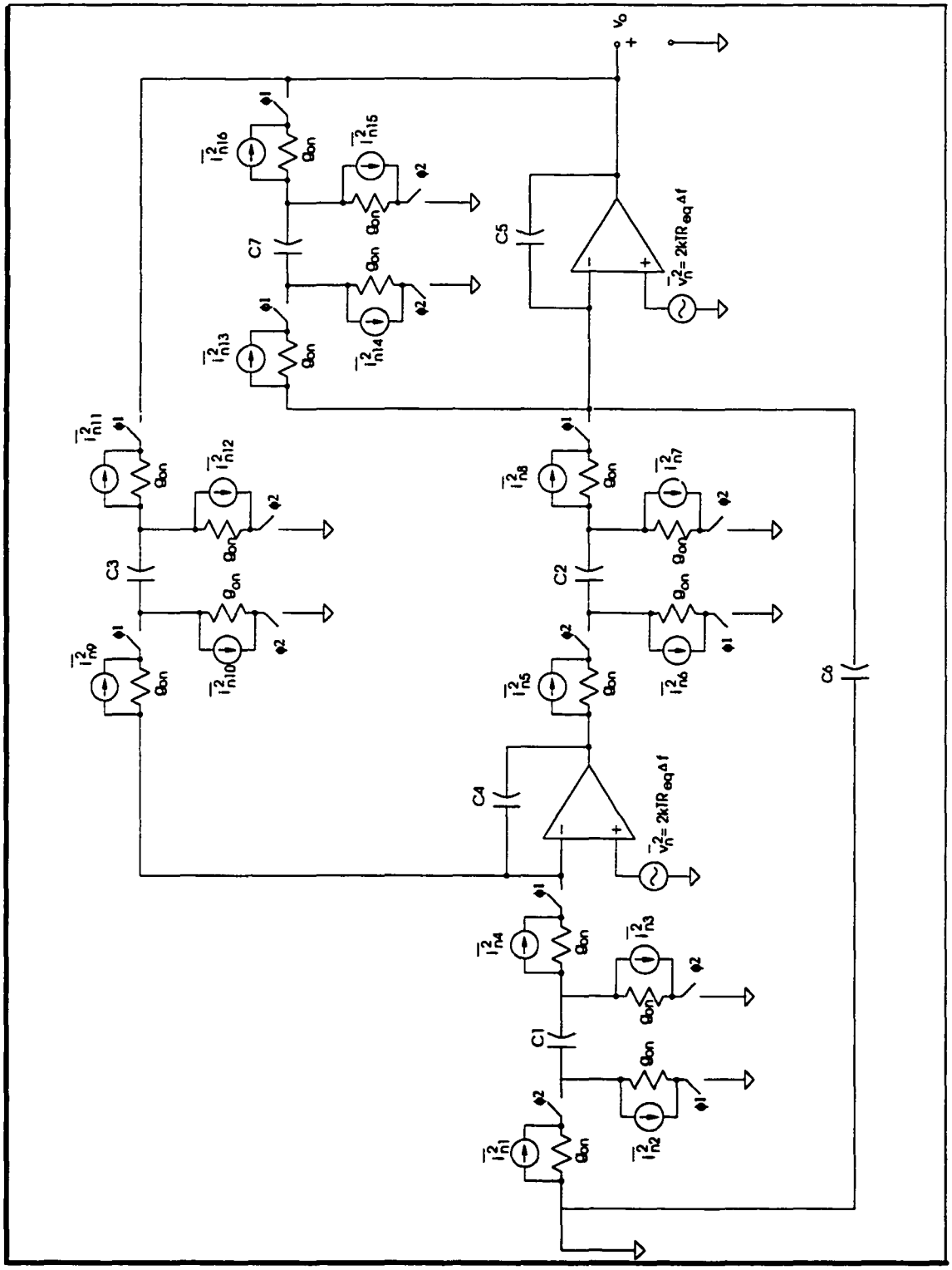


Figure 4.12: Equivalent circuit of band-pass filter

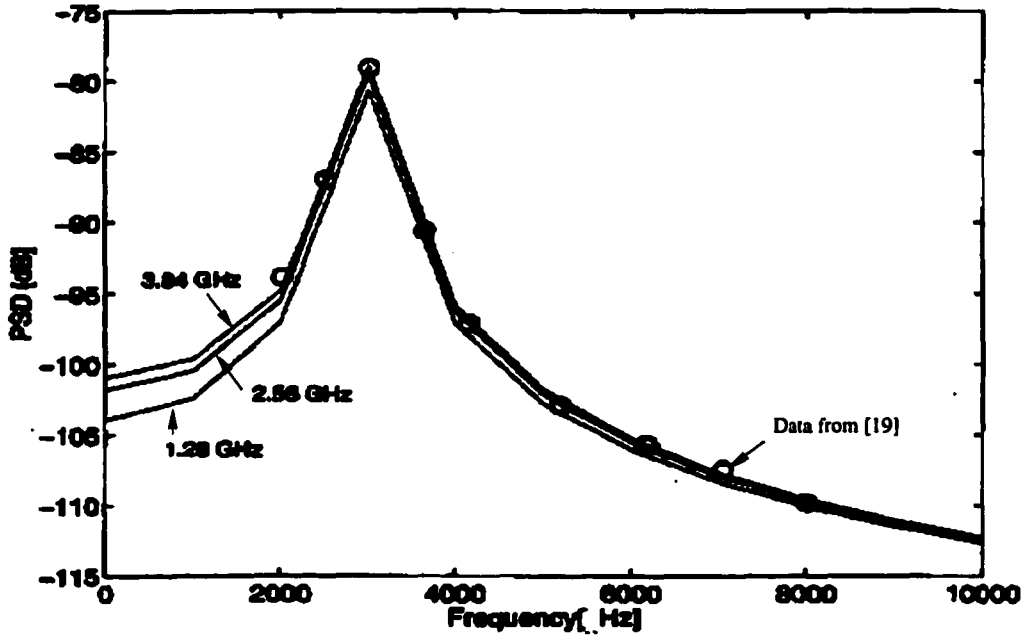


Figure 4.13: PSD of band-pass filter

Chapter 5

Sensitivity Analysis of PSL Circuits

This chapter investigates the frequency domain sensitivity of PSL circuits [138]. The incremental form of Tellegen's theorem for PSL circuits in phase domain is introduced. The frequency-domain sensitivity of PSL circuits is derived using the adjoint network approach. The sensitivity networks of PSL circuits are introduced and the sensitivity of PSL circuits is obtained using the sensitivity network approach. The theory is assessed using numerical examples and the results are compared with those from other CAD tools.

5.1 Introduction

Sensitivity is a mathematical measure that helps in understanding the effect of parameter variation on the response of electrical networks. It plays an essential role in circuit optimization and tolerance design [38]. Sensitivity considered in this

thesis is the change of the response of PSL circuits due to small variation in the element value of the circuit. Changes caused by external sources, such as clock jitter, are excluded. The normalized small-change sensitivity is defined as [39]

$$S_{\lambda}^{V_o}(\omega) = \frac{\lambda}{V_o(\omega)} \frac{\partial V_o(\omega)}{\partial \lambda} \qquad \lambda, V_o(\omega) \neq 0 \tag{5.1}$$

where $V_o(\omega)$ is the response, or other design objectives, such as the zeros or poles of the transfer function of a given circuit, λ is usually a circuit element to which the sensitivity is evaluated. Sensitivity to parasitic elements can also be defined in a similar but modified manner [39]. In practice, particularly in filter design, the normalized sensitivity of the magnitude of the response to circuit elements is often needed. This sensitivity is computed from

$$S_{\lambda}^{|V_o|}(\omega) = \frac{\lambda}{|V_o(\omega)|} \frac{\partial |V_o(\omega)|}{\partial \lambda} \tag{5.2}$$

where

$$\frac{\partial |V_o(\omega)|}{\partial \lambda} = |V_o(j\omega)| \mathrm{Re}\left[\frac{1}{V_o(j\omega)} \frac{\partial V_o(j\omega)}{\partial \lambda}\right] \tag{5.3}$$

To determine the quality of a designed circuit, the sensitivities of one variable with respect to a large number of the elements are usually required. An issue essential to sensitivity analysis is how to compute these sensitivities efficiently.

As reviewed in Chapter 1, various methods have been developed for sensitivity analysis of electronic circuits. Each has its pros and cons. The adjoint network approach has been proven to be one of the most efficient methods in computing sensitivities of the responses of linear time-invariant and Switched-capacitor circuits

with respect to all circuit elements. Its applications to sensitivity analysis of PSL circuits, however, have seldom been explored. This is mainly due to the fact that closed-form solutions exist for switched-capacitor networks while the solution of general PSL circuits rely upon numerical integration. In this chapter, we make use of the Tellegen's theorem for PSL circuit developed in Chapter 3 to facilitate sensitivity analysis and show that the sensitivity of PSL circuits can be represented by a summation of infinite series.

5.2 Incremental Form of Tellegen's Theorem in Phasor Domain

In steady state, let there be perturbations in the element values of a PSL circuit $\mathcal{N}$. The corresponding change of a network variable $v_b(t)$ of $\mathcal{N}$ is obtained from (3.4)

$$\Delta v_b(t) = \sum_{n=-\infty}^{\infty} \Delta V_b(\omega_o + n\omega_s) e^{j(\omega_o + n\omega_s)t} \tag{5.4}$$

where $\Delta V_b(\omega_o + n\omega_s)$ is the variation of the phasor of $v_b(t)$ at $\omega_o + n\omega_s$. The summation of (3.4) and (5.4) gives

$$v_b(t) + \Delta v_b(t) = \sum_{n=-\infty}^{\infty} \Big[V_b(\omega_o + n\omega_s) + \Delta V_b(\omega_o + n\omega_s) \Big] e^{j(\omega_o + n\omega_s)t}. \tag{5.5}$$

Thus, $v_b(t) + \Delta v_b(t)$, a perturbed network variable in time domain, is echoed with $V_b(\omega_o + n\omega_s) + \Delta V_b(\omega_o + n\omega_s), n = 0, \pm 1, \pm 2, ...$, a set of perturbed phasors in phasor domain. Substituting (5.5) into (3.12)

$$\sum_{b=1}^{B} \sum_{n=-\infty}^{\infty} \Big\{ [V_b(\omega_o + n\omega_s) + \Delta V_b(\omega_o + n\omega_s)] \hat{I}_b(\omega_o + n\omega_s)$$

$$- \left. [I_b(\omega_o + n\omega_s) + \Delta I_b(\omega_o + n\omega_s)]\hat{V}_b(\omega_o + n\omega_s) \right\} = 0. \quad (5.6)$$

Utilizing (3.12), we have

$$\sum_{b=1}^{B} \sum_{n=-\infty}^{\infty} \left[\Delta V_b(\omega_o + n\omega_s)\hat{I}_b(\omega_o + n\omega_s) - \Delta I_b(\omega_o + n\omega_s)\hat{V}_b(\omega_o + n\omega_s) \right] = 0. \quad (5.7)$$

Similarly, one can also show

$$\sum_{b=1}^{B} \sum_{n=-\infty}^{\infty} \Delta V_b(\omega_o + n\omega_s)\hat{I}_b(\omega_o + n\omega_s) = 0$$
$$\sum_{b=1}^{B} \sum_{n=-\infty}^{\infty} \Delta I_b(\omega_o + n\omega_s)\hat{V}_b(\omega_o + n\omega_s) = 0. \quad (5.8)$$

Eqs.(5.8) and (5.7) characterize the relation between the incremental changes of the phasors of the network variables of $\mathcal{N}$ and $\hat{\mathcal{N}}$. Note that in the above derivation, the adjoint network $\hat{\mathcal{N}}$ is not perturbed. The perturbation occurs in $\mathcal{N}$ only.

Theorem 5.1 (Incremental Form of Tellegen's Theorem for PSL Circuits) *For a given PSL circuit with input $e^{j\omega_o t}$ and clock frequency ω_s, the incremental form of Tellegen's theorem for PSL circuit in phasor domain is given by (5.7) and (5.8).*

5.3 Frequency-Domain Sensitivity of PSL Circuits

For the purpose of illustration, let a PSL circuit $\mathcal{N}$ consist of linear resistors (R), inductors (L), capacitors (C), ideal switches and VCVSs. Further, let the input of $\mathcal{N}$ be an ideal voltage source, $v_i(t) = e^{j\omega_o t}/(2\pi)$, and the output be the voltage across an open branch. The adjoint network $\hat{\mathcal{N}}$ of $\mathcal{N}$ is constructed in accordance with the guidelines given in Chapter 3, as shown in Fig. 5.1.

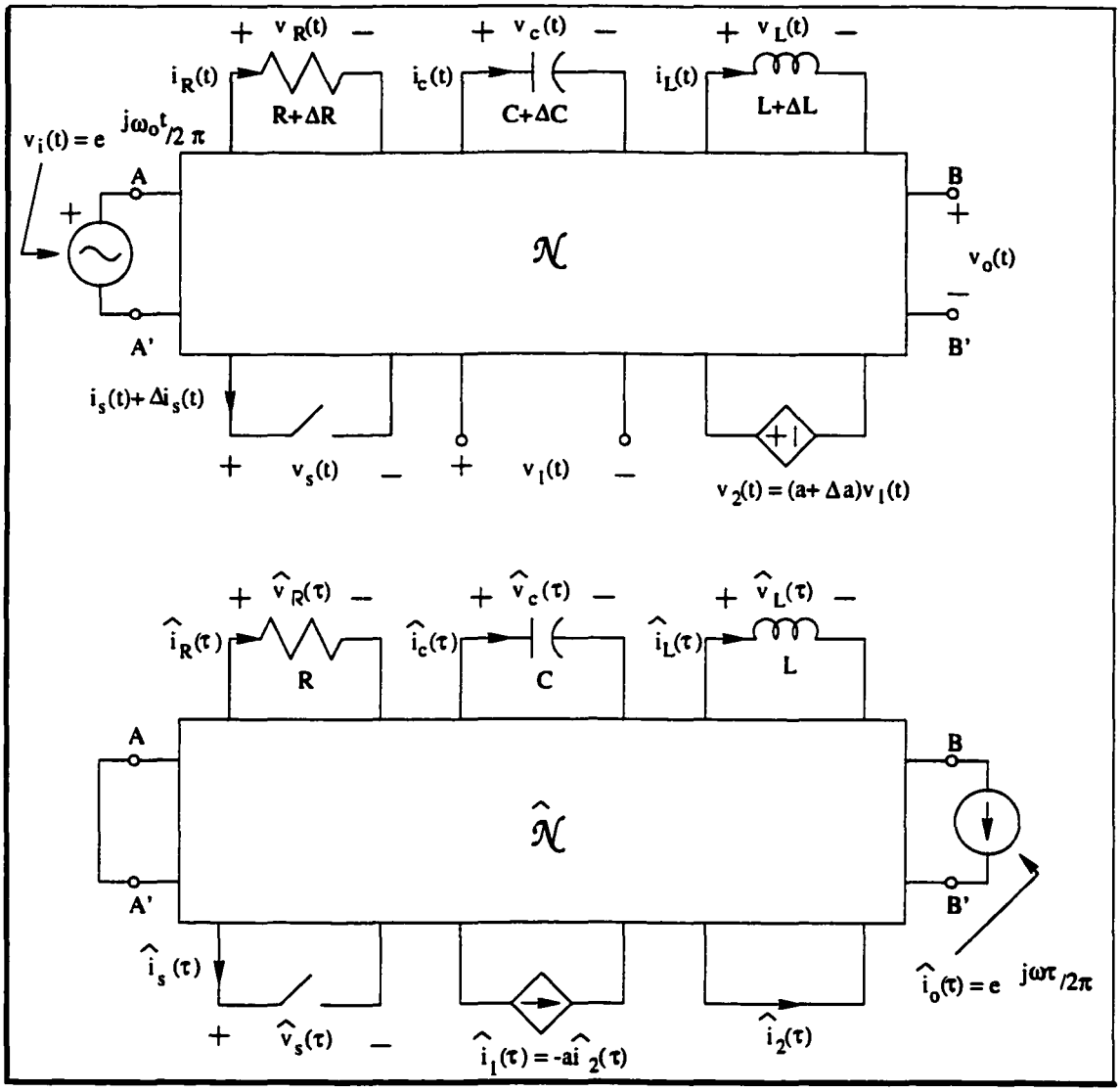


Figure 5.1: Sensitivity analysis of PSL circuits

5.3.1 Resistors

Consider a LTI resistor R in $\mathcal{N}$. Using Ohm's law, together with Theorem 3.1, and the identities of exponential series, we obtain the constitutive equations of the

resistor and its adjoint network in phasor domain

$$\begin{cases} V_R(\omega_o + n\omega_s) = RI_R(\omega_o + n\omega_s) \\ \hat{V}_R(\omega_o + n\omega_s) = R\hat{I}_R(\omega_o + n\omega_s) \end{cases} \qquad \forall n \tag{5.9}$$

Let there be a perturbation ΔR in R. The corresponding voltage variation is obtained by using Taylor series exapnsion

$$\begin{aligned} \Delta V_R &= \left[\frac{\partial V_R}{\partial R}\Delta R + \frac{\partial V_R}{\partial I_R}\Delta I_R\right] + \ldots + \left[\frac{\partial^n V_R}{\partial R^n}(\Delta R)^n + \frac{\partial^n V_R}{\partial I_R^n}(\Delta I_R)^n\right] + \ldots \\ &\approx I_R\Delta R + R\Delta I_R. \end{aligned} \tag{5.10}$$

Note we have neglected all high-order terms as we are only interested in small-change sensitivity. Making use of (5.9) and (5.10), we obtain

$$\begin{aligned} &\sum_{n=-\infty}^{\infty}\left[\Delta V_R(\omega_o + n\omega_s)\hat{I}_R(\omega_o + n\omega_s) - \Delta I_R(\omega_o + n\omega_s)\hat{V}_R(\omega_o + n\omega_s)\right] \\ \approx &\sum_{n=-\infty}^{\infty} I_R(\omega_o + n\omega_s)\hat{I}_R(\omega_o + n\omega_s)\Delta R. \end{aligned} \tag{5.11}$$

5.3.2 Capacitors and Inductors

Consider a LTI capacitor in $\mathcal{N}$. The phasor-domain representation of the constitutive equation of the capacitor is given by (3.22). The first-order approximation of the variation of the capacitor current due to a perturbation ΔC in C gives

$$\begin{aligned} &\sum_{n=-\infty}^{\infty}\left[\Delta V_C(\omega_o + n\omega_s)\hat{I}_C(\omega_o + n\omega_s) - \Delta I_C(\omega_o + n\omega_s)\hat{V}_C(\omega_o + n\omega_s)\right] \\ \approx &-\sum_{n=-\infty}^{\infty} j(\omega_o + n\omega_s)V_C(\omega_o + n\omega_s)\hat{V}_C(\omega_o + n\omega_s)\Delta C. \end{aligned} \tag{5.12}$$

In a like manner, one can show that for LTI inductors

$$\sum_{n=-\infty}^{\infty}\left[\Delta V_L(\omega_o+n\omega_s)\hat{I}_L(\omega_o+n\omega_s)-\Delta I_L(\omega_o+n\omega_s)\hat{V}_L(\omega_o+n\omega_s)\right]$$
$$\approx \sum_{n=-\infty}^{\infty} j(\omega_o+n\omega_s)I_L(\omega_o+n\omega_s)\hat{I}_L(\omega_o+n\omega_s)\Delta L. \tag{5.13}$$

5.3.3 Controlled Sources

Consider a VCVS with voltage gain a. Let the network variables of the controlling and controlled branches of the VCVS be identified with the subscripts "1" and "2", respectively. The adjoint network of the VCVS is a CCCS with controlling and controlled branches interchanged. The current gain of the CCCS is $-a$. Because $i_1(t)=0, \hat{v}_2(\tau)=0, v_2(t)=av_1(t)$, and $\hat{i}_1(\tau)=-a\hat{i}_2(\tau), \forall t,\tau$, using Corollary 3.1.1, we obtain, $I_1(\omega_o+n\omega_s)=0, \hat{V}_2(\omega_o+n\omega_s)=0$, $V_2(\omega_o+n\omega_s)=aV_1(\omega_o+n\omega_s)$, and $\hat{I}_1(\omega_o+n\omega_s)=-a\hat{I}_2(\omega_o+n\omega_s), \forall n$. As a result

$$\sum_{n=-\infty}^{\infty}\Big[\Delta V_1(\omega_o+n\omega_s)\hat{I}_1(\omega_o+n\omega_s)-\Delta I_1(\omega_o+n\omega_s)\hat{V}_1(\omega_o+n\omega_s)$$
$$+\ \Delta V_2(\omega_o+n\omega_s)\hat{I}_2(\omega_o+n\omega_s)-\Delta I_2(\omega_o+n\omega_s)\hat{V}_2(\omega_o+n\omega_s)\Big]$$
$$\approx \sum_{n=-\infty}^{\infty} V_1(\omega_o+n\omega_s)\hat{I}_2(\omega_o+n\omega_s)\Delta a. \tag{5.14}$$

Expressions for other types of controlled sources can be derived in a similar manner.

5.3.4 Ideal Switches

Let there be a perturbation in the element values of $\mathcal{N}$ such that the voltage across and current through an ideal switch, denoted respectively by $v_s(t)$ and $i_s(t)$,

vary from $v_s(t)$ to $v_s(t) + \Delta v_s(t)$,and $i_s(t)$ to $i_s(t) + \Delta i_s(t)$, respectively. If the switch is CLOSED at t, then, $v_s(t) = 0$ and $v_s(t) + \Delta v_s(t) = 0$, irrespective of the perturbation. Moreover, since its counterpart in $\hat{\mathcal{N}}$ is also a CLOSED switch at τ, we have $\hat{v}_s(\tau) = 0$. As a result

$$\Delta v_s(t)\hat{i}_s(\tau) - \Delta i_s(t)\hat{v}_s(\tau) = 0. \tag{5.15}$$

Similarly, one can show that (5.15) also holds if the switch is OPEN. We conclude that (5.15) is valid $\forall t, \tau$. We are therefore in the position to represent (5.15) using (3.4) and (5.4). This gives

$$\sum_{n=-\infty}^{\infty} \left[\Delta V_s(\omega_o + n\omega_s)\hat{I}_s(\omega_o + n\omega_s) - \Delta I_s(\omega_o + n\omega_s)\hat{V}_s(\omega_o + n\omega_s)\right] = 0. \tag{5.16}$$

5.3.5 Input and Output

Because the input of $\mathcal{N}$ is an ideal voltage source and the corresponding branch in $\hat{\mathcal{N}}$ is a short-circuit, $\Delta v_i(t) = 0, \hat{v}_i(\tau) = 0, \forall t, \tau$. From Corollary 3.1.1, $\Delta V_i(\omega_o + n\omega_s) = 0$, $\hat{V}_i(\omega_o + n\omega_s) = 0, \forall n$. As a result

$$\sum_{n=-\infty}^{\infty} \left[\Delta V_i(\omega_o + n\omega_s)\hat{I}_i(\omega_o + n\omega_s) - \Delta I_i(\omega_o + n\omega_s)\hat{V}_i(\omega_o + n\omega_s)\right] = 0. \tag{5.17}$$

The output branch of $\mathcal{N}$ is an open-circuit, $i_o(t) = 0, \forall t$. This results in $\Delta I_o(\omega_o + n\omega_s) = 0, \forall n$. Further, because the input of $\hat{\mathcal{N}}$ is a single tone of unity strength at ω_o

$$\hat{I}_o(\omega_o + n\omega_s) = \begin{cases} 1 & \text{if } n = 0 \\ 0 & \text{otherwise} \end{cases}.$$

Thus

$$\sum_{n=-\infty}^{\infty}\left[\Delta V_o(\omega_o+n\omega_s)\hat{I}_o(\omega_o+n\omega_s)-\Delta I_o(\omega_o+n\omega_s)\hat{V}_o(\omega_o+n\omega_s)\right]=\Delta V_o(\omega_o). \quad (5.18)$$

Substituting (5.11), (5.12), (5.13), (5.14), (5.16), (5.17) and (5.18) into (5.7), we obtain

$$\begin{aligned}\Delta V_o(\omega_o)\approx\ & -\sum_R\left[\sum_{n=-\infty}^{\infty} I_R(\omega_o+n\omega_s)\hat{I}_R(\omega_o+n\omega_s)\right]\Delta R\\ & +\sum_C\left[\sum_{n=-\infty}^{\infty} j(\omega_o+n\omega_s)V_C(\omega_o+n\omega_s)\hat{V}_C(\omega_o+n\omega_s)\right]\Delta C\\ & -\sum_L\left[\sum_{n=-\infty}^{\infty} j(\omega_o+n\omega_s)I_L(\omega_o+n\omega_s)\hat{I}_L(\omega_o+n\omega_s)\right]\Delta L\\ & -\sum_{VCVS}\left[\sum_{n=-\infty}^{\infty} V_1(\omega_o+n\omega_s)\hat{I}_2(\omega_o+n\omega_s)\right]\Delta a. \end{aligned} \quad (5.19)$$

Representing the variation of the output of $\mathcal{N}$ at ω_o using Taylor series expansion gives

$$\begin{aligned}\Delta V_o(\omega_o) &= \sum_{n=1}^{\infty}\left[\sum_R\frac{\partial^n V_o}{\partial R^n}(\Delta R)^n+\sum_C\frac{\partial^n V_o}{\partial C^n}(\Delta C)^n+\sum_L\frac{\partial^n V_o}{\partial L^n}(\Delta L)^n\right.\\ &\quad\left.+\sum_{VCVS}\frac{\partial^n V_o}{\partial a^n}(\Delta a)^n\right]\\ &\approx \sum_R\frac{\partial V_o}{\partial R}\Delta R+\sum_C\frac{\partial V_o}{\partial C}\Delta C+\sum_R\frac{\partial V_o}{\partial L}\Delta L+\sum_R\frac{\partial V_o}{\partial a}\Delta a \end{aligned} \quad (5.20)$$

We have neglected the high-order terms in simplifying (5.20) for the reason given earlier. Comparing (5.19) with (5.20), we obtain the sensitivities of the response of the circuit with respect to the elements. The results are given in Table 5.1.

Table 5.1: Sensitivity of PSL circuits

Element	Value	Sensitivity
Resistor	R	$\frac{\partial V_o(\omega_o)}{\partial R} = -\sum_{n=-\infty}^{\infty} I_R(\omega_o + n\omega_s)\hat{I}_R(\omega_o + n\omega_s)$
Capacitor	C	$\frac{\partial V_o(\omega_o)}{\partial C} = \sum_{n=-\infty}^{\infty} j(\omega_o + n\omega_s)V_C(\omega_o + n\omega_s)\hat{V}_C(\omega_o + n\omega_s)$
Inductor	L	$\frac{\partial V_o(\omega_o)}{\partial L} = -\sum_{n=-\infty}^{\infty} j(\omega_o + n\omega_s)I_L(\omega_o + n\omega_s)\hat{I}_L(\omega_o + n\omega_s)$
VCVS	a	$\frac{\partial V_o(\omega_o)}{\partial a} = -\sum_{n=-\infty}^{\infty} V_1(\omega_o + n\omega_s)\hat{I}_2(\omega_o + n\omega_s)$
VCCS	g	$\frac{\partial V_o(\omega_o)}{\partial g} = \sum_{n=-\infty}^{\infty} V_1(\omega_o + n\omega_s)\hat{V}_2(\omega_o + n\omega_s)$
CCVS	r	$\frac{\partial V_o(\omega_o)}{\partial r} = \sum_{n=-\infty}^{\infty} I_1(\omega_o + n\omega_s)\hat{I}_2(\omega_o + n\omega_s)$
CCCS	β	$\frac{\partial V_o(\omega_o)}{\partial \beta} = -\sum_{n=-\infty}^{\infty} I_1(\omega_o + n\omega_s)\hat{V}_2(\omega_o + n\omega_s)$

A few comments are made with respect to Table 5.1 : (a) Once the frequency response of $\mathcal{N}$, denoted by $\mathbf{V}(\omega_o + n\omega_s)$ and that of $\hat{\mathcal{N}}$, denoted by $\hat{\mathbf{V}}(\omega_o + n\omega_s)$, are available, the sensitivity of the response with respect to a element λ of $\mathcal{N}$ whose location is specified by a constant vector $\mathbf{g}_\lambda$ is obtained from

$$\frac{\partial V_o(\omega_o)}{\partial \lambda} = \sum_{n=-\infty}^{\infty} K_\lambda(\omega_o + n\omega_s)\mathbf{g}_\lambda^T \mathbf{V}(\omega_o + n\omega_s)\hat{\mathbf{V}}^T(\omega_o + n\omega_s)\mathbf{g}_\lambda \qquad (5.21)$$

where $K_\lambda(\omega_o + n\omega_s)$ is an element-type dependent parameter. For different elements, only $\mathbf{g}_\lambda$ and $K_\lambda(\omega_o + n\omega_s)$ need to be changed. Also, only one frequency analysis of $\mathcal{N}$ and $\hat{\mathcal{N}}$ at ω_o is required. The method is much more efficient as compared with the brute-force method in which the circuit must be solved each time the element to which the sensitivity is evaluated changes. (b) Both the base band and side band

components of the network variables contribute to sensitivity evaluated in the base band, as illustrated in Fig. 5.2. This is a unique characteristic of PSL circuits. (c) If there is no switching, i.e. $n\equiv 0$, Table 5.1 will simplify to the familiar sensitivities of LTI circuits. (d) For practical PSL circuits, the convergence of sensitivity is ensured by the effect of the parasitic capacitances at high frequencies because the amplitude of network variables decreases asymptotically with frequency, and eventually dies off. The above development is summarized in the following theorem.

Theorem 5.2 (Sensitivity Theorem of PSL Circuits) *For a given PSL circuit with input $e^{j\omega_o t}/(2\pi)$ and clock frequency ω_s, the sensitivities of the response with respect to circuit elements at a base band frequency ω_o are given by Table 5.1.*

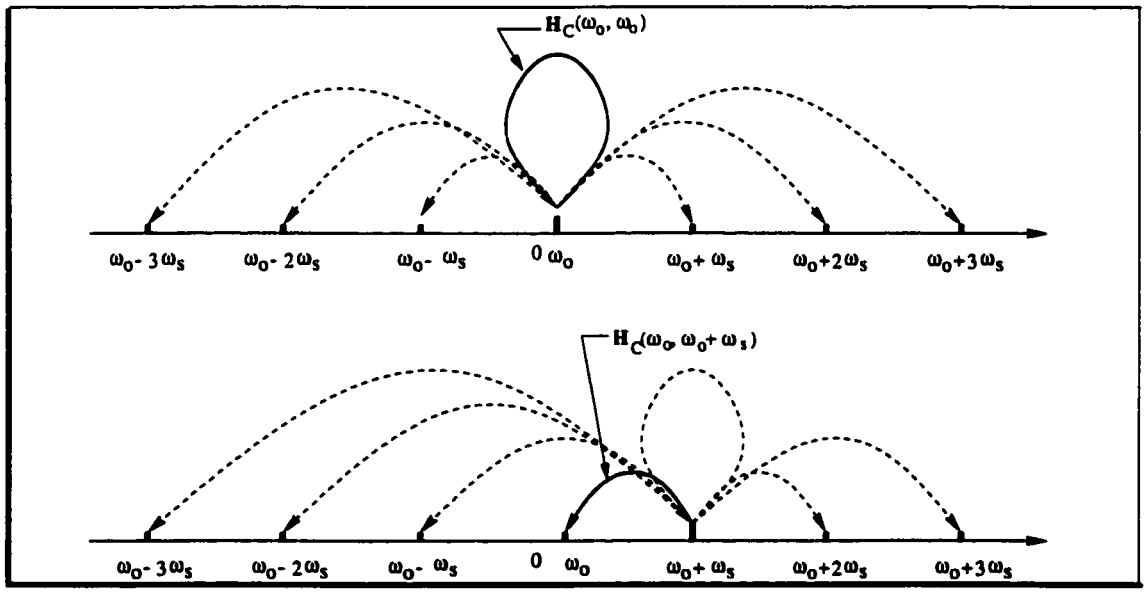


Figure 5.2: Fold-over effect in sensitivity analysis of PSL circuits

5.4 Sensitivity Analysis of PSL Circuits Using The Sensitivity Network Approach

5.4.1 Sensitivity Networks of PSL Circuits

In the preceding section, the sensitivity theorem of PSL circuits was developed rigorously. In this section, we show that the same results can also be obtained in a more illustrative manner by using a technique known as sensitivity network initially developed by Trick for LTI circuits [25] and Davis for switched-capacitor networks [27,28]. The essence of this approach is as follows : The fundamental laws governing a lumped circuit $\mathcal{N}$ are KCL and KVL [39]

$$\begin{cases} \mathbf{A}\mathbf{i}_b(t) = 0 \\ \mathbf{A}^T\mathbf{v}_n(t) = \mathbf{v}_b(t) \end{cases} \tag{5.22}$$

where $\mathbf{A}$ is the incidence matrix, $\mathbf{i}_b(t)$ and $\mathbf{v}_b(t)$ are the branch current and voltage vectors, respectively, $\mathbf{v}_n(t)$ is the nodal voltage vector. Differentiating (5.22) with respect to a circuit element λ_1 gives

$$\begin{cases} \mathbf{A}\dfrac{\partial \mathbf{i}_b(t)}{\partial \lambda_1} = 0 \\ \mathbf{A}^T\dfrac{\partial \mathbf{v}_n(t)}{\partial \lambda_1} = \dfrac{\partial \mathbf{v}_b(t)}{\partial \lambda_1} \end{cases} \tag{5.23}$$

Eqs.(5.23) are the governing equations of a derived network $\mathcal{N}_{\lambda_1}$ whose network variables are the derivatives of those of $\mathcal{N}$ with respect to λ_1. $\mathcal{N}_{\lambda_1}$ is called the sensitivity network of λ_1. Clearly, the solution of $\mathcal{N}_{\lambda_1}$ gives the sensitivity of $\mathcal{N}$ with respect to λ_1. Note that by changing the element λ_1 to λ_2, we obtain the sensitivity network of λ_2. Continuing this process, one can derive all sensitivity networks.

Important to note that these sensitivity networks have the same topology as that of $\mathcal{N}$. As an illustration, consider a capacitor C. Since $i_C(t) = C\frac{dv_C(t)}{dt}$, to derive the sensitivity network of the capacitor, we differentiate the above expression with respect to C

$$\frac{di_C(t)}{dC} = C\frac{d}{dt}\left(\frac{dv_C(t)}{dC}\right) + \frac{dv_C(t)}{dt} \tag{5.24}$$

The variables associated with the capacitor in the corresponding sensitivity network are the sensitivity current $\frac{di_C(t)}{dC}$ and sensitivity voltage $\frac{dv_C(t)}{dC}$. The capacitance remains the same. The constitutive equation of the capacitor in the sensitivity network is the same as that in the original circuit. An ideal current source $\frac{dv_C(t)}{dt}$ is added in parallel with the capacitor. It is the input of the corresponding sensitivity network. The substitution for the capacitor in the corresponding sensitivity network is given in Fig. 5.3. Similarly, one can derive the substitutions for other basic elements in the corresponding sensitivity networks.

5.4.2 Sensitivity Analysis of PSL Circuits Using The Sensitivity Network Approach

The sensitivity network concept of LTI circuits can be extended to general PSL circuits. To compute the sensitivity of the response of a PSL circuit $\mathcal{N}$ with respect to a capacitor C, the corresponding sensitivity network $\mathcal{N}_C$ is needed. The input of $\mathcal{N}_C$ is a current source of value $dv_C(t)/dt$ connected in parallel with C. From Theorem 3.1,

$$v_C(t) = \sum_{n=-\infty}^{\infty} V_C(\omega_o + n\omega_s)e^{j(\omega_o+n\omega_s)t} \tag{5.25}$$

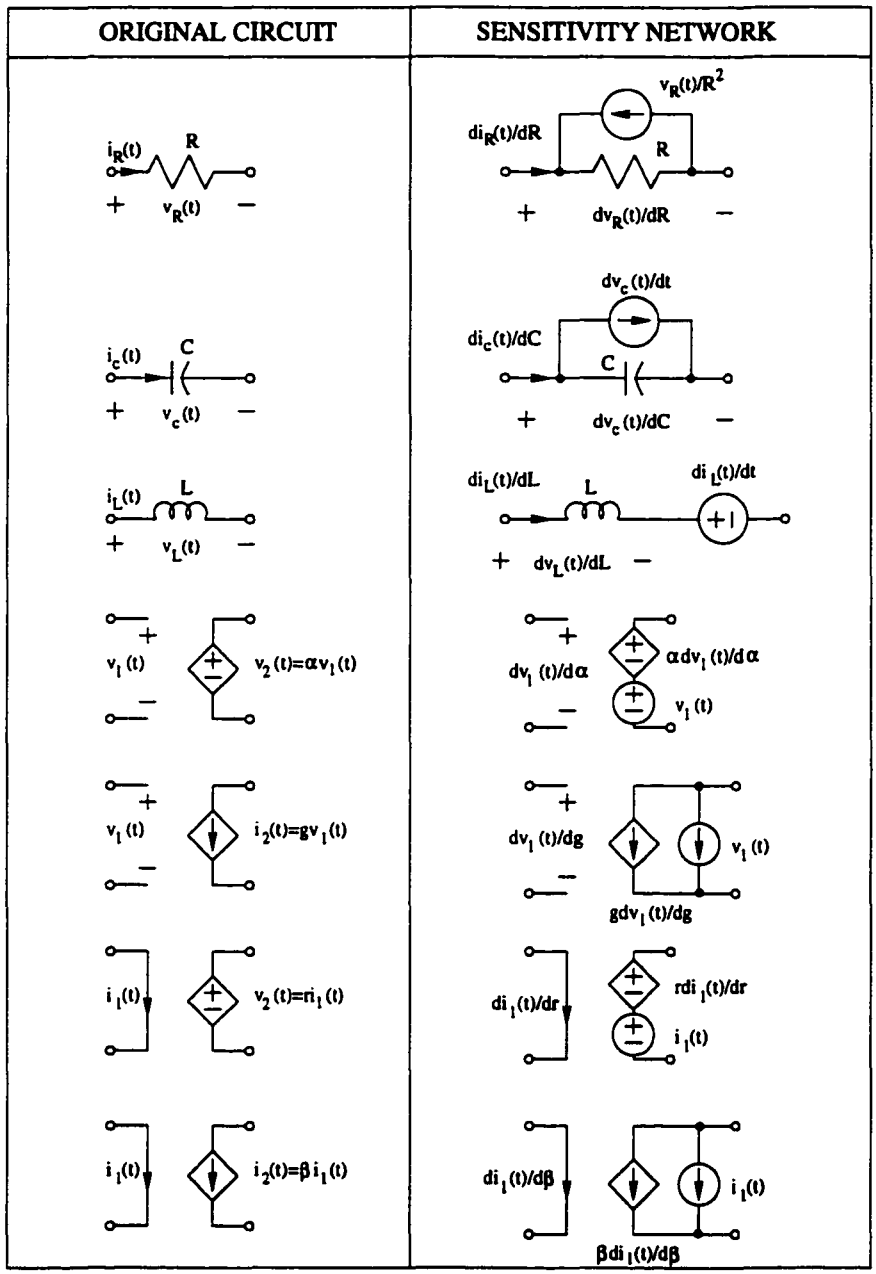


Figure 5.3: Sensitivity networks of basic elements

therefore

$$\frac{dv_C(t)}{dt} = \sum_{n=-\infty}^{\infty} j(\omega_o + n\omega_s)V_C(\omega_o + n\omega_s)e^{j(\omega_o+n\omega_s)t} \tag{5.26}$$

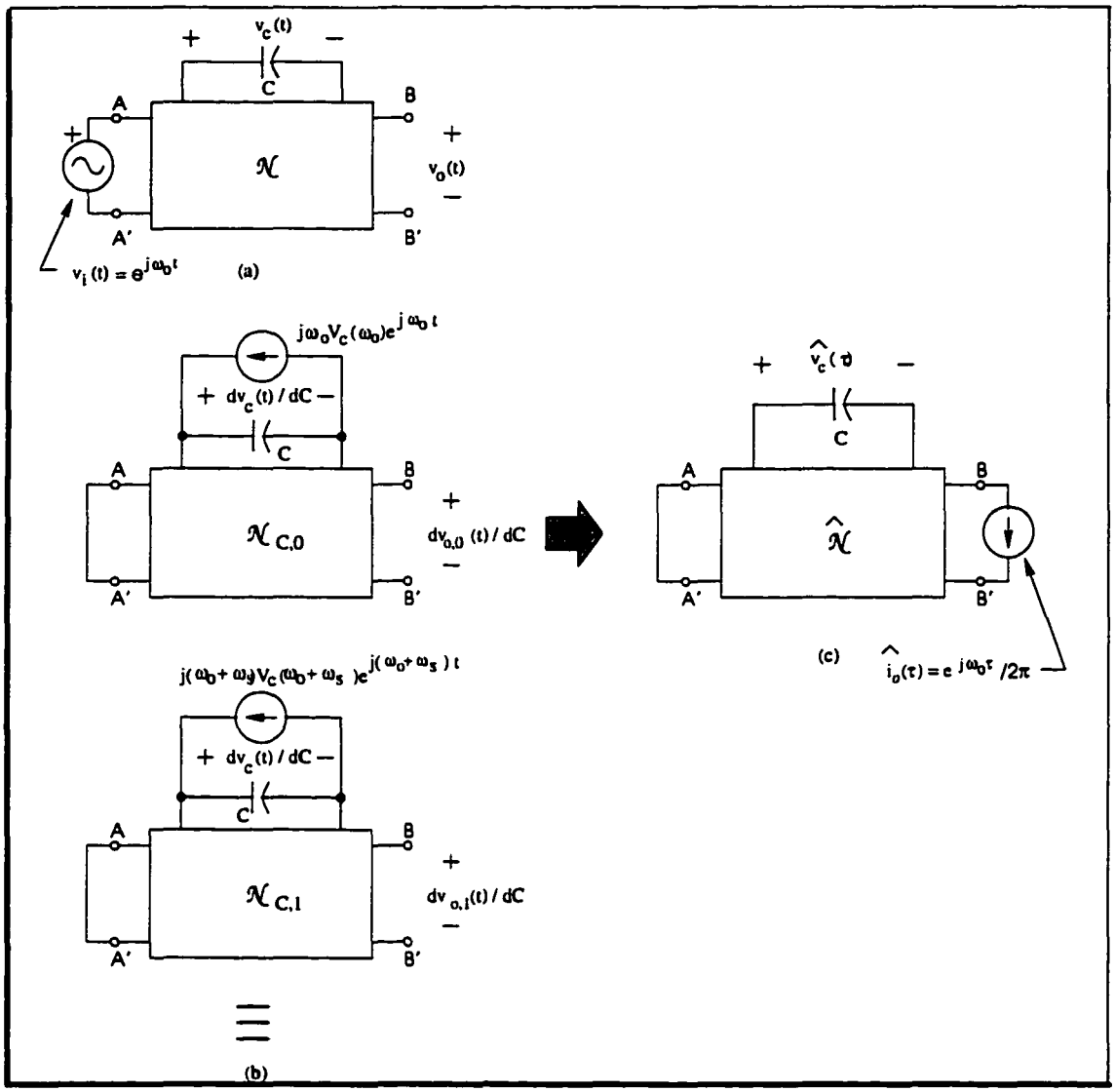


Figure 5.4: Sensitivity network of PSL circuits (a) PSL circuit $\mathcal{N}$, (b) Sensitivity networks $\mathcal{N}_{C,k}, k = 0, \pm 1, ...$, (c) Adjoint network of $\mathcal{N}$

This is equivalent to have an infinite number of current sources of value $j(\omega_o + n\omega_s)V_C(\omega_o + n\omega_s)e^{j(\omega_o+n\omega_s)t}$, $n = 0, \pm 1, \pm 2, ...$, connected in parallel with the capacitor, as depicted in Fig. 5.4. Each of these current sources generates an output that also contains an infinite number of frequency components. The complete out-

put of $\mathcal{N}_C$ at ω_o is obtained by summing up the contributions of all of the added current sources at ω_o

$$\frac{\partial V_o(\omega_o)}{\partial C} = \sum_{n=-\infty}^{\infty} \mathcal{H}_C(\omega_o, \omega_o + n\omega_s) j(\omega_o + n\omega_s) V_C(\omega_o + n\omega_s). \tag{5.27}$$

where $\mathcal{H}_C(\omega_o, \omega_o + n\omega_s)$ is the aliasing transfer function from the current source at $\omega_o + n\omega_s$ to the output of $\mathcal{N}_C$ at ω_o. A careful inspection shows that there exist two difficulties in solving (5.27). First, to obtain $\mathcal{H}_C(\omega_o, \omega_o + n\omega_s)$, $\mathcal{N}_C$ has to be solved at $\omega_o + n\omega_s, n = 0, \pm 1, ...$ Secondly, if the sensitivities of the response with respect to M elements are required, then a total of M sensitivity networks have to be constructed and solved. This amounts to excessive computation. To avert these difficulties, we notice that these sensitivity networks are topologically identical. This suggests that only one common adjoint network $\hat{\mathcal{N}}_C$ needs to be constructed for all sensitivity networks. In the above capacitor case, the magnitude of $\mathcal{H}_C(\omega_o, \omega_o + n\omega_s)$ is equal to that of the nth-order frequency component of the capacitor voltage in the adjoint network $\hat{\mathcal{N}}_C$, provided that the input of $\mathcal{N}_C$ is of unity strength. This is the result of Theorem 3.3. Because the adjoint network of $\mathcal{N}_C$ is the same as that of $\mathcal{N}$, we have

$$\mathcal{H}_C(\omega_o, \omega_o + n\omega_s) = \hat{V}_C(\omega_o + n\omega_s). \tag{5.28}$$

where $\hat{V}_C(\omega_o + n\omega_s)$ is the nth-order frequency component of the voltage of the capacitor in $\hat{\mathcal{N}}$. Substituting (5.28) into (5.27) gives

$$\frac{\partial V_o(\omega_o)}{\partial C} = \sum_{n=-\infty}^{\infty} j(\omega_o + n\omega_s) \hat{V}_C(\omega_o + n\omega_s) V_C(\omega_o + n\omega_s). \tag{5.29}$$

Note (5.29) is identical to the result given in Table 5.1. The above analysis reveals that the sensitivities of PSL circuits developed using the adjoint network approach can also be derived using the sensitivity network technique. The differences between the sensitivity networks of LTI and PSL circuits also become apparent. For each element of a LTI circuit, there is only one corresponding sensitivity network. However, for each element of a PSL circuit, there are an infinite number of sensitivity networks.

5.5 Numerical Examples

In this section, the sensitivities of the responses of several PSL circuits are analyzed using SLCSAP (Switched Linear Circuits Sensitivity Analysis Program, a computer program developed as a part of this research work) and the results are compared with those obtained from other CAD tools.

5.5.1 Sensitivity of Stray-insensitive Switched-capacitor Integrator

Consider a stray-insensitive switched capacitor integrator. The schematic of the integrator is shown Fig. 5.5, and the parameter values are given in Table 5.2. The models for MOSFET switches and the op amp are the same as those given in Chapter 3. The sensitivity of the output with respect to C_1 was computed using the proposed method and the results are plotted in Figs.5.6 and 5.7. As observed that both the real and imaginary parts of the sensitivity converges rapidly. For the purpose of comparison, the same sensitivity was computed using Watsnap [47] and the result is given here : $\partial V_o/\partial C_1 = -5.4817\times10^3 + j1.5158\times10^4$. To assist

Table 5.2: Parameter values of stray-insensitive Switched-capacitor integrator

Parameter	Numerical value	Unit	Remark
C_1	0.01592	μF	
C_2	10	μF	
R_{ON}	3.5	kΩ	Channel resistance
R_s	100	Ω	Source resistance
R_o	100	Ω	Output resistance of op amp
f_s	100	kHz	Clock frequency
T_s	$1/f_s$	Second	Clock period
f_T	700	kHz	Unit-gain freq. of op amp
τ_1	$0.488T_s$	Second	Width of phase 1
τ_2	$0.512T_s$	Second	Width of phase 2

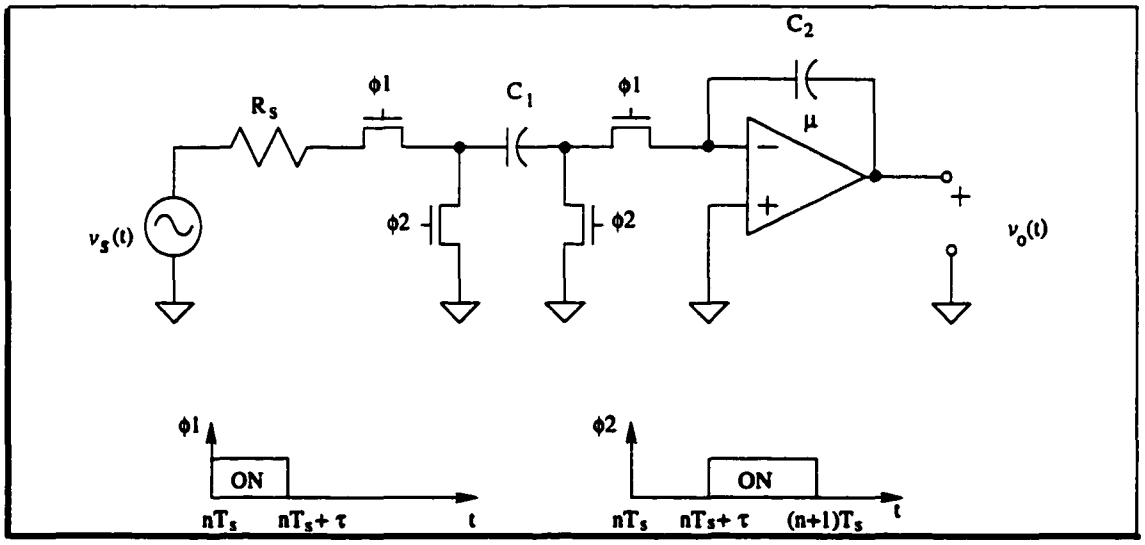


Figure 5.5: Stray-insensitive Switched-capacitor integrator

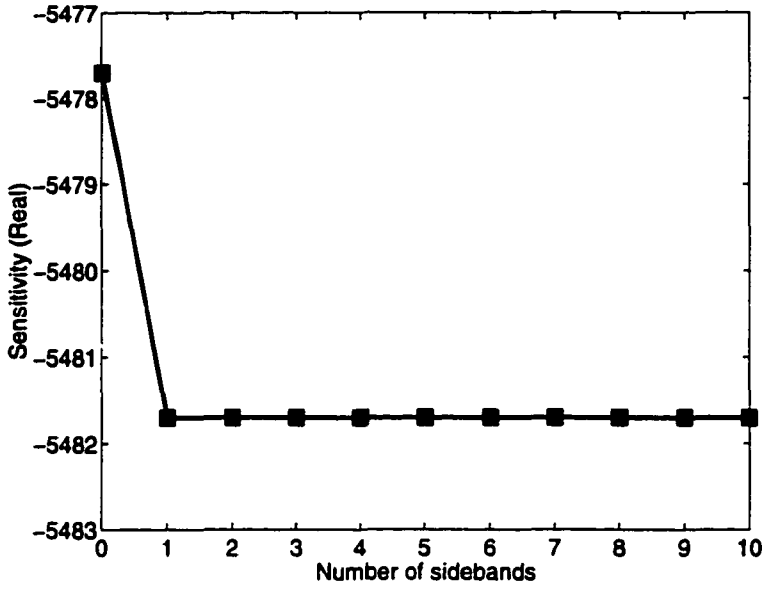


Figure 5.6: Sensitivity of the response of integrator to C1 (Real part)

analysis, we define the relative difference ϵ between the sensitivities computed from Watsnap and the proposed method as follows

$$\epsilon = \left| \frac{\partial V_o/\partial C_{Watsnap} - \partial V_o/\partial C_{Proposed}}{\partial V_o/\partial C_{Watsnap}} \right| \tag{5.30}$$

For this example, the relative difference is -62.38 dB with only base band components considered and -92.48 dB with one side band component considered. The normalized sensitivity of the magnitude of the response to C_1 is shown in Fig. 5.8. Clearly seen is that the normalized sensitivity converges as well. To further illustrate the convergence of sensitivity, the voltages of C_1 in both the integrator and its adjoint network are shown in Figs. 5.9 and 5.10 (20 side bands), respectively. It is seen that the voltages decrease rapidly with frequency. As a result, only a few side bands are needed to yield a converged sensitivity.

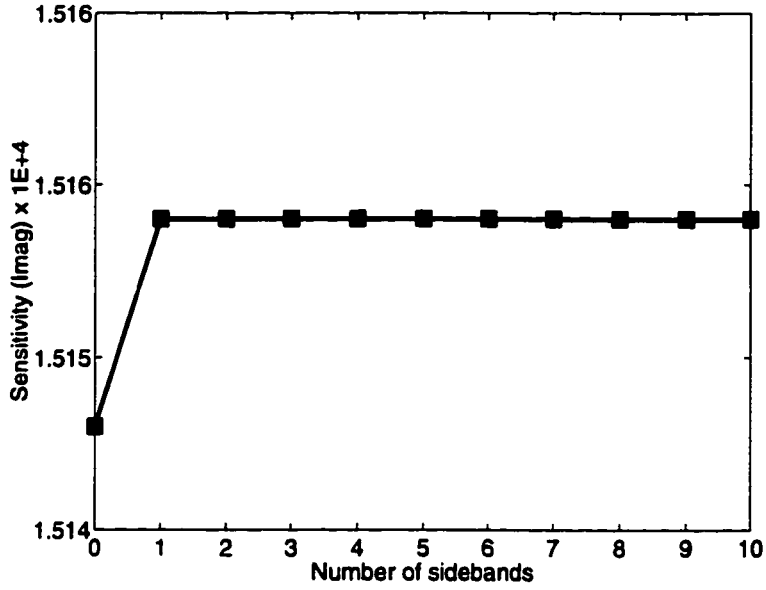


Figure 5.7: Sensitivity of the response of integrator to C1 (Imaginary part)

5.5.2 Sensitivity of Switched-capacitor Band pass Filter

Consider a switched capacitor band pass filter. The schematic of the filter is shown in Fig. 3.11. The sensitivity of the response with respect to C_2 at 1 kHz was computed using the proposed method and the results are plotted in Figs. 5.11 and 5.12. It is seen that both the real and imaginary parts of the sensitivity converge with the increase in the number of side bands considered. The rate of convergence is clearly slower as compared with the previous example. The normalized sensitivity of the magnitude of the response to C_2 is shown in Fig. 5.13. The relative difference ϵ versus the number of side bands considered in sensitivity analysis is plotted in Fig. 5.14. It is seen that the relative difference decreases with increase in the number of side bands monotonically. The convergence of the sensitivity can be further observed from the voltages of C_2 in both the band pass filter and its adjoint network as shown in Figs. 5.15 and 5.16 (100 side bands), respectively. The peaks

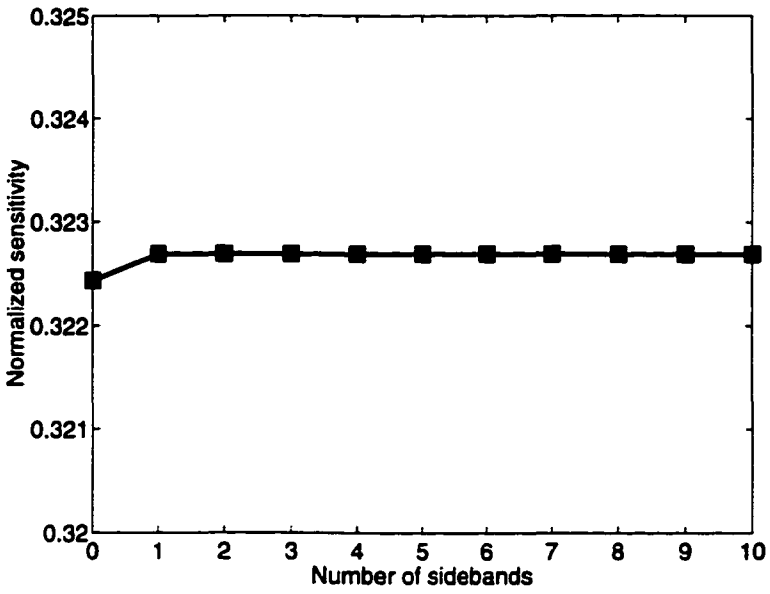


Figure 5.8: Normalized sensitivity of the response of integrator to C1

at the center of the plots represent the responses at 1kHz. As observed, the voltages decrease slowly with frequency. As a result, more side bands are needed to yield a converged sensitivity.

5.6 Summary

The frequency-domain sensitivity of multiphase PSL circuits was derived using the incremental form of Tellegen's theorem for PSL circuits in phasor domain. The theory yields sensitivities of the response of the circuit with respect to all circuit elements in one frequency analysis. It is shown that the sensitivity of PSL circuits is a series summation of the network variables of the element to which the sensitivity is evaluated. Both the base band and side band frequency components of the network variables contribute to the base band sensitivity. It is also shown that the

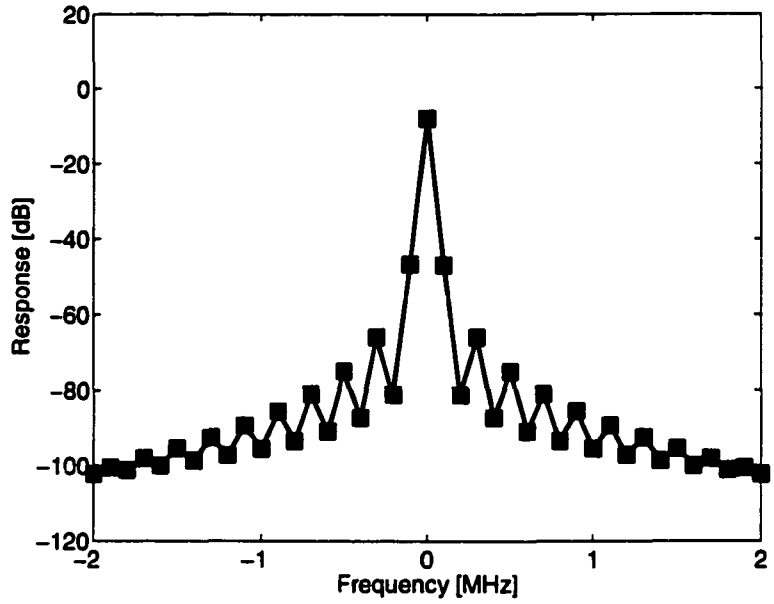


Figure 5.9: Voltage of C1 of Switched-capacitor integrator

sensitivity of LTI circuits is a special case of that of general PSL circuits. The sensitivity networks of PSL circuits were introduced. It is demonstrated that the sensitivities obtained using the adjoint networks are identical to those derived from the sensitivity networks. The theory is assessed using numerical examples and the results were compared with those from other CAD tools. An excellent agreement is observed.

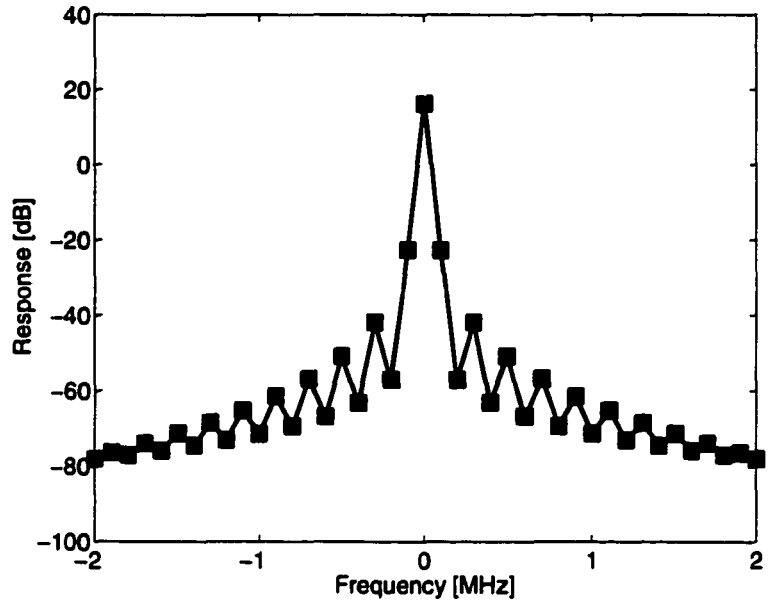


Figure 5.10: Voltage of C1 of the adjoint network of Switched-capacitor integrator

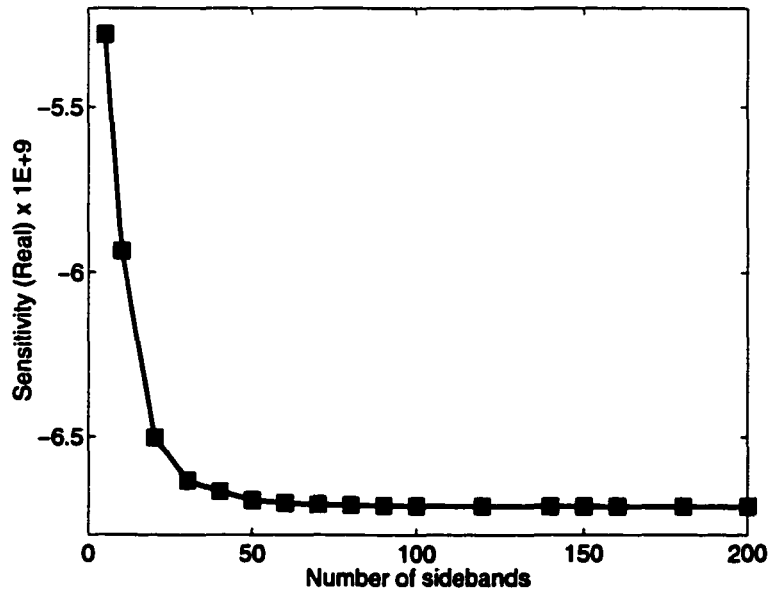


Figure 5.11: Sensitivity of the response of band pass to C2 (Real part)

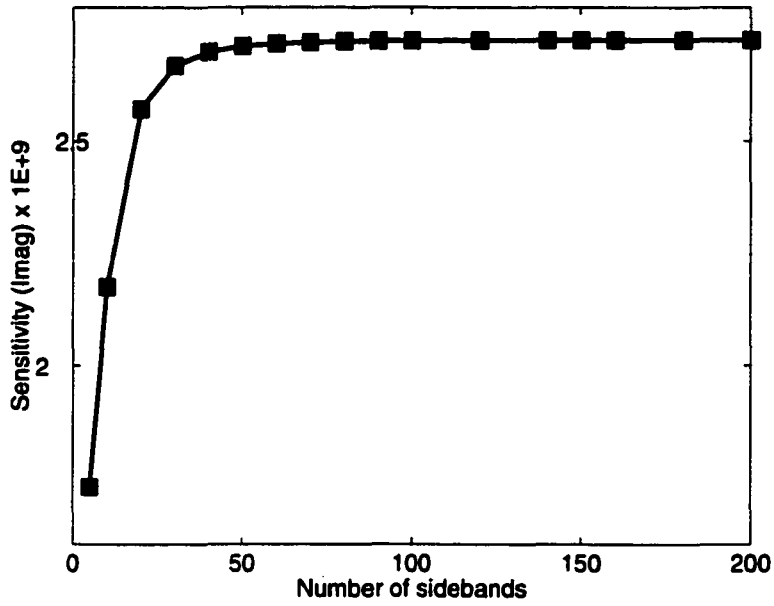


Figure 5.12: Sensitivity the response of band pass to C2 (Imaginary part)

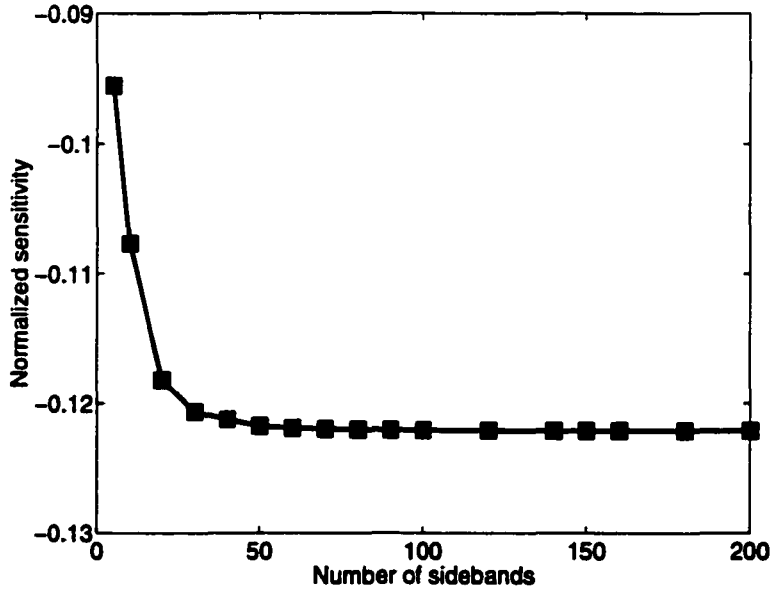


Figure 5.13: Normalized sensitivity of response of band pass

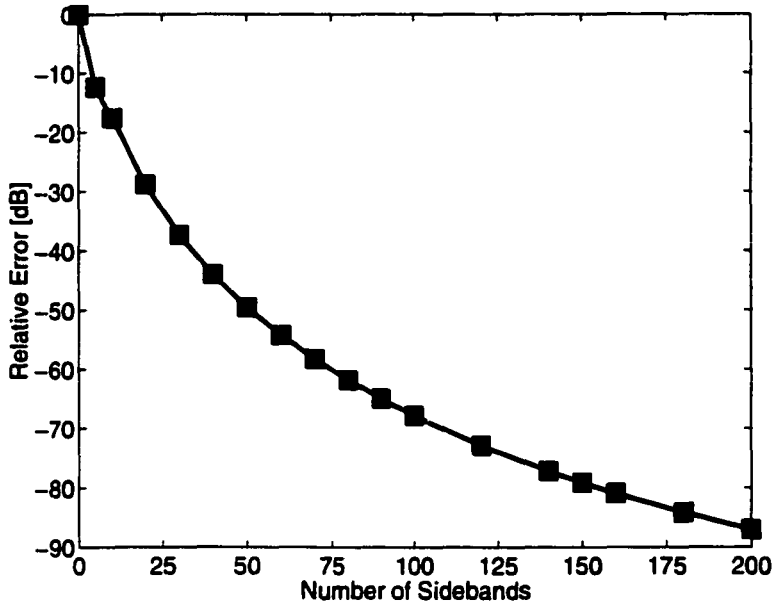


Figure 5.14: Relative difference

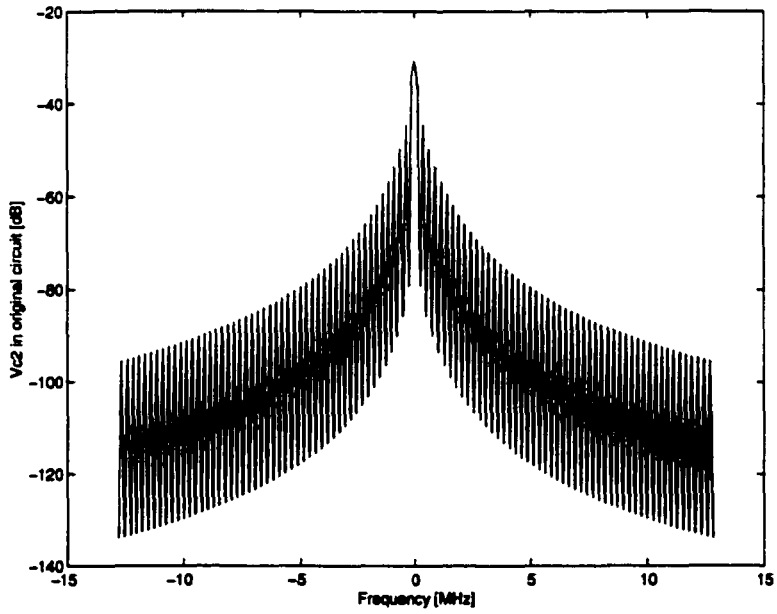


Figure 5.15: Voltage of C2 of band pass filter

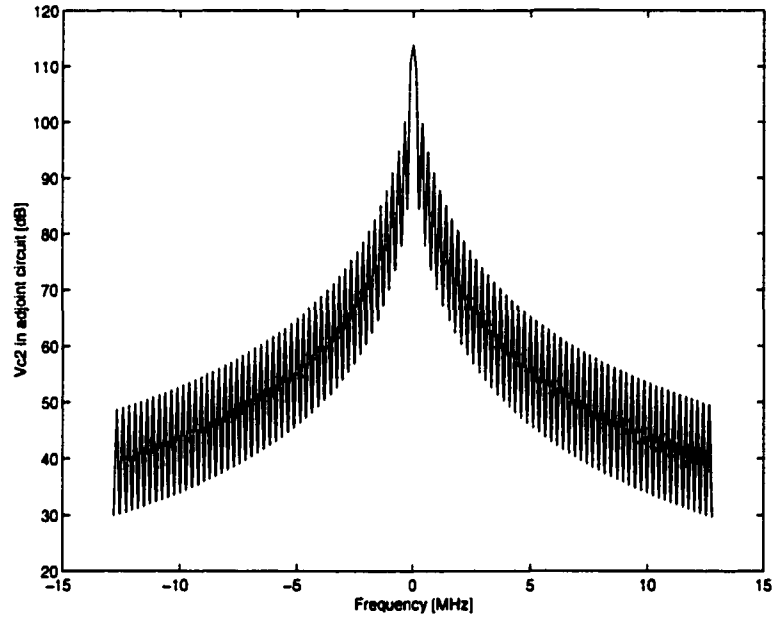


Figure 5.16: Voltage of C2 of the adjoint network of band pass filter

Chapter 6

Distortion Analysis of PSN Circuits

This chapter presents the original work on the theory of Volterra series for nonlinear time-varying (NTV) systems and its application to distortion analysis of periodically switched nonlinear circuits [139]. We first review Volterra functional series for nonlinear time-invariant and nonlinear time-varying systems. Time-varying network functions and multi-frequency transforms are then introduced to characterize the behavior of nonlinear time-varying systems. The network variable theorem of PSN circuits is introduced and the complete spectrum of PSN is obtained. The theory is applied to distortion analysis of PSN circuits. Both harmonic distortion and intermodulation distortion are analyzed. The effectiveness of the theory is assessed using numerical examples and the results are compared with SPICE simulation.

6.1 Volterra Series of Nonlinear Time-Invariant Systems

In steady state, the response of a LTI system $y(t)$ and its input $x(t)$ are related by

$$y(t) = \int_{-\infty}^{\infty} h_1(\tau)x(t-\tau)d\tau \tag{6.1}$$

where $h_1(t)$ is the impulse response of the system. This approach can be generalized to nonlinear time-invariant systems. The steady-state response of a nonlinear time-invariant system relates to its input by the Volterra functional series [73,75]

$$\begin{aligned} y(t) &= \int_{-\infty}^{\infty} h_1(\tau)x(t-\tau)d\tau \\ &+ \int_{-\infty}^{\infty}\int_{-\infty}^{\infty} h_2(\tau_1,\tau_2)x(t-\tau_1)x(t-\tau_2)d\tau_1 d\tau_2 \\ &+ \int_{-\infty}^{\infty}\int_{-\infty}^{\infty}\int_{-\infty}^{\infty} h_3(\tau_1,\tau_2,\tau_3)x(t-\tau_1)x(t-\tau_2)x(t-\tau_3)d\tau_1 d\tau_2 d\tau_3 \\ &+ \ldots \end{aligned} \tag{6.2}$$

where $h_n(\tau_1,...,\tau_n)$ is the nth-order Volterra kernel. Note $h_n(\tau_1,...,\tau_n)$ is casual for any n. The Fourier transform of the response of nonlinear time-invariant systems can be obtained using multi-dimensional Fourier transform [73]. It should be noted that (6.2) is only valid for nonlinear time-invariant systems. Volterra series have been used extensively in distortion analysis of time-invariant electronic circuits [74,140] and has been integrated in many CAD tools, such as HSPICE [142].

6.2 Volterra Series of Nonlinear Time-Varying Systems

If nonlinear systems are time-varying, then (6.2) is of no avail. A special subset of nonlinear time-varying systems are nonlinear sampled-data systems, such as SCNs with S/H inputs. Alper [76, 77] and Bush [78] modified the conventional Volterra series for nonlinear time-invariant systems by incorporating the characteristics of nonlinear sampled-data systems in the early 1960s and discrete Volterra series emerged. The response of a sampled-data system $y(mT_s)$ relates to the input $x(mT_s)$ by

$$\begin{aligned} y(mT_s) &= \sum_{k_1=0}^{\infty} h_1(mT_s)x[(k_1-m)T_s] \\ &+ \sum_{k_1=0}^{\infty}\sum_{k_2=0}^{\infty} h_2(k_1T_s,k_2T_s)x[(m-k_1)T_s]x[(m-k_2)T_s] \\ &+ \sum_{k_1=0}^{\infty}\sum_{k_2=0}^{\infty}\sum_{k_3=0}^{\infty} h_3(k_1T_s,k_2T_s,k_3T_s)x[(m-k_1)T_s]x[(m-k_2)T_s]x[(m-k_3)T_s] \\ &+ \ldots \end{aligned} \tag{6.3}$$

where T_s is the sampling period. Discrete Volterra series has been employed successfully in distortion analysis of SCNs with S/H inputs [27, 28, 79, 80].

If the input of SCNs is continuous or if the nonidealities of SCNs, such as channel resistances of MOSFET switches, are considered, then the circuits are no longer of piece-wise constant nature. Consequently, discrete Volterra series is nullified. A typical example is a Gilbert cell RF mixer shown in Fig.6.1 in which the mixing transistors M3-M6 are operated in ON/OFF modes whereas the amplifying transistors M1-M2 are biased in saturation and operated in the small-signal mode [83, 84].

Distortion generated by the mixer is mainly due to the nonlinear characteristic of the channel currents of M1 and M2 [82].

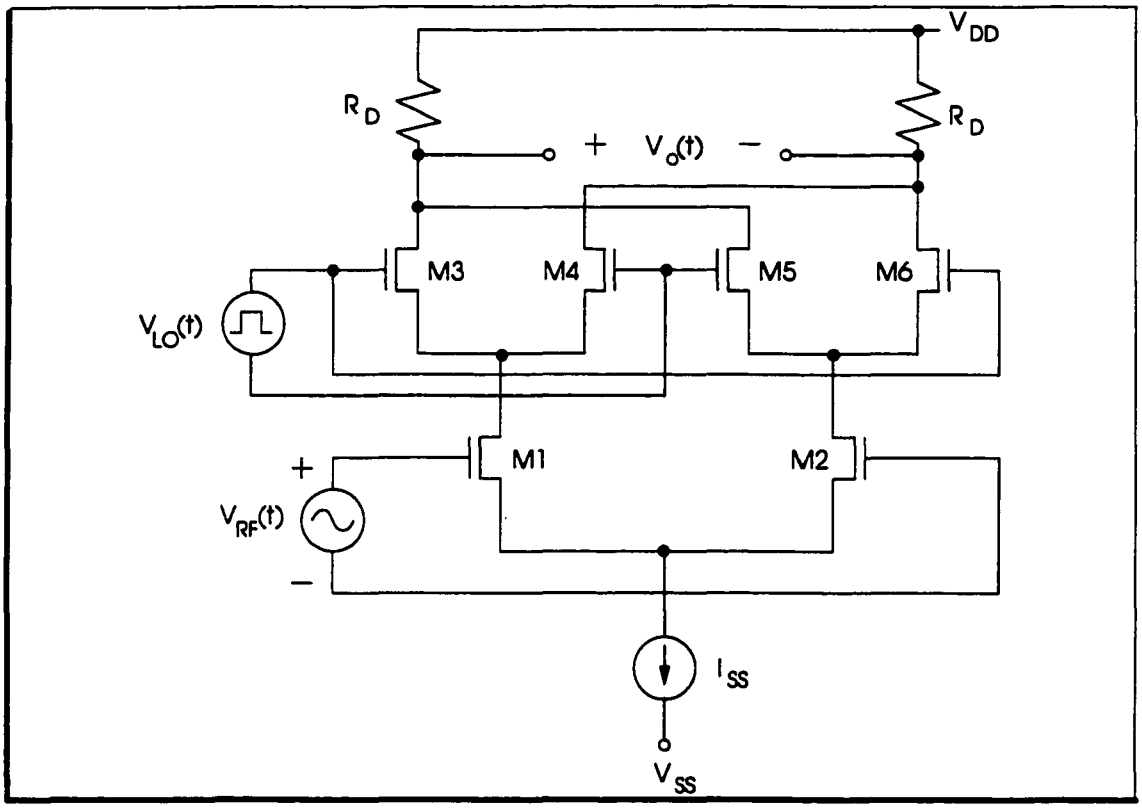


Figure 6.1: Gilbert-cell RF mixer

In [143], the response of linear time-varying systems (Eq.(2.7)) was extended to general nonlinear time-varying systems and time-varying Volterra functional series emerged. The steady-state response of a nonlinear time-varying system relates to the input by

$$\begin{aligned} y(t) &= \int_{-\infty}^{\infty} h_1(t,\tau)x(\tau)d\tau \\ &+ \int_{-\infty}^{\infty}\int_{-\infty}^{\infty} h_2(t,\tau_1,\tau_2)x(\tau_1)x(\tau_2)d\tau_1 d\tau_2 \\ &+ \int_{-\infty}^{\infty}\int_{-\infty}^{\infty}\int_{-\infty}^{\infty} h_3(t,\tau_1,\tau_2,\tau_3)x(\tau_1)x(\tau_2)x(\tau_3)d\tau_1 d\tau_2 d\tau_3 \end{aligned}$$

$$+ \ ...$$
$$= \mathbf{H}_1[x(t)] + \mathbf{H}_2[x(t)] + \mathbf{H}_3[x(t)] + ... \tag{6.4}$$

in which

$$\mathbf{H}_n[x(t)] = \int_{-\infty}^{\infty} ... \int_{-\infty}^{\infty} h_n(t, \tau_1, ..., \tau_n) x(\tau_1) ... x(\tau_n) d\tau_1 ... d\tau_n \tag{6.5}$$

is called the nth-order Volterra operator, $h_n(t, \tau_1, ..., \tau_n)$ is the kernel of the nth-order Volterra operator. If $x(t)$ is replaced with $\epsilon x(t)$, where ϵ is a nonzero constant, then

$$\mathbf{H}_n[\epsilon x(t)] = \epsilon^n \mathbf{H}_n[x(t)]. \tag{6.6}$$

Consequently

$$y(t) = \mathbf{H}_1[x(t)]\epsilon + \mathbf{H}_2[x(t)]\epsilon^2 + \mathbf{H}_3[x(t)]\epsilon^3 + ... \tag{6.7}$$

The right-hand side of (6.7) is a power series in ϵ. The convergence of $y(t)$ is ensured by an appropriate choice of the value of ϵ.

6.3 Frequency Response of Nonlinear Time-Varying Systems

6.3.1 Time-Varying Transfer Functions

In Chapters 2 and 3, the time-varying transfer function of linear time-varying systems $H_1(t, \omega)$ was used in noise analysis of PSL circuits. Note we have added the

subscript "1" to emphasize that linear time-varying systems are first-order systems. If the systems to be analyzed are nonlinear time-varying, then a set of time-varying Volterra kernels, $h_1(t,\tau_1), h_2(t,\tau_1,\tau_2), ...$, are needed to characterize the systems in time domain. To depict the behavior of the systems in frequency domain, we extend the definition of the time-varying transfer function for linear time-varying systems to nonlinear time-varying systems by defining a set of time-varying transfer functions, $H_1(t,\omega_1)$, $H_2(t,\omega_1,\omega_2)$, ..., as follows

$$H_n(t,\omega_1,...,\omega_n) = \int_{-\infty}^{\infty}...\int_{-\infty}^{\infty} h_n(t,\tau_1,...,\tau_n)e^{-j\omega_1(t-\tau_1)}...e^{-j\omega_n(t-\tau_n)}d\tau_1...d\tau_n \quad n=1,2,... \tag{6.8}$$

The corresponding Volterra kernel is obtained via the inverse transform

$$h_n(t,\tau_1,...,\tau_n) = \left(\frac{1}{2\pi}\right)^n \int_{-\infty}^{\infty}...\int_{-\infty}^{\infty} H_n(t,\omega_1,...,\omega_n)e^{j\omega_1(t-\tau_1)}...e^{j\omega_n(t-\tau_n)}d\omega_1...d\omega_n \quad n=1,2,... \tag{6.9}$$

The usefulness of these time-varying transfer functions is best demonstrated if the input of the system is $x(t) = e^{j\omega_o t}$. In this case, the response of the system becomes

$$y(t) = H_1(t,\omega_o)e^{j\omega_o t} + H_2(t,\omega_o,\omega_o)e^{j2\omega_o t} + H_3(t,\omega_o,\omega_o,\omega_o)e^{j3\omega_o t} + ... \tag{6.10}$$

Clearly seen is that once $H_n(t,\omega_o...,\omega_o), n=1,2,...,$ are known, the time-domain response of the system $y(t)$ will be defined.

6.3.2 Multi-Frequency Transform

It was demonstrated in Chapter 3 that the bi-frequency transform $\mathcal{H}_1(\Omega,\omega)$ fully characterizes the behavior of PSL circuits in frequency domain. Again, the subscript "1" was used to emphasize that the transform is first-order. Analogous to $H_1(t,\omega_1)$, $H_2(t,\omega_1,\omega_2)$,..., defined in the preceding section, a set of multi-frequency transforms, in addition to the bi-frequency transform, are defined to characteristize nonlinear time-varying systems in frequency domain. To begin with, we define the *tri-frequency transform* $\mathcal{H}_2(\Omega,\omega_1,\omega_2)$ and its inverse $H_2(t,\omega_1,\omega_2)$ as follows

$$\begin{cases} \mathcal{H}_2(\Omega,\omega_1,\omega_2) = \int_{-\infty}^{\infty} H_2(t,\omega_1,\omega_2)e^{-j(\Omega-\omega_1-\omega_2)t}dt \\ H_2(t,\omega_1,\omega_2) = \dfrac{1}{2\pi}\int_{-\infty}^{\infty} \mathcal{H}_2(\Omega,\omega_1,\omega_2)e^{j(\Omega-\omega_1-\omega_2)t}d\Omega \end{cases} . \tag{6.11}$$

The high-order transforms are defined similarly

$$\begin{cases} \mathcal{H}_n(\Omega,\omega_1,...,\omega_n) = \int_{-\infty}^{\infty} H_n(t,\omega_1,...,\omega_n)e^{-j(\Omega-\omega_1-...-\omega_n)t}dt \\ H_n(t,\omega_1,...,\omega_n) = \dfrac{1}{2\pi}\int_{-\infty}^{\infty} \mathcal{H}_n(\Omega,\omega_1,...,\omega_n)e^{j(\Omega-\omega_1-...-\omega_n)t}d\Omega \\ \qquad\qquad n = 1,2,... \end{cases} \tag{6.12}$$

The usefulness of these multi-frequency transforms will become evident in the next section where the frequency response of nonlinear time-varying systems is derived.

6.3.3 Frequency Response of Nonlinear Time-Varying Systems

When time-varying Volterra functional series is used, the time-domain response of a NTV system is obtained from

$$y(t) = \sum_{n=1}^{\infty} y^{(n)}(t) \tag{6.13}$$

where $y^{(n)}(t) = \mathbf{H}_n[x(t)]$. The complete spectrum of the response is obtained by taking Fourier transform

$$Y(\Omega) = \sum_{n=1}^{\infty} Y^{(n)}(\Omega) \tag{6.14}$$

It was shown in Chapter 3 that the Fourier transform of the 1st-order response $y^{(1)}(t)$ is given by

$$\begin{aligned} Y^{(1)}(\Omega) &= \mathcal{F}[y^{(1)}(t)] \\ &= \frac{1}{2\pi}\int_{-\infty}^{\infty} \mathcal{H}_1(\Omega,\omega_1)X(\omega_1)d\omega_1. \end{aligned} \tag{6.15}$$

The Fourier transform of $y^{(2)}(t)$ is obtained by making use of the tri-frequency transform introduced earlier

$$\begin{aligned} Y^{(2)}(\Omega) &= \mathcal{F}[y^{(2)}(t)] \\ &= \left(\frac{1}{2\pi}\right)^2 \int_{-\infty}^{\infty}\int_{-\infty}^{\infty} \mathcal{H}_2(\Omega,\omega_1,\omega_2)X(\omega_1)X(\omega_2)d\omega_1 d\omega_2. \end{aligned} \tag{6.16}$$

Similarly, one can show that

$$\begin{aligned} Y^{(n)}(\Omega) &= \mathcal{F}[y^{(n)}(t)] \\ &= \left(\frac{1}{2\pi}\right)^n \int_{-\infty}^{\infty} \cdots \int_{-\infty}^{\infty} \mathcal{H}_n(\Omega, \omega_1, ..., \omega_n) X(\omega_1) ... X(\omega_n) d\omega_1 ... d\omega_n. \end{aligned} \tag{6.17}$$

Substituting these results into (6.14) gives

$$\begin{aligned} Y(\Omega) &= \frac{1}{2\pi} \int_{-\infty}^{\infty} \mathcal{H}_1(\Omega, \omega_1) X(\omega_1) d\omega_1 \\ &+ \left(\frac{1}{2\pi}\right)^2 \int_{-\infty}^{\infty} \int_{-\infty}^{\infty} \mathcal{H}_2(\Omega, \omega_1, \omega_2) X(\omega_1) X(\omega_2) d\omega_1 d\omega_2 \\ &+ \left(\frac{1}{2\pi}\right)^3 \int_{-\infty}^{\infty} \int_{-\infty}^{\infty} \int_{-\infty}^{\infty} \mathcal{H}_3(\Omega, \omega_1, \omega_2, \omega_3) X(\omega_1) X(\omega_2) X(\omega_3) d\omega_1 d\omega_2 d\omega_3 \\ &+ \cdots \\ &= \mathbf{H}_1[X(\Omega)] + \mathbf{H}_2[X(\Omega)] + \mathbf{H}_3[X(\Omega)] + ... \end{aligned} \tag{6.18}$$

in which

$$\mathbf{H}_n[X(\Omega)] = \left(\frac{1}{2\pi}\right)^n \int_{-\infty}^{\infty} \cdots \int_{-\infty}^{\infty} \mathcal{H}_n(\Omega, \omega_1, ..., \omega_3) X(\omega_1) ... X(\omega_n) d\omega_1 ... d\omega_n \tag{6.19}$$

Eq.(6.18) is a frequency-domain representation of the time-varying Volterra series. Analogous to the time-domain representation of time-varying Volterra series given by (6.4), $(1/2\pi)^n \mathcal{H}_n(\Omega, \omega_1, ..., \omega_n)$ can be considered as the kernel of the nth-order frequency-domain Volterra series. Clearly seen is that once $\mathcal{H}_n(\Omega, \omega_1, ..., \omega_n)$ are known, the spectrum of the response of nonlinear time-varying systems will be defined completely. For example, if $x(t) = e^{j\omega_o t}$, because $X(\omega) = 2\pi\delta(\omega - \omega_o)$, then

$$Y(\Omega) = \mathcal{H}_1(\Omega, \omega_o) + \mathcal{H}_2(\Omega, \omega_o, \omega_o) + \mathcal{H}_3(\Omega, \omega_o, \omega_o, \omega_o) + ... \tag{6.20}$$

Eq.(6.18) provides a general means to characterize the behavior of nonlinear time-varying system in frequency domain. It is, however, generally difficult to compute $\mathcal{H}_n(\omega_1, ..., \omega_n)$ if the nonlinear time-varying system is arbitrary. In the next section, we will focus upon a special subset of nonlinear time-varying systems - nonlinear periodically time-varying (NPTV) systems.

6.4 Nonlinear Periodically Time-Varying Systems

It was shown in Chapter 3 that due to the periodic nature of linear periodically time-varying systems, the time-varying transfer function $H_1(t, \omega)$ is periodic in t. Consequently, $H_1(t, \omega)$ can be represented using Fourier series and the network variable theorem for PSL circuits was deduced. In this section, we extend this result to NPTV systems. Because of the periodically time-varying nature of NPTV systems, the time-varying network functions of NPTV systems, $H_1(t, \omega)$, $H_2(t, \omega_1, \omega_2)$, ..., are periodic in t with the same period T_s. Due to the periodicity, these time-varying network functions can be represented using Fourier series

$$H_n(t, \omega_1, ...\omega_n) = \sum_{k=-\infty}^{\infty} H_{n,k} e^{jk\omega_s t} \qquad n = 1, 2, ... \tag{6.21}$$

where

$$H_{n,k} = \frac{1}{T_s} \int_0^{T_s} H_n(t, \omega_1, ..., \omega_n) e^{-jk\omega_s t} dt \qquad n = 1, 2, ... \tag{6.22}$$

If the input of the NPTV system is $x(t) = e^{j\omega_o t}$, then by making use of (6.10), (6.21) and (6.22), we obtain

$$y(t) = \sum_{n=1}^{\infty} \sum_{k=-\infty}^{\infty} H_{n,k} e^{j(n\omega_o + k\omega_s)t} \tag{6.23}$$

Consequently

$$Y(\Omega) = 2\pi \sum_{n=1}^{\infty} \sum_{k=-\infty}^{\infty} H_{n,k} \delta(\Omega - n\omega_o - k\omega_s) \tag{6.24}$$

The bi-, tri-,... frequency transforms can be determined by comparing (6.24) with (6.20).

$$\mathcal{H}_n(\Omega, \omega_1, ..., \omega_n) = 2\pi \sum_{k=-\infty}^{\infty} H_{n,k} \delta(\Omega - n\omega_o - k\omega_s) \tag{6.25}$$

A few comments regarding (6.23) are made prior to further development.

(1) Eq. (6.23) is a generalization of the network variable theorem for PSL circuits derived in Chapter 3. $H_{1,k}, H_{2,k}, H_{3,k}, ...$ are the phasor representations of $y(t)$ at $\omega_o + k\omega_s, 2\omega_o + k\omega_s, 3\omega_o + k\omega_s, ...$, respectively. Eq.(6.23) represents a fundamental characteristic of NPTV systems.

Theorem 6.1 (Network Variable Theorem for PSN Circuits) *In steady state, the network variables of a periodically switched nonlinear circuit with input $e^{j\omega_o t}$ and clock frequency ω_s contain an infinite number of frequency components. They can be represented by*

$$v(t) = \sum_{n=1}^{\infty} \sum_{k=-\infty}^{\infty} V_{n,k} e^{j(n\omega_o + k\omega_s)t} \tag{6.26}$$

where $V_{1,k}, V_{2,k}, V_{3,k}, \ldots$ *are the phasors of* $v(t)$ *at* $\omega_o + k\omega_s, 2\omega_o + k\omega_s, 3\omega_o + k\omega_s, \ldots$, *respectively.*

(2) If the system is LPTV, then the corresponding $H_2(t, \omega_1, \omega_2)$, $H_3(t, \omega_1, \omega_2, \omega_3)$,... are identically zero. As a result, Theorem 6.1 simplifies to Theorem 3.1.

(3) The complete spectrum of a NPTV system to a single-tone input $x(t) = e^{j\omega_o t}$ is given by (6.24). In the base band where $n = 0$, the fundamental component is given by $H_{1,0}$ whereas the 2nd-, 3rd-, ..., harmonic components are given by $H_{2,0}, H_{3,0}$, ..., respectively. The similar pattern repeats in side bands ($n \neq 0$).

(4) To obtain the harmonic components of the response of nonlinear time-varying systems to a sinusoidal input $x(t) = A\cos(\omega_o t)$, note $\cos(\omega_o)t = (e^{j\omega_o t} + e^{-j\omega_o t})/2$, we have

$$\begin{aligned} y(t) &= \left[\frac{A^2}{2}H_2(t, \omega_o, -\omega_o) + \ldots\right] \\ &+ \left[\frac{A}{2}H_1(t, \omega_o) + \frac{3A^3}{8}H_3(t, \omega_o, \omega_o, -\omega_o) + \ldots\right]e^{j\omega_o t} \\ &+ \left[\frac{A}{2}H_1(t, -\omega_o) + \frac{3A^3}{8}H_3(t, \omega_o, -\omega_o, -\omega_o) + \ldots\right]e^{-j\omega_o t} \\ &+ \left[\frac{A^2}{4}H_2(t, \omega_o, \omega_o) + \ldots\right]e^{j2\omega_o t} + \left[\frac{A^2}{4}H_2(t, -\omega_o, -\omega_o) + \ldots\right]e^{-j2\omega_o t} \\ &+ \left[\frac{A^3}{8}H_3(t, \omega_o, \omega_o, \omega_o) + \ldots\right]e^{j3\omega_o t} + \left[\frac{A^3}{8}H_3(t, -\omega_o, -\omega_o, -\omega_o) + \ldots\right]e^{-j3\omega_o t} \\ &+ \ldots \end{aligned} \tag{6.27}$$

Note we have assumed symmetrical kernels in the above derivation. The 2nd- and 3rd-order harmonic distortion are computed from

$$HD_2(t) = \left|\frac{\frac{A^2}{4}H_2(t, \omega_o, \omega_o) + \ldots}{\frac{A}{2}H_1(t, \omega_o) + \frac{3A^3}{8}H_3(t, \omega_o, \omega_o, -\omega_o) + \ldots}\right|. \tag{6.28}$$

$$HD_3(t) = \left| \frac{\frac{A^3}{8} H_3(t, \omega_o, \omega_o, \omega_o) + \ldots}{\frac{A}{2} H_1(t, \omega_o) + \frac{3A^3}{8} H_3(t, \omega_o, \omega_o, -\omega_o) + \ldots} \right|. \tag{6.29}$$

The harmonic distortion is a function of time. Note the similarity between (6.28), (6.29) and those of nonlinear time-invariant systems given in [74]. If the system is nonlinear time-invariant, then (6.28) and (6.29) simplify to the familiar expressions of HD_2 and HD_3 of nonlinear time-invariant systems.

If the system is NPTV, then using Theorem 6.1 and neglecting terms whose order is higher than 3 in (6.27), we have

$$\begin{aligned} y(t) \approx & \sum_{k=-\infty}^{\infty} \frac{A^2}{2} H_{2,k} e^{jk\omega_s t} \\ & + \sum_{k=-\infty}^{\infty} \left[\frac{A}{2} H_{1,k} + \frac{3A^3}{8} H_{3,k} \right] e^{j(\omega_o + k\omega_s)t} + \sum_{k=-\infty}^{\infty} \left[\frac{A}{2} H_{1,k} + \frac{3A^3}{8} H_{3,k} \right] e^{j(-\omega_o + k\omega_s)t} \\ & + \sum_{k=-\infty}^{\infty} \frac{A^2}{4} H_{2,k} e^{j(2\omega_o + k\omega_s)t} + \sum_{k=-\infty}^{\infty} \frac{A^2}{4} H_{2,k} e^{j(-2\omega_o + k\omega_s)t} \\ & + \sum_{k=-\infty}^{\infty} \frac{A^3}{8} H_{3,k} e^{j(3\omega_o + k\omega_s)t} + \sum_{k=-\infty}^{\infty} \frac{A^3}{8} H_{3,k} e^{j(-3\omega_o + k\omega_s)t}. \end{aligned} \tag{6.30}$$

The complete spectrum of the response is obtained by taking Fourier transform on (6.30) and is given in Fig.6.2. Note that only up-to 3rd-order terms are considered and plotted in the figure. The 2nd-order and 3rd-order harmonic distortion in the base band are computed from

$$HD_2 = \left| \frac{\frac{A^2}{4} H_{2,0}}{\frac{A}{2} H_{1,0} + \frac{3A^3}{8} H_{3,0}} \right| \approx \frac{A}{2} \left| \frac{H_{2,0}}{H_{1,0}} \right|. \tag{6.31}$$

$$HD_3 = \left| \frac{\frac{A^3}{8} H_{3,0}}{\frac{A}{2} H_{1,0} + \frac{3A^3}{8} H_{3,0}} \right| \approx \frac{A^2}{4} \left| \frac{H_{3,0}}{H_{1,0}} \right|. \tag{6.32}$$

provided that $\left| \frac{3A^3}{8} H_{3,0} \right| \ll \left| \frac{A}{2} H_{1,0} \right|$.

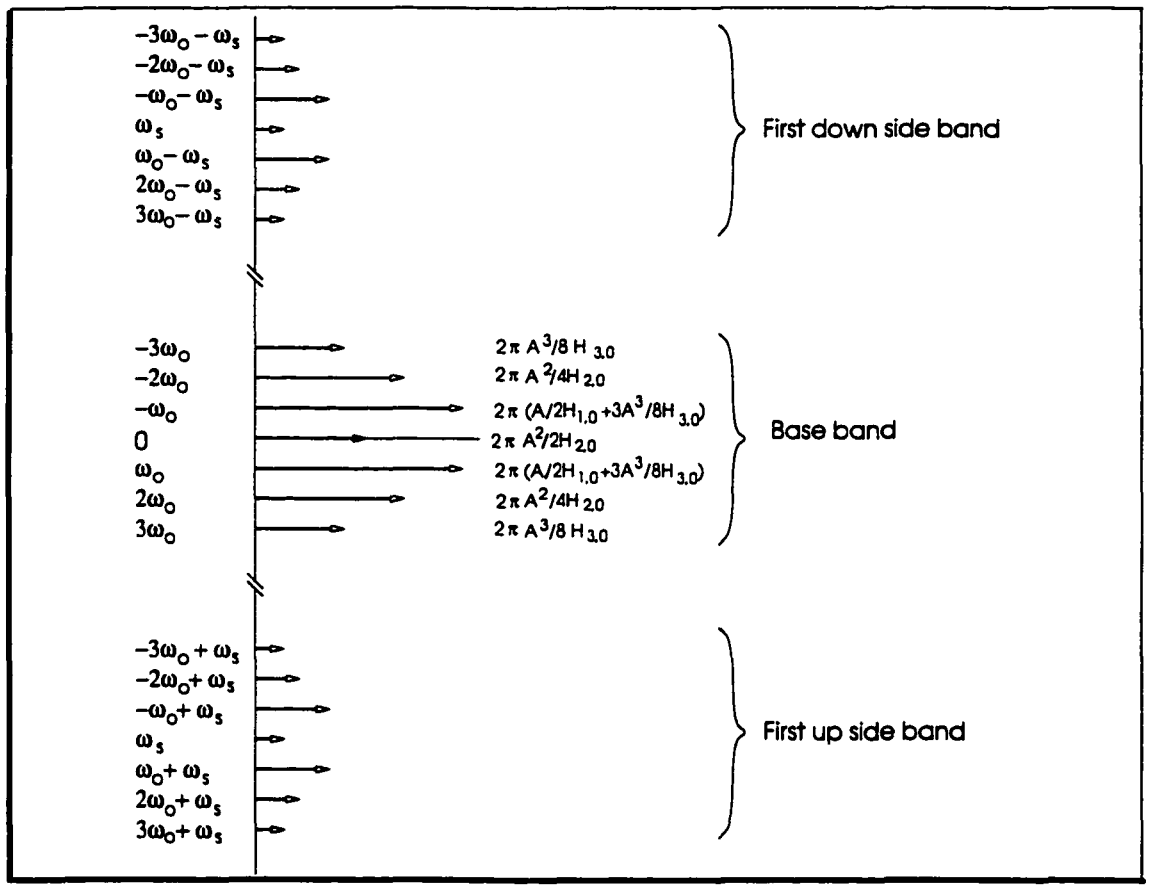


Figure 6.2: Spectrum of PSN circuits with input $x(t) = A\cos\omega_o t$

(5) If the input of a nonlinear time-varying system contains two different frequencies, i.e. $x(t) = A(\cos\omega_1 t + \cos\omega_2 t)$, $\omega_1 \neq \omega_2$, the spectrum of the response can also be obtained in a similar manner. It can be shown that the 3rd-order intermodulation

distortion is computed from

$$IM_3(t) = \left| \frac{\frac{3A^3}{8} H_3(t, \omega_1, \omega_1, -\omega_2) + \ldots}{\frac{A}{2} H_1(t, \omega_1) + \frac{9A^3}{8} H_3(t, \omega_1, \omega_1, -\omega_1) + \ldots} \right|. \tag{6.33}$$

If the system is further NPTV, then it can be shown that the spectrum of the response is given in Fig.6.3. The 3rd-order intermodulation distortion at $2\omega_1 - \omega_2$ in the base band is computed from

$$IM_3 = \left| \frac{\frac{3A^3}{8} H_{3,0}}{\frac{A}{2} H_{1,0} + \frac{9A^3}{8} H_{3,0}} \right| \approx \frac{3A^2}{4} \left| \frac{H_{3,0}}{H_{1,0}} \right|. \tag{6.34}$$

provided that $\left| \frac{9A^3}{8} H_{3,0} \right| \ll \left| \frac{A}{2} H_{1,0} \right|$

6.5 Distortion Analysis of PSN Circuits

Having developed the general theory of Volterra series for nonlinear time-varying systems, in this section we make use of this theory to compute the distortion of PSN circuits.

6.5.1 Nonlinear Elements

Nonlinear elements considered in this thesis are time-invariant weak nonlinearities. The characteristics of these nonlinearities can be modeled sufficiently using a truncated Taylor series expansion (usually up-to the 3rd-order). Such a limitation is justified as a large number of nonlinearities encountered in switched analog circuits fall into this category. In this section, the equivalent circuits of nonlinear controlled

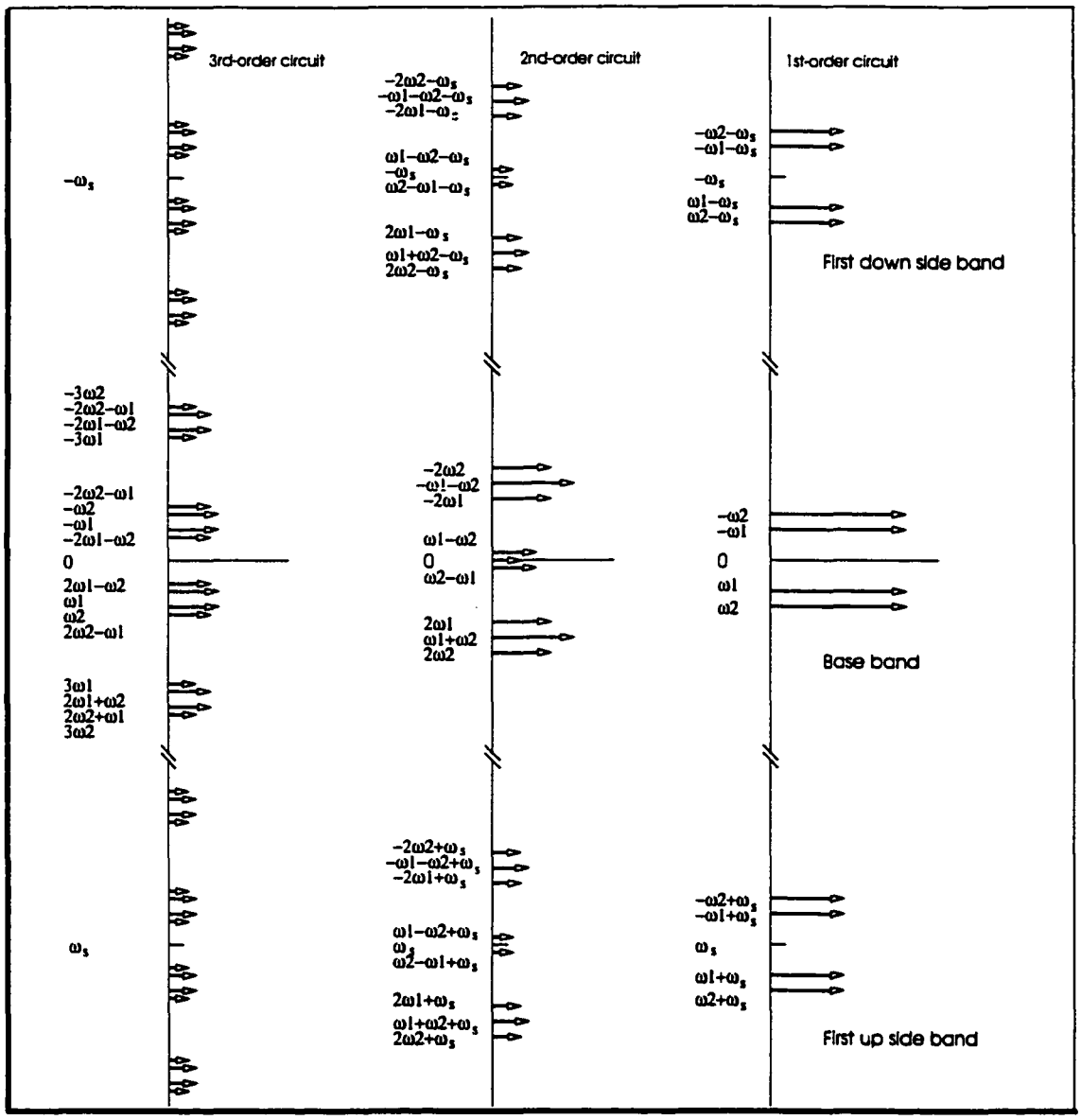


Figure 6.3: Spectrum of PSN circuits with input $x(t) = A(\cos\omega_1 t + \cos\omega_2 t)$

sources and nonlinear capacitors in switched circuits are derived. The equivalent circuits of other nonlinear elements can be derived similarly.

Nonlinear Controlled Sources Nonlinear controlled sources are used extensively in modeling many types of nonlinear elements. For the purpose of illustration,

only nonlinear VCVSs are investigated here. Let a VCVS in a switched circuit be modeled by

$$v_{2,k}(t) = a_1 v_{1,k}(t) + a_2 v_{1,k}^2(t) + a_3 v_{1,k}^3(t) \qquad k = 1, 2, ..., K \tag{6.35}$$

where $v_{1,k}(t)$ and $v_{2,k}(t)$ are the controlling and controlled voltages of the VCVS in phase k, respectively. a_1, a_2, and a_3 are constants. Representing the voltages of both the controlling and controlled branches of the VCVS in Volterra series of the input $w(t)$ and substituting the results into (6.35) gives

$$\begin{aligned} &\left[v_{2,k}^{(1)}(t) - a_1 v_{1,k}^{(1)}(t)\right]\epsilon + \left[v_{2,k}^{(2)}(t) - a_1 v_{1,k}^{(2)}(t) - a_2\left(v_{1,k}^{(1)}(t)\right)^2\right]\epsilon^2 \\ + &\left[v_{2,k}^{(3)}(t) - a_1 v_{1,k}^{(3)}(t) - 2a_2 v_{1,k}^{(1)}(t) v_{1,k}^{(2)}(t) - a_3\left(v_{1,k}^{(1)}(t)\right)^3\right]\epsilon^3 + ... = 0. \end{aligned} \tag{6.36}$$

Since a power series equals to zero if and only if all the coefficients of the power series are identically zero, we obtain

$$\begin{cases} v_{2,k}^{(1)}(t) = a_1 v_{1,k}^{(1)}(t) \\ v_{2,k}^{(2)}(t) = a_1 v_{1,k}^{(2)}(t) + a_2 [v_{1,k}^{(1)}(t)]^2 \\ v_{2,k}^{(3)}(t) = a_1 v_{1,k}^{(3)}(t) + 2a_2 v_{1,k}^{(1)}(t) v_{1,k}^{(2)}(t) + a_3 [v_{1,k}^{(1)}(t)]^3 \end{cases} \tag{6.37}$$

Eq.(6.37) reveals that the nonlinear VCVS can be represented equivalently by three linear VCVSs as shown in Fig.6.4. These three linear VCVSs are termed respectively as the 1st, 2nd, and 3rd-order Volterra circuits of the nonlinear VCVS.

Nonlinear Capacitors Nonlinear capacitors encountered in periodically switched nonlinear circuits are mainly the depletion layer capacitances, such as the base-collector junction capacitance of BJT, the source-substrate, and drain-substrate junction capacitances of MOS transistors. These capacitances are nonlinear func-

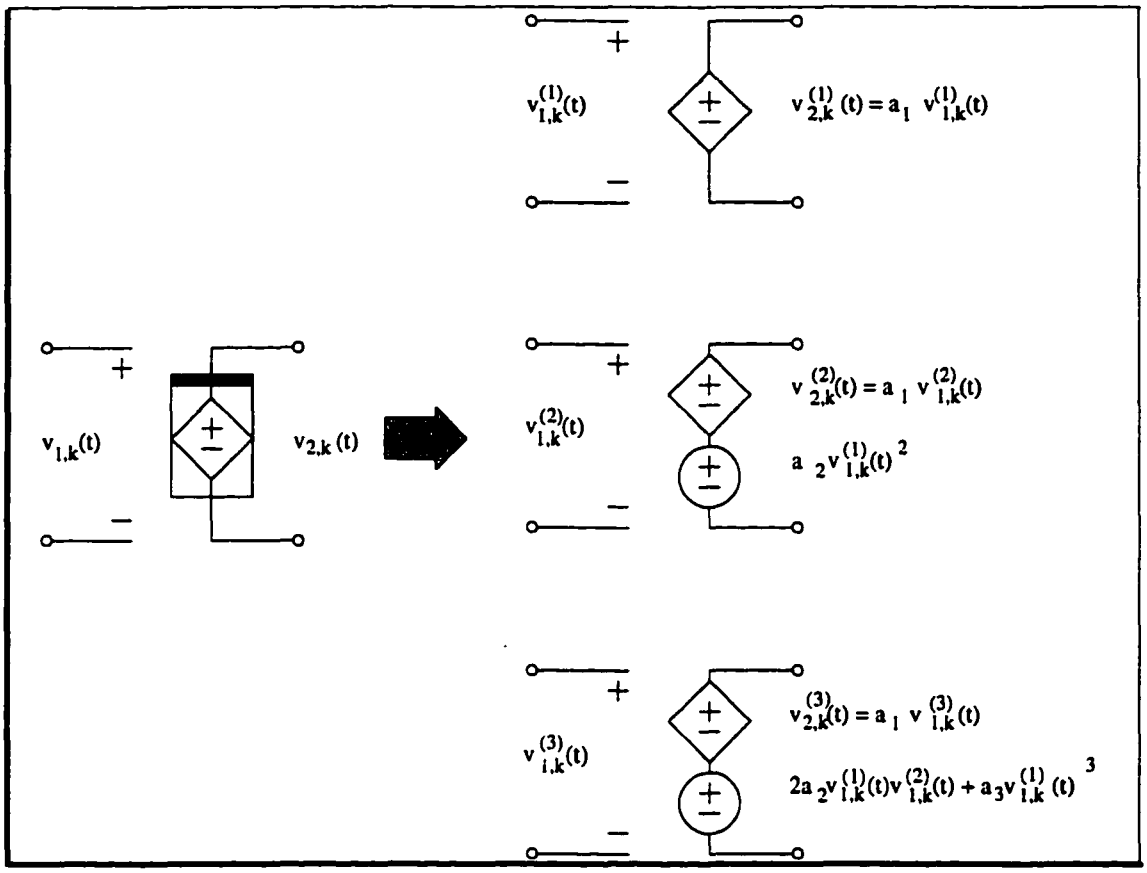


Figure 6.4: Equivalent circuits of nonlinear VCVS

tions of the junction voltages [16] and are modeled as voltage-controlled charge sources

$$q(t) \approx C_1 v(t) + C_2 v^2(t) + C_3 v^3(t). \tag{6.38}$$

where $q(t)$ and $v(t)$ are the AC components of the charge stored in the capacitor and the reverse biasing voltage of the capacitor. C_1, C_2, and C_3 are constants. Note C_1 is the incremental capacitance. When these capacitors are in switched circuits, the effect of the initial conditions of these capacitors must be considered. To assist

analysis, we first review the technique used in dealing with linear capacitors in switched circuits. We will then extend this approach to nonlinear capacitors in switched circuits.

Consider a LTI capacitor with initial voltage $v(0^+)$ at $t = 0^+$. Because $i(t) = C\frac{dv(t)}{dt}$, where $i(t)$ and $v(t)$ are the current and voltage of the capacitor, respectively. Laplace transform of this relation gives

$$I(s) = sCV(s) - Cv(0^+) \tag{6.39}$$

where $I(s)$ and $V(s)$ are the Laplace transform of $i(t)$ and $v(t)$, respectively. Eq.(6.39) can be written equivalently in time domain as

$$i(t) = C\frac{dv(t)}{dt} - Cv(0^+)\delta(t) \qquad t > 0^+ \tag{6.40}$$

Now, consider a LTI capacitor in a PSL circuit. Let there be a phase k specified by $nT + \sigma_{k-1} < t \leq nT + \sigma_k$](see Fig. 3.8). The voltage of the capacitor at $t = nT + \sigma_{k-1}^+$ is given by $v_{k-1}(nT + \sigma_{k-1}^+)$. Making use of the result in (6.40), we obtain

$$i(t) = C\frac{dv(t)}{dt} - Cv_{k-1}(nT + \sigma_{k-1}^+)\delta(t - nT - \sigma_{k-1}^+) \qquad t > nT + \sigma_{k-1}^+ \tag{6.41}$$

To ensure that $i(t)$ is zero for $t > nT + \sigma_k$, the effect of the charge on the capacitor at $t = nT + \sigma_k^-$ must be considered. This is achieved by subtracting $Cv_k(nT +$

$\sigma_k^-)\delta(t-nT-\sigma_k^-)$ from $i(t)$. As a result

$$\begin{aligned} i_k(t) = C\frac{dv_k(t)}{dt} &- Cv_{k-1}(nT+\sigma_{k-1}^+)\delta(t-nT-\sigma_{k-1}^+) \\ &+ Cv_k(nT+\sigma_k^-)\delta(t-nT-\sigma_k^-) \end{aligned} \tag{6.42}$$

where

$$i_k(t) = \begin{cases} i(t) & nT+\sigma_{k-1} < t \leq nT+\sigma_k \\ 0 & \text{elsewhere} \end{cases} \tag{6.43}$$

An equivalent circuit of the capacitor in phase k is shown in Fig. 6.5(a). The formulation of capacitors in PSL circuits is exclusively based on (6.42), as was shown in [47].

If capacitors are nonlinear, the characterizing variable is the charge $q(t)$, rather than the voltage $v(t)$, of the capacitors. Consider a nonlinear capacitor with an initial charge $q(0^+)$ at $t = 0^+$. The current of the nonlinear capacitor is obtained from $i(t) = \frac{dq(t)}{dt}$. Laplace transform gives

$$I(s) = sQ(s) - q(0^+) \tag{6.44}$$

where $Q(s) = \mathcal{L}[q(t)]$. This equation can be written equivalently in time domain as

$$i(t) = \frac{dq(t)}{dt} - q(0^+)\delta(t) \qquad\qquad t > 0^+ \tag{6.45}$$

Now consider a nonlinear capacitor in a switched circuit. In phase k, let the charge of the capacitor at $t = nT+\sigma_{k-1}^+$ be given by $q_{k-1}(nT+\sigma_{k-1}^+)$. When taking into consideration of the initial charge on the capacitor, the current of the capacitor

is obtained from

$$i(t) = \frac{dq(t)}{dt} - q_{k-1}(nT + \sigma_{k-1}^{+})\delta(t - nT - \sigma_{k-1}^{+}) \qquad t > nT + \sigma_{k-1}^{+} \tag{6.46}$$

Analogous to LTI capacitors in PSL circuits, to ensure that $i(t)$ vanishes for $t > nT + \sigma_k$, the effect of the charge on the capacitor at the end of the phase must be considered. This is realized by subtracting $q_k(nT + \sigma_k^{-})\delta(t - nT - \sigma_k^{-})$ from $i(t)$. As a result

$$\begin{aligned} i_k(t) = \frac{dq_k(t)}{dt} &- q_{k-1}(nT + \sigma_{k-1}^{+})\delta(t - nT - \sigma_{k-1}^{+}) \\ &+ q_k(nT + \sigma_k^{-})\delta(t - nT - \sigma_k^{-}) \end{aligned} \tag{6.47}$$

Eq.(6.47) is illustrated in Fig.6.5(b). The formulation of the capacitor in switched circuits is based on (6.38) and (6.47). The system matrices of the nonlinear capacitor in phase k are given in Fig.6.6.

Nonlinear inductors can be analyzed in a similar manner. The formulating variable is the magnetic flux of the inductor.

6.5.2 Volterra Series Representation of Network Variables

Periodically switched nonlinear circuits are NPTV systems. The network variable of a periodically switched nonlinear circuit $v(t)$ can be represented by a time-varying Volterra series of the input.

$$v(t) = \sum_{m=1}^{\infty} v^{(m)}(t) \tag{6.48}$$

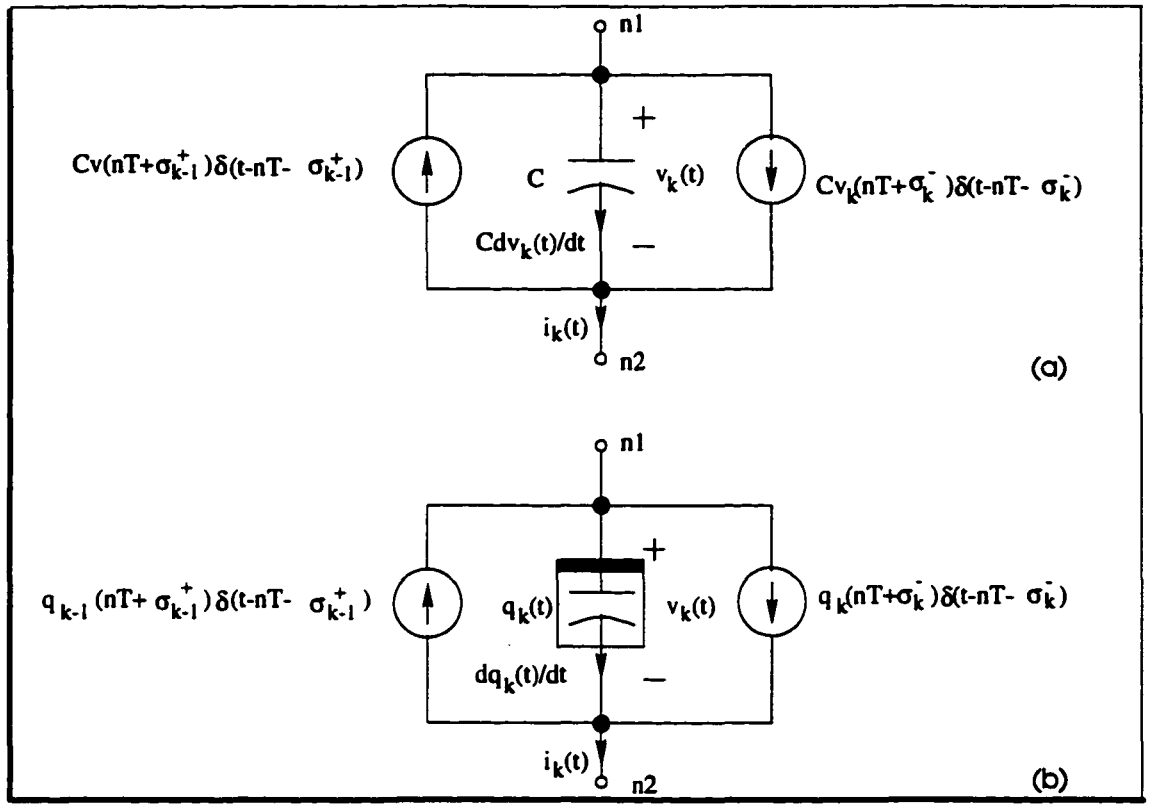


Figure 6.5: Equivalent circuits of linear and nonlinear capacitors in phase k. (a) Linear capacitor, (b) Nonlinear capacitor

where $v^{(m)}(t) = \mathbf{H}_m[w(t)]$, $w(t)$ is the input of the circuit. Multiplying (6.48) by the window function $\xi_k(t)$ defined in (3.44) gives

$$v_k(t) = \sum_{m=1}^{\infty} v_k^{(m)}(t) \qquad k = 1, 2, ..., K \tag{6.49}$$

where

$$v_k(t) = \begin{cases} v(t) & nT + \sigma_{k-1} < t \leq nT + \sigma_k \\ 0 & \text{elsewhere} \end{cases} \tag{6.50}$$

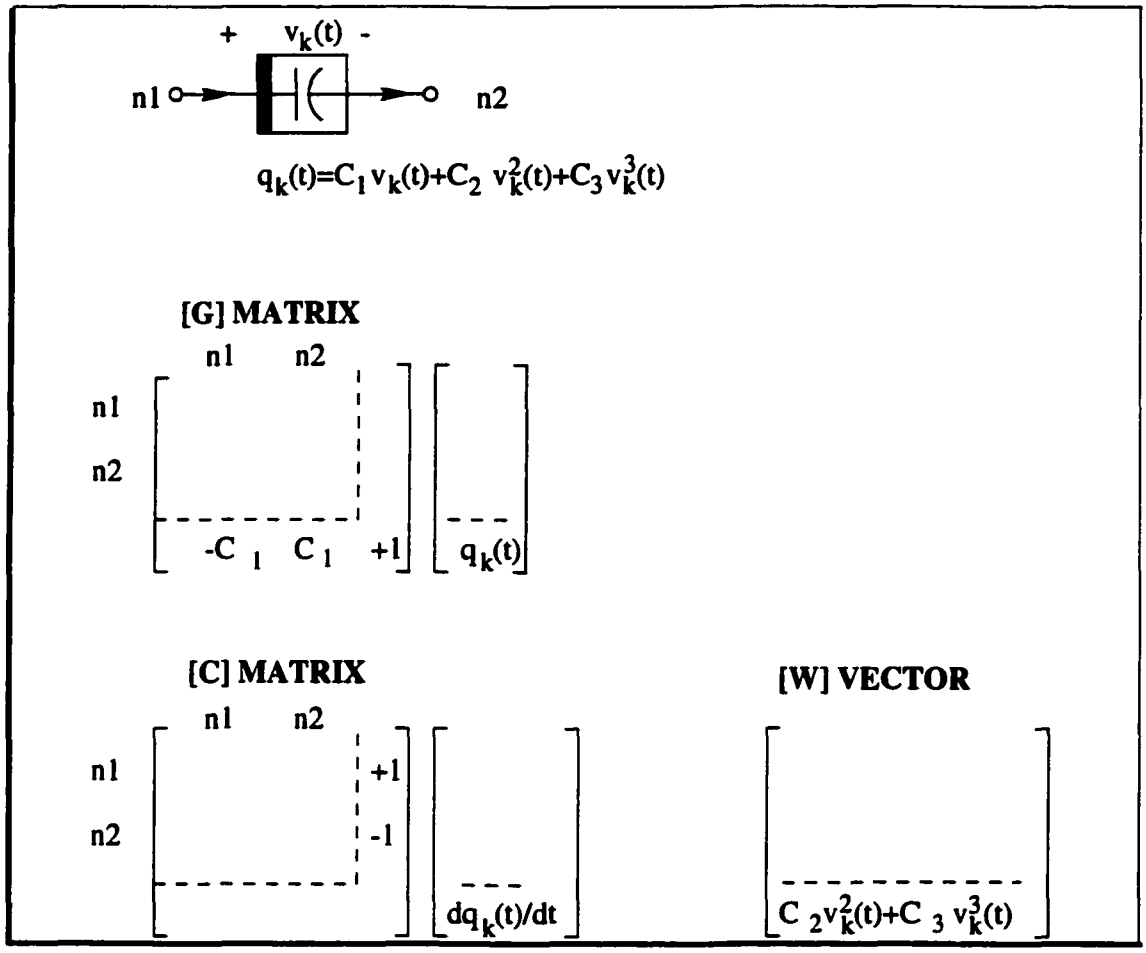


Figure 6.6: Stamps for nonlinear capacitors

$$v_k^{(m)}(t) = \begin{cases} v^{(m)}(t) & nT + \sigma_{k-1} < t \leq nT + \sigma_k \\ 0 & \text{elsewhere} \end{cases} \tag{6.51}$$

If $w(t)$ is replaced with $\epsilon w(t)$, then

$$v_k(t) = \sum_{m=1}^{\infty} v_k^{m)}(t)\epsilon^m \qquad k = 1, 2, ..., K \tag{6.52}$$

Further multiplying (6.52) by a Dirac delta function $\delta(t - nT - \sigma_k^-)$ gives

$$v_k(nT + \sigma_k^-) = \sum_{m=1}^{\infty} v_k^{(m)}(nT + \sigma_k^-)\epsilon^m \qquad k = 1, 2, ..., K \qquad (6.53)$$

where $v_k(nT + \sigma_k^-)$ is the network variable $v(t)$ at $t = nT + \sigma_k^-$ (final condition), $v_k^{(1)}(nT + \sigma_k^-)$, $v_k^{(2)}(nT + \sigma_k^-)$, ... are the 1st, 2nd,...,-order terms of Volterra series expansion of $v_k(nT + \sigma_k^-)$. Note $v_k(t)$, $v_k^{(1)}(t)$, $v_k^{(2)}(t)$,... , and $v_k^{(1)}(nT + \sigma_k^-)$, $v_k^{(2)}(nT + \sigma_k^-)$, ... are defined in the entire time domain. Fourier transform of (6.49) gives

$$V_k(j\omega) = \sum_{m=1}^{\infty} V_k^{(m)}(j\omega) \qquad k = 1, 2, ..., K \qquad (6.54)$$

Writing (6.54) for all phases and summing up the resultant equations give the complete response of the periodically switched nonlinear circuit

$$V(j\omega) = \sum_{m=1}^{\infty} V^{(m)}(j\omega) \qquad (6.55)$$

6.5.3 Distortion Analysis of PSN Circuits

In the analysis of PSL circuits, the difficulties associated with periodically time-varying topology are overcome by decomposing the circuits into a set of LTI circuits connected via the initial and final conditions of the network variables [47]. Analogously, in distortion analysis of PSN circuits, a PSN circuit can be considered as a set of nonlinear time-invariant circuits connected via the initial and final conditions of the network variables of the circuits, as shown in Fig.6.7. Assume that the nonlinearities encountered can be modeled sufficiently by the third-order Taylor series expansions of their constitutive equations. Further assume that the network

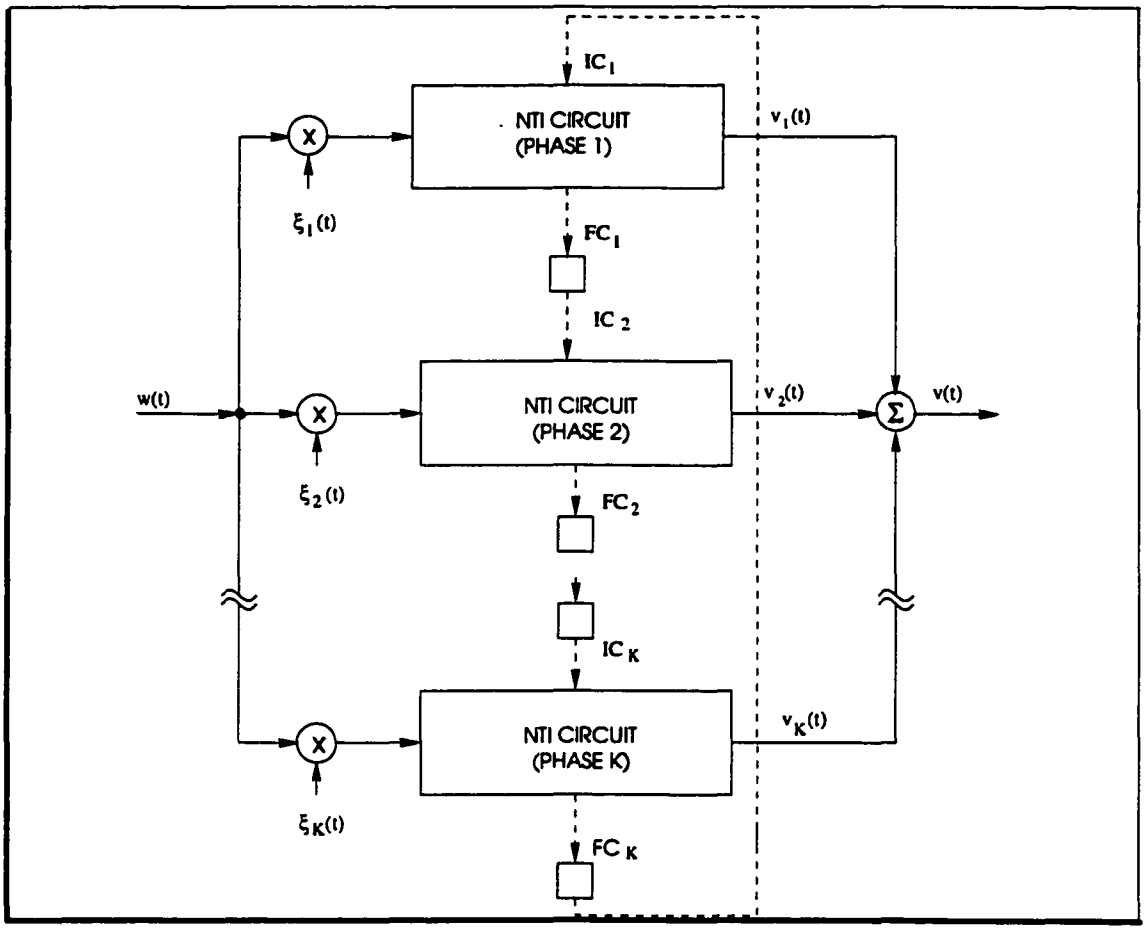


Figure 6.7: Block diagram of PSN circuits. IC - initial condition, FC - final condition

variables of PSN circuits can be represented by the 3rd-order Volterra series of the input. It can be shown that when one-graph formulation method is used, the nonlinear time-invariant circuit in phase k is characterized by

$$\begin{aligned} \mathbf{G}_k\mathbf{v}_k(t) + \mathbf{C}_k\frac{d\mathbf{v}_k(t)}{dt} &= \mathbf{w}^{(1)}(t)\xi_k(t) \\ &+ \mathbf{C}_k\mathbf{v}_{k-1}(nT+\sigma_{k-1}^{+})\delta(t-nT-\sigma_{k-1}^{+}) \\ &- \mathbf{C}_k\mathbf{v}_k(nT+\sigma_k^{-})\delta(t-nT-\sigma_k^{-}) \end{aligned}$$

$$+ \quad \mathbf{A}_2\mathbf{v}_k^2(t) + \mathbf{A}_3\mathbf{v}_k^3(t) \tag{6.56}$$

where $\xi_k(t)$ is the kth window function defined earlier in Chapter 3. A useful identity of the window function $\xi_k(t)$ is that

$$\xi_k^n(t) = \xi_k(t) \tag{6.57}$$

where n is any positive integer. Eq.(6.57) can be readily verified. $\mathbf{v}_k(t)$ is the network variable vector consisting of nodal voltages, some branch currents, charges of nonlinear capacitors and fluxes of nonlinear inductors of the circuit, $\mathbf{G}_k$ and $\mathbf{C}_k$ are the conductance and capacitance matrices, $\mathbf{w}^{(1)}(t)$ is the input, $\mathbf{A}_2$ and $\mathbf{A}_3$ are constant matrices depicting respectively the 2nd, 3rd-order nonlinearities of the circuits. The elements of the vectors $\mathbf{v}_k^2(t)$ and $\mathbf{v}_k^3(t)$ are the square and cube of the corresponding elements of $\mathbf{v}_k(t)$, respectively. Note we have employed scalar-like conventions here for their self-explanation feature.

If the input is changed from $\mathbf{w}(t)$ to $\epsilon\mathbf{w}(t)$, then using (6.52) and (6.53) with only up-to the 3rd-order terms considered, Eq.(6.56) becomes

$$\begin{aligned}
\mathbf{G}_k \sum_{m=1}^{3} \epsilon^m \mathbf{v}_k^{(m)}(t) \quad &+ \quad \mathbf{C}_k \sum_{m=1}^{3} \epsilon^m \frac{d\mathbf{v}_k^{(m)}(t)}{dt} = \epsilon\mathbf{w}^{(1)}(t)\xi_k(t) \\
&+ \quad \mathbf{C}_k \sum_{m=1}^{3} \epsilon^m \mathbf{v}_{k-1}^{(m)}(nT + \sigma_{k-1}^+)\delta(t - nT - \sigma_{k-1}^+) \\
&- \quad \mathbf{C}_k \sum_{m=1}^{3} \epsilon^m \mathbf{v}_k^{(m)}(nT + \sigma_k^-)\delta(t - nT - \sigma_k^-) \\
&+ \quad \mathbf{A}_2\Big[\sum_{m=1}^{3} \epsilon^m \mathbf{v}_k^{(m)}(t)\Big]^2 + \mathbf{A}_3\Big[\sum_{m=1}^{3} \epsilon^m \mathbf{v}_k^{(m)}(t)\Big]^3
\end{aligned} \tag{6.58}$$

Eq.(6.58) is essentially a power series in ϵ. Following the same arguments as those in deriving (6.37), we obtain the following set of linear differential equations

$$\begin{aligned}\mathbf{G}_k\mathbf{v}_k^{(1)}(t) + \mathbf{C}_k\frac{d\mathbf{v}_k^{(1)}(t)}{dt} &= \mathbf{w}^{(1)}(t)\xi_k(t) \\ &+ \mathbf{C}_k\mathbf{v}_{k-1}^{(1)}(nT+\sigma_{k-1}^+)\delta(t-nT-\sigma_{k-1}^+) \\ &- \mathbf{C}_k\mathbf{v}_k^{(1)}(nT+\sigma_k^-)\delta(t-nT-\sigma_k^-). \qquad (6.59)\end{aligned}$$

$$\begin{aligned}\mathbf{G}_k\mathbf{v}_k^{(2)}(t) + \mathbf{C}_k\frac{d\mathbf{v}_k^{(2)}(t)}{dt} &= \mathbf{w}^{(2)}(t)\xi_k(t) \\ &+ \mathbf{C}_k\mathbf{v}_{k-1}^{(2)}(nT+\sigma_{k-1}^+)\delta(t-nT-\sigma_{k-1}^+) \\ &- \mathbf{C}_k\mathbf{v}_k^{(2)}(nT+\sigma_k^-)\delta(t-nT-\sigma_k^-). \qquad (6.60)\end{aligned}$$

$$\begin{aligned}\mathbf{G}_k\mathbf{v}_k^{(3)}(t) + \mathbf{C}_k\frac{d\mathbf{v}_k^{(3)}(t)}{dt} &= \mathbf{w}^{(3)}(t)\xi_k(t) \\ &+ \mathbf{C}_k\mathbf{v}_{k-1}^{(3)}(nT+\sigma_{k-1}^+)\delta(t-nT-\sigma_{k-1}^+) \\ &- \mathbf{C}_k\mathbf{v}_k^{(3)}(nT+\sigma_k^-)\delta(t-nT-\sigma_k^-) \qquad (6.61)\end{aligned}$$

where

$$\mathbf{w}^{(2)}(t) = \mathbf{A}_2[\mathbf{v}^{(1)}(t)]^2 \qquad (6.62)$$

$$\mathbf{w}^{(3)}(t) = 2\mathbf{A}_2\mathbf{v}^{(1)}(t)\mathbf{v}^{(2)}(t) + \mathbf{A}_3[\mathbf{v}^{(1)}(t)]^3 \qquad (6.63)$$

$\mathbf{v}^{(2)}(t)$ and $\mathbf{v}^{(3)}(t)$ are the complete responses of the PSL circuits characterized by (6.60) and (6.61), respectively. Note $\mathbf{v}^{(1)}(t)\mathbf{v}^{(2)}(t)$ and $[\mathbf{v}^{(1)}(t)]^3$ are vectors whose dimensions are the same as $\mathbf{v}^{(1)}(t)$. The elements of $\mathbf{v}^{(1)}(t)\mathbf{v}^{(2)}(t)$ are the products

of the corresponding elements of $\mathbf{v}^{(1)}(t)$ and $\mathbf{v}^{(2)}(t)$ whereas those of $[\mathbf{v}^{(1)}(t)]^3$ are the cube of the corresponding elements of $\mathbf{v}^{(1)}(t)$. Fourier transform of (6.59)-(6.61) gives

$$\begin{aligned}(\mathbf{G}_k + j\omega\mathbf{C}_k)\mathbf{V}_k^{(1)}(j\omega) &= \mathcal{F}[\mathbf{w}^{(1)}(t)\xi_k(t)] \\ &+ \mathbf{C}_k\mathcal{F}[\mathbf{v}_{k-1}^{(1)}(nT+\sigma_{k-1}^+)\delta(t-nT-\sigma_{k-1}^+)] \\ &- \mathbf{C}_k\mathcal{F}[\mathbf{v}_k^{(1)}(nT+\sigma_k^-)\delta(t-nT-\sigma_k^-)]. \qquad (6.64)\end{aligned}$$

$$\begin{aligned}(\mathbf{G}_k + j\omega\mathbf{C}_k)\mathbf{V}_k^{(2)}(j\omega) &= \mathcal{F}[\mathbf{w}^{(2)}(t)\xi_k(t)] \\ &+ \mathbf{C}_k\mathcal{F}[\mathbf{v}_{k-1}^{(2)}(nT+\sigma_{k-1}^+)\delta(t-nT-\sigma_{k-1}^+)] \\ &- \mathbf{C}_k\mathcal{F}[\mathbf{v}_k^{(2)}(nT+\sigma_k^-)\delta(t-nT-\sigma_k^-)]. \qquad (6.65)\end{aligned}$$

$$\begin{aligned}(\mathbf{G}_k + j\omega\mathbf{C}_k)\mathbf{V}_k^{(3)}(j\omega) &= \mathcal{F}[\mathbf{w}^{(3)}(t)\xi_k(t)] \\ &+ \mathbf{C}_k\mathcal{F}[\mathbf{v}_{k-1}^{(3)}(nT+\sigma_{k-1}^+)\delta(t-nT-\sigma_{k-1}^+)] \\ &- \mathbf{C}_k\mathcal{F}[\mathbf{v}_k^{(3)}(nT+\sigma_k^-)\delta(t-nT-\sigma_k^-)]. \qquad (6.66)\end{aligned}$$

Eqs.(6.64)-(6.66) reveal that the behavior of a PSN circuit can be characterized by three intrinsically related PSL circuits. The input of the circuit characterized by (6.65) is obtained from the solution of (6.64) whereas that of the circuit depicted by (6.66) is from the solutions of (6.64) and (6.65). These PSL circuits are solved in a sequential order. The circuits characterized by (6.64)- (6.66) are termed respectively as the 1st-, 2nd-, and 3rd-order Volterra circuits of the PSN circuit and are denoted by $\mathcal{N}^{(1)}$, $\mathcal{N}^{(2)}$,and $\mathcal{N}^{(3)}$, respectively. It should be noted that

because the frequency components of $\mathcal{N}^{(1)}$, $\mathcal{N}^{(2)}$, and $\mathcal{N}^{(3)}$ differ from each other, LU-decomposition of $(\mathbf{G}_k + j\omega\mathbf{C}_k)$ has to be performed each time the output frequency changes. The implementation of the theory in computing the harmonic and intermodulation distortion of PSN circuits are detailed in the following sections.

6.6 Harmonic Distortion of PSN Circuits

The harmonic distortion of a PSN circuit is obtained by finding the harmonic components of the response of the circuit to a sinusoidal input. When Volterra series-based approach is employed, it is obtained by solving $\mathcal{N}^{(1)}$, $\mathcal{N}^{(2)}$,and $\mathcal{N}^{(3)}$ of the circuit.

6.6.1 The First-order Volterra Circuit $\mathcal{N}^{(1)}$

Let the input of a PSN circuit be $w(t) = A\cos\omega_o t = A(e^{j\omega_o t} + e^{-j\omega_o t})/2$. The input signal contains two distinct frequency components at ω_o and $-\omega_o$. Using Theorem 3.1 and the principle of superposition, it can be shown that the complete response of $\mathcal{N}^{(1)}$, denoted by $v^{(1)}(t)$, contains frequency components $\pm\omega_o + k\omega_s, k = 0, \pm1, \pm2,...$, and can be represented by

$$v^{(1)}(t) = \sum_{k=-\infty}^{\infty} V_{p,k}^{(1)}(\omega_o + k\omega_s)e^{j(\omega_o+k\omega_s)t} + \sum_{k=-\infty}^{\infty} V_{n,k}^{(1)}(-\omega_o + k\omega_s)e^{j(-\omega_o+k\omega_s)t} \quad (6.67)$$

where $V_{p,k}^{(1)}(\omega_o + k\omega_s)$ and $V_{n,k}^{(1)}(-\omega_o + k\omega_s)$ are the phasors of $v^{(1)}(t)$ at frequencies $\omega_o + k\omega_s$ and $-\omega_o + k\omega_s$, respectively. The subscripts p and n specify respectively the positive and negative base band frequencies. The contribution of $\mathcal{N}^{(1)}$ to the fundamental component at ω_o is given by $V_o^{(1)}(\omega_o) = V_{p,0}^{(1)}(\omega_o)$.

6.6.2 The Second-order Volterra Circuit $\mathcal{N}^{(2)}$

The input of $\mathcal{N}^{(2)}$, denoted by $w^{(2)}(t)$, is given by (6.62)

$$\begin{aligned} w^{(2)}(t) &= \sum_{k=-\infty}^{\infty} W_{p,k}^{(2)}(2\omega_o + k\omega_s)e^{j(2\omega_o+k\omega_s)t} + \sum_{k=-\infty}^{\infty} W_{z,k}^{(2)}(k\omega_s)e^{jk\omega_s t} \\ &+ \sum_{k=-\infty}^{\infty} W_{n,k}^{(2)}(-2\omega_o + k\omega_s)e^{j(-2\omega_o+k\omega_s)t} \end{aligned} \tag{6.68}$$

where $W_{p,k}^{(2)}(2\omega_o + k\omega_s)$, $W_{z,k}^{(2)}(k\omega_s)$, and $W_{n,k}^{(2)}(-2\omega_o + k\omega_s)$ are phasors of $w^{(2)}(t)$ at $2\omega_o + k\omega_s, k\omega_s$, and $-2\omega_o + k\omega_s$, respectively. The subscript z specifies zero base band frequency. Among the frequency components of $w^{(2)}(t)$, only those at $2\omega_o+k\omega_s$ contribute to the 2nd-order harmonic [1]. The 2nd-order harmonic $V_o^{(2)}(2\omega_o)$ of the output is obtained by summing up the response of $\mathcal{N}^{(2)}$ at frequency $2\omega_o$ with input at frequencies $2\omega_o + k\omega_s, k = 0, \pm 1, ...$

$$V_o^{(2)}(2\omega_o) = \sum_{k=-\infty}^{\infty} \mathcal{H}^{(2)}(2\omega_o, 2\omega_o + k\omega_s)W_{p,k}^{(2)}(2\omega_o + k\omega_s) \tag{6.69}$$

where $\mathcal{H}^{(2)}(2\omega_o, 2\omega_o + k\omega_s)$ is the aliasing transfer function of $\mathcal{N}^{(2)}$. Further from Theorem 3.1, the complete solution of $\mathcal{N}^{(2)}$, denoted by $v^{(2)}(t)$, with inputs given by (6.68) is given by

$$\begin{aligned} v^{(2)}(t) &= \sum_{k=-\infty}^{\infty} V_{p,k}^{(2)}(2\omega_o + k\omega_s)e^{j(2\omega_o+k\omega_s)t} + \sum_{k=-\infty}^{\infty} V_{z,k}^{(2)}(k\omega_s)e^{jk\omega_s t} \\ &+ \sum_{k=-\infty}^{\infty} V_{n,k}^{(2)}(-2\omega_o + k\omega_s)e^{j(-2\omega_o+k\omega_s)t} \end{aligned} \tag{6.70}$$

[1] In saying so, we have assumed that $-2\omega_o + k\omega_s$ and $k\omega_s$ will not be multiples of $2\omega_o$ for any k. This is often the case in reality as ω_s is usually much higher than ω_o.

where $V^{(2)}_{p,k}(2\omega_o + k\omega_s)$, $V^{(2)}_{z,k}(k\omega_s)$, and $V^{(2)}_{n,k}(-2\omega_o + k\omega_s)$ are the phasors of $v^{(2)}(t)$ at $2\omega_o + k\omega_s$, $k\omega_s$, and $-2\omega_o + k\omega_s$, respectively. These phasor quantities are needed in solving $\mathcal{N}^{(3)}$, as will be shown in the sequel.

6.6.3 The Third-order Volterra Circuit $\mathcal{N}^{(3)}$

The input of $\mathcal{N}^{(3)}$ is given by (6.63). Let us examine these two inputs in more detail. $v^{(1)}(t)v^{(2)}(t)$ contains frequency components $\pm 3\omega_o + k\omega_s$ and $\pm\omega_o + k\omega_s$. Among them, only those at $3\omega_o + k\omega_s$ contributes to the third-order harmonic. The input at $\omega_o + k\omega_s$, however, affects the fundamental. Note that it was assumed that $-\omega_o + k\omega_s$ and $-3\omega_o + k\omega_s$ will not be multiples of either ω_o or $3\omega_o$ for any k. $\mathcal{N}^{(3)}$ only needs to be solved with (a) the input at $3\omega_o + k\omega_s$ and the output at $3\omega_o$ for its contribution to the 3rd-order harmonic and (b) the input at $\omega_o + k\omega_s$ and the output at ω_o for its contribution to the fundamental.

Important to note that in computing the input of $\mathcal{N}^{(3)}$, the solutions of $\mathcal{N}^{(1)}$ at $\omega_o + n\omega_s$ and $\mathcal{N}^{(2)}$ at $2\omega_o + n\omega_s$ are needed. $\mathcal{N}^{(1)}$ and $\mathcal{N}^{(2)}$ therefore need to be solved at all relevant side band frequencies with output at these frequencies. $\mathcal{N}^{(3)}$, however, needs only to be solved at specific frequencies because only the responses at ω_o and $3\omega_o$ are of concern. The output of $\mathcal{N}^{(3)}$ at ω_o due to $v^{(1)}(t)v^{(2)}(t)$ is obtained from

$$V^{(3)}_{o,1}(\omega_o) = \sum_{k=-\infty}^{\infty} \mathcal{H}^{(3)}(\omega_o, \omega_o + k\omega_s) W^{(3)}_{p,k}(\omega_o + k\omega_s) \tag{6.71}$$

where $\mathcal{H}^{(3)}(\omega_o, \omega_o + k\omega_s)$ is the aliasing transfer function of $\mathcal{N}^{(3)}$ with input at $\omega_o + k\omega_s$ and output at ω_o, $W^{(3)}_{p,k}(\omega_o + k\omega_s)$ is computed from

$$\begin{aligned} W^{(3)}_{p,k}(w_o + k\omega_s) &= \sum_{k_1,k_2=-\infty;k_1\neq k_2}^{\infty} V^{(1)}_{n,k_1}(-\omega_o + k_1\omega_s)V^{(2)}_{p,k_2}(2\omega_o + k_2\omega_s) \\ &+ \sum_{k_1,k_2=-\infty;k_1\neq k_2}^{\infty} V^{(1)}_{p,k_1}(\omega_o + k_1\omega_s)V^{(2)}_{z,k_2}(k_2\omega_s) \end{aligned} \tag{6.72}$$

The third-order harmonic component generated by $v^{(1)}(t)v^{(2)}(t)$ is obtained from

$$V^{(3)}_{o,1}(3\omega_o) = \sum_{k=-\infty}^{\infty} \mathcal{H}^{(3)}(3\omega_o, 3\omega_o + k\omega_s)W^{(3)}_{p,k}(3\omega_o + k\omega_s) \tag{6.73}$$

where

$$W^{(3)}_{p,k}(3\omega_o + k\omega_s) = \sum_{k_1,k_2=-\infty;k_1\neq k_2}^{\infty} V^{(1)}_{p,k_1}(\omega_o + k_1\omega_s)V^{(2)}_{p,k_2}(2\omega_o + k_2\omega_s) \tag{6.74}$$

and $\mathcal{H}^{(3)}(3\omega_o, 3\omega_o + k\omega_s)$ is the aliasing transfer function of $\mathcal{N}^{(3)}$ with the input at $3\omega_o + k\omega_s$ and output at $3\omega_o$. The other input of $\mathcal{N}^{(3)}$, $[v^{(1)}(t)]^3$, also contributes to both the fundamental and third-order harmonics. Its contribution can be computed in a similar manner as that of $v^{(1)}(t)v^{(2)}(t)$. Let its contribution to the base band and the 3rd-order harmonic be denoted by $V^{(3)}_{o,2}(\omega_o)$ and $V^{(3)}_{o,2}(3\omega_o)$, respectively.

In summary, the fundamental component of the complete response of the circuit is obtained by summing up the contributions of $\mathcal{N}^{(1)}$ and $\mathcal{N}^{(3)}$ at ω_o. The 2nd-order harmonic component of the complete response is solely determined by the solution of $\mathcal{N}^{(2)}$ at $2\omega_o$. The 3rd-order harmonic is obtained by summing up the contribution of $\mathcal{N}^{(3)}$ with inputs $v^{(1)}(t)v^{(2)}(t)$ and $[v^{(1)}(t)]^3$. The 2nd-order harmonic distortion

is computed from

$$HD_2 = \left| \frac{V_o^{(2)}(2\omega_o)}{V_o^{(1)}(\omega_o) + V_{o,1}^{(3)}(\omega_o) + V_{o,2}^{(3)}(\omega_o)} \right| \tag{6.75}$$

and the 3rd-order harmonic distortion

$$HD_3 = \left| \frac{V_{o,1}^{(3)}(3\omega_o) + V_{o,2}^{(3)}(3\omega_o)}{V_o^{(1)}(\omega_o) + V_{o,1}^{(3)}(\omega_o) + V_{o,2}^{(3)}(\omega_o)} \right| \tag{6.76}$$

6.6.4 The Fold-over Effect

Eqs.(6.69), (6.71) and (6.73) demonstrate that the high-order side band components of the inputs of $\mathcal{N}^{(2)}$ and $\mathcal{N}^{(3)}$ contribute to the distortion in the base band. This is analogous to the fold-over effect encountered in noise analysis of PSL circuits. The folding effect in computing $V_o^{(3)}(3\omega_o)$ is illustrated in Fig.6.8. The frequency reversal theorem can be employed to minimize the cost of computation in calculating these aliasing transfer functions.

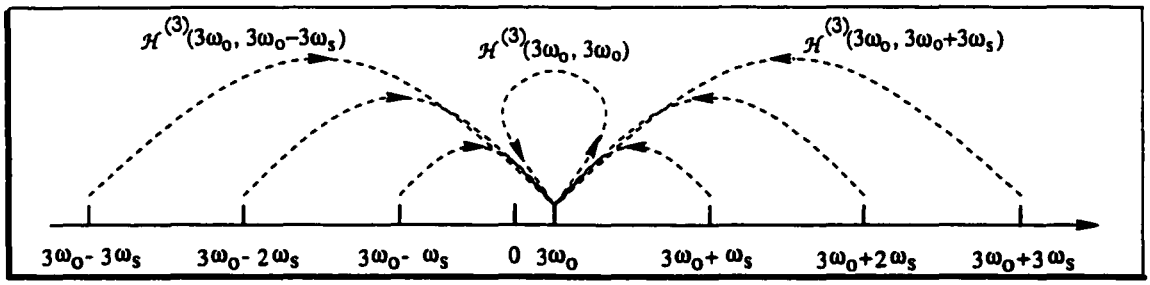


Figure 6.8: Fold-over effect in distortion analysis

6.7 Intermodulation Distortion of PSN Circuits

Intermodulation distortion arises when the input of a PSN circuit contains two sinusoidal signals of different frequencies. For example, in a RF receiver, the frequency difference between two adjacent channels is very small. Due to the nonlinearities in the receiver, frequency components other than those of the carriers are generated. The harmonic components in the output of the mixer are usually not of concern in this case as they will be filtered out by a downstream loop filter. The third-order intermodulation components, however, are critical because their spectra fall so close to those of the carriers that the loop filter fails to eliminate them. The analysis of the third-order intermodulation distortion is of practical importance.

6.7.1 The Solution of $\mathcal{N}^{(1)}$

Let the input of a PSN circuit be

$$w(t) = A(\cos\omega_1 t + \cos\omega_2 t) = \frac{A}{2}[e^{j\omega_1 t} + e^{-j\omega_1 t} + e^{j\omega_2 t} + e^{-j\omega_2 t}] \tag{6.77}$$

From Theorem 3.1 and the principle of superposition, the complete response of $\mathcal{N}^{(1)}$ of the PSN network, denoted by $v^{(1)}(t)$, contains frequency components $\pm\omega_1 + k\omega_s$ and $\pm\omega_2 + k\omega_s, k = 0, \pm 1, \pm 2, ...$, and can be represented by

$$\begin{aligned} v^{(1)}(t) &= \sum_{k=-\infty}^{\infty} V_{1p,k}^{(1)}(\omega_1 + k\omega_s)e^{j(\omega_1+k\omega_s)t} + \sum_{k=-\infty}^{\infty} V_{1n,k}^{(1)}(-\omega_1 + k\omega_s)e^{j(-\omega_1+k\omega_s)t} \\ &+ \sum_{k=-\infty}^{\infty} V_{2p,k}^{(1)}(\omega_2 + k\omega_s)e^{j(\omega_2+k\omega_s)t} + \sum_{k=-\infty}^{\infty} V_{2n,k}^{(1)}(-\omega_2 + k\omega_s)e^{j(-\omega_2+k\omega_s)t} \end{aligned} \tag{6.78}$$

where $V^{(1)}_{1p,k}(\omega_1 + k\omega_s)$, $V^{(1)}_{1n,k}(-\omega_1 + k\omega_s)$, $V^{(1)}_{2p,k}(\omega_2 + k\omega_s)$, and $V^{(1)}_{2n,k}(-\omega_2 + k\omega_s)$ are the phasors of $v^{(1)}(t)$ at $\omega_1 + k\omega_s$, $-\omega_1 + k\omega_s$, $\omega_2 + k\omega_s$, and $-\omega_2 + k\omega_s$respectively.

6.7.2 The Solution of $\mathcal{N}^{(2)}$

The input of $\mathcal{N}^{(2)}$ contains frequency components $\pm 2\omega_1 + k\omega_s$, $\pm 2\omega_2 + k\omega_s$, $k\omega_s$, $(\omega_1 \pm \omega_2) + k\omega_s$ and $(\omega_2 \pm \omega_1) + k\omega_s, k = 0, \pm 1, \pm 2, \ldots$. Consequently, the output of $\mathcal{N}^{(2)}$ consists of frequency components $\pm 2\omega_1 + k\omega_s$, $\pm 2\omega_2 + k\omega_s$, $k\omega_s$, $(\omega_1 \pm \omega_2) + k\omega_s$, $(\omega_2 \pm \omega_1) + k\omega_s$. Further analysis shows that the input of $\mathcal{N}^{(2)}$ at $\pm(\omega_1 + \omega_2) + k\omega_s$ and $k\omega_s$ do not contribute to the 3rd-order intermodulation. As a result, the output of $\mathcal{N}^{(2)}$ at these frequencies is not required. The output at other frequencies, however, must be computed.

6.7.3 The Solution of $\mathcal{N}^{(3)}$

The input of $\mathcal{N}^{(3)}$ consists of $v^{(1)}(t)v^{(2)}(t)$ and $[v^{(1)}(t)]^3$. It can be shown that among the frequency components of $v^{(1)}(t)v^{(2)}(t)$, only those at $(2\omega_1 - \omega_2) + k\omega_s$ and $(2\omega_2 - \omega_1) + k\omega_s$ contribute to the 3rd-order intermodulation whereas those at $\omega_1 + k\omega_s$ and $\omega_2 + k\omega_s$ contribute to the fundamentals at ω_1 and ω_2, respectively. $\mathcal{N}^{(3)}$ therefore needs to be solved with (a) input at $(2\omega_1 - \omega_2) + k\omega_s$ and $(2\omega_2 - \omega_1) + k\omega_s$, and outputs at $2\omega_1 - \omega_2$ and $2\omega_2 - \omega_1$, respectively; (b) input at $\omega_1 + k\omega_s$ and $\omega_2 + k\omega_s$ and output at ω_1 and ω_2, respectively.

Note the amplitude of the inputs at these frequencies must be calculated prior to solving $\mathcal{N}^{(3)}$. Similarly, Among the frequency components of $[v^{(1)}(t)]^3$, only (a) $(2\omega_1 - \omega_2) + k\omega_s$ and $(2\omega_2 - \omega_1) + k\omega_s$, (b) $\omega_1 + k\omega_s$ and $\omega_2 + k\omega_s$ are of concern as they contribute to the third-order intermodulation. The frequency reversal theorem can be used in both cases to minimize the cost of computation.

The 3rd-order intermodulation distortion at $2\omega_1 - \omega_2$ is computed from

$$IM_3 = \left| \frac{V_{o,1}^{(3)}(2\omega_1 - \omega_2) + V_{o,2}^{(3)}(2\omega_1 - \omega_2)}{V_{1p,0}^{(1)} + V_{o,1}^{(3)}(\omega_1) + V_{o,2}^{(3)}(\omega_1)} \right| \tag{6.79}$$

where $V_{o,1}^{(3)}(2\omega_1 - \omega_2)$ and $V_{o,2}^{(3)}(2\omega_1 - \omega_2)$ are the contributions of $v^{(1)}(t)v^{(2)}(t)$ and $[v^{(1)}(t)]^3$ at $2\omega_1 - \omega_2$, respectively. $V_{o,1}^{(3)}(\omega_1)$ and $V_{o,2}^{(3)}(\omega_1)$ are the contributions of $v^{(1)}(t)v^{(2)}(t)$ and $[v^{(1)}(t)]^3$ at ω_1, respectively.

6.8 Numerical Examples

The above algorithms for harmonic and intermodulation distortion analysis of PSN circuits have been implemented in a computer program SNCDAP (Switched Nonlinear Circuits Distortion Analysis Program). In this section, the harmonic and intermodulation distortion of several PSN circuits are analyzed using SNCDAP and the results are compared with SPICE simulation.

6.8.1 Harmonic Distortion of Modulator

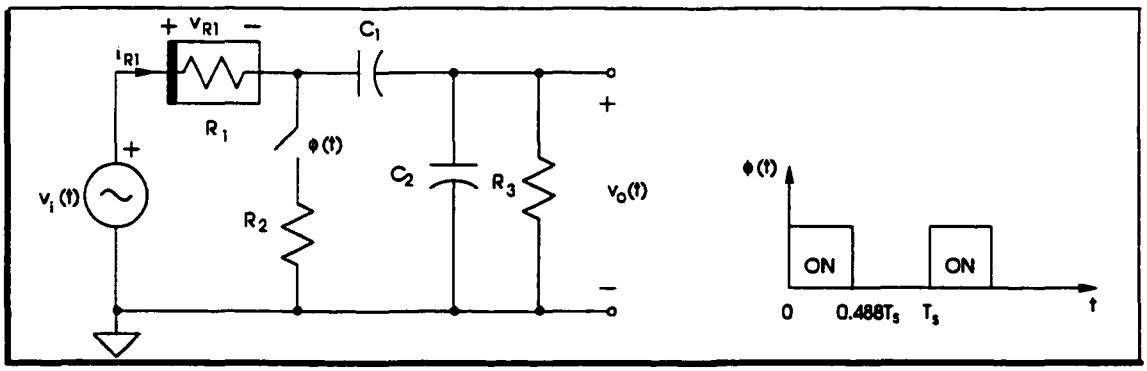


Figure 6.9: Modulator

Table 6.1: Parameter values of modulator

Parameter	Numerical value	Unit	Remark
C_1	2200	pF	
C_2	80	pF	
R_1	$v_{R1} = 206.95935 i_{R1} + 100 i_{R1}^2$		
R_2	35	Ω	
R_3	300	Ω	
f_s	8	kHz	Clock frequency
τ_1	$0.488 T_s$	Second	Width of phase 1
τ_2	$0.512 T_s$	Second	Width of phase 2

Consider a modulator shown in Fig.6.9 with the parameter values given in Table 6.1 [146]. The resistor R_1 is modeled as a nonlinear current-controlled voltage source. The circuit was solved using SNCDAP and results are shown in Table 6.2. Results from HPSICE simulation are also shown in the table. Care was taken in choosing the step size in transient analysis, collecting steady-state response data, and selecting the number of data points and windows in FFT analysis [147–149]. As observed that the results from SNCDAP and HSPICE compare well. To demonstrate the fold-over effect in distortion analysis, the 2nd-order harmonic components at 1 kHz from SNCDAP are plotted versus the number of side bands considered in Fig.6.10. As can be seen that the 2nd-order harmonic component converges rapidly.

6.8.2 Harmonic Distortion of Stray-insensitive SC Integrator

Table 6.2: Harmonic distortion of modulator

Frequency (kHz)	HSPICE (dB)		SNCDAP (dB)	
	Fundamental	Second-order	Fundamental	Second-order
1	-53.90	-166.9	-53.91	-167.0
2	-47.88	-160.4	-47.89	-160.8
3	-44.36	-157.2	-44.38	-157.1
4	-41.87	-154.2	-41.87	-154.3
5	-39.93	-152.2	-39.93	-151.9
6	-38.35	-149.9	-38.35	-149.8
7	-37.01	-147.7	-37.02	-147.9
8	-35.86	-145.8	-35.86	-146.0

Table 6.3: Parameter values of stray-insensitive SC integrator

Parameter	Numerical value	Unit	Remark
C_1	0.015926	μF	
C_2	10	μF	
R_{ON}	3.5	kΩ	
f_s	100	kHz	Clock frequency
τ_1	$0.488T_s$	Second	Width of phase 1
τ_2	$0.512T_s$	Second	Width of phase 2

Consider a stray-insensitive switched capacitor integrator shown in Fig.6.11 with parameters given in Table 6.3. MOSFET switches M_2, M_3, and M_4 are modeled as a linear resistor with resistance 3.5kΩ in series with an ideal switch. M_1 is modeled as a nonlinear resistor in series with an ideal switch. The nonlinear resistor is

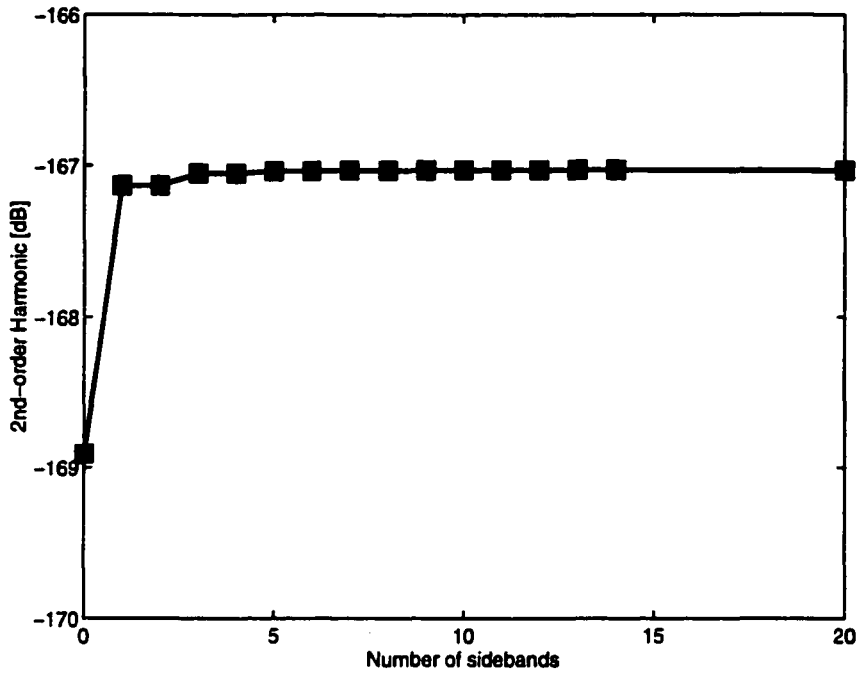


Figure 6.10: Convergence of 2nd-order harmonic of modulator

characterized by $v_R = 3500i_R + 500i_R^2$. The model of the op amp is the same as those used in Chapter 4. The circuit was solved using SNCDAP and the results are shown in Table 6.4, together with HSPICE simulation results. To ensure that the second-order harmonic components are free of numerical errors, several HSPICE simulations with different step sizes used in transient analysis were conducted. The absolute errors between the harmonic components obtained from using different step sizes in transient analysis are less than 0.2 decibels. It is seen that the SNCDAP gives good prediction of both the fundamental and the second-order harmonic components. The 2nd-order harmonic component at 1 kHz is plotted in Fig.6.12 versus the number of side bands considered. It is seen that the 2nd-order harmonic converges with the increase in the number of side bands. Also observed that the rate of convergence is slower as compared with the modulator.

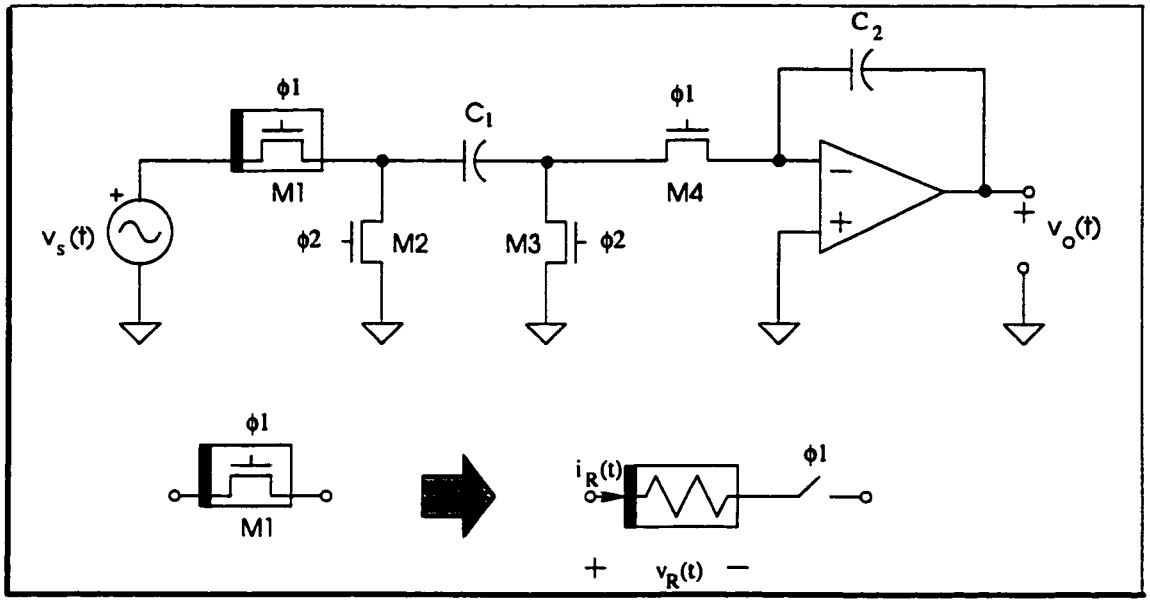


Figure 6.11: Stray-insensitive SC integrator

Table 6.4: Harmonic distortion of stray-insensitive integrator

Frequency	HSPICE (dB)		SNCDAP (dB)	
(kHz)	Fund.	2nd-order	Fund.	Second-order
1	-27.87	-99.85	-27.87	-100.4
2	-31.89	-99.57	-31.89	-101.1
3	-34.42	-100.4	-34.42	-101.9
4	-36.17	-103.7	-36.17	-102.4
5	-37.38	-102.0	-37.39	-102.4
6	-38.22	-102.4	-38.22	-102.2

To further demonstrate the effectiveness of the proposed method, another nonlinear switched capacitor integrator shown in Fig.6.13 with parameters given in Table 6.5 was analyzed. The only nonlinearity is the amplifier modeled by $v_2(t) =$

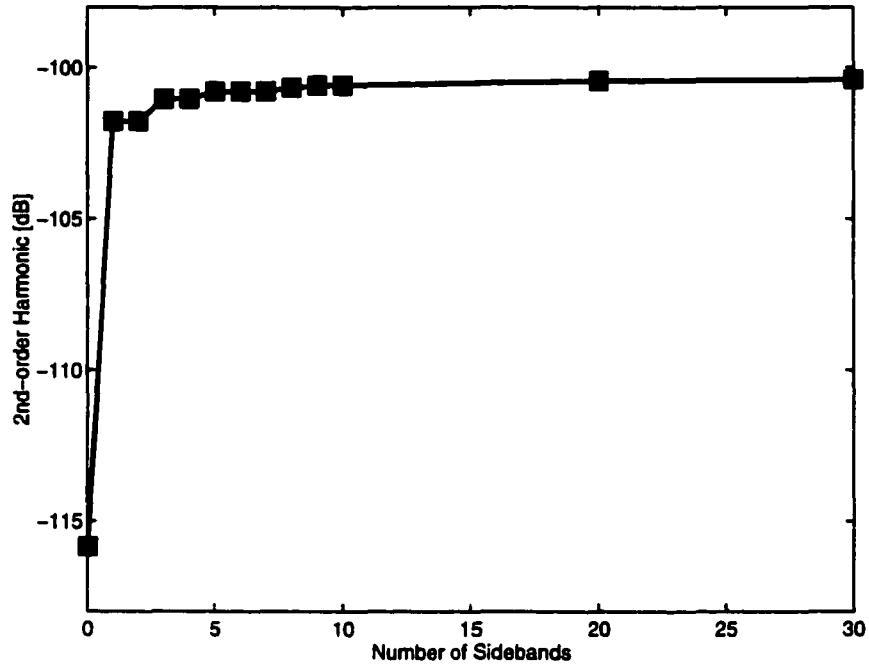


Figure 6.12: Convergence of 2nd-order harmonic of stray-insensitive SC integrator

Table 6.5: Parameter values of stray-insensitive SC integrator

Parameter	Numerical value	Unit	Remark
C_1	10	nF	
C_2	1.0	nF	
R_{ON}	3.5	kΩ	
f_s	100	kHz	Clock frequency
τ_1	$0.5T_s$	Second	Width of phase 1
τ_2	$0.5T_s$	Second	Width of phase 2

$a_1v_1(t) + a_2v_1^2(t) + a_3v_1^3(t)$. Two tests were carried out for two sets of coefficients : $(a_1, a_2, a_3) = (100, 0, 10)$ and $(a_1, a_2, a_3) = (100, 10, 10)$. The harmonic components

of the output were computed using SNCDAP and the results are tabulated in Table 6.6 for the first set of coefficients and Table 6.7 for the second set. HSPICE simulation results are also shown in the tables. It is seen that the results from SNCDAP are in good agreement with HSPICE simulation. Also, in Table 6.6, since $a_2 = 0$, zero second-order harmonic is predicted by SNCDAP as both the first- and third-order PSL circuits do not contribute to the 2nd-order harmonic. This agrees with HSPICE simulation. HSPICE results for $(a_1, a_2, a_3) = (100, 10, 10)$ are plotted in Figs. 6.14 and 6.15 [2]. By comparing these plots with Fig.6.2, it is evident that the theory gives accurate prediction of the fundamental second-, and third-order harmonic components of the response. Since only third-order Volterra series expansion was considered in our implementation, SNCDAP is not capable of predicting high-order harmonics.

The CPU time used by SNCDAP (implemented in MATLAB) for computing the distortion at a single frequency is 4.1 minutes while HSPICE consumed 2.78 hours. The efficiency gain from using the proposed method is evident.

To demonstrate the efficiency gain obtained from using the frequency reversal theorem in distortion analysis of PSN circuits, the same circuit was solved using SNCDAP with frequency reversal theorem implemented and without (brute-force). The results are tabulated in Table 6.8. It is seen that the results from both methods agree well. The marginal differences are mainly due to the numerical errors caused by the differences of the two algorithms. The efficiencies of the two algorithm are also compared via their CPU time. It was observed that the method with the

[2]The estimated time constant due to the sampling capacitor and channel resistance of MOSFET switches is about 1 μs. To ensure the establishment of the steady state, the first 1000 samples were discarded from DFT analysis. Also the number of samples used in DFT analysis was 64k. Rectangular window was employed.

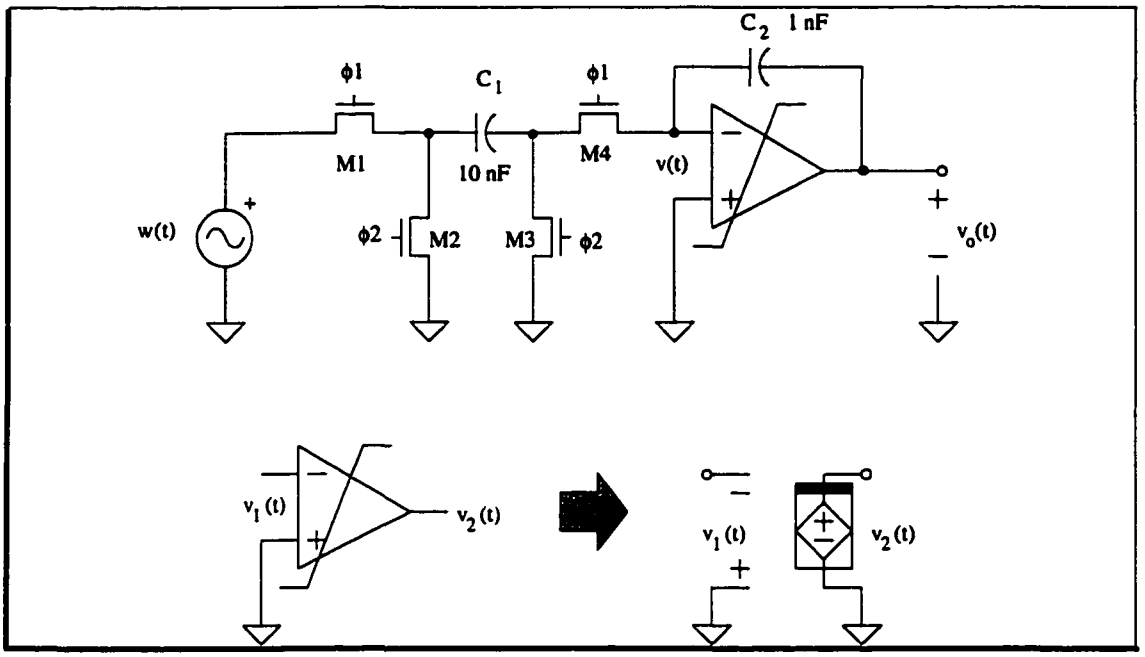


Figure 6.13: SC integrator

frequency reversal theorem implemented is 3 times faster than those without. The speedup is less than those in noise analysis shown in Chapter 4. This is because the frequency reversal theorem was only employed in solving $\mathcal{N}^{(3)}$ because $\mathcal{N}^{(2)}$ needs to be solved at all relevant side band frequencies. Our experience shows that a significant portion of the CPU time was spent on solving $\mathcal{N}^{(2)}$.

The intermodulation distortion of the circuit with $(a_1, a_2, a_3) = (100, 10, 10)$ was also investigated. The input consists of two sinusoidals with frequency difference of 100 Hz. The third-order intermodulation components were computed using SNC-DAP and the results are tabulated in Table 6.9, together with HSPICE simulation results. A good agreement is observed. HSPICE simulation results for $f_1 = 1.0$ kHz and $f_2 = 1.1$ kHz are plotted in Figs.6.16 and 6.17. A careful comparison of these plots with Fig.6.3 reveals that all major beats of the response predicted by the proposed method match HSPICE simulation.

Table 6.6: Harmonic distortion of stray-insensitive integrator ($a_1 = 100, a_2 = 0, a_3 = 10$)

Frequency	HSPICE (dB)			SNCDAP (dB)		
(kHz)	Fund.	2nd-order	3rd-order	Fund.	2nd-order	3rd-order
1.0	27.62	-135.0	-20.65	27.64	$-\infty$	-20.38
2.0	26.45	-137.1	-28.09	26.46	$-\infty$	-27.83
3.0	25.02	-132.3	-35.28	25.03	$-\infty$	-35.16
4.0	23.61	-161.4	-41.77	23.61	$-\infty$	-41.85
5.0	22.30	-145.0	-47.53	22.31	$-\infty$	-47.83
6.0	21.12	-127.9	-52.54	21.13	$-\infty$	-53.13
7.0	20.07	-140.0	-56.97	20.07	$-\infty$	-57.82
8.0	19.12	-105.0	-60.95	19.13	$-\infty$	-61.93

To demonstrate the analysis of harmonic distortion due to the existence of nonlinear capacitors, the circuit in Fig.6.11 is considered. The only nonlinear element is capacitor C_1 modeled by $C_1 = 10\times10^{-9} + 5\times10^{-9}v_{C_1} + 1.5\times10^{-9}v_{C_1}^2$ while C_2 remains unchanged. The switching frequency is 100 kHz with two equal clock phases. To avoid numerical difficulties, the circuit is impedance scaled by 10^4 and frequency scaled by 100. As a result, the ON-resistance of MOSFET switches is changed from 3.5 kΩ to 0.35 Ω. The capacitance of C_2 is changed from 1.0×10^{-9} F to 10^{-3} F. C_1 becomes $C_1 = 10\times10^{-3} + 5\times10^{-3}v_{C_1} + 1.5\times10^{-3}v_{C_1}^2$. The clock frequency is changed from 100 kHz to 1000 Hz. The operational amplifier is modeled as an ideal VCVS with gain 1000. The distortion of the output at frequency 100 Hz was analyzed. For the purpose of comparison, it was also computed using HSPICE. Both results are tabulated in Table 6.10. As can be seen that the results obtained using

Table 6.7: Harmonic distortion of stray-insensitive integrator ($a_1 = 100, a_2 = 10, a_3 = 10$)

Frequency	HSPICE (dB)			SNCDAP (dB)		
(kHz)	Fund.	2nd-order	3rd-order	Fund.	2nd-order	3rd-order
1.0	27.62	-6.738	-21.14	27.63	-6.525	-20.87
2.0	26.44	-11.91	-29.14	26.45	-11.65	-28.92
3.0	25.02	-17.23	-36.63	25.03	-17.03	-36.59
4.0	23.61	-22.10	-43.28	23.61	-21.99	-43.47
5.0	22.30	-26.42	-49.14	22.31	-26.42	-49.58
6.0	21.12	-30.23	-54.20	21.13	-30.33	-54.98
7.0	20.07	-33.61	-58.67	20.07	-33.79	-59.74
8.0	19.12	-36.60	-62.69	19.13	-36.87	-63.90

the proposed method are in good agreement with those from HSPICE simulation. HSPICE simulation results are also plotted in Fig.6.18 for verification purpose.

6.9 Summary

A Volterra series-based frequency-domain method for distortion analysis of general PSN circuits with mild nonlinearities was developed. It is shown that the behavior of these circuits can be characterized by a set of intrinsically related PSL circuits. The complete spectrum of the PSN circuit is obtained by summing up those of these PSL circuits. The analysis of PSL circuits is exact. The only approximation made is the truncation of the Volterra series expansion of network variables. The proposed method is a generalization of the multilinear theory for NTI circuits [150]

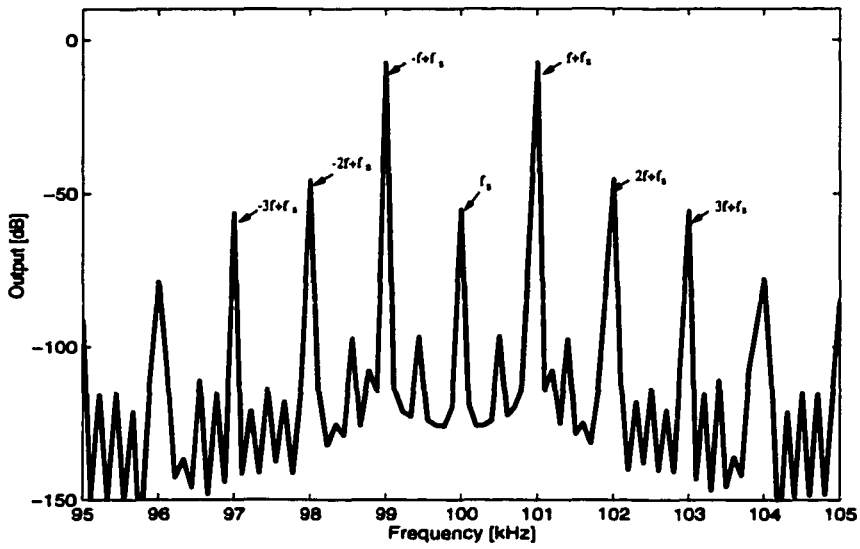


Figure 6.14: Harmonic distortion of SC integrator

and nonlinear SCNs [27, 80]. It unifies distortion analysis of nonlinear nonlinear time-invariant circuits and general PSN circuits, including nonlinear SCNs in a single algorithm.

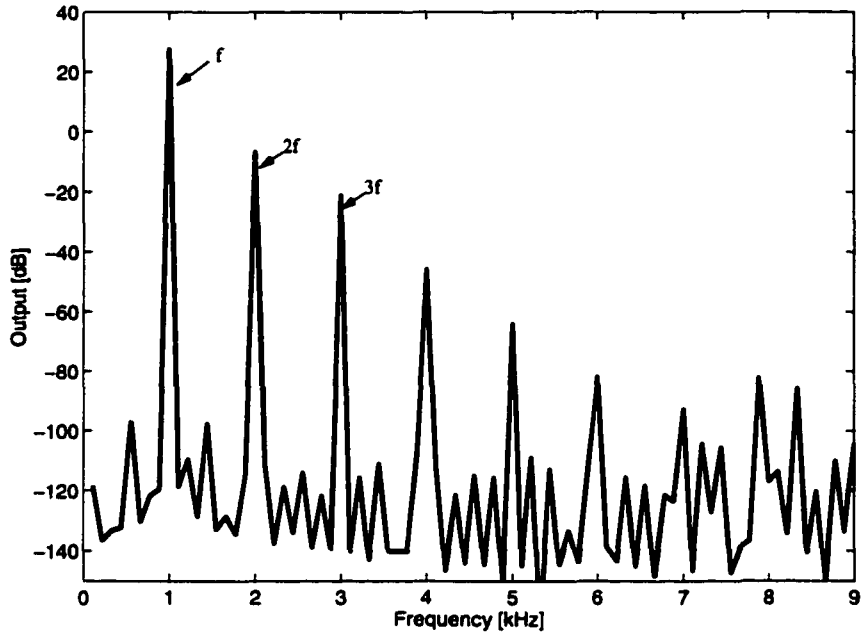


Figure 6.15: Harmonic distortion of SC integrator

Table 6.8: Harmonic distortion using adjoint network and brute-force methods

Frequency	Brute-force(dB)			Adjoint Network(dB)		
(kHz)	Fund.	2nd-order	3rd-order	Fund.	2nd-order	3rd-order
1.0	27.628	-6.525	-20.994	27.633	-6.525	-20.873
2.0	26.450	-11.645	-29.003	26.454	-11.645	-28.921
3.0	25.025	-17.027	-36.608	25.028	-17.027	-36.588
4.0	23.611	-21.988	-43.413	23.613	-21.988	-43.473
5.0	22.304	-26.415	-49.433	22.305	-26.415	-49.577
6.0	21.215	-30.328	-54.765	21.126	-30.328	-54.975
7.0	20.070	-33.791	-59.512	20.07	-33.791	-59.737
8.0	19.126	-36.874	-63.760	19.127	-36.874	-63.897

Table 6.9: Intermodulation distortion

Frequency (kHz)		HSPICE (dB)				SNCDAP (dB)	
f_1	f_2	Fund. f_1	Fund. f_2	Intermod $2f_1 - f_2$	Intermod $2f_2 - f_1$	Intermod $2f_1 - f_2$	Intermod $2f_2 - f_1$
1.0	1.1	27.85	27.76	-8.894	-9.304	-8.475	-8.860
2.0	2.1	26.58	26.44	-13.80	-14.37	-13.18	-13.74
3.0	3.1	25.09	24.95	-19.49	-20.09	-18.87	-19.47
4.0	4.1	23.65	23.51	-25.09	-25.65	-24.56	-25.12
5.0	5.1	22.32	22.20	-30.27	-30.78	-29.84	-30.36
6.0	6.1	21.14	21.02	-34.95	-35.42	-34.64	-35.10
7.0	7.1	20.08	19.98	-39.17	-39.59	-38.94	-39.36
8.0	8.1	19.13	19.04	-42.95	-43.35	-42.80	-43.18

Table 6.10: Harmonic distortion of stray-insensitive integrators with nonlinear capacitors

Frequency (Hz)	HSPICE (dB)	SNCDAP (dB)
100	14.95	14.92
200	-27.60	-27.64
300	-45.60	-46.52

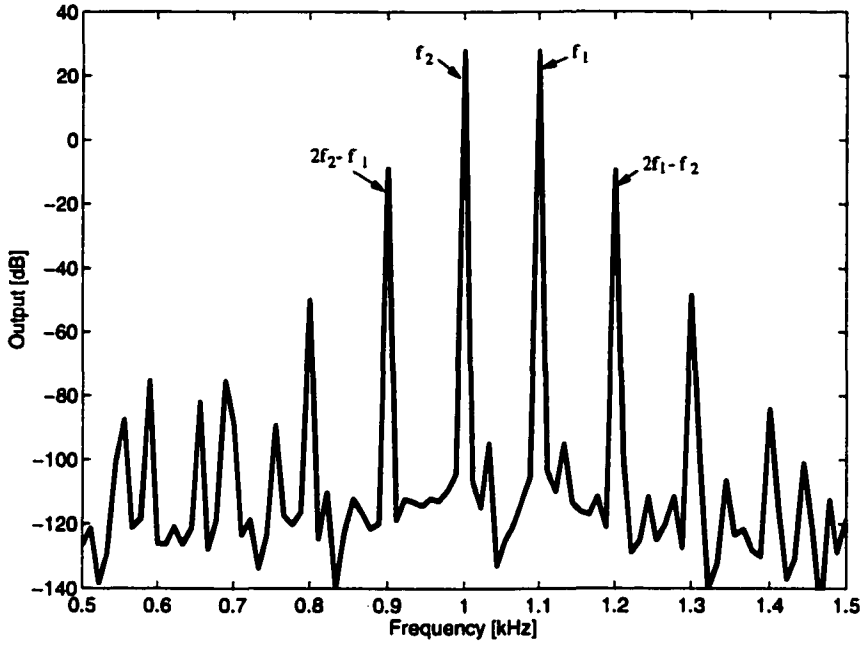


Figure 6.16: Intermodulation distortion of SC integrator

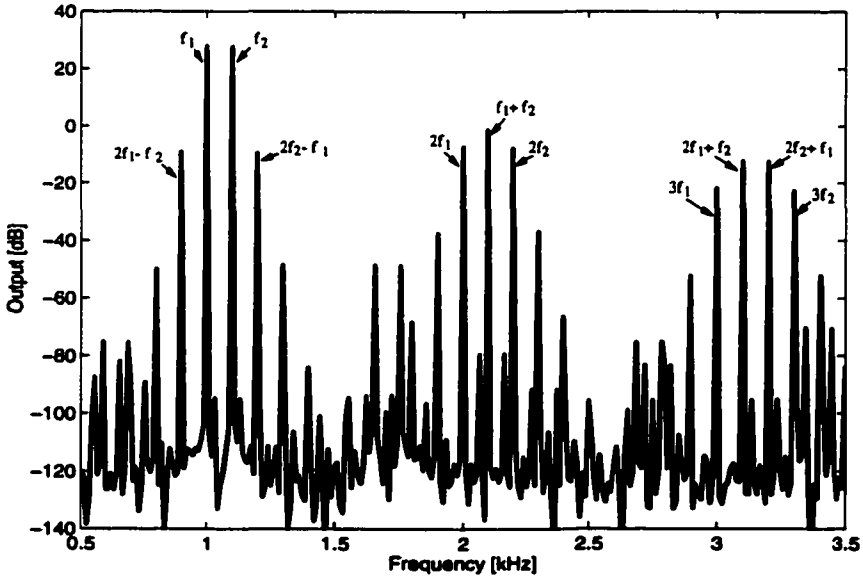


Figure 6.17: Intermodulation distortion of SC integrator

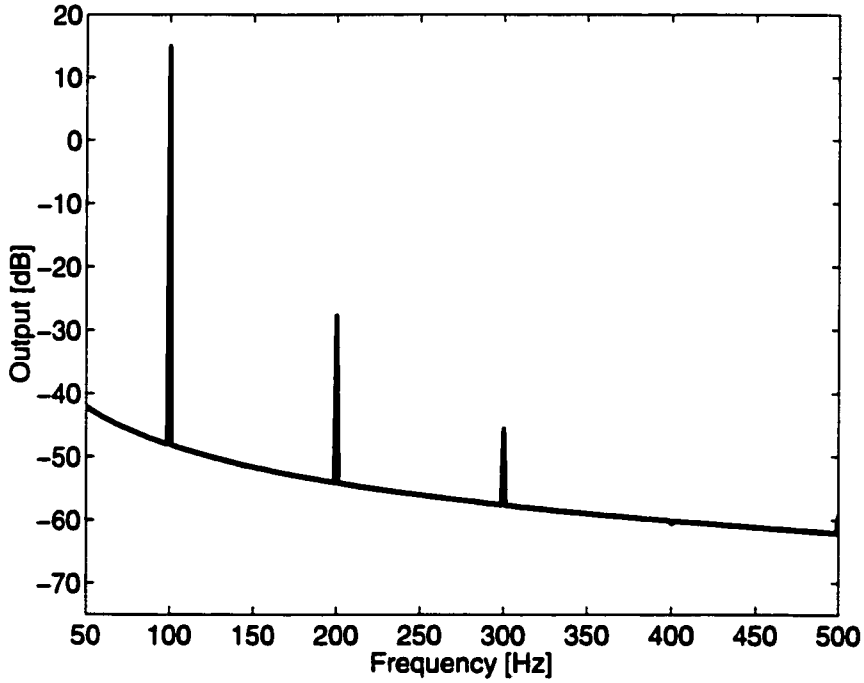


Figure 6.18: Harmonic distortion of SC integrator with nonlinear capacitors

Chapter 7

Conclusions

This thesis dealt with the analysis of the noise and sensitivity of general periodically switched linear circuits, and the distortion of periodically switched nonlinear circuits in frequency domain.

Using the characteristics of LPTV systems, we derived the Tellegen's theorem for PSL circuits in phase domain. The theory of the adjoint network of PSL circuits was developed. The frequency reversal theorem and transfer function theorem, were also developed. The adjoint network theory provides a powerful means in reducing the computational cost associated with the noise analysis of PSL circuits in two aspects : (i) It derives the transfer functions from multiple inputs to the single output of PSL circuits at a given frequency by solving its adjoint network at the same frequency only once. (ii) It computes the aliasing transfer functions by evaluating the corresponding high-order frequency components of the response of the adjoint network.

In noise analysis, an adjoint network-based algorithm was developed and implemented in a computer program to compute the output noise power of general

PSL circuits. Several PSL circuits were analyzed. The numerical results obtained using the proposed algorithm are compared with measurements and an excellent agreement is observed. The algorithm is exact and is orders of magnitude faster than the brute-force method.

In sensitivity analysis, the incremental form of Tellegen's theorem for PSL circuits in phase domain was introduced, and the frequency-domain sensitivity of PSL was obtained. The theory yields sensitivities of the response with respect to all circuit elements in one frequency analysis. The sensitivity networks of PSL circuits were introduced. It is demonstrated that the sensitivities obtained using the adjoint network technique are identical to those from the sensitivity network approach. The sensitivities of several PSL circuits were analyzed. The numerical results obtained using the proposed methods match those obtained from other CAD tools.

In distortion analysis, the time-varying Volterra series initially proposed by Yu *et al.* [143] was further developed. The time-varying network functions and multi-frequency transforms were introduced to characterize the behavior of NTV systems in frequency domain. The network variable theorem for PSN circuits was introduced and the complete spectrum of PSN was obtained. The theory was applied to frequency-domain distortion analysis of general PSN circuits. It is shown that the behavior of PSN circuits can be characterized by a set of intrinsically related PSL circuits. The complete frequency-domain spectrum of the response of the PSN circuit is obtained by summing up the spectra of the corresponding PSL circuits. These PSL circuits are solved using exact frequency-domain method, the only approximation made is the truncation of the Volterra series expansion of the network variables.

The work reported in this thesis can be extended in many areas. Suggestions for further research include :

- Extending the adjoint network theory of general periodically switched circuits to general periodically switched nonlinear circuits. This extension could be used to speed up noise and sensitivity analysis of general PSN circuits.

- Extending the theories of noise and sensitivity analysis of general PSL circuits developed in this thesis to general PSN circuits. This extension is of practical significance as there is no efficient and accurate method currently available to compute both noise and sensitivity of general PSN circuits.

- Extending the noise analysis of PSL circuits to include the effect of clock jitter. The available methods on the analysis of the effect of jitter timing are mostly time-domain approaches which requires Monte Carlo analysis. Such an analysis is time-consuming.

- Extending the frequency-domain analysis of PSL and PSN circuits to include the effect of clock signal. Specifically, the gate-source and gate-drain capacitances, as well as parasitic capacitances of MOSFET switches, will be included in modeling MOSFET switches. This will not only allow us to directly analyze the effect of clock feed-through, it will also extend the application of the theories of PSL and PSN circuits to circuits operated at intermediate and high frequencies, such as RF mixers and modulators.

- Extending the frequency-domain analysis of general switched circuits to permit rising and falling time of sampling clock. Most of the CAD tools currently available for analysis of PSL circuits and SCNs are based on the assumption of a square-wave clock signal. This assumption neglects the effect of finite rising and falling slopes of the clock signal. The operation of MOSFET switches can hence not be described accurately.

Appendix A

Numerical Inversion of Laplace Transform

In computing the frequency response of PSL circuits, numerical integration of the circuit equation is required to yield the quasi-state-transition matrix $\mathbf{N}_k$ and the zero-state response vector $\mathbf{P}_k$. There are many integration methods available. We have used numerical inversion of Laplace transform because it is equivalent to high-order numerical integration. It gives very accurate results with absolute numerical stability [97,98]. More importantly, computation is performed in frequency domain where impulse functions can be handled with ease. This appendix reviews the fundamentals of this technique. A detail description can be found in [39,97,98].

Consider a LTI circuit depicted by

$$\mathbf{G}\mathbf{v}(t) + \mathbf{C}\frac{d\mathbf{v}(t)}{dt} = \mathbf{w}(t) \qquad \mathbf{v}(t)|_{t=0} = \mathbf{v}(0^+) \tag{A.1}$$

where **G** and **C** are conductance and capacitance matrices formulated using the modified nodal analysis. $\mathbf{w}(t)$ is the input vector and $\mathbf{v}(t)$ is the network variable vector. Laplace transform of $\mathbf{v}(t)$ is obtained from

$$\mathbf{V}(s) = (\mathbf{G} + s\mathbf{C})^{-1}[\mathbf{W}(s) + \mathbf{v}(0^+)] \tag{A.2}$$

The time domain solution of $\mathbf{v}(t)$ is obtained from the inverse Laplace transform of $\mathbf{V}(s)$

$$\mathbf{v}(t) = \frac{1}{2\pi j}\int_{c-j\infty}^{c+j\infty} \mathbf{V}(s)e^{st}ds \tag{A.3}$$

with $c > |\mathrm{Re}(s_i)|$, where s_i are the poles of $\mathbf{V}(s)$. Replacing s with a new complex variable $s = z/t$, $t \neq 0$ in (A.3) leads to

$$\mathbf{v}(t) = \frac{1}{2\pi jt}\int_{\hat{c}-j\infty}^{\hat{c}+j\infty} \mathbf{V}\left(\frac{z}{t}\right)e^{z}dz \tag{A.4}$$

The key of numerical inversion of Laplace transform is to approximate e^z term in (A.4) with a special rational complex function - the Pade function, denoted by $\xi_{N,M}(z)$

$$e^z \approx \xi_{N,M}(z) = \frac{P_N(z)}{Q_M(z)} \tag{A.5}$$

where $P_N(z)$ and $Q_M(z)$ are polynomials in z of orders of N and M, respectively. The Pade function matches the first $M + N$ term of e^z exactly. The values of M and N are selected carefully such that all poles of the Pade function are *simple* and

are in the *right half* of the complex plane. Thus

$$\xi_{M,N} = \sum_{i=1}^{M} \frac{K_i}{z - z_i} \tag{A.6}$$

where z_i are the poles of $\xi_{M,N}(z)$ and K_i is the residue of $\xi_{M,N}(z)$ at z_i. The integral in (A.5) can be evaluated using the Residue theorem by closing the path of integration along an infinite arc around the poles z_i in the right half plane. The resultant time domain response is given by

$$\hat{\mathbf{v}}(t) = -\frac{1}{t} \sum_{i=1}^{M} K_i \mathbf{V}\left(\frac{z_i}{t}\right) \tag{A.7}$$

where t is the step size used in numerical integration. It is observed that the computation of the time-domain response involves frequency-domain evaluation of the network function at frequencies z_i/t. Since $\xi_{M,N}$ is independent of the network and time, the values of z_i and K_i can be precomputed and stored.

Bibliography

[1] Y. Tsividis, *Mixed analog-digital VLSI devices and technology : An introduction*, New York : McGraw-Hill, 1996.

[2] P. V. A. Mohan, V. Ramachandran, and M. N. S. Swamy, *Switched capacitor filters, theory, analysis and design*, Hertfordshire, UK : Prentice-Hall International, 1995.

[3] H. M. Wey and W. Guggenbuhl, "Noise transfer characteristics of a correlated doubling sampling circuits," *IEEE Trans. Circuits Syst.*, vol. 33, pp. 1028-1031, October 1986.

[4] J. M. Pimbley and G. J. Michon, "The output power spectrum produced by correlated double sampling" *IEEE Trans. Circuits Syst.*, vol.38, pp. 1086-1090, September 1991.

[5] V. F. Dias, G. Palmisano, and F. Maloberti, "Noise in mixed continuous-time switched capacitor sigma-delta modulators," *IEE Proc.- Circuits Devices Syst.* vol. 139, pp. 680-684, December 1992.

[6] V. F. Dias, G. Palmisano, P. O'Leary, and F. Maloberti, "Fundamental limitations of switched capacitor sigma-delta modulators," *IEE Proc.- Circuits Devices Syst.* vol. 139, pp. 27-32, February 1992

[7] K. Nakayama and Y. Kuraishi, "Present and future applications of switched-capacitor circuits," *IEEE Circuits and Devices*, pp. 10-21, September 1987.

[8] D. J. Allstot and W. C. Black, JR., "Technological design considerations for monolithic MOS switched-capacitor filtering systems," *Proc. IEEE*, vol. 71, pp. 967-985, August 1983.

[9] B. P. Lathi, *Signals, systems and communication*, New York : John Wiley and Sons, 1965.

[10] D. L. Fred, "Analog sampled-data filter,", *IEEE J. Solid-State Circuits*, vol. 7, August 1972.

[11] C. A. Gobet and A. Knob, "Noise analysis of switched capacitor networks," *IEE Electronics Letters*, vol. 16, pp. 734-735, 1980.

[12] C. A. Gobet and A. Knob, "Noise generated in switched capacitor networks," in *Proc. IEEE Int'l Symp. Circuits Syst.*, Chicago, Illinois, pp. 856-859, July 1981.

[13] C. A. Gobet and A. Knob, "Noise analysis of switched capacitor networks," *IEEE Trans. Circuits Syst.*, vol. 30, pp. 37-43, January 1983.

[14] B. Furrer and W. Guggenbuhl, "Noise analysis of sampled-data circuits," in *MOS sampled-capacitor filters : analysis and design*, edited by G. S. Moschytz, IEEE Press, pp. 142-146, 1984.

[15] J. H. Fischer, "Noise sources and calculation technique for switched capacitor filters," *IEEE J. of Solid-State Circuits*, vol. 17, pp. 742-752, August 1982.

[16] P. R. Gray and R. G. Meyer, *Analysis and design of analog integrated circuits*, 3rd-edition, New York : John Wiley and Sons, 1993.

[17] M. L. Liou and Y. L. Kuo, "Exact analysis of switched capacitor circuits with arbitrary inputs," *IEEE Trans. Circuits Syst.*, vol. 26, pp. 213-223, April 1979.

[18] J. Gobette and C. A. Gobet, "Exact noise analysis of SC circuits and an approximate computer implementation," *IEEE Trans. Circuits Syst.*, vol. 36, pp. 508-521, April 1989.

[19] L. Toth and K. Suyama, "Exact noise analysis of ideal SC networks," in *Proc. IEEE Int'l Symp. Circuits Syst.*, pp. 1585-88, New Orlean, May 1996.

[20] L. Toth and K. Suyama, "Efficient noise analysis of ideal switched-capacitor networks with experimental verification," in *Proc. IEEE Int'l Symp. Circuits Syst.*, Hong Kong, pp. 1054-1057, June 1997.

[21] D. O. Pederson, "A historical review of circuit simulation," *IEEE Trans. Circuits Syst.*, vol. 31, pp. 103-111, January 1984.

[22] J. Vlach and A. Opal, "Modern CAD methods for analysis of switched networks," *IEEE Trans. Circuits Syst. I*, vol. 44, pp. 759-762, August 1997.

[23] S. W. Director and R. A. Rohrer, "The generalized adjoint network and network sensitivity," *IEEE Trans. Circuit Theory*, vol. 16, pp. 318-323, August 1969.

[24] A. K. Seth, "Comments on time-domain network sensitivity using the adjoint network concept," *IEEE Trans. Circuit Theory*, vol. 19, pp. 367-370, July 1972.

[25] T. N. Trick, *Introduction to circuit analysis*, New York : John Wiley and Sons, 1977.

[26] R. Rohrer, L. Nagel, R. Meyer, and L. Weber, "Computationally efficient electronic-circuit noise calculations," *IEEE J. of Solid-State Circuits*, vol.6, pp. 204-213, August 1971.

[27] R. D. Davis, *Computer analysis of switched capacitor filters including sensitivity and distortion effects*, Ph.D. dissertation, University of Illinois at Urbana-Champion, 1981.

[28] R. D. Davis, "Distortion analysis of switched capacitor filters", in *Proc. IEEE Int'l Symp. Circuits Syst.*, Chicago, Illinois, pp. 876-879, April 1981.

[29] R. D. Davis, "A derivation of the switched-capacitor adjoint network based on a modified Tellegen's theorem," *IEEE Trans. Circuits Syst.*, vol.29, pp. 215-220, April 1982.

[30] J. Vandewalle, H. De Man, and J. Rabaey, "The adjoint switched capacitor network and its applications," in *Proc. IEEE Int'l Symp. Circuits Syst.*, Houston, Texas, 1031-1034, June 1980.

[31] J. Vandewalle, H. J. De Man, and J. Rabaey, "The adjoint switched capacitor network and its application to frequency, noise and sensitivity analysis," *Int'l J. of Circuit Theory Appl.*, vol. 9, pp. 77-88, 1981.

[32] C. F. Lee, R. D. Davis, W. L. Jenkins, and T. N. Trick, "Sensitivity and nonlinear distortion analysis for switched capacitor circuits using SCAPN," *IEEE Trans. Circuits Syst.*, vol. 31, pp. 213-221, February 1984.

[33] M. Okumura, H. Tanimoto, T. Itakura, and T. Sugawara, "Noise analysis method for nonlinear circuits with two frequency excitations using the computer," *Electronics and Communications in Japan*, Part 3, vol.3, pp. 41-50, 1991.

[34] M. Okumura, H. Tanimoto, T. Itakura, and T. Sugawara, "Numerical noise analysis for nonlinear circuits with a periodic large signal excitation including cyclo-stationary noise sources," *IEEE Trans. Circuits Syst. I*, vol. 40, pp. 581-589, September 1993.

[35] Z. Q. Shang and J. I. Sewell, "Efficient noise analysis methods for large non-ideal SC and SI circuits," in *Proc. IEEE Int'l Symp. Circuits Syst.*, pp. 565-68, Piscataway, NJ, 1994.

[36] Z. Q. Shang and J. I. Sewell, "Development of efficient switched network and mixed-mode simulators," *IEE Proc. - Circuits Devices Syst.*, vol. 145, pp. 24-34, February 1998.

[37] C. Hull and R. G. Meyer, "A systematic approach to the analysis of noise in mixers," *IEEE Trans. Circuits Syst. I*, vol. 40, pp. 909-919, December 1993.

[38] R. Spence and R. S. Soin, *Tolerance design of electronic circuits*, London : Imperial College Press, 1988.

[39] J. Vlach and K. Singhal, *Computer methods for circuit analysis and design*, 2nd edition, New York : Van Nostrand Reinhold, 1994.

[40] L. O. Chua and P. M. Lin, *Computer-aided analysis of electronic circuits - algorithms and computational techniques*, Englewood Cliffs, NJ : Prentica-Hall, 1975.

[41] S. W. Director, *Circuit theory - a computational approach*, New York : John Wiley and Sons, 1975.

[42] C. W. Ho, "Time-domain sensitivity computation for networks containing transmission lines," *IEEE Trans. Circuits Syst.*, vol.18, pp. 114-121, January 1971.

[43] B. D. H. Tellegen, "A general network theorem and applications," *Philip Res. Rept.*, 7, pp. 259-269, 1952.

[44] J. G. Ye and O. Wing, "Sensitivity analysis of SCN's with arbitrary inputs," in *Proc. IEEE Int'l Symp. Circuits Syst.*, pp.56-59, 1983.

[45] K. L. Lee and R. G. Meyer, "Low-distortion switched-capacitor filter design techniques," *IEEE J. Solid-State Circuits*, vol.20, pp. 1103-1112, February 1984.

[46] Y. Elcherif and P. M. Lin, "Transient analysis and sensitivity computation in piecewise-linear circuits," *IEEE Trans. Circuits Syst.*, vol. 38, pp. 1525-1533, December 1991.

[47] A. Opal and J. Vlach, "Analysis and sensitivity of periodically switched linear networks," *IEEE Trans. Circuits Syst.*, vol. 36, pp. 522-532, April 1989.

[48] Z. Q. Shang and J. I. Sewell, "Efficient sensitivity analysis for large non-ideal switched capacitor networks," in *Proc. IEEE Int'l Symp. Circuits Syst.*, vol. 2, pp.1405-1407, May 1993, New York.

[49] L. B. Wolovitz and J. I. Sewell, "General analysis of large linear switched capacitor networks," *IEE Proc. Circuits, Devices Syst.*, vol. 135, pp. 119-124, June 1988.

[50] L. E. Larson, editor, *RF and Microwave circuit design for wireless communications*, Boston : Artech House, 1996.

[51] T. J. Aprille and T. N. Trick, "Steady-state analysis of nonlinear circuits with periodic inputs," *Proc. IEEE*, vol. 60, pp. 108-114, January 1972.

[52] T. J. Aprille and T. N. Trick, "A computer algorithm to determine the steady-state response of nonlinear oscillators," *IEEE Trans. Circuit Theory*, vol. 19, pp. 354-360, July 1972.

[53] F. Colon and T. N. Trick, "Fast periodic steady-state analysis of large-signal electronic circuits," *IEEE J. Solid-State Circuits*, vol. 8, pp. 260-269, August 1973.

[54] D. Bedrosian and J. Vlach, "Analysis of switched networks," *Int'l J. of Circuit Theory and Applications*, May-June 1992, vol. 20, pp. 309-325.

[55] D. Bedrosian and J. Vlach, "Time-domain analysis of networks with internally controlled switches", *IEEE Trans. on Circuits Syst. I*, vol. 39, March 1992, pp. 199-212.

[56] J. Vlach and D. Bedrosian, "Switched networks," *The IMA Volumes in Mathematics and its Applications*, vol. 58, Semiconductors Part I, Springer Verlag, pp. 147-154, 1994.

[57] A. Opal and J. Vlach, "Consist initial conditions of linear switched networks," *IEEE Trans. Circuits Syst.*, vol.37, pp. 364-372, March 1991.

[58] J. Vlach, J., M., Wojciechowski, and A. Opal, "Analysis of Nonlinear networks with inconsistent initial conditions," *IEEE Trans. Circuits Syst. I*, vol. 42, 195-200, April 1995.

[59] A. Opal and J. Vlach, "Consistent initial conditions of nonlinear networks with switches," *IEEE Trans. Circuits Syst.*, vol. 78, pp. 698-710, July 1991.

[60] W. J. Cunningham, *Introduction to nonlinear analysis*, New York : McGraw-Hill, 1958.

[61] J. K. Hale, *Oscillations in nonlinear systems*, New York : McGraw-Hill, 1963.

[62] K. Gopal, M. S. Nakhla, K. Singhal, and J. Vlach, "Distortion analysis of transistor networks," *IEEE Trans. Circuits Syst.*, vol. 25, pp. 99-106, February 1978.

[63] K. S. Kundert and A. Sangiovanni-Vincentelli, "Simulation of nonlinear circuits in the frequency domain," *IEEE Trans. Computer-Aided Design*, vol.5, pp. 521-535, October 1986.

[64] M. S. Nakhla and J. Vlach, "A piecewise harmonic balance technique for determination of periodic response of nonlinear systems," *IEEE Trans. Circuits Syst.*, vol. 23, pp. 85-91, February 1976.

[65] L.O. Chua, *Introduction to nonlinear network theory*, New York : McGraw-Hill, 1969.

[66] A. Ushida and L. O. Chua, "Frequency-domain analysis of nonlinear circuits derived by multi-tone signals," *IEEE Trans. Circuits Syst.*, vol.31, pp. 766-777, September 1984.

[67] H. Flogerg and S. Mattisson, "Symbolic distortion analysis of nonlinear elements in feedback amplifiers using describing functions," *Int'l J. Circuit Theory and Application*, vol. 23, pp. 345-356, 1995.

[68] J. J. Slotinex and W. Li, *Applied Nonlinear Control*, London : Prentice-Hall International, 1991.

[69] A. T. Behr, M. C. Scheneider, S. N. Filho, and C. G. Montoro, "Harmonic distortion caused by capacitors implemented with MOSFET gates," *IEEE J. Solid-State Circuits*, vol. 27, pp. 1470-1475, October, 1992.

[70] M. C. Schneider, C. Galup-Montoro, and J. C. M. Bermudez, "Explicit formula for harmonic distortion in SC filters with weakly nonlinear capacitors," *IEE Proc.- Circuits Devices Syst.* vol. 141, pp. 505-509, December 1994.

[71] D. O. Pederson, *Analog integrated circuits for communications : principle, simulation and design*, Boston : Kluwer Academic, 1991.

[72] D. D. Weiner and J. E. Spina, *Sinusoidal analysis and modeling of weakly nonlinear circuits with application to nonlinear interference effects*, New York : Van Nostrand Reinhold, 1980.

[73] M. Schetzen, *The Volterra and Wiener theory of nonlinear systems*, New York : John Wiley and Sons, 1981.

[74] P. Wambacq and W. Sansen, *Distortion analysis of analog integrated circuits*, Boston : Kluwer Academic, 1998.

[75] L. O. Chua and C. Y. Ng, "Frequency domain analysis of nonlinear systems : general theory," *Electronic Circuits Syst.*, vol. 3, pp. 165-185, July 1979.

[76] P. Alper and D. C. J. Poortvliet, "On the use of Volterra series representation and higher order impulse responses for nonlinear systems," *Revue*, vol. 6, pp. 19-33, January 1964.

[77] P. Alper, "A consideration of the discrete Volterra series," *IEEE Trans. Automatic Control*, vol. 10, pp. 322-327, July 1965.

[78] A. M. Bush, "Some techniques for the synthesis of nonlinear systems," Technical Report 441, Research Laboratory of Electronics, Massachusetts Institute of Technology, Cambridge, Mass., 1966.

[79] J. Rabaey, *A unified computer-aided design technique for switched capacitor systems in the time and the frequency domain*, Ph.D. dissertation, Katholieke Universiteit Leuv, 1981.

[80] J. Vandewalle, J. Rabaey, W. Vercruysse, and H. J. De Man, "Computer-aided distortion analysis of switched capacitor filters in the frequency domain," *IEEE J. Solid-State Circuits*, vol.18, pp.324-332, June 1983.

[81] C. D. Keys, *Low-distortion mixers for RF communications*, Ph.D. Dissertation, Department of Electrical Engineering and Computer Science, University of California at Berkeley, 1994.

[82] S. Sen, *The design of sampling mixer and A/D converter for high IF digitization*, Ph.D. Dissertation, Department of Electrical and Computer Engineering, University of Waterloo, 1997.

[83] B. Gilbert, "A high-performance monolithic multiplier using active feedback," *IEEE J. Solid-State Circuits*, vol. 9, pp. 364-373, December 1974.

[84] P. J. Sullivan, B. A. Xavier, and W. H. Ku, "Low voltage performance of a microwave CMOS Gilbert cell mixer," *IEEE J. of Solid-State Circuits*, vol.32, pp. 1151-1155, July 1997.

[85] K. Kimura, "Some circuit design techniques using two cross-coupled emitter-coupled pairs," *IEEE Trans. Circuits Syst. I*, vol. 41, pp. 411-423, May 1994.

[86] A. Papoulis, *Probability, random variables and stochastic processes*, New York : McGraw-Hill, 1965.

[87] H. Dangelo, *Linear time-varying systems : analysis and synthesis*, Boston : Allyn and Bacon, 1970.

[88] A. van der Ziel, *Noise, sources, characterization, measurement*, Englewood Cliffs, NJ : Prentice-Hall, 1970.

[89] L. A. Zadeh, "Frequency analysis of variable networks," *Proc. IRE*, vol. 32, pp. 291-299, March 1950.

[90] M. E. Brinson and D. J. Faulkner, "A SPICE noise macromodel for operational amplifiers,", *IEEE Trans. Circuits Syst. I*, vol. 42, pp. 166-168, March 1995.

[91] F. Yuan and A. Opal, "Adjoint network of periodically switched linear circuits", in *Proc. IEEE Int'l Symp. Circuits Syst.*, vol. 6, pp. 298-301, Monterey, CA, May 1998.

[92] P. Penfield, R. Spence, Jr., and S. Duinker, *Tellegen's theorem and electrical networks*, Research monograph No. 58, Cambridge : MIT Press, Mass, 1970.

[93] G. W. Robert and A. S. Sedra, "Adjoint networks revisited," in *Proc. IEEE Int'l Symp. Circuits Syst.*, vol. 1, pp. 540-544, 1990.

[94] J. L. Bordewijk, "Interreciprocity applied to electrical networks," *Applied Sci. Res.*, B6, pp. 1-74, 1956.

[95] L. A. F. Schwarz, *Computer-aided design of microelectronic circuits and systems : fundamentals, methods and tools*, vol.1, London : Academic Press, 1987.

[96] S. Porta and A. Carlosena, "On the experimental methods to characterize the opamp response : a critical view," *IEEE Trans. Circuits Syst. I*, vol. 43, pp. 245-249, March 1996.

[97] J. Vlach, "Numerical method for transient responses of linear networks with lumped, distributed or mixed parameters," *J. Franklin Institute.*, vol. 288, pp. 99-113, August 1969.

[98] K. Singhal and J. Vlach, "Computation of time domain response by numerical inversion of the Laplace transform," Technical Report No. 74.6, 1974, University of Waterloo.

[99] R. Piessens, "On a numerical method for the calculation of transient response," *J. of Franklin Institute*, vol. 292, pp. 57-65, July 1971.

[100] K. Martin and A. Sedra, "Stray-insensitive switched-capacitor filters based on bilinear z-transform," *IEE Electronic Letters*, vol. 15, pp. 356-366, June 1979.

[101] P. E. Allen and E. Sanchez-Sinencio, *Switched capacitor circuits*, New York : van Nostrand Reinhold, 1984.

[102] L. Huelsman, *Active and passive analog filter design*, New York : McGraw-Hill, 1993.

[103] F. Yuan and A. Opal, "Noise analysis of periodically switched linear circuits", in *Proc. 1998 IEEE Canadian Conf. on Electrical and Computer Engineering*, vol. 1, pp. 153-156, Waterloo, Ont., May 1998.

[104] J. B. Johnson, "Thermal agitation of electricity in conductors," *Nature*, vol. 119, pp. 50-51, 1927.

[105] W. A. Gardner, *Introduction to random processes with applications to signals and systems*, 2nd edition, New York : McGraw-Hill, 1990.

[106] H. Nyquist, "Thermal agitation of electric charge in conductors,", *Physical Review*, vol. 32, pp. 110-113, 1928.

[107] A. G. Jordan and N. A. Jordan, "Theory of noise in metal oxide semiconductor devices," *IEEE Trans. Electron Devices*, pp. 148-157, March 1965.

[108] S. O. Rice, "Mathematical analysis of random noise," *Bell Syst. Tech. J.*, vol. 23, 1944, pp. 282-332.

[109] S. O. Rice, "Mathematical analysis of random noise," *Bell Syst. Tech. J.*, vol. 24, 1945, pp. 46-156.

[110] F. N. Hooge, "1/f noise,", *Physica*, 83B, pp. 14-23, 1976.

[111] A. L. McWhorter, "1/f noise and related surface effects in germanium," R.L.E. 295 and Lincoln Lab Tech Rep. 80, M.I.T., 1955.

[112] M. A. Caloyannides, "Microcycle spectral estimates of 1/f noise in semiconductors," *J. of Applied Physics*, vol. 45, pp. 307-310, 1974.

[113] B. Razavi, "A study of phase noise in CMOS oscillators," *IEEE J. Solit-State Circuits*, vol. 31, pp. 331-343, March 1996.

[114] B. E. Jonsson, "Sampling jitter in high-speed SI circuits," in *Proc. Int'l Symp. Circuits Syst.*, pp. I-524-526, 1998.

[115] M. Shinagawa, Y. Akazawa, and T. Wakimoto, "Jitter analysis of high-speed sampling system," *IEEE J. Solid-State Circuits*, vol. 25, pp. 22-224, February 1990.

[116] T. M .Souders, D. R. Flach, C. Hagwood, and G. L. Yang, "The effects of timing jitter in sampling systems," *IEEE Trans. Instrumentation and Measurement*, vol. 39, pp. 80-85, February 1990.

[117] A. A. Beex and M. P. Fargues, "Analysis of clock jitter in switched-capacitor systems," *IEEE Trans. Circuits Syst. I*, vol. 39, pp. 506-519, July 1992.

[118] Y. Dong and A. Opal, "Fast time-domain noise simulation of sigma-delta converters and periodically switched linear networks,", in *Proc. Int'l Symp. Circuits Syst.*, New York, vol. 6, pp. 114-117, 1998.

[119] Z. Y. Chang and W. M. C. Sansen, *Low-noise wide-band amplifiers in bipolar and CMOS technologies*, Boston : Kluwer Academic, 1991.

[120] R. C. Jaeger and A.J. Brodersen, "Low-frequency noise source in bipolar junction transistor," *IEEE Trans. Electron Devices*, vol. 17, pp. 128-136, February 1970,

[121] W. M. C. Sansen and R. G. Meyer, "Characterization and measurement of the base and emitter resistances of bipolar transistors,", *IEEE J. Solid-State Circuits*, vol. 7, pp. 492-498, December 1972.

[122] C. D. Motchenbacher, J. A. Connelly, *Low-noise electronic system design*, New York : John Wiley and Sons, 1993.

[123] Y. Tsividis,*Operation and modeling of the MOS transistor*, New York : McGraw-Hill, 1987.

[124] S. Christensson and L. Lundstrom, "Low frequency noise in MOS transistors," *Solid-State Electronics*, vol. 11, pp. 813-820, 1968.

[125] G. Nicollini, D. Pancini, and S. Pernici, "Simulation-oriented noise model for MOS devices," *J. Solit-State Circuits*, vol. 22, pp. 1209-1212, December 1987.

[126] P. Bolcato and R. Poujois, "A new approach for noise simulation in transient analysis," in *Proc IEEE Int'l Symp. Circuits Syst.*, pp. 887-890, 1992.

[127] R. M. Fox, "Comments on circuit models for MOSFET thermal noise," *J. Solid-State Circuits*, vol. 28, pp. 184-185, February 1993.

[128] A. van der Ziel, *Noise in solid-state devices and circuits*, New York : Wiley, 1986.

[129] S. Liu and L. W. Nagel, "Small-signal MOSFET models for analog circuit design," *IEEE J. Solide-State Circuits*, vol. 17, pp. 983-998, December 1982.

[130] B. Wang, J. R. Hellums, and C. G. Sodini, "MOSFET thermal noise modeling for analog integrated circuits," *J. Solid-State Circuits*, vol. 29, pp. 833-835, July 1994.

[131] R. Unbehauen and A. Cichocki, *MOS switched-capacitor and continuous-time integrated circuits and systems : analysis and design*, Berlin : Springer-Verlag, 1989.

[132] B. J. Sheu, D. L. Scharfetter, P. K. Ko, and M. C. Jeng, "BSIM:Berkeley short-channel IGFET model for MOS transistors," *J. Solid-State Circuits*, vol. 22, pp. 558-566, August 1987.

[133] R. P. Jindal, "Distributed substrate resistance noise in fine-line NMOS field-effect transistors," *IEEE Trans. Electron Devices*, vol. 32, pp. 2450-2453, November 1985.

[134] T. Manku, "Microwave CMOS - device Physics and design," *IEEE J. Solid-State Circuits*, vol. 34, pp. 277-285, March 1999.

[135] J. C. Bertails, "Low-frequency noise consideration for MOS amplifiers design," *IEEE J. of Solid-State Circuits*, vol.14, pp. 773-776, August 1979.

[136] S. Letzter and N. Webster, "Noise in amplifiers," *IEEE Spectrum*, vol.7, pp. 67-75, June 1970.

[137] Y. Netzer, "The design of low-noise amplifiers," *Proc. IEEE*, vol. 69, pp. 728-742, 1981.

[138] F. Yuan and A. Opal, "Sensitivity analysis of periodically switched linear circuit using an adjoint network technique", *IEEE Int'l Symp. Circuits Syst.*, Orlando, Florida, May 1999 (in press).

[139] F. Yuan and A. Opal, "Distortion analysis of periodically switched nonlinear circuits" in *Proc. IEEE Int'l Symp. Circuits Syst.*, Orlando, Florida, May 1999 (in press).

[140] Y. L. Kuo, "Distortion analysis of bipolar transistor," *IEEE Trans. Circuits Theory*, vol.20, pp. 709-716, 1973.

[141] R. G. Mayer, M. J. Shensa, and R. E. Schenbach, "Cross modulation and intermodulation in amplifiers at high frequencies," *IEEE J. of Solid-State Circuits*, vol.7, pp. 16-23, February 1972.

[142] *Hspice user's manual*, Meta-Software Inc. , 1992

[143] W. Yu, S. Sen, and B. Leung, "Time varying Volterra series and its applications to the distortion analysis of a sampling mixer", in *Proc. 40th Midwest Symp. Circuits Syst.*, vol. 1, pp. 245-248, Sacramento, CA. August 1997.

[144] M Bialko and S. Krawczyk, "Influence of nonlinear switch resistance on nonlinear distortion in switched-capacitor circuits," in *Proc. European Conf. Circuits Syst.*, pp. 780-783, 1987.

[145] S. Lachowicz and S. Krawczyk, "Influence of MOS switch ON resistance and parasitic capacitances on harmonic distortion of SC filters," in *Circuit Theory and Design 87*, edited by R. Gerber, Amsterdam : North-Holland, 1987.

[146] M. L. Liou, "Exact analysis of linear circuit containing periodically operated switches with applications," *IEEE Trans. Circuit Theory*, vol. 19, pp. 146-154, March 1972.

[147] G. W. Roberts, "Calculating distortion levels in sampled-data circuits using SPICE," in *Proc. IEEE Int'l Symp. Circuits Syst.*, pp. 2059-2062, 1995.

[148] P. Crewley and G. W. Roberts, "Predicting harmonic distortion in switched-current memory cell," *IEEE Trans. Circuits Syst. II*, vol. 41, pp. 73-86, February 1994.

[149] F. J. Harris, "On the use of windows for harmonic analysis with the discrete Fourier transform," *Proc. IEEE*, vol. 66, pp. 51-83, January 1978.

[150] M. Schetzen, "Multilinear theory of nonlinear networks," *J. of The Franklin Institute*, vol. 320, pp. 221-247, November 1985.

[151] F. M. Klaassen, "On the influence of hot carrier effects on the thermal noise of field-effect transistors," *IEEE Trans. Electron Devices*, vol. 17, pp. 858-862, October 1970.

[152] A. Demir, E. W. Y. Liu and L. Sangiovanni-Vincentelli, "Time-domain non-Monte Carlo noise simulation for nonlinear dynamic circuits with arbitrary

excitations," *IEEE Trans. Computer-Aided Design of Integrated Circuits Syst.*, vol. 15, pp. 493-505, 1996.